The Important Role of Post-translational Modifications, Neddylation and Acetylation, in Immunity

by

Nathan D. Mathewson

A dissertation submitted in partial fulfillment
of the requirements for the degree of
Doctor of Philosophy
(Immunology)
in The University of Michigan
2015

Doctoral Committee:

Professor Pavan R. Reddy, Chair
Associate Professor David Aronoff, Vanderbilt University
Professor Bethany Moore
Professor Gabriel Nuñez
Professor Benjamin S. Segal
Professor Yi Sun

DEDICATION

For my family. Your support and encouragement

have inspired and boosted my resolve.

ACKNOWLEDGMENTS

This dissertation would not have been possible without the support and mentorship of my advisor and mentor, Pavan Reddy. Pavan has always been willing to take time when I stop by and interrupt him at his office, a gesture of commitment that I am extremely appreciative of. Through his willingness and encouragement to discuss ideas critically, Pavan has trained me to think logically, clearly, and directly. He has thus been fundamental in molding me into a young scientist and has been the finest mentor I could imagine.

I am also indebted to the members of the Reddy lab, particularly Tomomi Toubai for his extensive and patient assistance in teaching me critical cellular techniques. I am also thankful for Yaping Sun and his knowledge and help in understanding molecular techniques. Julia Wu for being bay-buddies and for assistance in performing experiments. Katherine Oravecz-Wilson for managing the lab and Cynthia Zajac for your day to day help.

TABLE OF CONTENTS

LIST OF FIGURES

Figure

LIST OF TABLES

Table

LIST OF ABREVIATIONS

Abs	Antibodies
Allo-BMT	Allogeneic bone marrow transplant
APC	Antigen presenting cell
ASC	Apoptosis-associated speck-like protein containing CARD
BMDC	Bone marrow derived dendritic cells
BMDM	Bone marrow derived macrophage
CAND1	Cullin-associated and neddylation-dissociated protein 1
CRL	Cullin ring ligase
CTL	Cytotoxic T lymphocyte
DAMP	Danger associated molecular pattern
G-CSF	Granulocyte colony stimulating factor
GF	Germ free
GI	Gastrointestinal
GVHD	Graft versus host disease
GVT	Graft versus tumor
HAT	Histone acetyltransferase
HDAC	Histone deacetylase
HDACi	Histone deacetylase inhibitor

HECT	Homologous to the E6AP carboxyl terminus
HLA	Human leukocyte antigen
HSCs	Hematopoietic stem cell
IkB	Inhibitor of kappaB
KO	knockout
LPS	Lipopolysaccharide
MHC	Major histocompatibility complex
MLR	Mixed lymphocyte reaction
mRNA	messenger RNA
MYD88	Myeloid differentiation primary response gene 88
NAE	NEDD8 activating enzyme
NEDD8	Neural precursor cell expressed developmentally down-regulated protein 8
NF-kB	Nuclear factor-kappaB
NLR	NOD like receptor
PAMPS	Pathogen associated molecular patterns
PRRs	Pattern recognition receptors
PTM	Posttranslational modification
Rbx2	RING box protein 2
RING	Really interesting new gene
SAG	Sensitive to apoptosis gene
SPF	Specific pathogen free
TBI	Total body irradiation

TCR	T cell receptor
T_H	T helper cell
ThCTL	T helper cytoxic lymphocyte
TLR	Toll like receptor
Tregs	T regulatory cell
TSA	Tumor specific antigen
Ub	Ubiquitin
UBC12	Ubiquitin conjugating enzyme E2M
VDJ	Variable, joining, diversity
WT	Wild type

ABSTRACT

Proteins undergo posttranslational modifications (PTMs) by the attachment of various side chains including phosphate, acetate, sumo, ubiquitin, etc. Our lab has previously shown that the PTM acetylation is important for immune responses. To that end, acetylation of the non-histone protein STAT3 increases the expression of indoleamine 2,3-dioxygenase (IDO) in dendritic cells resulting in decreased responses in the context of allogeneic bone marrow transplant (allo-BMT) leading to attenuated graft versus host disease (GVHD). Further, histone deacetylase inhibitors (HDACi) enhance T regulatory cells. However, the role of other modifications, such as neddylation, remained unknown. Neddylation facilitates the degradation of proteins by the E3 ligase system known as cullin RING ligase (CRL) and has been identified to regulate the proliferation and survival of liver, breast, and pancreatic cancer cells. Further, the neddylation pathway has previously been suggested to regulate the function of NF-κB, a critical transcription factor for several immune cell functions. Therefore, we systematically examined the role of neddylation in the function of innate (DCs, macrophages, and neutrophils) and adaptive (T cells) immune cells. We found that neddylation affects immunity in a cell specific manner. It positively regulates NF-κB in DC and macrophage functions where, by contrast, it negatively regulates neutrophils and T cells in a non NF-κB manner. Our data suggest that the loss of a critical adapter element of the CRL, sensitive to apoptosis

gene (SAG), in neutrophils leads to increased reactive oxygen species (ROS) resulting in increased inflammatory responses. Examination of T cells revealed that inhibition of the neddylation pathway results in less degradation of SOCS proteins attenuating T cell functions following allo-stimulation.

Expanding on the previous observations made in our lab, we further explored the role of acetylation in regulating immunopathology, such as graft versus host disease (GVHD). We found that the endogenous histone deacetylase inhibitor (HDACi) butyrate – which is also a primary energy source of intestinal epithelial cells (IECs) and is derived exclusively from the GI microbiota – is critical for the survival of IECs and the negative regulation of GVHD severity. Our data show that diminutive levels of butyrate are found within the intestinal tissue following allo-BMT. Furthermore, the loss in butyrate leads to decreased acetylation of histone-H4, decreased IEC junctional integrity, and increased allo-mediated damage – effects that were restored upon local intragastric gavage with exogenous butyrate leading to mitigated GVHD pathology and improved mortality. Furthermore, rationally altering the microbiota to high butyrate-producing Clostridial strains recapitulates the effects of synthetic butyrate by decreasing GVHD severity and improving survival.

Collectively, these data further our knowledge of the roles of PTMs in immunity – specifically the heretofore-unknown functions of neddylation in the regulation of immune cells and acetylation in the regulation of immune pathology.

CHAPTER I

INTRODUCTION

Overview of the Immune System

The collection of cells that protect vertebrates from surrounding pathogenic foreign microorganisms is known as the immune system. The specialized cells of the immune system are categorized under two main arms of defense and are comprised of innate immunity and adaptive immunity[1].

The innate immune system is the host's first line of cellular mediated defense against invading bacteria, fungi, and viruses that express pathogen associated molecular patterns (PAMPs). Although a wide array of PAMPs are almost immediately detected by pattern recognition receptors (PRRs) encoded in the germ line of innate immune cells leading to the elimination of the invading microorganism, the innate immune system does not develop a lasting immunity to that pathogen[1].

The second arm of defense – the adaptive immune system – consists of a specific immune response driven by the production of pathogen-specific antibodies (Abs) by B cells and cellular recognition by cytotoxic T cells. Generation of specific antigen receptors consisting of Ab immunoglobulin production by B cells and αβ T cell receptors (TCR) in T cells, is accomplished through the somatic rearrangement of variable, diversity, and joining [V(D)J] regions of the antigen receptor encoding genes[2]. This rearrangement leads to an extremely diverse repertoire of individual TCRs (upwards of

10^{11} TCRs) with an approximate $3.6x10^{7}$ distinct T cell clones comprehensively increasing the host's ability to fight infection[3,4]. Upon T cell recognition of cognate antigen, pathogen-specific clonal expansion occurs leading to the elimination of the antigen source[1]. Following antigen clearance, the immune response ceases and the majority of the effector cells undergo apoptosis[5,6]. The remaining effector cells are then converted to memory cells resulting in the development of the hallmark lifelong immunity known as immunological memory[6,7]. Immunological memory allows the adaptive immune response to be shortened from a time period requiring days upon the first pathogenic insult, to only a fraction of the time following reinfection[8].

Detection of pathogen

The epithelium of the skin, gut, and lungs is an important part of host defense against invading pathogens, as it is often the first point of contact with the infection[1]. When a pathogen crosses the physical epithelial barrier, the innate immune system composes the first line of *cell-mediated* host defense. As mentioned above, innate immune cells possess PRRs to detect invading pathogens. There are several categories of PRRs that exist to recognize PAMPs in various cellular surfaces and compartments. One type of PRR is known as toll-like receptors (TLRs). Many TLRs have been described and are known to recognize various PAMPs. These include TLR4 recognition of lipopolysaccharide (LPS), TLR2 of bacterial lipoproteins, TLR5 of flagellin, TLR3 and 7 of RNA, and TLR9 of DNA[9]. The engagement of extracellular TLR receptors requires the adaptor protein known as myeloid differentiation primary response protein 88 (MYD88) for downstream signaling[10,11].

While TLRs are both extracellular and intracellular, another type of PRR, known as NOD-like receptors (NLR), is found in the intracellular compartment[12,13]. Indeed, NLRs function through the recognition of intracellular PAMPs and danger- associated molecular patterns (DAMPs)[14]. NOD1 and NOD2 are the most well studied members of the NLR family and are often viewed as the prototypical NLRs. NOD1 is ubiquitously expressed, where NOD2 expression is restricted to innate immune cells and intestinal Paneth cells[13]. Signaling through the NLR has differential functional effects dependent upon which class of NLR is stimulated. NLR signaling is critical for the function of the inflammasome, a multiprotein complex that plays an important role in inflammatory responses. Activation of NOD1 and NOD2 triggers MAPK and NF-κB pathways, where activated NLRP1, NLRP3, and NLRC4 act as scaffolding platforms for the formation of inflammasomes. A commonality of these three inflammasomes is their association with the protein apoptosis-associated speck-like protein containing a CARD (ASC), which enables the recruitment of caspase-1. The activation of caspase-1 by the inflammasome is required for the processing of IL-1β and IL-18. Although NLRs and TLRs have disparate cellular locations, these PRRs can have both non-redundant and complimentary functions. For example, when cells have become refractory to TLR agonists, NOD1/2 signaling is not mitigated highlighting the non-redundant roles for these PRRs. However, TLR-mediated NF-κB is required for the production of pro-IL-1β, where NLR activation of caspase-1 is required for the cleavage of pro-IL-1β to active IL-1β, leading to its secretion.

Amongst the first PRR-expressing cellular responders to pathogen are known as

neutrophils. While neutrophils are short-lived compared to another type of innate immune cell called macrophages, they are the most numerous and the most important cells that compose innate immune responses[1]. The main function of a neutrophil is phagocytosis and efficient destruction of collected material in intracellular vesicles. Neutrophils are also an important source of TNFα which triggers local containment of infection and increases extravasation of immune cells into the infected area[1]. While neutrophils react quickly to pathogen based upon expressed PAMPs, the response is not pathogen specific. Several immune cell types, whose function is to generate and present antigen peptide to adaptive immune cells for a pathogen specific response, continually sample the physical barrier[1,15]. These surveying cells are known as antigen presenting cells (APCs).

Antigen Presenting Cells

There are three cell types known to have the capability of presenting antigen to activate T cells – DCs, macrophages, and B cells. While all three cell types are indeed professional APCs, it is DCs that are the most potent and can collect, process, and present antigen from myriad sources[1,16]. By contrast, macrophages and B cells specialize in presenting antigens from intracellular compartments and mainly interact with T cells that have been previously primed by DCs[1,15].

It is well known that the innate and adaptive immune systems work in concert to provide protection from invading pathogens. Dendritic cells serve as a bridge between the two arms of the immune system – that is, ingesting pathogen and presenting peptide to T cells with appropriate activating cytokines, such as IL-12[1]. When sampling the peripheral

environment via phagocytosis, the DC is in an immature state. Maturation of a DC occurs by 1) PRR recognition of PAMPs expressed on collected material, 2) the cytokine environment present during an inflammatory response, or 3) by mediators released during tissue damage[1,15]. The mature DC state is distinct from immature in that the phagocytic nature of the DC is down regulated. Further, DC maturation up-regulates the expression of both class I and II major histocompatibility complex (MHC) molecules increasing the display of processed peptide on the cell surface. In addition, activated DCs migrate to the lymph node and increase co-stimulatory B7 molecules (CD80 and CD86) necessary for T cell activation.

Macrophages are found in most tissues, including the lymphoid tissue, and are activated through PRRs, similarly to DCs[1]. Although an important role of these cells is the presentation of antigen to primed T cells (T cells previously activated by DCs), a primary role of macrophages is the ingestion of microbes and particulate antigens thereby preventing their systemic escape into the blood[1]. Indeed, macrophages constitutively scavenge dead or dying cells of the liver sinusoids, the splenic red pulp, and especially clear the large numbers of cells of the blood that die daily[1,17]. Notably, macrophages that have engulfed microorganisms, but are unable to destroy them, use their antigen presentation capabilities to recruit the adaptive immune system for assistance[1].

B cells internalize soluble molecules that bind to their cell surface immunoglobulin. Protein components of the antigen are processed and presented via peptide:MHC class II complexes[1]. This allows for the interaction with CD4 T cells and may result in

immunoglobulin class switching to better refine Ab responses[18]. B cells do not constitutively express B7 co-stimulatory molecules necessary for the activation of T cells. However, PRR stimulation – as also seen in DCs and macrophages – results in these molecules expression on the B cell surface[1].

T cell Subsets

Following T cell development in the thymus (discussed below), two principal types of naïve T cell migrate into the periphery known as $CD4^+$ and $CD8^+$ – based upon the cells surface expression of CD4 and CD8 glycoproteins[19]. CD4 T cells are either naïve effector cells or T regulatory cells (Tregs). Upon stimulation by cognate antigen, naïve CD4 T cells differentiate into several effector T cell subsets, often referred to as T helper cells (T_H) as they provide activation, growth, and survival signals to accessory cells[20]. CD4 T cells must be presented with antigen by MHC class II-expressing APCs which result in their differentiation into three main categories of T_H cells distinguished as T_H1, T_H2, and T_H17 cells that each promote distinct types of responses based upon the form of infection[1]. T_H1 cells assist in the eradication of the bacterial invasion of intracellular vesicles of macrophages through the release of IFNγ and IL-2. IFNγ instructs the macrophage to increase intracellular killing and it also promotes $CD8^+$ T cell function (discussed below)[1].

By contrast, T_H2 cells produce a wide array of cytokines[21], including IL-4, that evoke a strong antibody response and recruit eosinophils culminating in a robust reaction to parasitic infections. These effector activities of T_H2 cells are shared with those indicated in allergic responses which increase the production of protective barrier mucus at

mucosal sites[1].

T_H17 cells are being increasingly associated with inflammatory diseases, are known to play a strong role in mucosal immunology, and are also indicated in autoimmune diseases[1,22]. Upon stimulation, T_H17 cells release cytokine mediators including IL-17 and IL-22, which induce a substantial tissue reaction. The receptor of IL-17 is expressed on nearly every cell type of the body promoting the recruitment of neutrophils to the site of inflammation[22,23].

The function of Tregs in the adaptive immune response is to suppress T effector responses. There are two main groups of Tregs, both of which express the transcription factor FoxP3. One subset is committed to a regulatory function during development in the thymus known as natural Tregs. The other subset, known as induced Tregs, differentiate from naïve CD4 T cells into Treg cells in the periphery influenced by local environmental conditions[24]. Treg cells require a source of IL-2 which is detected by the constitutive expression of $CD25^+$ on the Treg cell surface[1,24]. Tregs release an anti-inflammatory cytokine known as IL-10 which inhibits the activity of T_H1 cells and macrophages[25]. This regulation of immune responses diminishes optimal pathogen clearance but also protects from immune-mediated tissue damage. Thus, Tregs and the release of IL-10 cytokine can both hinder pathogen clearance and mitigate immunopathology[25].

Although CD4 T cells are classically referred to as 'helper cells' due to their release of cytokines that result in accessory cell activation, CD4 T cells also function as cytoxic-killing cells (ThCTL). Indeed, ThCTLs have been found in the peripheral blood of

humans seropositive for human cytomegalovirus, hepatitis, and human immunodeficiency-1[26-28]. Similar to $CD8^+$ cytotoxic T lymphocytes (CTLs, discussed below), ThCTLs induce target cell apoptosis through the release of granulocytes[29,30] and Fas/Fas ligand mediated apoptosis[31,32].

CD8 CTLs responding to foreign antigen become potent and specific cytotoxic killers known as effectors[20]. CTLs target cells that are infected with viruses present in the cytosol of the invaded cell. Classically, CTLs were once thought to require CD4 T_H cells for a measureable effector response. A strong primary response is now, however, clearly measured in animals that lack $CD4^+$ T cells. Indeed, mice that lack expression of CD4 T cells – either by $CD4^+$ T cell depletion, genetic deletion of major MHC class II molcules (discussed further below), or mice deficient in CD4 glycoprotein co-receptor – still generate $CD8^+$ CTL-mediated killing similar to wild type (WT) mice[33-35]. However, while a primary CTL response is similar in animals that lack $CD4^+$ T cell help, the formation of memory CTLs is now understood to require CD4 T_H cells, rendering a secondary response unattainable in CD4 T cell-deficient animals[36,37]. These studies have given great insight into the hallmark immune memory response required for effective immunity.

T cell development

Adaptive immune cells derive from the pluripotent hematopoietic stem cells (HSCs) of the bone marrow[1]. T cell-progenitors migrate from the bone marrow via the blood to the thymus[1] and differentiate into new T cells, known as lymphopoiesis. Developing T cells

undergo rigorous selection based upon TCR interaction with MHC molecules expressed by thymic cells[19]. When the TCR of the developing T cell is capable of interacting with MHC molecules presented in the thymus, that T cell is positively selected (approximately 10-30% of somatically rearranged TCRs). In the absence of positive selection, the developing T cell dies due to neglect[19]. All possible self-peptide antigens are next presented to the positively selected developing T cells in the context of MHC:self-peptide. If, however, the developing T cell responds strongly to the self-peptide, that T cell clone is deleted to ensure an autoimmune attack does not occur upon migration to the periphery – a process known as negative selection[1,19].

Activation of T cells

For a T cell to be stimulated and undergo clonal expansion, specialized cell-surface peptide-presentation proteins called MHC molecules must present the cells cognate antigen. There are two classes of MHC molecules which are termed class I and class II molecules[1]. Class I MHC molecules are expressed by all nucleated cells and present antigen-peptide derived from the cytosol of cells to $CD8^+$ T cells[38]. MHC-I molecules consist of two polypeptide chains known as the three subunit 'α-chain' which is noncovalently associated with a smaller chain termed β_2-microglobulin[1]. The α_1 and α_2 subunits compose the peptide binding cleft and the region that interacts with the TCR on $CD8^+$ T cells. Genetic inactivation of the β_2 subunit blocks MHC-I function effectively preventing presentation of class I antigen to T cells enabling studies to explore class I dynamics[39].

Class II MHC molecules are expressed by accessory cells functioning as professional APCs – such as DCs, macrophages, and B cells. These APCs sample the extracellular environment and present peptide derived from phagocytosed antigen, contained within intracellular vesicles, to only $CD4^+$ T cells[1]. MHC-II molecules are composed of two chains, α and β each consisting of two subunits. Although similar in name, the α chain of MHC-II is distinct from that found in MHC-I[1]. The MHC-II peptide binding cleft is comprised of the α_1 and β_1 subunits of the corresponding chains[40].

Importantly, TCRs of both CD4 and CD8 T cells only recognize peptide presented in the context of the appropriate MHC-class molecule. Furthermore, the TCR interacts with both the antigen-peptide *and* the MHC molecule[1,38,40].

Upon activation by the MHC complex, new T effector cells fall into three broad categories: killing, activation, and regulation[1].

Primary activation of naïve T cells requires additional signaling through co-stimulatory receptors for the T cell to become fully activated. A consequence of TCR-only stimulation results in anergic T cells – that is, T cells that respond very poorly upon future interaction with cognate peptide[41]. The best characterized co-stimulatory molecules are known as B7 molecules and interact with the CD28 receptor on T cells[1]. Stimulation through CD28 stabilizes the life of IL-2 messenger RNA (mRNA) transcripts allowing for copious amounts of IL-2 protein to be produced. The existence of other co-stimulatory receptors serve to modify the co-activation signal received by the T cell[42]. For example CTLA-4 receptor bind B7 molecules on an order of 20 times more avidly than CD28[1,43]. Rather than stimulate the T cell, CTLA-4 signaling has an inhibitory effect

on the T cell and restricts the production of IL-2. Another type of co-stimulation occurs through the interaction of inducible co-stimulator (ICOS) on T cells with ICOS ligand expressed on APCs. Although ICOS signaling too inhibits IL-2 production – by contrast with CTLA-4 – ICOS regulates the expression of other T cell cytokines such as IFNγ and IL-4 thereby having a strong indication in 'helper' roles of the T cell including isotype switching in B cells[1,44].

Posttranslational modifications

Posttranslational modifications (PTMs) are a broad array of versatile, reversible chemical alterations of newly translated proteins[45]. PTMs are crucial for a proteins function and control its cellular location, lifespan, and activity[46]. PTMs can occur at any step during the life of a protein[47] and include (but are not limited to) acetylation, phosphorylation, ubiquitylation, and neddylation[48-50], which are all critical for an immune response. For example, in immunity the most common modus to terminate a signaling event is the ubiquitination of a protein leading to subsequent proteolytic degradation via the proteasome[1]. Similarly, phosphorylation of inhibitor-κB (IκB) protein releases the transcription factor nuclear factor-κB (NF-κB) allowing its translocation into the nucleus initiating the production of inflammatory cytokines, such as TNFα and IL-6[51].

Acetylation

Acetylation is most often associated with modification of histone proteins, around which chromatin is wound[52,53], known as nucleosomes. The chromatin structure of a eukaryotic cell has a major impact on the level of gene transcription[52]. Within the cell, DNA exists

as nucleosome repeats wherein 146bp of DNA are wound around a histone octamer – composed of two of each of the H2A, H2B, H3, and H4 histone proteins[52]. Dynamics of H3 and H4 tail acetylation are the best understood and most commonly studied[54].

The attachment of acetyl groups by histone acetyltransferases (HATs) to the tails of histone-solenoids results in an open chromatin conformation, allowing gene expression. By contrast, histone deacetylases (HDAC) remove acetyl groups thereby returning the chromatin to a closed state and thus inhibiting gene expression[52]. There are several classes of HDAC; Class I (HDACs 1, 2, 3, and 8), Class II (HDACs 4, 5, 6, 7, 9, and 10), and Class IV (HDAC 11) are zinc dependent enzymes, whereas Class III HDAC enzymes are known as sirtuins and rely on nicotinamide adenine dinucleotide (NAD) and are zinc independent[55]. HDAC enzymes are frequently disregulated in cancer[56], thus HDAC inhibitors (HDACi) have been shown to have a profound effect on many disease states including cancers of the blood[55,57,58] through myriad cell death pathways[56]. While many synthetic HDACi have been developed and are currently either approved or in various stages of clinical trial[53], the commensal microbiota found in the gastrointestinal (GI) tract exclusively make an endogenous HDACi, called butyrate (explained in depth later) [59-61].

Acetylation can, however, occur on non-histone proteins, such as STAT3[48]. STAT3 acetylation promotes the transcription of indoleamine 2,3-deoxygenase (IDO) on DCs which promotes the induction of Tregs[1].

Ubiquitylation

Attachment of the small 23 kD ubiquitin (Ub) molecule is most often associated with

degradation of a target protein[62]. Ubiquitylation can, however, serve non proteolytic roles such as in the NF-κB pathway[1]. Nevertheless, attachment of Ub requires three enzymes to facilitate the lysine residue modification of the protein substrate. The E1 molecule activates Ub in an ATP-dependent manner and transfers the activated Ub molecule to an E2 molecule. The E2-Ub conjugate interfaces with an adaptor protein on the E3-ligase scaffolding to catalyze target protein mono- or poly-ubiquitylation[63,64]. There are two main classes of E3 ligases – those that contain either a homologous to the E6AP carboxyl terminus (HECT) domain or a really interesting new gene (RING) domain[65] – with the vast majority containing RING finger domains. A major difference between E3 classes is that those with a HECT domain form a catalytic intermediate with Ub and, by contrast, RING domain E3s do not. Furthermore, RING E3s serve as a scaffold that brings the E2-Ub conjugate within close proximity of the substrate[65]. RING finger Ub-ligase family members can function as monomers, dimers, or multi-subunit complexes. Multi-subunit RING domains are most often cullin RING ligases (CRLs)[66].

CRL function must first be activated by the attachment of a 16 kD Ub-homolog called neural precursor cell expressed developmentally downregulated protein 8 (NEDD8) through a process known as neddylation[67]

Neddylation

Similar to Ub molecule activation and transfer, NEDD8 requires an ATP dependent specific E1 enzyme known as NEDD8 activating enzyme (NAE) (Fig. 1.1).

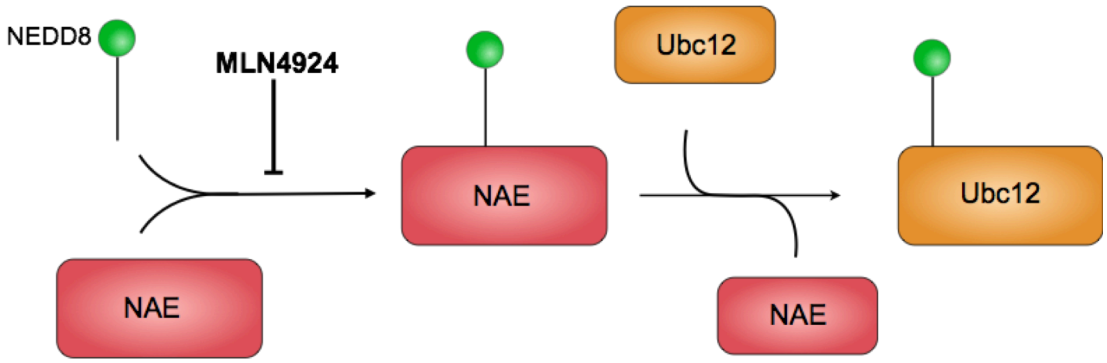

Fig 1.1 – Activation of NEDD8 molecule. NEDD8 is activated by NEDD8 activating enzyme (NAE) in an ATP dependent process. Once activated, NEDD8 is transferred to the E2 molecule, Ubc12. A small molecule inhibitor, MLN4924, prevents the activation of NEDD8 molecule by NAE. MLN4924 is an AMP-mimetic with potent and specific inhibitory capabilities.

Following activation, NAE transfers NEDD8 to an E2 molecule called NEDD8-conjugating enzyme (UBC12), which in turn transfers NEDD8 to the cullin backbone[66,67], displacing cullin-associated NEDD8-dissociated protein 1 (CAND1) – a competitive inhibitor of cullin protein. The attachment of NEDD molecule to cullin protein allows the recruitment of the multi-subunit components composing the CRL complex[67] which serves as the scaffolding to complete substrate ubiquitylation of a specific subset of proteins[68] (Fig. 1.2).

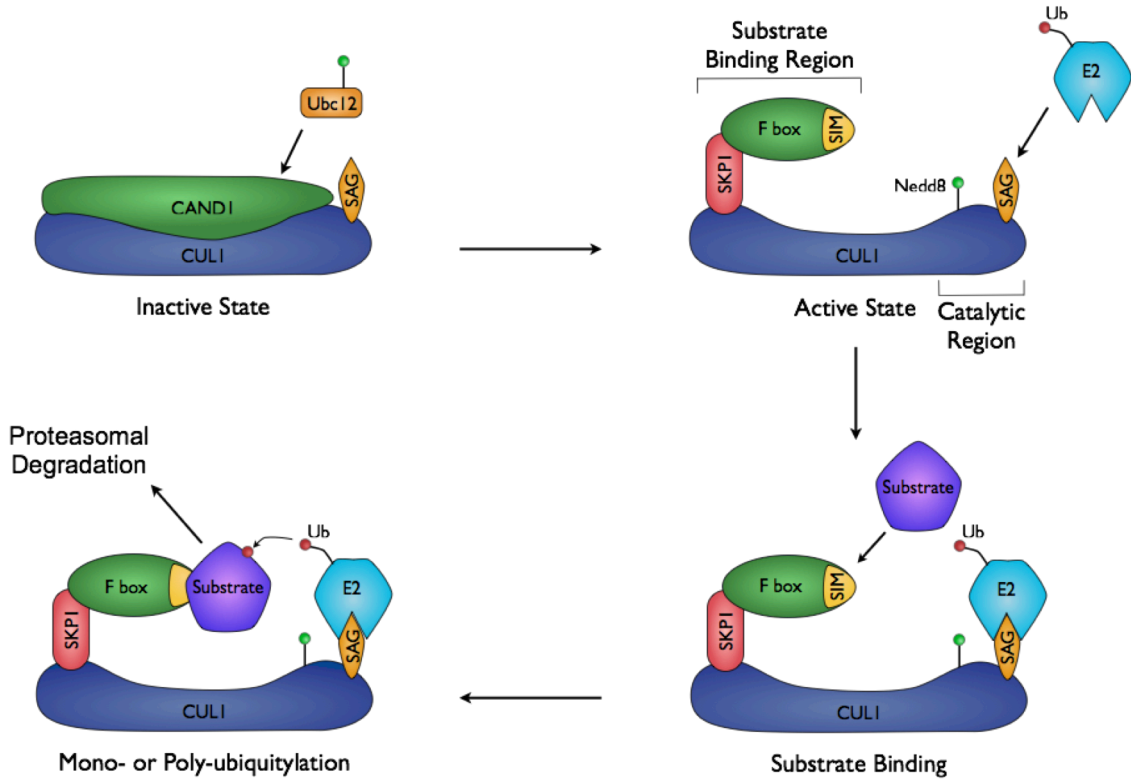

Fig 1.2 – Neddylation. Following the activation of NEDD8 (Fig. 1.1), it is transferred to cullin protein of the CRL complex. This displaces the inhibitor of CRL activity, CAND1. Upon initiation of the CRL by NEDD8, multi-subunit components are recruited forming the substrate-binding region. Target proteins are next recruited and mono- or poly-ubiquitylated followed by subsequent degradation by the proteasome.

There at least seven cullins (CUL1, CUL2, CUL3, CUL4A, CUL4B, CUL5, and CUL7) that each facilitate ubiquitylation based on their substrate binding region specificity[67,68].

An adaptor molecule – sensitive to apoptosis gene (SAG) / RING-box protein 2 (Rbx2) – is a critical component of the CRL5 complex and interfaces with the Ub-E2 conjugate (Fig. 1.2)[69-71]. Initially, SAG was cloned and found to be a redox inducible agent that protected cells from apoptosis[69]. Subsequent studies found SAG to be over expressed in human primary tumor tissues and that silencing SAG inhibited the growth of the

cancerous cells[71]. Together these studies suggest that knockdown / knockout of SAG protein would block CRL function regulating neddylation[72-74].

Recent attempts to find a pharmacological inhibitor of neddylation were met with the discovery of MLN4924, a potent and selective inhibitor of NAE[75]. MLN4924 is an AMP-mimetic and binds the nucleotide-binding site of NAE (Fig. 1.1)[75-77]. The differences between MLN4924 and AMP are 4-fold as MLN4924 has: 1) a deazapurine base substituted with an aminoindane at N6 in place of the adenine base; 2) a carbocycle with a 2'-hydroxyl group absent in place of the ribose sugar; 3) a sulphamate in place of the phosphate; and 4) contrasts the stereochemistry of AMP with a non-natural anti-relationship to the deazapurine (Fig. 1.3)[75]. Although MLN4924 is an AMP-mimetic, it does not inhibit other enzymes that utilize ATP due to its binding site specificity[75].

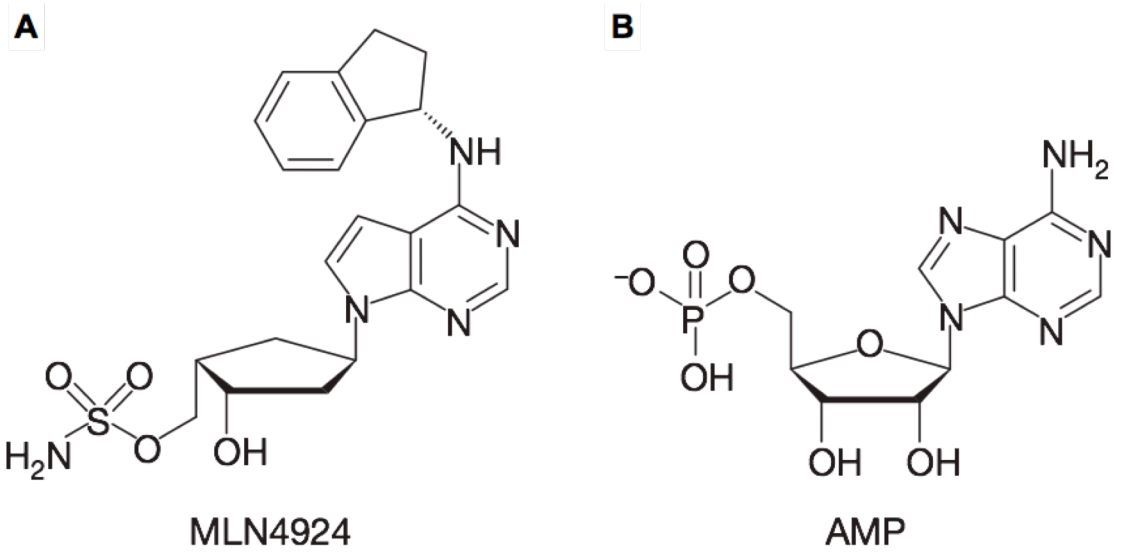

Fig 1.3 – Comparison of MLN4924 to AMP. (**A**) Chemical structure of MLN4924 ((1S,2S,4R)-4-{4-[(1S)-2,3-dihydro-1H-inden-1-ylamino]-7H-pyrrolo[2,3-d]pyrimidin-7-yl}-2-hydroxycyclopentyl)methyl sulphamate. (**B**) The structure of adenosine monophosphate (AMP).

Proteins that are polyubiquitinylated are degraded by cellular proteasomes under homeostatic conditions and studies have shown that inhibition of the proteasome, results in substantially preventing intracellular protein turnover[78]. However, inhibition of NAE with MLN4924 only affects the degradation of proteins whose ubiquitylation is performed using the CRL neddylation scaffolding[68,75]. Indeed, Soucy et. al. found MLN4924 treatment of HCT-116 cells inhibited overall protein turnover by just 9%, compared to ~50% when cells were treated with the proteasome inhibitor, bortezomib.

Subsequent studies have revealed that global inhibition of neddylation – inhibition of all five CRL ligases – with MLN4924 causes radiosensitization of human pancreatic cancer cells[79] and breast cancer cells[80], as well as induces autophagy prior to apoptosis in liver cancer cells[81].

Thus, neddylation regulates the ubiquitylation and subsequent degradation of a specific subset of proteins[68]. Furthermore, the neddylation pathway can be regulated utilizing the small molecule, global inhibitor MLN4924[50,75,79-81] and by knocking-down or knocking-out SAG protein[69-71].

Hematopoietic stem cell transplantation

Allogeneic hematopoietic bone marrow transplantation (allo-BMT) is a curative therapy by conferring a donor graft versus tumor (GVT) effect for many patients who would otherwise succumb to hematological malignant diseases[82]. Allo-BMT recipients undergo a conditioning regimen to prepare for the donor stem cells and post-transplantation

therapy[83]. These steps eradicate any underlying malignancy, ensure that the donor stem cells engraft in the recipient bone marrow, and attempt to minimize the incidence and severity of immune-mediated graft-versus-host disease (GVHD)[83]. Conditioning regimens typically involve a combination of total body irradiation (TBI) and cytoxic chemotherapeutics. Chemotherapeutic use has progressed from using a single-agent methotrexate to modern calcineurin-inhibitor based combinations[83]. Stem cells can either be harvested directly from a donor's bone marrow or – now more commonly – from the donor's peripheral blood by pretreating the patient with granulocyte-colony stimulating factor (G-CSF), which effectively induces egress of stem cells from the bone marrow into the blood stream[84]. Soon after the recipient has undergone myeloablative therapy and allo-BMT, the patient often experiences a period of severe febrile immunodeficiency (leukopenia and lymphopenia) putting the recipient at an increased risk for infection[85]. The recovery of neutrophils is one of the first signs of donor engraftment[86].

Graft versus host disease

Although BMT increases survival of patients with hematological malignancies, 40–50% of recipients experience complications or secondary disease associated with BMT known as GVHD[87]. GVHD is a complex disease that is modified by the extent of the conditioning regimen, degree of human leukocyte antigen (HLA) mismatch, activation of donor cells, and destruction of target tissues[88,89].

Conditioning of the host with myeloablative therapy results in damage to host tissues. Damaged tissues respond by producing proinflammatory cytokines (TNFα, IL-1β, IL-6)

and by increasing the expression of cellular adhesion molecules and chemokines[90-93]. This inflammatory milieu activates host antigen presenting cells (APC) and results in the upregulation of MHC antigens and co-stimulatory molecules[88]. In addition, damage conferred on the gastrointestinal tract sets up the milieu for future stimulation of the immune cells by PAMPs and metabolic by-products produced by the microbiome. We are beginning to understand the impacts of the GI tract microbiome on GVHD. The discussion below will therefore primarily focus on the GI microbiome and its impact on GVHD and not on the microbiota from other mucosal surfaces.

The Microbiome of the GI Tract

The body is colonized by commensals including bacteria, fungi, and viruses. The human GI tract contains trillions of microorganisms, which is estimated to outnumber human cells 10 to 1[94,95]. The gut of a human adult is largely dominated by the phyla Bacteroidetes, Firmicutes, Proteobacteria, and Actinobacteria[96]. While only a small fraction of these microorganisms may be pathogenic, it is now appreciated that the relationship between the host and the commensal microbiome as a whole impacts several aspects of the host biology[97,98]. Microbiota-associated molecular patterns are directly recognized by PRRs. In addition, they secrete a multitude of metabolites that also affect host immunity and biology.

Pathogen Recognition Receptors

Innate immune cells of the host express certain PRRs encoded in the germ-line to detect PAMPs associated with microbes[99] (discussed in depth above). Recognition of PAMPs

through PRRs results in the activation of innate immune cells, such as neutrophils and APCs. In addition to cells of hematopoietic origin, such as the innate and adaptive immune system, PRRs are also expressed on epithelial and endothelial cells.

The Metabolome

The microbiota are known to perform key metabolic functions[100]. The microbiota of the gut can metabolize not only material directly ingested by the host but also produce by-products of its own metabolism. The intestinal metabolome thus consists of products from discrete host metabolism, microbial metabolism, and mammalian-microbial co-metabolism[101]. The critical impact of microbiota-derived metabolites is being increasingly appreciated. Donohoe et al. demonstrates that the microbiota plays a critical effect on the energy homeostasis of colonocytes through the generation of short chain fatty acids (SCFAs). Recent studies show that colonocytes from germ-free mice are in an energy-deprived state demonstrating a decreased ratio of $NADH/NAD^+$, oxidative phosphorylation, and levels of ATP which in turn result in autophagy[102].

In addition to the effects of microbial metabolites on non-immune cells, the impact of the metabolome on immune cells is now increasingly being understood. Recent studies have shown that 17 rationally selected strains of Clostridia, known to produce the SCFA butyrate, directly result in the increased presence of regulatory T cells (Tregs) in the gut. Tregs play a critical role in maintaining gastrointestinal homeostasis by modulating inflammatory responses via the release of the anti-inflammatory molecule IL-10, which also directly impact macrophages[103-106]. Similarly, other groups have utilized a cocktail of altered Schaedler flora which too resulted in the de novo generation of colonic Tregs[107].

With the emerging importance of the effects of microbial metabolites on host biology beginning to be appreciated, recent studies have shown diet to play a role in regulating rapid changes in the taxonomic composition of the gut microbiome[108,109]. These findings suggest that an appropriate diet conducive to homeostatic microbiota may be an important factor when treating comorbidities as the associated metabolome is correspondingly altered[110,111].

Together, these data suggest the microbial metabolome could impact GVHD, although this hypothesis remains to be formally tested.

Antimicrobial Peptides

It has long been established that colonization of commensal microflora provides protection against invading pathogenic bacteria, referred to as colonization resistance[112]. Further, intestinal epithelial cells (IECs) provide a physical barrier against contaminating factors found in the lumen of the gut (Fig. 1.4). IECs are known to produce both antimicrobial peptides (AMPs) which inhibit the growth of and kill microorganisms, and a polysaccharide-rich mucus layer which functions in a manner similar to biofilms[113]. The biofilm-like mucus promotes various functions of the microbiota including metabolism of luminal contents, fortification of host defenses, and resistance to hydrodynamic forces due to peristalsis[113].

Defensins and cathelicidins are AMPs that have been identified in many mammals. Defensins interact with, and potentially destroy, both Gram-negative and Gram-positive bacteria through membrane disruption[114,115]. Several studies have also described the ability of defensins to sequester components of the bacterial cell wall, thus inhibiting its

synthesis[114,116]. These findings emphasize the ability of defensins to mount a multifaceted attack on bacterial targets. Cathelicidin (LL-37) is chiefly produced and stored in granules of neutrophils; however, it is also an inducible product of epithelial cells, T cells, and monocytes[117]. Recent studies have demonstrated the rapid release of defensins not only neutralizes pathogenic bacteria, but they are also sufficient to initiate and amplify an adaptive immune response resulting in both Th1-dependant cellular responses and Th2-dependent humoral responses by activation of immature dendritic cells (DC)[118].

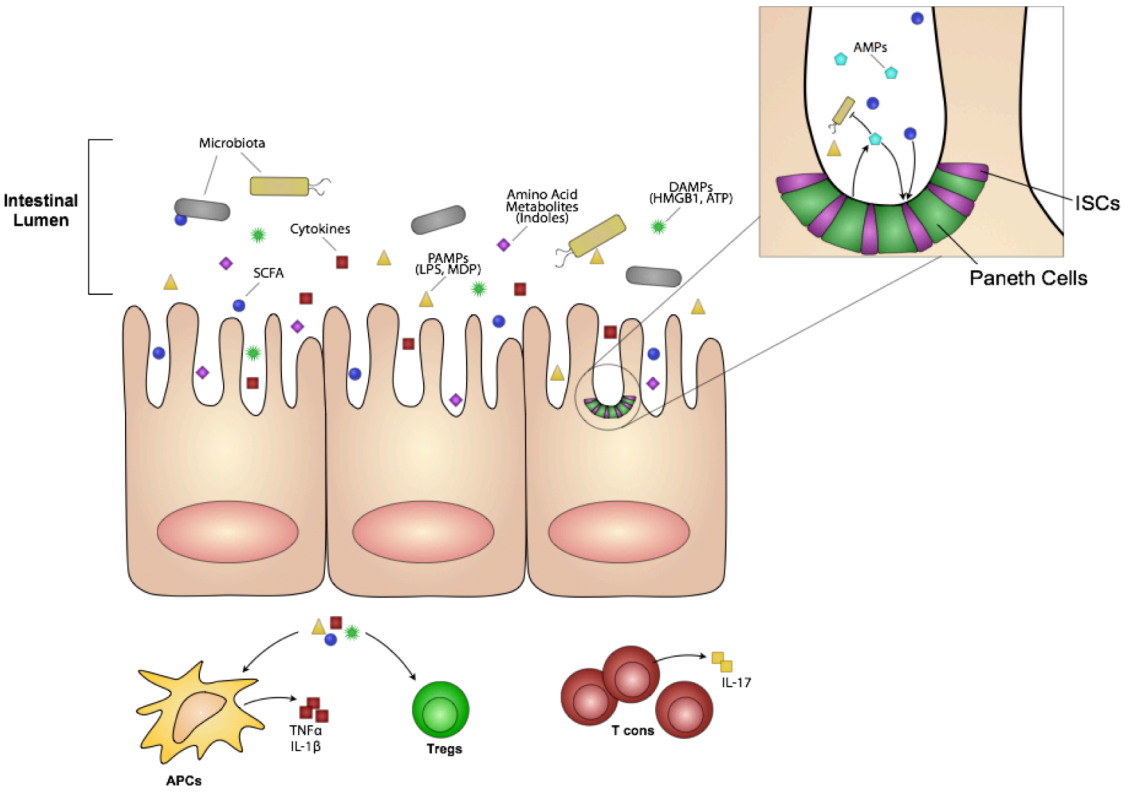

Fig 1.4 – The intestinal barrier and gut homeostasis. The intestinal lumen contains by-products of microbial fermentation – both commensal (SCFAs) and pathogenic (PAMPs). Host intestinal epithelial cells (IECs) provide a physical barrier against contaminating PAMPs and produce cytokines, amino acid metabolites (Indoles), and DAMPs that are found in the lumen. Specialized IECs, known as Paneth cells, produce antimicrobial peptides (AMPs) that selectively inhibit pathogenic bacteria while preserving commensal microbiota and provide critical trophic factors for intestinal stem cells. Damage to IEC homeostasis results in loss of barrier function and activation of immune cells.

Another type of AMP, RegIIIα (RegIIIγ in mice), is a C-type lectin, found primarily in the intestine, and is generated by Paneth cells. RegIII is composed of a combination of α-helical structures and beta sheets[119] that binds to peptidoglycan carbohydrates of Gram-positive bacterial cell walls, in a calcium independent process.

Studies have shown that RegIIIα adopts a hexameric membrane-permeating pore structure to kill bacteria[120,121].

In addition to AMPs, IECs also secrete chemotactic cytokines (chemokines) resulting in the recruitment of innate immune cells and produce proinflammatory enzymes such as inducible nitric oxide synthase (iNOS) and cyclooxygenase-2 (COX-2) which activate neutrophils resulting in their degranulation upon pathogenic stimuli[122].

Thus, in coordination with immune cells, IECs can have a significant influence on both the microbiota and homeostasis of the host tissue.

The Role of the Microbiome in GVHD

Early Experimental Studies

A role for the microbiome in modulating the severity of GVHD was first identified in the early 1960s by the seminal studies of van Bekkum et al. using germ-free recipient mice. The authors made the observation that the severity of GVHD was markedly decreased when compared to conventional BMT controls[123,124]. Subsequent studies by the same and other groups confirmed and expanded these findings[125,126]. Further studies by van Bekkum et al. isolated colonization resistant microflora which inhibited colonization of *Escherichia coli*, *K. pneumoniae*, and *P. aeruginosa* by treating conventionally housed mice with antibiotics (streptomycin, neomycin, and pimaricin)[127]. The colonization

resistant microflora were then transferred to germ-free mice prior to BMT resulting in decreased GVHD severity, thus indicating that select microorganisms may be beneficial in the context of BMT. These studies formed the basis for clinical utilization of antibiotic prophylaxis prior to BMT and the establishment of standard practice gut decontamination prior to BMT in the clinic, at many transplants centers.

Clinical Studies

The early experimental studies described above led to initial clinical trials designed to determine the role of GI bacterial decontamination in BMT patients. In a study performed nearly 30 years ago, patients were divided into 3 groups: administration of oral nonabsorbable antibiotics with isolation and decontamination in laminar airflow isolation (LAF) rooms, prophylactic granulocyte transfusions from a single family member donor, or conventional treatment in single rooms with hand-washing and mask precautions[128]. Following engraftment, significantly fewer infections were observed in patients isolated in LAF rooms and acute GVHD occurred much later than control groups. More importantly, day 100 overall survival was significantly improved in patients in LAF isolation (92 %) compared to groups in conventional treatment (64 %)[128]. Another study in which patients were either treated with meropenem, a broad-spectrum antibiotic, starting on the first day of febrile episode, or prophylactically treated beginning the first day with $<500/mm^3$ granulocytes, demonstrated fewer febrile episodes in patients receiving meropenem prophylaxis. Prophylactic use of meropenem during the period of neutropenia favorably affected the morbidity of the BMT procedure suggesting that reduced febrile episodes were due to decreased bacterial infections[129].

Other studies indicate that increased survival in patients treated in LAF rooms resulted in less transplant-related mortality (TRM) independent of prophylactic antibiotic use[130], whereas other studies indicated that there is no benefit to isolation in LAF room following BMT[131]. Several groups have performed additional studies utilizing antibiotic prophylaxis prior to BMT or during granulocytopenic period following BMT with conflicting results. One such study housed all patients in LAF rooms with one group receiving prophylactic systemic antibiotics (PSA). However, overall survival at day 100 of groups in LAF rooms with PSA was 72.2 % where groups in LAF rooms only was 70.6 % suggesting no improvement in survival, even though LAF + PSA groups had significantly lower incidence of infections[132]. However, many of these studies have sought to answer disparate questions and lacked sufficient power to determine the validity of prophylactic antibacterial use on GVHD severity in the patients.

The Impact of the Microbiome of the Host on GVHD: Recent Observations

Despite early observations as noted above, the role that the host microbiome plays in the severity of GVHD was largely unexplored until recent years. Recent studies have made significant strides in illuminating alterations in the intestinal microbiota following allogeneic BMT in mice and humans[133,134]. Jenq et al. described observations utilizing clinical models of BMT (B10.BR → B6) where recipients were subjected to lethal irradiation and received donor BM with or without isolated T cells. A loss of overall diversity was seen consisting of an expansion of Lactobacillales with a simultaneous loss of Clostridiales in allo-recipients of BM with isolated T cells. Elegant experiments where the predominant pre-BMT species of Lactobacillus (L. johnsonii) was reintroduced

following gut decontamination and allo-BMT, resulted in improved overall survival compared to recipients of allo-BMT receiving only gut decontamination[133]. Likewise, unpublished observations from our laboratory suggest that intragastric introduction of a cocktail of 17 rationally selected strains of predominantly Clostridiales[103] with salutary effects on the GI epithelium, results in decreased GVHD and improved overall survival[59]. Another recent study illuminated the impact of the loss of diversity in the gut further, following allo-BMT. The study observed that Paneth cells are targets of GVHD[134]. Paneth cells, located next to intestinal stem cells (ISC) within the crypts of the intestinal lumen (Fig. 1.4), are essential regulators of the composition of the intestinal microbiota[135,136]. Further, Paneth cells are known to secrete antimicrobial peptides and α-defensins which largely function by forming pores in bacterial cell walls[137,138]. Eriguchi et al. revealed that the loss of Paneth cells from GVHD resulted in decreased expression of α-defensins. The authors further suggest that α-defensins selectively kill non-commensal bacteria while preserving commensal microbiota[134]. The study suggests that the decrease in the expression of α-defensins resulted in the loss of microbial diversity (as also observed in Jenq et al.) and an overwhelming expansion of E. coli, leading to septicemia.

A recent study demonstrated the importance of bacterial diversity in the intestinal tract on mortality outcomes following BMT. The authors collected fecal specimens from patients that received allo-BMT, at the time of stem cell engraftment[139]. Microbial diversity was then determined by performing bacterial 16S rRNA gene sequencing. Patients with lower bacterial diversity exhibited significantly worse mortality. Overall survival at 3 years was 36 % for low, 60 % for intermediate, and 67 % for high diversity groups[139]. These results

suggest that diversity of the intestinal microbiota at time of engraftment may be a predictor of mortality in recipients of allo-BMT and thus highlight the consequences of dysbiosis of the intestinal flora.

The Impact of the Microbiome of the Donor

The microbiome is known to play a key role in the development and maturation of T cells[103,140,141]. The influence of the donor microbiota on the donor allograft and its impact on GVHD was recently examined[142]. Using clinically relevant murine models of BMT, the authors observed the severity of GVHD induced by T cells harvested from germ-free (GF) donors and specific pathogen-free (SPF) donors. Interestingly, there was no difference in the frequency of Treg cells in the periphery of the host or levels of lineage-specific cytokines in the sera such as IFNγ, IL-5, IL-17, or the anti-inflammatory cytokine IL-10. Further, clinical observation revealed that GVHD progression and severity was similar between recipients of the GF and SPF donor T cells with no difference in histopathological scores of the small intestine and liver. In addition, no survival benefit was observed in the recipients of donor T cells from GF or SPF donor T cells. Furthermore, when SPF donor mice were treated with broad-spectrum antibiotics prior to T cell isolation, no difference in survival was determined.

These data indicate that absence of the effects of the microbiome on T cells may be lost once they have been removed from the germ-free environment.

PAMPs and GVHD

There is mounting evidence that microorganisms and PRRs of the innate immune system

play a critical role in the pathogenesis of acute GVHD[124,133,143]. Products of Gram-negative bacteria, such as LPS, were suggested to be contributors to the severity and progression of GVHD in certain experimental models[144-146]. Cooke et al. utilized a potent antagonist of LPS and observed significantly reduced production of TNFα and intestinal damage. While donor T cell responses were unaltered, overall GVHD severity was reduced[145]. However, a recent study utilized a different model system with myeloid differentiation primary response gene (88) (MYD88) and TIR-domain-containing adapter-inducing interferon-β (TRIF) double knockout cells, thus the donor allograft was deficient in all TLR signaling[147]. The authors demonstrated that loss of TLR signaling did not protect from GVHD nor improve overall survival, suggesting that TLR signaling is dispensable for GVHD severity.

Human genetic association studies wherein patients possessing TLR4 polymorphisms, who also received grafts from HLA-matched donor siblings, demonstrated an increased risk for Gram-negative bacteremia and GVHD severity[148].

In another study, TLR9 deficient recipients of allo-BMT have demonstrated decreased systemic GVHD[149]. The authors observed that APCs isolated from $TLR9^{-/-}$ mice had a decreased ability to stimulate allogeneic T cells. Further, utilizing cytosine-phosphorothioate guanine oligodeoxynucleotides (CpG ODNs), which mimics bacterial and viral DNA and stimulates TLR9, Blazar et al. found that CpG treatment enhanced allo-T cell responses leading to increased GVHD severity and mortality[150]. These TLR9 dependent studies emphasize the importance of TLR signaling for host APC function during GVHD[151]. The analysis of TLR9 gene associated polymorphisms on the clinical outcome of 413 donors showed no association of the TLR9 polymorphisms with

incidence or severity of GVHD[148,151]. However, patients with the T1486C mutation exhibited significantly improved survival due to reduced TRM and relapse rate.

The importance of TLRs in neutrophils on the severity of GVHD has recently been demonstrated. Neutrophils are the largest human white blood cell population and have important roles in cleaving chemokines and the production of reactive oxygen species (ROS). During allogeneic immune responses, neutrophils amplify tissue damage caused by conditioning regimens[152]. Schwab et al. utilized clinical models of BMT where donor neutrophils were TLR2, TLR3, TLR4, TLR7, and TLR9 deficient. GVHD severity was significantly reduced suggesting that TLR signaling is important for neutrophil-mediated inflammation in the context of allo-BMT.

The role of NLRs in GVHD has been examined in several recent studies. NOD2 deficiency in recipients of experimental BMT resulted in increased GVHD of both MHC-mismatched and MHC-matched models[153,154] corresponding with enhanced activation and proliferation of donor T cells, due to increased activation status of DCs.

The presence of certain cytokines, such as IL-1β, was suggested to predict the outcome and severity of GVHD[91]. IL-1β is one such proinflammatory cytokine that is released following NLR stimulation. A study examining the genotypes of 133 patients undergoing BMT from (HLA)-matched donor siblings demonstrated a strong correlation between genetic variants of NLRP2 and NLRP3 genes and the clinical outcome and severity of GVHD[155].

Immune-mediated tissue destruction, which is often found in acute GVHD, is a result of cellular damage or response to DAMPs. Although critical for the function of the cell, extracellular ATP released from a damaged cell is subsequently internalized and serves as

a strong activating signal of NLRP3[156]. In response to accumulated ATP and NLRP3 stimulation, APCs increased expression of co-stimulatory molecules which resulted in enhanced proinflammatory signals and expansion of donor T cells with a reduction of Treg cells and increased GVHD severity[157].

Siglec-G recognition of non-infectious DAMPs regulates innate immune responses[158]. A recent study examined the role of Siglec-G expression on host APCs, specifically on hematopoietic cells, and its ability to negatively regulate GVHD in multiple clinically relevant murine models[159]. The authors demonstrate that recipients deficient in Siglec-G exhibit significantly increased GVHD severity and mortality, in a CD24 dependent manner. Upon administration of CD24 fusion protein to WT recipients of allo-BMT, improved overall survival is observed. However, administration of CD24 fusion protein to recipients deficient in Siglec-G did not improve survival, suggesting that Siglec signaling is required for the effects of CD24[159].

These data suggest that the Siglec-G–CD24 axis controls the severity of GVHD and that enhancing this interaction may represent a method of mitigating clinical GVHD.

The Metabolome and GVHD

Many recent studies have made strides to identify the taxonomic composition and activity of the host microbiome[103,111,133]. However, few publications examine the role of microbial metabolites (e.g., SCFAs) in the homeostasis of host physiology. While it is increasingly evident that alterations in the microbiome correlate with many disease states[160-162], the mechanism through which these alterations confer their effects is poorly understood.

The most studied microbial metabolites are SCFAs, of which butyrate, acetate, and propionate are the most abundant. As described earlier in this review, SCFAs are produced by microbial fermentation of complex polysaccharides in the gut and are subsequently absorbed by the intestinal epithelium[100]. Butyrate is utilized as a major energy source for IECs and is a known histone deacetylase inhibitor (iHDAC)[163]. Thus, microbial metabolites may play an important role in maintaining the health of the physical barrier of the gut epithelium as well as protecting the host from the influences of PAMPs and DAMPs.

SCFAs may have a particularly important role in the protection of the host from GVHD. Unpublished observations from our lab demonstrate that there is a significantly decreased concentration of butyrate found in the tissue of the GI tract following allo-BMT. In addition, this coincides with a substantial and significant decrease in the acetylation state of histones in IECs of allo-BMT recipients. When butyrate was supplemented via intragastric gavage, it increased histone acetylation in IECs and significantly improved junction integrity mitigating GVHD severity[59].

AMPs and GVHD

AMPs, produced by Paneth cells, have been shown to be a critical "first line of defense" of the innate immune system among epithelial barriers[164,165]. As discussed above, a recent study observed a loss of α-defensins in the gut due to a GVHD-mediated decrease of Paneth cells[134]. Furthermore, non-commensal bacteria were selectively targeted and killed by α-defensins, while commensal microbiota were preserved. Equally, several studies have observed that the composition of the intestinal microbiome is directly

influenced by alterations in the expression of AMPs[166,167].

Another recent study by Ferrara et al. identified the AMP RegIIIα as a biomarker found in the plasma indicative of acute GVHD in the lower GI tract. The authors found RegIIIα to be 3-fold higher at GI GVHD onset in a large cohort of patients, compared to control cohorts[168].

The effects of the microbiome on GVHD, and that of GVHD on the microbiome, are now being increasingly appreciated. The differential role that the microbiota plays in the host[133,134] and the donor[142] and the effects of polymorphisms of PRRs on GVHD severity highlight the complex interactions between the microbiome and GVHD that remain to be meticulously examined. Further studies examining the functions and mechanisms are needed to identify new targets for treating GVHD and other diseases affected by dysbiosis of the microbiota.

Statement of purpose

Activation of donor T cells by APCs is critical for the GVT effect following allogeneic BMT. However, inappropriate activation of lymphocytes by nonhematopoietic cells results in GVHD (Fig. 1.5).

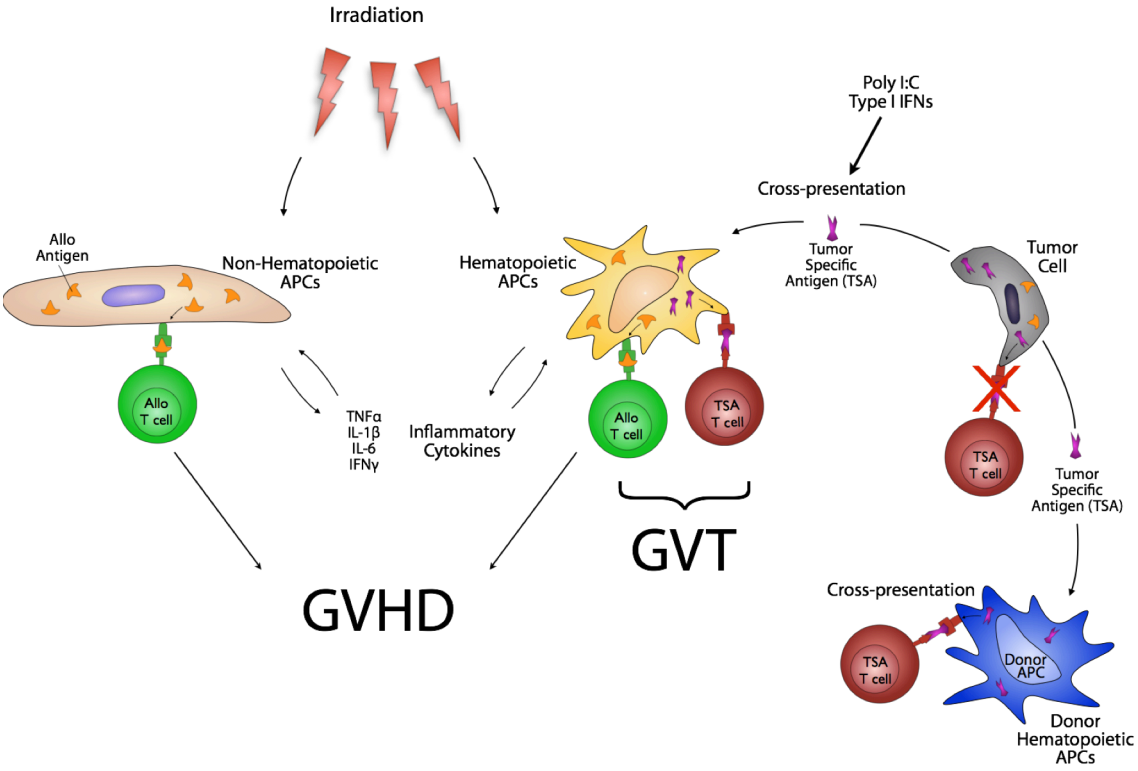

Fig 1.5 – Antigen presenting cells in GVT: to maximize GVT responses, two important factors must be considered: antigen presentation and donor T cells. Although both host and donor DCs have been shown to play an important role in GVHD, their role in GVT is only beginning to be understood. To induce GVT, although donor T cells must recognize both alloantigens and tumor specific antigens (TSAs) that presented either directly by the tumor or indirectly by the professional APCs, tumor themselves are generally poor presenters and activators of T cell effector responses. Therefore, professional APCs are required for optimizing GVT. While alloantigen responses are also elicited by many APCs including both hematopoietic-derived and non-hematopoietic-derived APCs cause GVHD, TSAs are exclusively directed to tumors and thus considered to GVHD without concomitantly causing GVHD. In cases where tumors are poor APCs of TSAs to donor T cells, the TSAs have to be efficiently presented by professional APCs, especially DCs, derived from either donor or host. This mechanism of presentation includes cross-presentation.

Current methods of GVHD prophylaxis are often indiscriminate and kill both disease causing and non-disease causing cells. Recent advances have shown that the microbiota as well as PTMs, such as acetylation, play a role in regulating GVHD pathogenesis. However, the effects that the metabolites that are produced exclusively by the commensal

bacteria within the gastrointestinal tract – such as butyrate, an endogenous HDACi – have on GVHD are unknown. Furthermore, the role that neddylation (a type of PTM) plays in the immune system, and thus immune-mediated diseases such as GVHD, have heretofore been unknown.

Therefore, the goal of my research is to further understand the role of PTMs in immunity and their impacts on GVHD pathogenesis. In Chapter II, the PTM neddylation is shown to regulate both mouse and human DC function. Mechanistic studies in murine DCs showed that inhibiting neddylation prevented the degradation of IκB and thus impeded the translocation of NF-κB to nucleus. This resulted in not only decreased inflammatory cytokines, but also decreased GVHD and mortality in mice treated with neddylation inhibitor, MLN4924. In Chapter III, inhibiting neddylation is shown to have a disparate function in regulating macrophages compared with activation of neutrophils. Indeed, generation of a novel mouse possessing a conditional macrophage knockout of SAG protein exhibited increased LPS-induced mortality even though the neddylation-deficient macrophages released less cytokines. Disruption of neddylation in neutrophils was demonstrated to increase ROS and also resulted in the increased release of TNFα and IL-6. In Chapter IV, the generation of a different novel mouse that had a T cell-specific deletion of SAG revealed that T cell functions may be regulated by the inhibition of neddylation, including ameliorating the effects of GVHD. Furthermore, utilization of a small molecule inhibitor of neddylation, MLN4924 (currently in phase I/II clinical trials) recapitulated the results seen in the knockout mouse, suggesting that carefully designed clinical trials may find therapeutic efficacy for MLN4924 and thus may be a new agent for regulating GVHD in the clinic. Chapter V describes the findings that the SCFA

butyrate (an endogenous HDACi) – produced exclusively by the commensal microbiota – is diminished in the intestinal tissue following allo-BMT. This lack of butyrate resulted in decreased histone-H4 acetylation in IECs and increased IEC allo-mediated damage, the effects of which are reversed by the local intragastric gavage of butyrate. Indeed, restoration of histone-H4 acetylation improved junctional integrity and resulted in less severe GVHD and improved survival.

CHAPTER II

NEDDYLATION PLAYS AN IMPORTANT ROLE IN THE REGULATION OF MURINE AND HUMAN DENDRITIC CELL FUNCTION

ABSTRACT

Posttranslational protein modifications (PTMs) are necessary for cells to function properly. The role of PTMs in regulating immune responses, specifically those mediated by dendritic cells (DCs), which are critical for both innate and adaptive immunity, is not well understood. Utilizing multiple but complementary approaches, we determined the role of an important but less understood type of PTM, namely, neddylation, in regulating DC functions. Inhibition of neddylation suppressed the release of proinflammatory cytokines by DCs in response to Toll-like receptor, nucleotide oligomerization domain–like receptor, and noninfectious CD40L stimulation. These effects were more profound than those mediated by the proteasome inhibitor bortezomib or a commonly used antiinflammatory agent, dexamethasone. Targeting neddylation also suppressed the ability of DCs to stimulate murine allogeneic T cells in vitro and in vivo and human allogeneic T-cell responses in vitro. Mechanistic studies demonstrated that inhibition of neddylation reduced both canonical and noncanonical nuclear factor-κB (NF-κB) activity. Neddylation inhibition prevented the degradation of inhibitor-κB and thus reduced the translocation and activation of NF-κB, but without perturbation of the mitogen-activated protein kinase/extracellular signal-regulated kinase pathway. Thus, blocking neddylation could be a novel strategy for mitigating immune-mediated disease processes.

INTRODUCTION

Post-translational protein modifications (PTM) are critical for immunity[46]. PTMs include, but are not limited to, acetylation[48], phosphorylation, and ubiquitination.[49] These PTMs are necessary for the proper function of all cells, including dendritic cells (DCs). DCs are critical for both innate and adaptive immunity[169,170]. Following an encounter with inflammatory stimuli or components of microbial or viral origin, DCs upregulate costimulatory molecules[171] and release proinflammatory cytokines[172]. Proinflammatory cytokines released by DCs play an important role in immunity through an autocrine and paracrine fashion on surrounding cells; the molecular processes regulating cytokine release from DCs are, however, not completely understood. Proinflammatory cytokines have profound impact on causing or exacerbating many diseases states including chronic inflammatory diseases, shock, autoimmunity, and alloimmunity[92,173-175].

Pattern recognition receptors (PRRs) such as Toll-like receptor (TLR) and NOD-like receptor (NLR) on DCs interact with pathogen-associated molecular patterns (PAMPS) allowing selective recognition of microorganisms[13,176]. A series of signaling events leads to the phosphorylation of IKKβ, which in turn phosphorylates inhibitor-κB (IκB) for degradation resulting in the activation of the transcription factor NF-κB[177]. At basal conditions, IκB sequesters canonical NF-κB in the cytosol. However, the critical molecular regulators of the degradation of phosphorylated IκB are not well understood. Activation and translocation of NF-κB results in the transcription of the proinflammatory cytokines TNFα and IL-6[178]. Activation of NF-κB occurs through two distinct, canonical and non-canonical NF-κB pathways[178]. NF-κB is comprised of heterodimers of the Rel protein family. The canonical NF-κB is a union of p65 (RelA) and p50 and responds to

numerous PRR stimuli resulting in diverse functions. In contrast, the noncanonical pathway consists of RelB and p52 constituting NF-κB and responds to a subset of TNFR signals such as CD40L[179].

Upon PRR stimulation, IκB is phosphorylated and subsequently ubiquitinated resulting in its degradation allowing NF-κB to translocate to the nucleus[180]. Phosphorylation of IκB is followed by its ubiquitination and degradation by the E3 ligase complex. This complex consists of the proteins Skp1 (S-phase kinase associated protein 1), an F-box protein, Cullin1 (Cul1) and a RING box protein (RBX1 or RBX2, also known as SAG), which together comprise the Cullin RING Ligase 1 (CRL-1)[68,80]. The ability of CRL-1 to ubiquitinate target proteins, including IκB, is dependent upon the covalent PTM of the Cullin1 subunit of the CRL by the attachment of a ubiquitin homolog called *Nedd8* (Neural precursor cell Expressed, Developmentally-Downregulated 8)[181]. Post-translational protein modification by the attachment of Nedd8 is known as neddylation[79,182]. Neddylation is an enzymatic process in which Nedd8 is activated in an ATP dependent manner by an E1 enzyme known as Nedd8 activating enzyme (NAE) and is subsequently transferred to the E2 enzyme, Ubc12[183]. Nedd8-Ubc12 transfers Nedd8 to Cullin displacing CAND1, an inhibitor of Cullin activity[183,184]. Once activated, CRL-1 catalyzes the transfer of ubiquitin from the E2 to the substrate[183]. A small molecule called MLN4924 has been recently developed with remarkable specificity and potency for inhibiting NAE. MLN4924 forms a Nedd8-AMP mimetic and thereby prevents the initial activation of Nedd8[75]. This small molecule is in human clinical trials as an anti-cancer

agent, but the role of neddylation in regulating immune cells, specifically DCs, is not known.

Utilizing two distinct but complementary approaches (chemical inhibition with the small molecule MLN4924 and molecular knockdown of critical CRL proteins), we have examined the effect of inactivation of CRL-1 E3 ligase activity on murine and human DC function as determined by the release of proinflammatory cytokines and their ability to stimulate allogeneic T cells both in vitro and in vivo. We also compared these results to the known anti-inflammatory drug, dexamethasone and further determined the differential molecular mechanisms that underpin their anti-inflammatory responses. We found that inactivation of the CRL-1 E3 ligase resulted in significantly greater suppression of proinflammatory cytokine production than dexamethasone or the proteasome inhibitor bortezomib and mechanistic studies showed that in contrast to dexamethasone, inhibition of neddylation prevented the degradation of IκB as well as the translocation and activation of NF-κB without perturbation of the MAPK/ERK pathway.

RESULTS

Inhibition of neddylation attenuates LPS induced proinflammatory cytokine production by DCs

Previous studies have shown that MLN4924 prevents the neddylation of CRLs in several cell types[81,185]. Therefore, we first determined if MLN4924 and/or dexamethasone could inhibit neddylation in bone marrow-derived dendritic cells (BMDC). BMDCs pretreated with MLN4924 followed by TLR4 stimulation (LPS) exhibited reduced neddylation (Fig. 2.1).

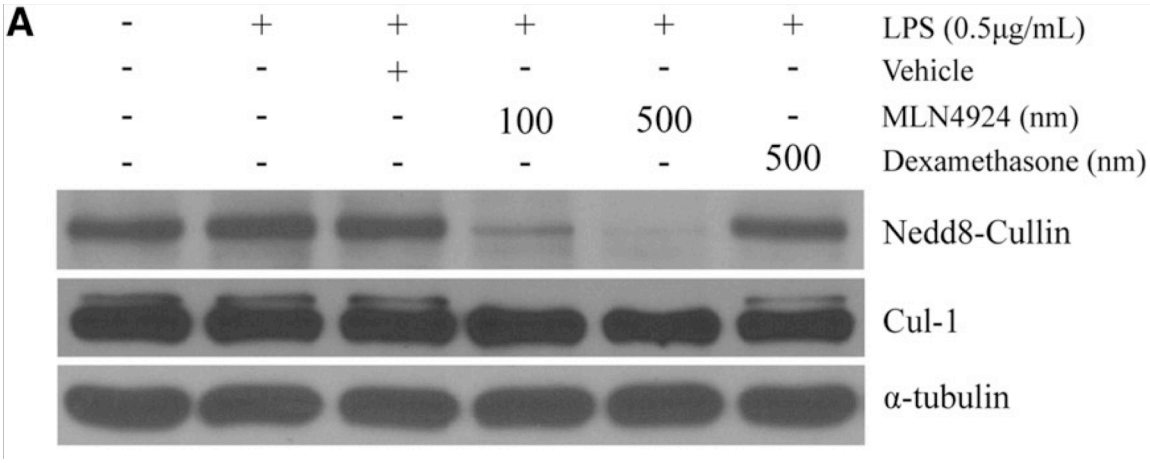

Fig 2.1 – Neddylation inhibition. Protein analysis by western blot of (A, top panel) neddylated Cullin proteins and (A, middle panel) Cul1 protein using whole cell lysate of BMDC stimulated with LPS in the presence or absence of MLN4924 or dexamethasone at the indicated doses. Cells receiving treatment were preincubated with MLN4924 or dexamethasone for 2 hours followed by concurrent LPS stimulation (0.5 μg/mL) for 4 hours. α-tubulin protein levels were analyzed as an equal loading control.

This inhibition of neddylation was detected using a Nedd8 antibody capable of binding Nedd8-conjugated Cullin protein at approximately 90 kDa (Fig. 2.1, top panel)[185,186]. We further confirmed it with an antibody specific for total Cullin-1[80] (Fig. 2.1, middle panel). By contrast, treatment with dexamethasone did not inhibit neddylation in BMDCs (Fig. 2.1).

Having established that MLN4924 inhibited neddylation, we next determined whether it modulated the production of proinflammatory cytokines such as TNFα and IL-6 following stimulation of BMDCs with LPS[187]. TNFα (Figure 2.2A) and IL-6 (Figure 2.2B) cytokine levels in the supernatants were significantly inhibited by MLN4924 in a dose dependent manner. Furthermore, MLN4924 suppressed LPS-induced inflammatory cytokines significantly more than dexamethasone treatment (Fig. 2.2).

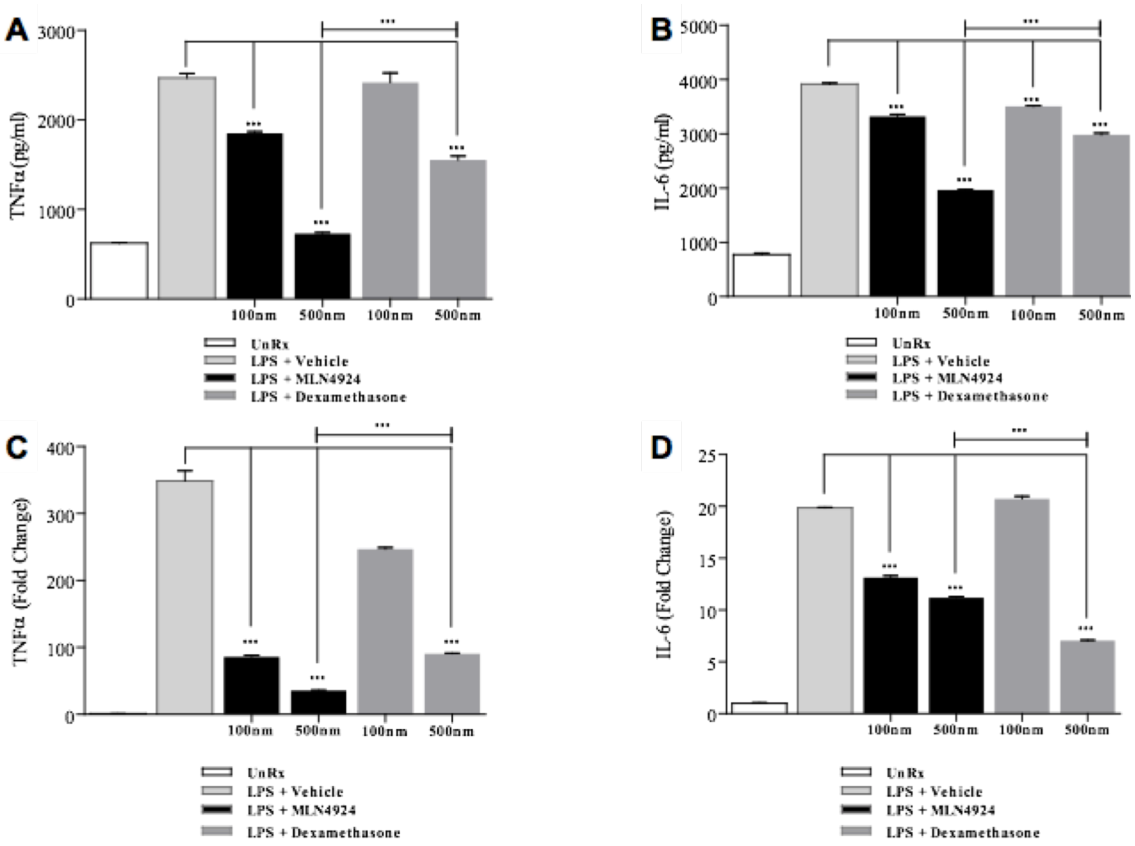

Fig. 2.2 - Neddylation inhibition attenuates LPS-induced TNF-α and IL-6 release and gene expression in BMDC. Quantification via ELISA of cytokines TNF-α (A) and IL-6 (B) and qPCR analysis of TNF-α (C) and IL-6 (D) transcripts in BMDC stimulated with LPS in the presence or absence of MLN4924 or dexamethasone at the indicated doses. Cells receiving treatment were preincubated with MLN4924 or dexamethasone for 2 hours followed by concurrent LPS stimulation (0.5 μg/mL) for 4 hours. One representative experiment of 3 is shown. ***$P < .0001$.

Because LPS increases the expression of TNFα and IL-6 at the transcriptional level[188-190] we next assessed the impact of MLN4924 and dexamethasone on LPS-induced transcriptional expression of TNFα and IL-6 mRNA. As shown in Figures 1D and 1E, both MLN4924 and dexamethasone inhibited LPS-induced TNFα and IL-6 mRNA levels. The impact of MLN4924 on mitigating LPS-induced increases of TNFα and IL-6 mRNA was dose-dependent (Figure 2.2C-D).

These data collectively suggest that MLN4924 and dexamethasone differentially affect cullin1 neddylation in DCs and that they may not have interrelated molecular targets. More importantly, the data show that inhibition of neddylation results in a more significant attenuation of LPS induced TNFα and IL-6 production than dexamethasone in BMDC.

Neddylation modulates DC responses to both infectious and non-infectious stimuli

Next, to determine whether the effects of MLN4924 observed thus far were specific only to TLR4 ligation (LPS), we stimulated BMDC with Pam3CSK4 (a TLR1/2 ligand), peptidoglycan (PGN, a NOD2 stimulator) and non-infectious CD40L agonist. Treatment of DCs in the presence or absence of MLN4924 or dexamethasone, caused a significant reduction in the secretion of TNFα by both MLN4924 and dexamethasone, regardless of whether they were stimulated with Pam3CSK4 (Figure 2.3A), PGN (Figure 2.3B) or CD40L (Figure 2.3C).

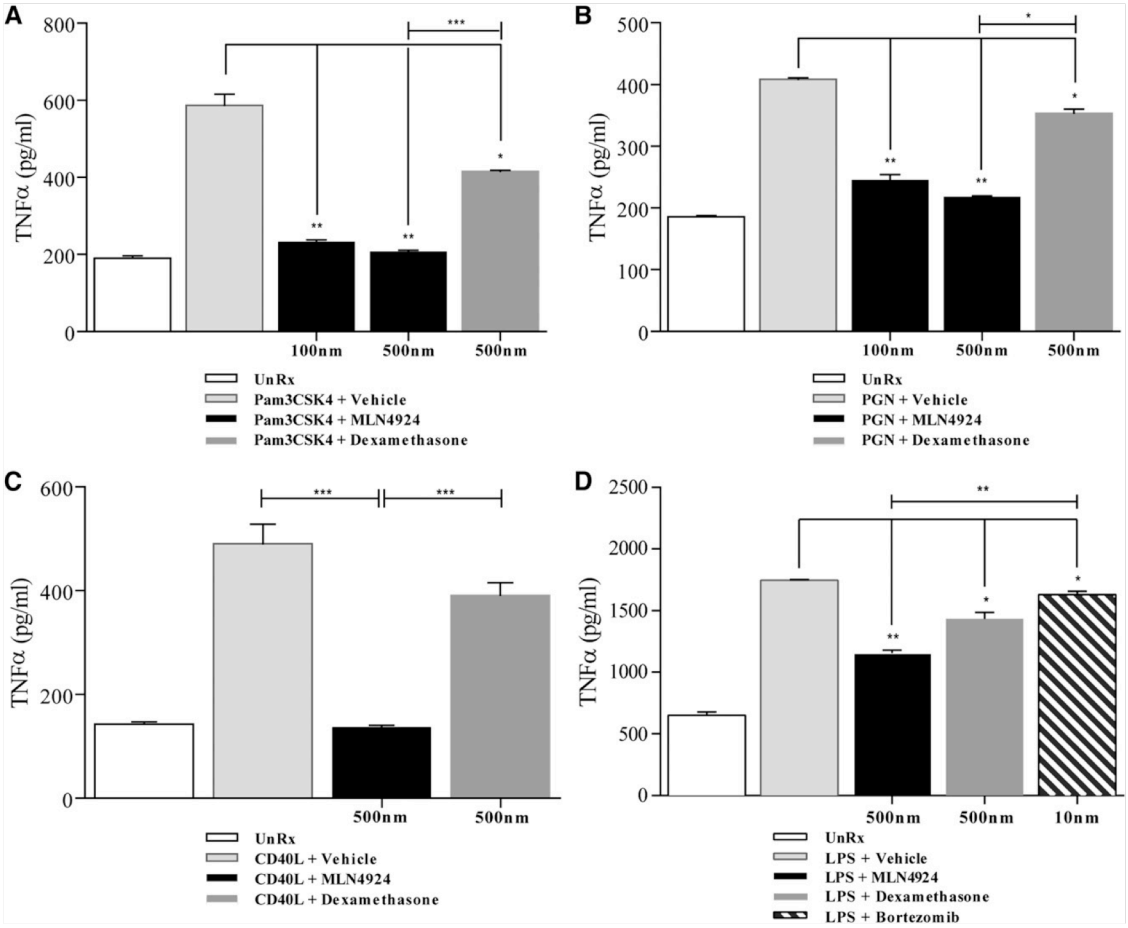

Fig. 2.3 - Neddylation inhibition in BMDC mitigates release of non-TLR4–stimulated cytokines in vitro. ELISA quantification of TNF-α release in Pam3CSK4 (300 ng/mL) stimulated (A), PGN (5 μg/mL) stimulated (B), and CD40L (1 μg/mL) stimulated (C) BMDC in the presence or absence of vehicle, MLN4924, or dexamethasone at the indicated doses. (D) Comparison of TNF-α release via ELISA of cells treated with vehicle, MLN4924, dexamethasone, or bortezomib followed by concurrent stimulation with LPS (0.5 μg/mL). Cells receiving treatment were preincubated with vehicle, MLN4924, dexamethasone, or bortezomib for 2 hours followed by concurrent stimulation for 4 hours. One representative experiment of 3 is shown in cells treated in triplicate. **P* < .05; ***P* < .01; ****P* < .0001.

These data suggest that the effects on suppression of proinflammatory cytokines through inactivation of the CRL-1 E3 ligase are not specific to only TLR4, but extend to an array of PRR and cellular stimuli such as CD40L. Furthermore, these data also show that inhibition of neddylation regulated both canonical (TLR/NLR) and non-canonical (CD40L) activated NF-**κ**B pathways. To further compare the effects of neddylation

inhibition to another clinically used inhibitor of the proteasome and NF-κB pathway, we next stimulated BMDC with LPS and concurrently treated with either the diluent vehicle, MLN4924, dexamethasone, or bortezomib. As shown in Figure 2.3D, blocking neddylation inhibited TNFα secretion from the DCs far more potently than the proteasome inhibitor bortezomib (Figure 2.3D).

Inhibition of neddylation mitigates the ability of DCs to induce proliferation of allogeneic T cells

To further characterize the effect of inhibition of neddylation on the functions of DCs, we determined the impact of treatment of DCs with MLN4924 on their ability to stimulate allogeneic T cells[169,170] in a mixed lymphocyte reaction (MLR). BALB/C T cells were cultured with C57BL/6 irradiated (30Gy) BMDC at 40:1 and 100:1 ratios for 72 (Figure 2.4A) and 96 (Figure 2.4B) hours. Addition of MLN4924 to the cultures upon plating cells significantly reduced the proliferation of T cells (Figure 2.4A-B). To determine whether this reduction is due to a direct impact of MLN4924 on DCs, BMDCs were preincubated with MLN4924 for 6 hours, washed and then used as stimulators in the MLR. Pretreatment of DCs with MLN4924 also reduced proliferation of allo-T cells at both 72 (Figure 2.4A) and 96 (Figure 2.4B) hours suggesting that MLN4924 treatment of DCs reduced their ability to induce proliferation of allo-T cells.

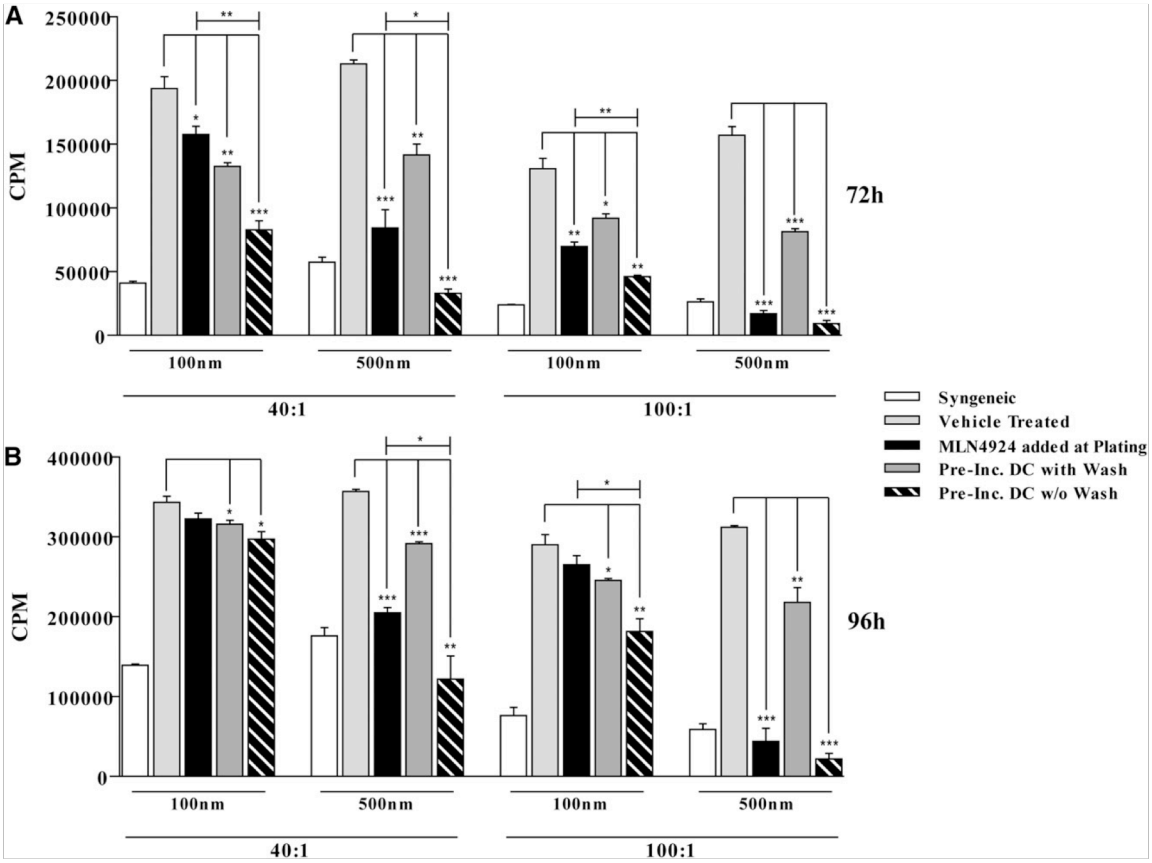

Fig. 2.4 - Neddylation inhibition mitigates allogeneic T-cell proliferation. BALB/C T cells were cultured with C57BL/6 irradiated (30 Gy) BMDC at 40:1 and 100:1 ratios in the presence or absence of MLN4924 for 72 hours (A) and 96 hours (B). Where indicated, BMDC were preincubated in the presence or absence of vehicle or MLN4924 at specified dosage for 6 hours. One representative experiment of 3 is shown of groups treated in triplicate. *P < .05; **P < .01; ***P < .0001.

To specifically determine whether inhibition of neddylation can also suppress T cells directly, we next stimulated BALB/C CD90.2^{+} T cells with α-CD3 and α-CD28 functional Abs for 48 hours following their pre-treatment in the presence or absence of MLN4924. MLN4924 significantly reduced the proliferation of T cells (Figure 2.5A) and caused a significant decrease in the secretion of IFNγ (Figure 2.5B).

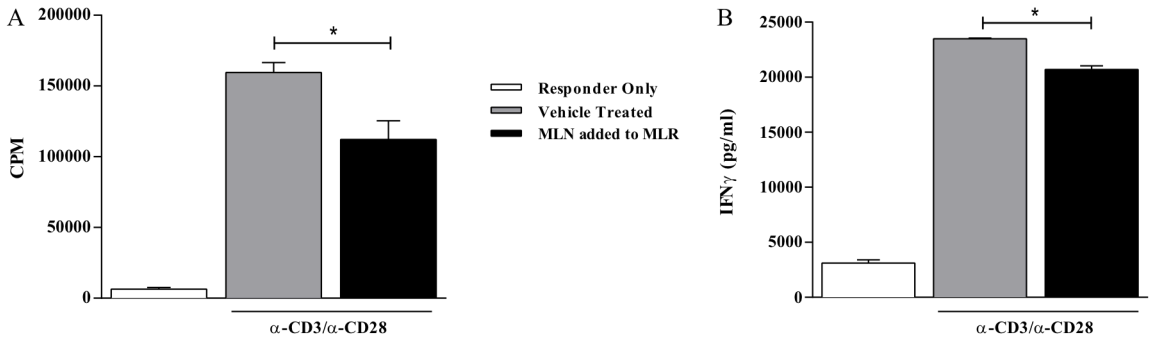

Fig. 2.5 - T cell proliferation and Th1 lineage cytokines are decreased following stimulation with α-CD3 and α-CD28 functional Ab. Balb/c T cells were stimulated with α-CD3 and α-CD28 functional Abs in the presence or absence of MLN4924. After 42h incubation, 3H (1μCi/well) was added for and additional 6 hours followed by (A) determination of proliferating T cells. Supernatants were removed prior to 3H stimulation and analyzed for (B) IFNγ via ELISA.

Inhibition of neddylation regulates DC functions in vivo

We next investigated the effects of neddylation inhibition on in vivo DC functions. Because host antigen presenting cells modulate GVHD, and DCs are the most potent APCs, we utilized a clinically relevant, MHC mismatched B6 (H-2^b) → BALB/C (H-2^d) model of allogeneic BMT to test the effect of inhibition of neddylation on induction and severity of GVHD. Recipient BALB/C animals were lethally irradiated with 8Gy on day -1 and transplanted with 0.5×10^6 CD90.2^+ T cells and 5×10^6 BM cells from either syngeneic BALB/C or allogeneic MHC-mismatched C57BL/6 donors on day 0. The recipients also received either MLN4924 (20mg/kg) or vehicle from day -1 to +3 because host DCs typically cannot be recovered beyond this time following allo-BMT. All of the syngeneic recipients survived with no signs of GVHD demonstrating absence of non-specific toxicity by MLN4924 (Figure 2.6). The allogeneic recipients receiving only vehicle showed signs of severe GVHD and greater mortality than syngeneic animals (Figure 2.6A). By contrast, allogeneic recipients receiving MLN4924 exhibited

significantly improved survival compared to vehicle control (Figure 2.6A) suggesting that in vivo blockade of neddylation mitigated GVHD.

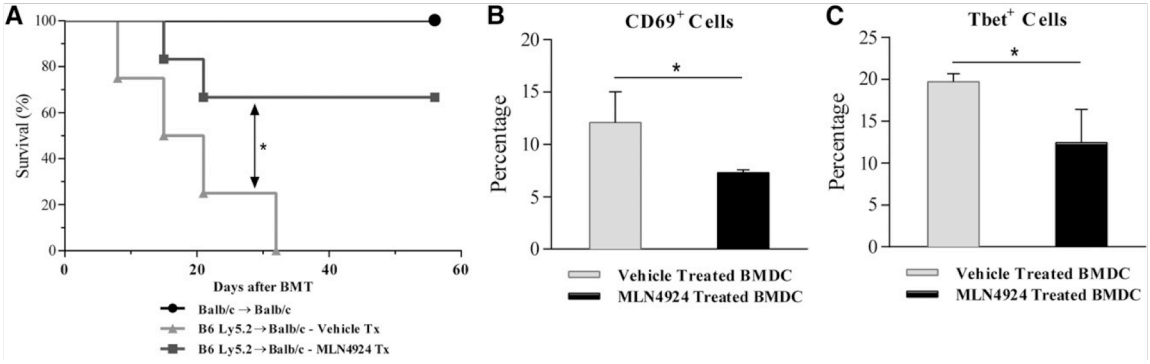

Fig. 2.6 - Neddylation blockade regulates DC-mediated T-cell activation. (A) Survival of BALB/C animals lethally irradiated and transplanted with BM and CD90.21 T cells from either syngeneic BALB/C or allogeneic C57BL/6 donors. Following lethal irradiation (8 Gy) on day 1, MLN4924 (20 mg/kg) was administered in 5 daily doses, day 1 to day 3 relative to BMT. Data are combined from 2 independent experiments (n 5 10 to 12 animals in the allogeneic groups). (B-C) Abb animals were lethally irradiated (10 Gy) on day 1 and WT B6 BMDC (10 3 106) pretreated with vehicle or MLN4924 overnight and subsequently transferred in 2 doses separated by 24 hours (day 1 and day 0). CD90.21 T cells (2 3 106) from syngeneic WT-C57BL/6 or allogeneic bm12 animals were transferred on day 0. Following sacrifice on day 6, spleens were analyzed for CD69 (B) and Tbet (C).

Because systemic administration of MLN4924 is likely to impact not just DCs but also several other cells, particularly donor T cells that are critical for GVHD, the reduction in GVHD mortality might be a reflection of its effects on these other cells in vivo. Therefore, in order to evaluate the effects of neddylation inhibition only on the in vivo function of BM-derived DCs without the confounding effects on other tissues or expression of target antigens, we devised a model in which allogeneic $CD4^+$ T cells would respond only to MHC class II alloantigens on exogenously administered DCs in an acute GVHD model. MHC class II–deficient (Abb (H2-Ab1) C57BL/6 mice ($H2^b$) received 10 Gy total body irradiation and were injected with 1×10^7 BMDCs from syngeneic WT C57BL/6 ($H2^b$) animals that were incubated overnight with either vehicle

or MLN4924 in 2 doses separated by 24 h. We then injected 2 × 10^6 CD90.2$^+$ T cells from either syngeneic C57BL/6 or allogeneic bm12 donors (see Methods and Figure 2.7), which differ from the recipient animals by a single MHC class II antigen. Analysis of donor T cells in the spleen at 6 days revealed fewer activated CD69$^+$ (Figure 2.6B) and differentiated Tbet$^+$ (Figure 2.6C) CD4$^+$ T cells in animals that received DCs pretreated with MLN4924.

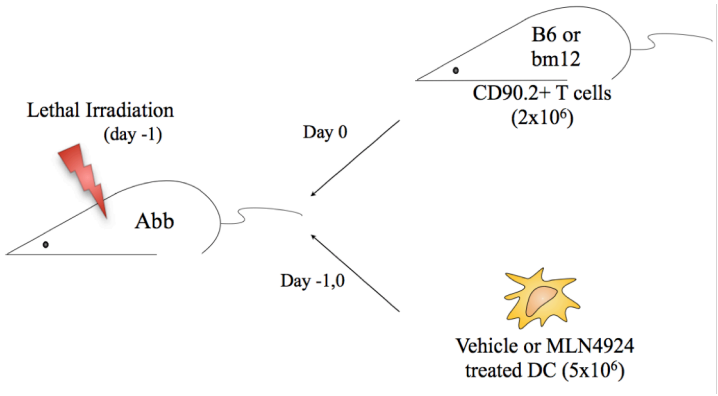

Fig. 2.7 - Description of in vivo transplant scheme. Abb recipient mice, which lack expression of MHC II, were lethally irradiated (10 Gy) and transplanted with vehicle or MLN4924 treated WT B6 BMDC (10x106) in 2 doses separated by 24 hours, on d-1 and d0. CD90.2+ T cells (2x106) were transferred on d0 to Abb recipients. The spleens of recipient mice were analyzed for T cell activation following sacrifice on day 6.

Blockade of neddylation attenuates the functions of human DCs

To determine the clinical relevance of our observations we determined whether the effects of inhibition of neddylation on DCs was also germane to DCs derived from healthy human PBMCs. Human peripheral blood monocyte-derived dendritic cells (moDC) were harvested and cultured with and without MLN4924 and stimulated with LPS. LPS induces the secretion of both TNFα and IL-6[191] from moDCs, but were significantly reduced by MLN4924 compared to vehicle control (Figure 2.8A). Similar

to the effect on murine DCs, the reduction of proinflammatory cytokines was also significantly greater than dexamethasone (Figure 2.8A).

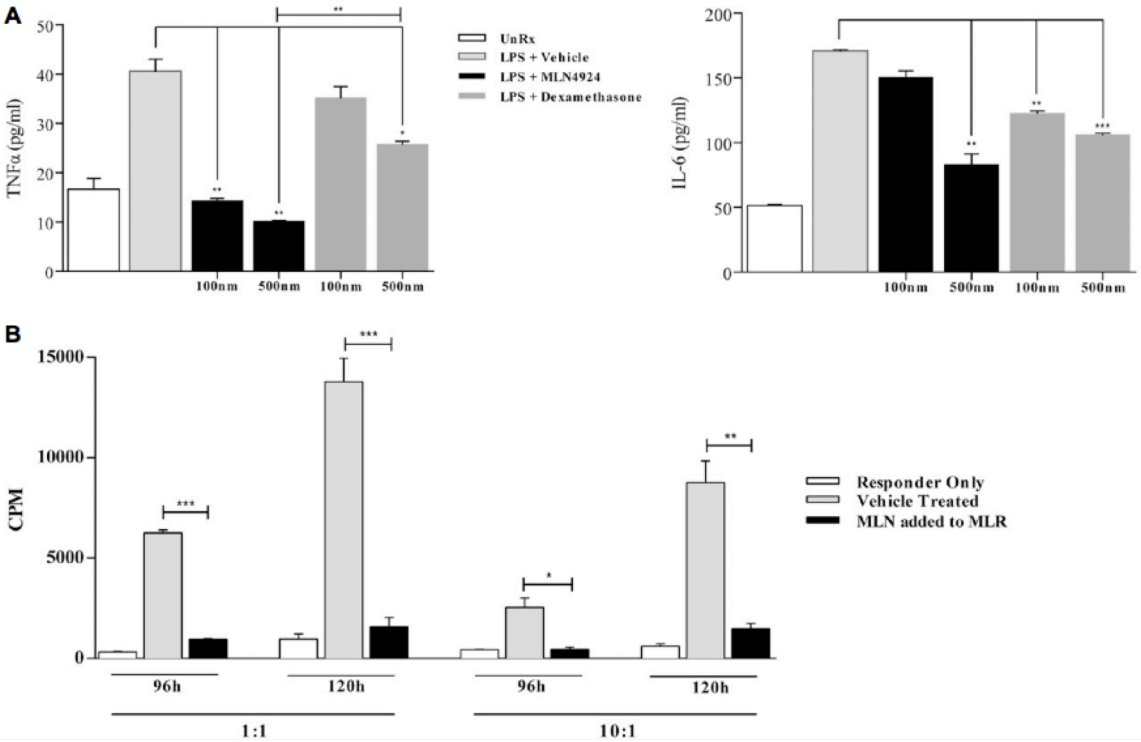

Fig. 2.8 – Neddylation modulates human DC function. (A) Quantification via ELISA of TNF-a (left) and IL-6 (right) released from human moDCs stimulated with LPS in the presence or absence of MLN4924 or dexamethasone at the indicated doses. Cells receiving treatment were preincubated with vehicle, MLN4924, or dexamethasone for 2 hours followed by concurrent LPS stimulation (0.5 mg/mL) for 4 hours. One representative experiment of 3 is shown of groups treated in triplicate. (B) Human PBMCs (1 3 105/well) and moDCs were obtained from 2 healthy donors and cocultured at 1:1 and 10:1 ratios in an MLR in the presence or absence of MLN4924 for 96 and 120 hours.

Next, we determined whether MLN4924 attenuated the ability of human PBMC derived DCs to stimulate allogeneic PBMCs. Peripheral blood mononuclear cells (PBMC) and moDCs were obtained from two healthy donors and cultured in an MLR at 1:1 and 10:1 ratios in the presence or absence of MLN4924. Following culture for 96 hours and 120 hours, a significant decrease in proliferation of PBMCs was observed in cultures incubated with MLN4924 (Figure 2.8B), similar to the results observed in murine cells.

Inhibition of neddylation does not increase apoptosis or alter the phenotype of DCs

Studies have shown previously that MLN4924 reduces the viability of cancer cell lines.[81] Therefore we determined whether the observed effects of inhibition of neddylation through inactivation of Cul-1 E3 ligase by MLN4924 was due to reduced BMDC viability.

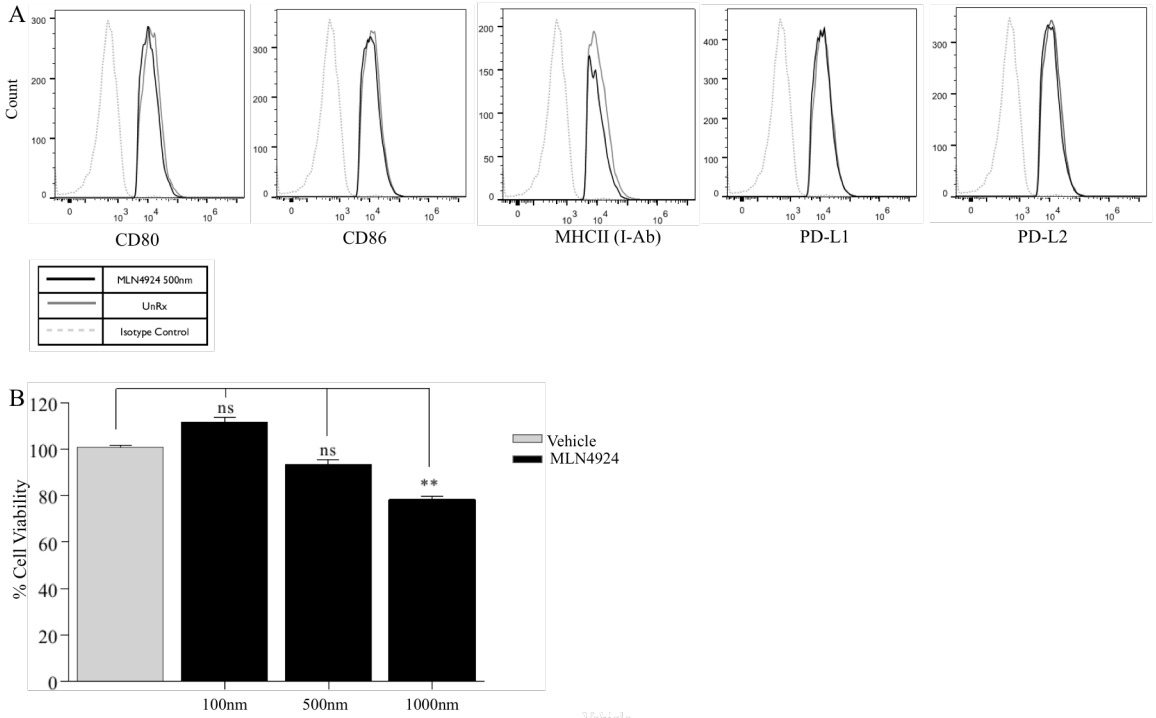

Fig. 2.9 – Inhibition of neddylation does not alter phenotype or cell viability in BMDC. (A) Flow cytometric analysis of cell surface phenotypic markers on BMDC. (B) Cell viability of BMDC cultured in the presence or absence of vehicle or MLN4924 for 24 hours. One representative experiment of three is shown. ** P<0.01

Treatment of BMDCs with MLN4924 for 24 hours at the doses that reduced their function did not cause greater apoptosis and thus did not affect cell viability (Figure 2.9B). We next assessed whether MLN4924 arrested the maturation of DCs as determined by the expression of surface co-stimulatory molecules. To determine this, we

supplemented the culture media during BMDC generation with vehicle or MLN4924 for the last 24 hours and then examined cell surface expression of CD80, CD86, MHC II, PD-L1, and PD-L2 with flow cytometry. Addition of MLN4924 did not cause phenotypic changes (Figure 2.9A). These data taken together suggest that the reduction of DC function following treatment with MLN4924 is not due to the result of decreased cell viability or phenotypic change, but that these are intrinsic to inhibition of neddylation.

Inhibition of SAG reduces LPS-induced cytokine production in DCs

The inhibition of LPS-induced cytokine production by MLN4924 suggests that de-neddylation is critical to this process by inactivation of CRL-1 E3 ligase activity. Next, to determine the specificity of the approach and to rule out any potential off-target effects of MLN4925, we utilized siRNA mediated knock-down of RBX2/SAG, a critical and specific component of the CRL-1 induced neddylation pathway. We next performed siRNA-mediated knockdown of RBX1 and RBX2/SAG alone or in combination in JAWSII cells. First, we confirmed the efficiency and specificity of knock-down of targeting SAG transcripts with siRNA as indicated by reduced levels of SAG (Figure 2.10A). We next compared TNFα cytokine release following LPS stimulation in JAWSII cells transfected with the control scrambled siRNA or SAG specific siRNA. Upon LPS stimulation, JAWSII cells transfected with SAG siRNA exhibited a significant reduction in expression of TNFα compared with the scrambled siRNA (Figure 2.10B). Interestingly double knockdown of Rbx1 and SAG/Rbx2 had little or no effect on cytokine production, which could be because Rbx1 may antagonize or cause feedback inhibition of SAG (Rbx2). Future studies will address this issue. Nonetheless, collectively, these data

suggest that inhibition of neddylation through inactivation of the CRL-1 mediated either by siRNA knockdown of SAG or by the small molecule MLN4924, reduced proinflammatory cytokine release by DCs.

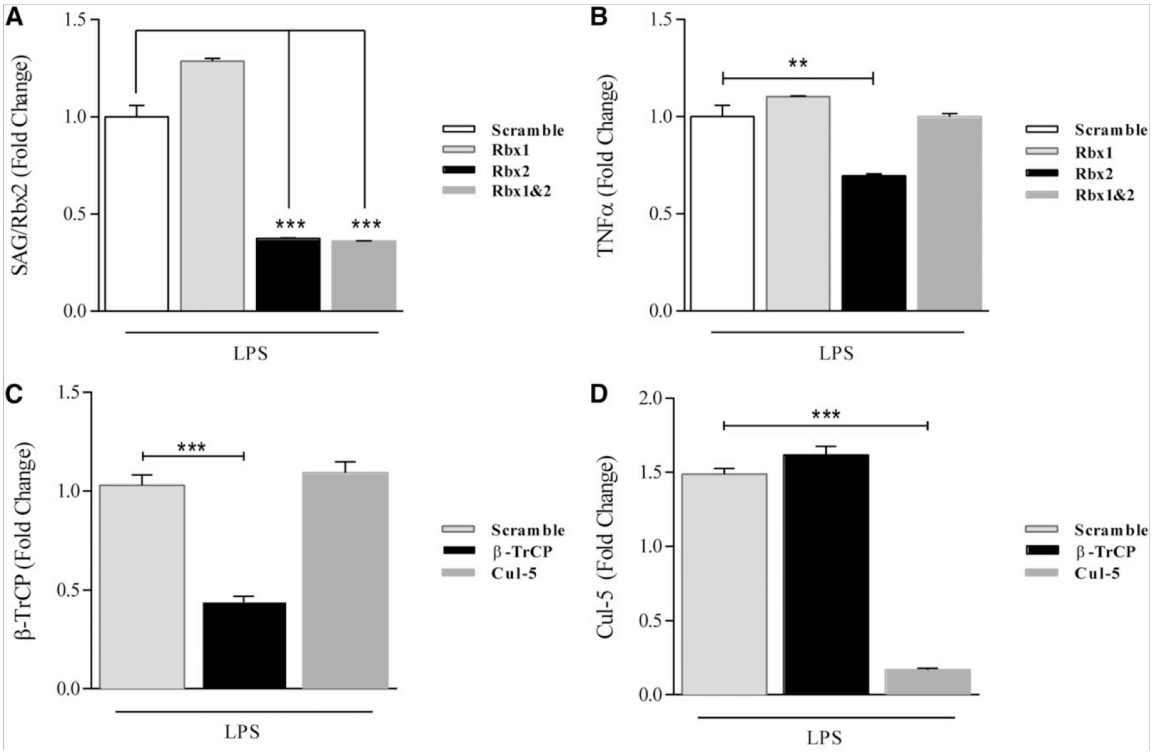

Fig. 2.10 – siRNA-mediated neddylation inhibition. (A) qPCR analysis of SAG expression in JAWSII cells transfected with indicated siRNA (3 mg). Scramble transfection performed as control. (B) qPCR analysis of TNF-a expression in JAWSII cells transfected with indicated siRNA and stimulated with LPS (0.5 mg/mL). Scramble transfection performed as control. One representative experiment of 3 is shown. (C-E) JAWSII cells transfected with siRNA for βTrCP, Cul5, or scramble as described in Materials and methods. Expression of βTrCP (C) and Cul5 (D) mRNA transcripts in JAWSII cells receiving indicated siRNA- mediated knockdown. *P < .05; **P < .01; ***P < .0001

Inhibition of βTrCP but not Cul-5 reduces LPS-induced cytokine expression in DCs

Inhibition of neddylation via MLN4924 and molecular knockdown of Rbx2 results in global CRL inactivation. Therefore, to determine if the observed results are specific to CRL-1, we silenced βTrCP as well as Cul-5 using siRNA mediated knockdown in

JAWSII cells. We first ensured efficient knockdown of both βTrCP (Figure 2.10C) and Cul-5 (Figure 2.10D). Next, we examined the expression of TNFα as a functional readout from the cells transfected with scramble, βTrCP, or Cul-5 and subsequently stimulated with LPS. A significant decrease in TNFα expression was observed in cells receiving knockdown of βTrCP, but not in cells with Cul-5 knockdown (Figure 2.11). These data suggest that the function of CRL-1 is critical for the underlying mechanism of immune suppression following inhibition of neddylation.

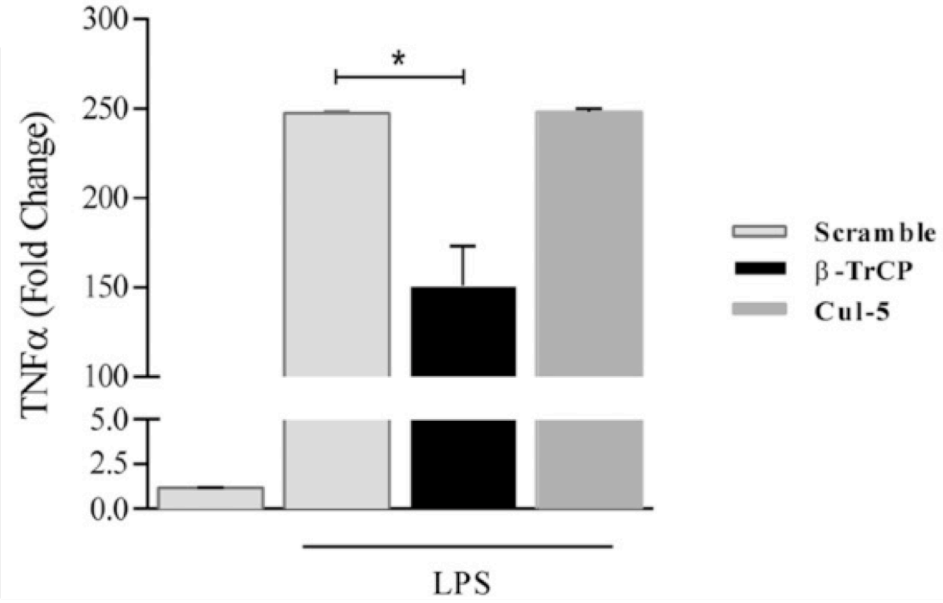

Fig. 2.11 – siRNA-mediated neddylation inhibition inhibits LPS-induced TNF-a production. Expression of TNF-a mRNA transcripts in cells transfected with indicated siRNA and cultured in the presence or absence of LPS (0.5 mg/mL) for 4 hours. *P < .05

MLN4924 inhibits translocation and activation of NF-κB

To determine if inhibition of neddylation prevents transcriptional activity of LPS-induced NF-κB, we assessed p65 NF-κB translocation to the nucleus in BMDCs treated with MLN4924 or dexamethasone following stimulation with LPS. As anticipated, in cells

cultured in the presence of vehicle and stimulated with LPS for 30 minutes, p65 NF-κB was present in the nuclear fraction (Figure 2.12A, top panel). Cells pretreated with dexamethasone 500nm and stimulated with LPS, exhibited a similar level of p65 NF-κB in the nuclear fraction (Figure 2.12A, top panel). However, pretreating cells with MLN4924 prior to LPS stimulation inhibited protein levels of p65 NF-κB in the nuclear fraction of BMDCs (Figure 2.12A). Interestingly, these doses of MLN4924 and dexamethasone both inhibited LPS-induced release and gene expression of TNFα and IL-6 (Figure 2.2A-D). These data indicate that LPS-induced nuclear accumulation of p65 NF-κB in BMDCs is blocked by MLN4924, but not dexamethasone suggesting that MLN4924 and dexamethasone have divergent molecular effects.

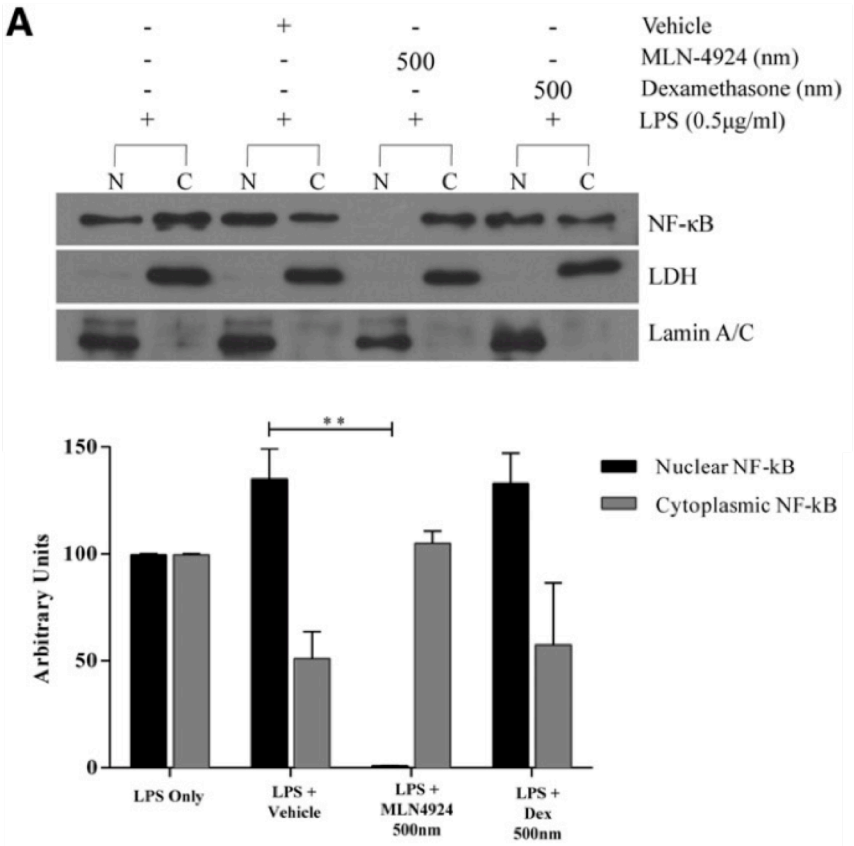

Fig. 2.12 – Neddylation inhibition and dexamethasone differentially affect NF-κB translocation in BMDC. (A) Protein analysis by western blot (left) of p65 isoform of NF-κB protein using nuclear (N) and cytosolic (C) fractions of BMDC in the presence or absence of 500 nm MLN4924 or 500 nm dexamethasone and stimulated concurrently with LPS (0.5 mg/mL) for 30 minutes. Plot (right) shows densitometric and statistical analysis of p65 NF-κB presence in the nuclear fraction and cytosolic fraction. Lamin A/C and LDH proteins were analyzed to demonstrate the presence of nuclear and cytosolic fractions, respectively. One representative experiment of 3 is shown. **P < .01

Next, to visualize and demonstrate the translocation of p65, we performed immunocytochemistry. BMDC cultured only with vehicle exhibited a diffuse cytoplasmic localization of NF-κB (Figure 2.13, top row). By contrast, BMDCs stimulated with LPS for 1 hour and treated with vehicle, revealed prominent NF-κB accumulation in the nucleus (Figure 2.13, middle row). However, LPS stimulated cells treated with MLN4924 showed a dispersed cytoplasmic localization of NF-κB similar to unstimulated

controls (Fig 2.13, bottom row). These complementary methods of examining NF-κB translocation showed prevention of translocation of NF-κB to the nuclei in BMDC treated with MLN4924.

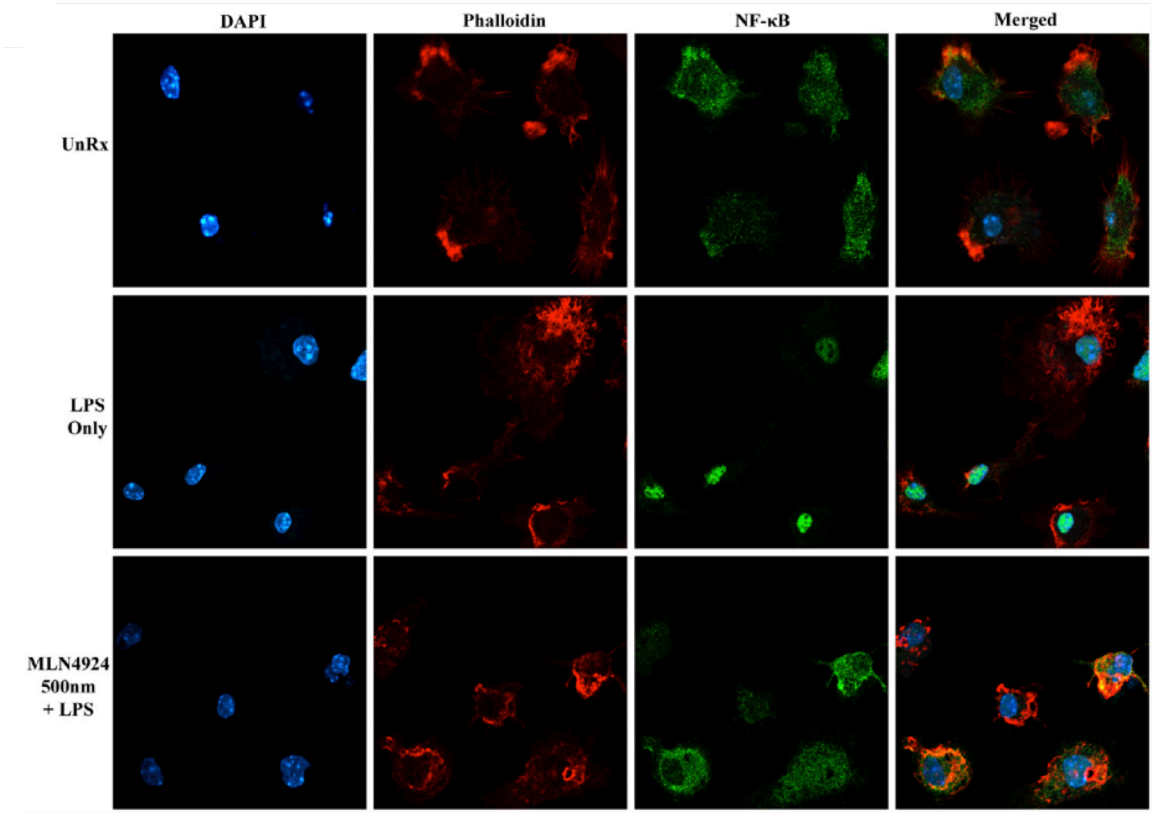

Fig. 2.13 – Neddylation inhibition affects NF-κB translocation in BMDC. Immunocytochemistry analysis of p65 NF-κB (column 3) localization in BMDC cultured in the presence or absence of MLN4924 and stimulated with LPS (0.5 mg/mL) for 1 hour. Cell nuclei were stained using DAPI (column 1). Cytoplasmic actin was stained with phalloidin (column 2). Merged images of staining (column 4). One representative experiment of 3 is shown.

Inhibition of neddylation prevents IκB degradation in BMDC

Previous studies have shown that IκB is a target of CRLs[192]. Therefore, we examined the effect of MLN4924 on the degradation of IκB in BMDCs when stimulated with LPS. Similar to previous studies in BMDCs[193] and other APCs[194], stimulation with LPS

resulted in the reduction of IκB protein levels within 30 minutes in vehicle treated BMDCs. Levels of IκB were slowly restored over a 6-hour period (Figure 2.14A left, middle panel).

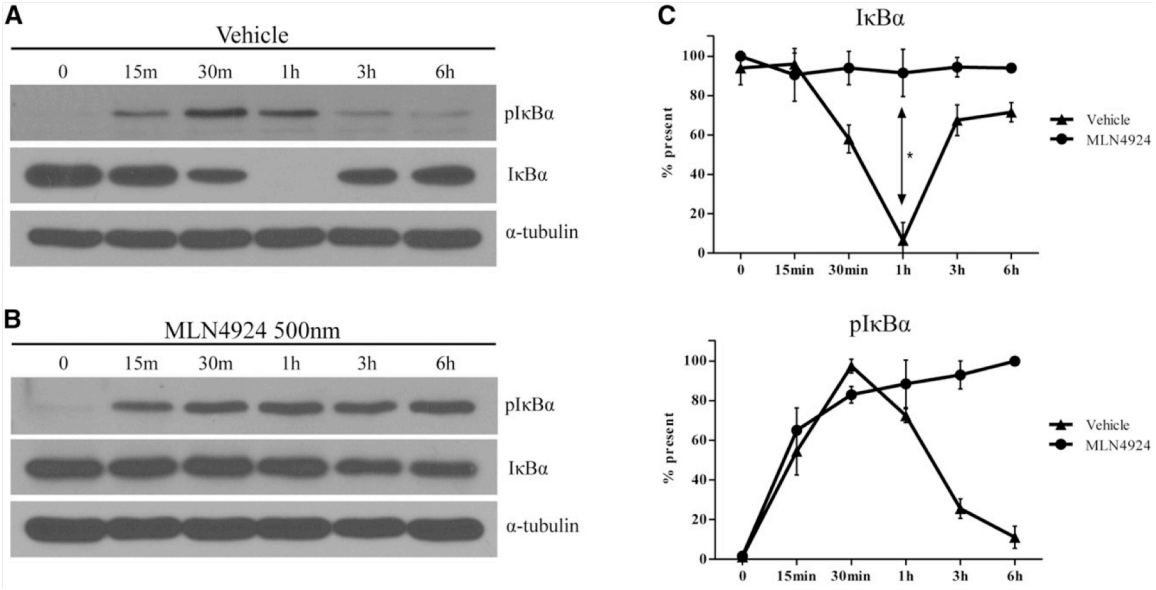

Fig. 2.14 – Neddylation inhibition prevents IκB degradation in BMDC. Protein analysis via western blot of phosphorylated IκBa protein (A-B, top panels) and total IκBa (A-B, middle panels) using whole cell lysate of BMDC stimulated with LPS (0.5 mg/mL) for 6 hours in the presence of vehicle (A) or 500 nm MLN4924 (B). Densitometric and statistical analysis of total IκB (C, top) or pIκB (C, bottom) of vehicle or MLN4924-treated cells. α-tubulin protein levels were analyzed as an equal loading control. One representative experiment of 3 is shown. * $P < 0.05$

The observed decrease in IκB following LPS stimulation coincided with increased phosphorylation of IκB at Serine-32 and Serine-36 during the first 30 minutes of treatment. The increased p-IκB slowly returned to lower levels during the remaining 5 hours of treatment (Figure 2.14A left, top panel). Treatment of BMDCs with MLN4924 500nM inhibited any LPS-mediated decrease in IκB (Figure 21.4B left, middle panel) while levels of phosphorylated IκB in the same cells were elevated within 15 minutes following LPS treatment (Figure 2.14B left, top panel). Further, the levels of phosphorylated IκB remained elevated for the duration of the 6 hour treatment (Figure

2.14B). Following densitometric and statistical analysis, the decrease in IκB in vehicle treated cells was significantly greater than MLN4924 treated cells (Figure 2.14C, top panel). These data indicate that inhibition of neddylation blocks the degradation of phosphorylated $I\kappa B^{Ser32/Ser36}$ protein in BMDCs.

Neddylation blockade does not perturb LPS induced activation of MAPK/ERK pathway

Previous studies have shown that LPS stimulation of cells results in activation of the MAPK/ERK pathway[193]. We therefore examined whole cell lysates of BMDC stimulated with LPS cultured in the presence of vehicle or MLN4924. Western blot analysis showed that ERK protein levels were similar in vehicle treated (Figure 2.15A) and MLN4924 treated (Fig 2.15B) cells. In addition, levels of pERK increased in a similar manner in both vehicle and MLN4924 treated cells (Figure 2.15A-B). These data suggest that MLN4924 treatment specifically reduced proinflammatory cytokines through regulation of NF-κB pathway without affecting MAPK/ERK pathway.

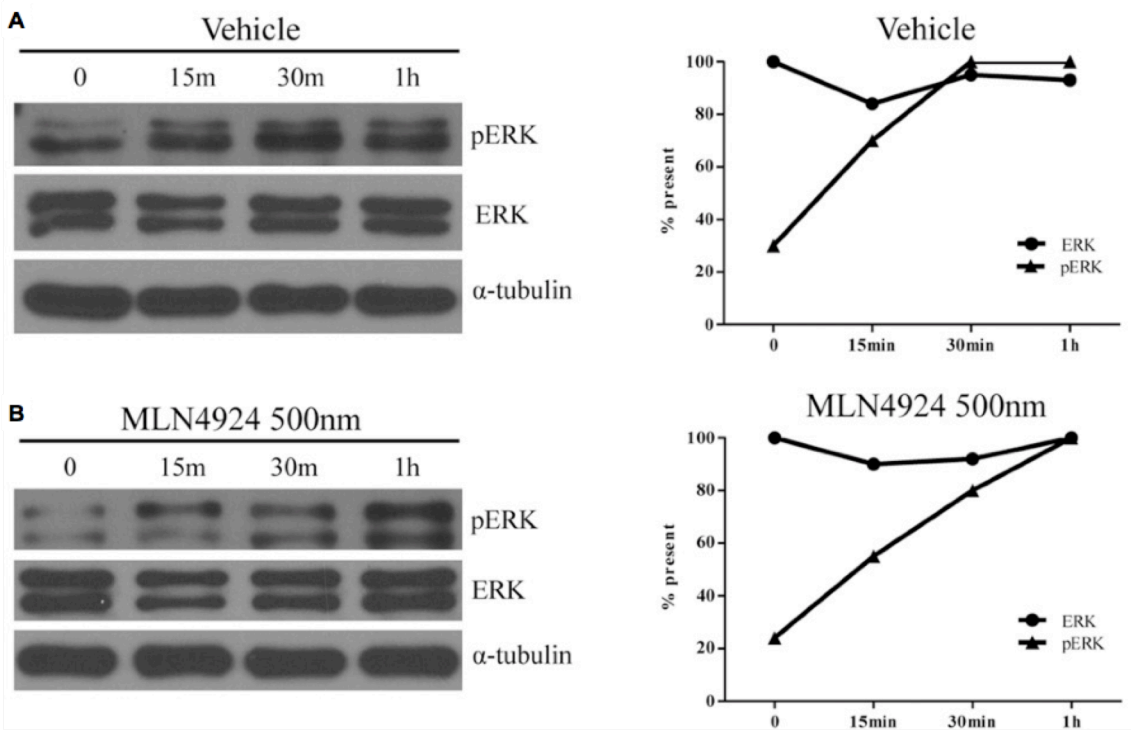

Fig. 2.15 – Neddylation inhibition does not perturb the MAPK/ERK pathway. Protein analysis via western blot of phosphorylated ERK protein (A-B, top panels) and total ERK (A-B, middle panels) using whole cell lysate of BMDC stimulated with LPS for 6 hours in the presence of vehicle (A) or 500 nm MLN4924 (B). Densitometric analysis of vehicle-treated cells (A, right) or 500 nm MLN4924-treated cells (B, right) of phosphorylated ERK and total ERK protein. α-tubulin protein levels were analyzed as an equal loading control. One representative experiment of 3 is shown.

DISCUSSION

PTMs modulate immunity[46]. Proteins critical for an effective immune response, such as NF-κB, are known to be phosphorylated and acetylated[195,196]. However, the role that neddylation plays in regulating immune cells, such as DCs, through the translocation of NF-κB is not clear. Our results demonstrate a novel role for the PTM neddylation in the regulation of DC mediated immunity. The mechanism of neddylation characterizes a novel molecular target for the inhibition of secretion and transcription of certain LPS-induced proinflammatory cytokines in dendritic cells. We show that following inhibition of neddylation and stimulation via TLR and NLR, release and gene expression of the proinflammatory cytokines TNFα and IL-6 are greatly mitigated (Figure 2.2 & 2.3).

Studies have previously shown the ability of MLN4924 to suppress the growth of tumor cell lines as well as primary human AML cells[79,80,186]. Inhibition of NEDD8 pathway by MLN4924 has been reported to result in apoptosis[75,197]. However, our data suggests that MLN4924 did not affect BMDC viability (Figure 2.9B) demonstrating that the reduction in the production of proinflammatory cytokines was not due to loss of cells, but a functional consequence of inhibition of neddylation. Our data also suggest that treatment with MLN4924 had significantly greater impact on suppression of the release of proinflammatory cytokines than dexamethasone or bortezomib (Figures 2.1 to 2.3) in the nanomolar dose range. Moreover inhibition of neddylation with MLN4924 reduced DC functions in vivo and attenuated GVHD (Figure 2.6) suggesting that this pathway could be targeted to mitigate in vivo inflammatory diseases.

Mechanistic studies have uncovered a distinct molecular pathway for MLN4924 mediated suppression of DC functions when compared with dexamethasone. The primary molecular target of dexamethasone is the glucocorticoid receptor (GR)[198]. Binding of steroid results in activation of the receptor and subsequent translocation to the nucleus[199] and is known to interact with transcription factors such as NF-κB and AP-1[200]. These interactions repress the expression of genes coding a number of cytokines that play key roles in the immune and inflammatory systems. By contrast MLN4924 specifically targets NEDD8 activating enzyme (NAE), a heterodimer of NAE1 and UBA3 subunits[75]. By doing so, MLN4924 inactivates CRLs and impedes the ubiquitination rate of the subset of proteins whose degradation is dependent on CRLs[75].

Although dexamethasone significantly inhibited secretion of TNFα and IL-6, which are known to be regulated by NF-κB[178], it did not directly prevent the translocation of NF-κB to the nucleus after LPS stimulation (Figure 2.12), in contrast to MLN4924. The ability of MLN4924 to directly prevent the degradation of IκB in LPS stimulated cells (Figure 2.14B) suggests a specific and distinct mechanism from that of dexamethasone. The role of inhibiting neddylation by MLN4924 in suppressing the release of TNFα and IL-6 through the inactivation of CRL-1 causing IκBα accumulation and subsequent prevention of NF-κB activation, is further supported by molecular inactivation of CRL-1 by the siRNA knockdown of SAG and βTrCP (Figure 2.10). These data together suggest that MLN4924 and dexamethasone block LPS-induced cytokine release through distinct mechanisms.

Our study is in agreement with previous reports in cell lines demonstrating an effect on NF-κB activation[201]. We extend those observations for the first time in primary cells, DCs and their functional immune responses. More importantly we show a similar effect on primary human dendritic cells. Furthermore, we uncover the molecular mechanism that is dependent on IκB degradation but independent of MAPK/ERK pathway (Figure 2.14 and 2.15) and show that it is germane to both canonical and non-canonical NF-κB signaling mediated release of proinflammatory cytokines. Other studies have shown that degradation of IκB and release of proinflammatory cytokines can be altered by proteasome inhibitors[202]. However, these proteasome inhibitors also activate the transcription factor AP-1 which is known to contribute to LPS induced cytokines[193]. Our results show that upon treatment of LPS-stimulated BMDC with MLN4924, the MAPK/ERK pathway is unperturbed (Figure 2.15) suggesting that AP-1 activity is unaltered by inhibition of neddylation. This is likely due to the degradation of IRAK1 through its association with the E3 ligases TRAF6 and Pellino[203]. Previous studies have shown that Pellino, not CRL, is a likely candidate to serve as the degradation scaffold for IRAK1[204]. Thus inhibition of the neddylation pathway may be a more specific approach of inhibiting the degradation of IκB and thereby blocking the increase in proinflammatory cytokines as compared to the effects seen by proteasome inhibitors.

Promising preclinical results led to the advancement of MLN4924 to Phase 1 clinical trials for both non-hematological and hematological cancers[205,206]. However, MLN4924s immune-modulatory effects have heretofore been largely unrecognized. Our results suggest that, at non-cytotoxic doses, drugs such as MLN4924 that specifically target

neddylation, may provide novel therapeutic strategies for diseases associated with deregulated immune responses such as GVHD, chronic inflammatory disease, shock, autoimmunity and allo-transplantation[81,92,173-175].

MATERIALS AND METHODS

Cell isolation and cultures: Briefly, bone marrow cells were flushed from the femurs of 8- to 12-week-old female C57BL/6 mice and cultured in 150 x 15-mm CytoOne petri dishes (USA Scientific, Ocala, FL) at $1x10^7$ in 20ml of RPMI supplemented with 10% FCS, 4mM L-glutamine, 10 U/ml penicillin, 100 µg/ml streptomycin, 0.5 mM 2-ME, 20ng/ml GM-CSF. On day 4, 20ml of fresh complete RPMI containing 20ng/ml GM-CSF was added to each culture. After 7 days of culture, the loosely adherent cells were harvested and purified using anti-CD11c magnetic microbeads (Miltenyi Biotec Ltd., Auburn, CA) and the autoMACS (Miltenyi Biotec).

Human peripheral blood mononuclear cells (PBMCs) were isolated from the blood of healthy donor volunteers. PBMCs were isolated according to a protocol obtained from Current Protocols in Immunology. Briefly, whole heparinized blood was centrifuged (2000 rpm, 20ºC, 30 min) using a Ficoll Hypaque density gradient. The mononuclear layer was removed from the gradient and washed in complete RPMI and used as either responders in human MLR or monocytes were cultured at $1x10^6$ cells/ml in complete RPMI containing 800 U/ml human recombinant GM-CSF and 500 U/ml human recombinant IL-4. On day 5, fresh complete RPMI containing 100 U/ml TNF-α as well as 800 U/ml human recombinant GM-CSF and 500 U/ml human recombinant IL-4 was added to the culture. Cells were harvested on day 9 to 10 of incubation. All human recombinant cytokines were purchased from Peprotech (Rocky Hill, NJ).

The DC cell line, JAWSII, was established from bone marrow cells of a p53-knockout C57BL/6 mouse, and was purchased from the American Type Culture Collection (CRL-11904; ATCC, Manassas, VA). Cells were grown in a CO_2 incubator at 37ºC and 5%

CO_2 in complete culture medium consisting of α-MEM with 10% FCS, 4mM L-glutamine, 10U/ml penicillin and 100μg/ml streptomycin, 0.5mM 2-ME, 1mM sodium pyruvate, and 5ng/ml murine GM-CSF. Cultures were maintained by transferring nonadherent cells to a centrifuge tube and treating attached cells with 0.25% trypsin-0.03% EDTA (Gibco) at 37ºC for 5 min after rinsing culture flask with pre-warmed PBS. The two populations were pooled together, washed once (1000rpm, 10min) and distributed into new culture flasks

Cytokine Detection: Isolated BMDC and human moDCs were seeded on 60mm culture dishes at $3x10^6$ cells/well and a 24-well plate at $2x10^5$ cells/well, respectively. Pretreated cells were cultured with DMSO (Sigma), MLN4924 (Active Biochem), dexamethasone (APP Pharmaceuticals), or bortezomib (Fisher Scientific) at the indicated dosages for 2 hours. Cells were then stimulated with *E. coli*-derived LPS (Invivogen), synthetic Pam3CSK4 (Invivogen), PGN (Invivogen), or CD40L (Shenandoah Biotechnology) at the indicated concentrations for a concurrent 4 hours. Supernatants were subsequently collected and stored at -20ºC until analysis. TNFα and IL-6 ELISA kits (mouse and human) were purchased from R&D Systems and performed as per the manufacturers' instructions and read at 450nm by a SpectraMax microplate reader (Molecular Devices, Sunnyvale, CA).

Quantitative PCR: Using 1μg of each RNA template, cDNA was synthesized using SuperScript VILO (Invitrogen; Carlsbad, CA). qPCR primers for murine GAPDH (Forward: CCACAGTCCATGCCATCACTGC; Reverse: GCCCAAGATGCCCTTCAGTGGG), TNF α (Forward: CGACGTGGAGGCAGAAGAGGC; Reverse: CGTGGGCTACAGGCTTGTCACTC),

IL-6 (Forward: CGGAGAGGAGACTTCACAGAGG; Reverse: GCAAATTTCCTGATTATATCCAG), Rbx2 (Forward: GGACGTTGAGTGCGATACCT; Reverse: TGCCGATTCTTTGGACTACC), βTrCP (Forward: TCTGCACCTGCGCTTCAATA; Reverse: GAGGGTGATGTCAGTTGGGG), or Cul-5 (Forward: CAACGGAACTCCCAGATGCT; Reverse: GCTGCAAGCGTCCAATCAAA).

Flow Cytometry: To analyze DC surface phenotype, DCs were incubated in the presence or absence of MLN4924 or the vehicle (DMSO, Sigma). Cells were then harvested and stained with CD11c-conjugated APC (Clone: N418) and one of the following per triplicate group: Annexin V (BD Biosciences), CD80 (Clone: 16-10A1), CD86 (Clone: GL-1), MHCII-I-A^b (Clone: AF6-120.1), PD-L1 (Clone: MIH5), PD-L2 (Clone: TY25). All flow cytometry Abs were purchased from eBiosciences. Stained cells were then analyzed with an Accuri C6 Flow Cytometer (BD Biosciences).

Western Blot and Subcellular Fractionation: BMDCs were seeded in 60mm dishes with $3x10^6$ cells per dish. Pretreated cells were cultured with DMSO (Sigma), MLN4924 (Active Biochem), or dexamethasone (APP Pharmaceuticals) at the indicated dosages for 2 hours followed by concurrent stimulation with *E. coli*-derived LPS (100ng) for an additional 4 hours. Following treatment and stimulation, whole cell lysates where obtained and protein concentrations determined with Pierce BCA Protein Assay (Thermo Scientific). Equal amounts of protein were separated by SDS-PAGE gel (120V, 1.5h) and subsequently transferred to nitrocellulose membrane (20V, 1h). The following antibodies were used to analyze the membranes: Nedd8 (19E3), α-tubulin (11H10), NF-**κ**B p65 (D14E12), Lamin A/C (4C11), pIκBα (5A5), IκBα (L35A5), pERK (D13.14.4E), ERK

(137F5) were purchased from Cell Signaling (Danvers, MA). Cullin1 (EPR3103Y) and LDH (EP1566Y) were purchased from abcam (Cambridge, MA). Secondary antibodies conjugated to HRP (Jackson ImmunoResearch) were used to detect primary antibodies. Densitometric analysis performed by ImageJ software. Subcellular fractionation was performed on $3x10^6$ BMDC seeded in 60mm dishes. Cells were pretreated in the presence or absence of vehicle, MLN4924, or dexamethasone for 2 hours followed by concurrent LPS stimulation for 30 minutes. The cytoplasmic and nuclear fractions were isolated using the Nuclear Extract Kit (Active Motif) per the manufacturers instructions. The extracts where then analyzed via western blot.

Mixed Lymphoctye Reaction (MLR): Splenic T cells ($2x10^5$/well) were magnetically separated from WT-B6 or WT-BALB/c mice by autoMACS using CD90.2 microbeads and subsequently cultured with irradiated (30 Gy) WT-B6 DC at 40:1 ($5x10^3$/well) and 100:1 ($2x10^3$/well) for 72 hours and 96 hours. Human MLRs were performed by co-culture of PBMCs ($1x10^5$/well) and moDCs at 1:1($1x10^5$) and 10:1 ($1x10^4$) ratios for 96 hours and 120 hours. Incorporation of ^{3}H-thymidine (1µCi/well) by proliferating T cells or PBMCs during the final 6 hours of culture was measured by a TopCount (PerkinElmer).

Molecular Knockdown: JAWSII cells were seeded into a 24-well plate ($2.5x10^5$/well) overnight at 37ºC. Cells were transfected with siRNA (3µg) using Oligofectamine Reagent (Invitrogen) as per the manufacturers instructions. Cells were incubated with transfection medium and siRNA for 24 hours before stimulation with LPS for 4 hours. RNA was extracted from cell pellets using RNeasy Mini Kit (Qiagen) and analyzed via

qPCR. Rbx1, Rbx2, βTrCP, and Cul-5 siRNA were obtained from Ambion (Carlsbad, CA)

Confocal Microscopy: BMDC were seeded onto Corning glass cover slips ($1x10^5$ cells/slip) (Fisher Scientific) overnight at 37ºC. Pretreated cells were cultured with DMSO (Sigma) or MLN4924 (Active Biochem) at the indicated dosages for 2 hours followed by concurrent stimulation with *E. coli*-derived LPS for an additional 1 hour. Cover slips were then washed, fixed with 4% paraformaldehyde for 20 minutes, and subsequently permeabilized with 0.3% Triton X. Cells were stained with NF-**κ**B p65 (D14E12) primary (1:500) and Alexa Fluor 488 (Molecular Probes) secondary (1:1000), DAPI (Invitrogen), and Alexa Fluor 555 Phalloidin (1:500). Coverslips were then mounted using ProLong Gold Antifade Reagent (Molecular Probes) and Z-stack images were acquired at room temperature using a Nikon A-1 confocal microscope (Mellville, NY) using an oil immersion 60X objective with a numerical aperture = 1.4 and imported into NIS-Elements Software (Nikon). Excitation lasers 405nm, 488nm, and 561nm were used. Microscope laser exposure and settings were obtained using appropriate isotype controls and were retained for each experimental group.

CHAPTER III

SAG/RBX2 E3 UBIQUITIN LIGASE DIFFERENTIALLY REGULATES INFLAMMATORY RESPONSES OF MYELOID CELL SUBSETS

ABSTRACT

Macrophages form an important component of the innate immune system and serve as first responders against invading pathogens. While pathways critical for initiation of inflammatory responses between macrophages and other $LysM^{+}$ myeloid cells are largely similar, it remains unknown whether a specific pathway has differential effects on inflammatory responses mediated between these cells. Sensitive to apoptosis gene (SAG) protein has E3 ligase and antioxidant activities. Recent studies demonstrated that SAG negatively regulates *in vitro* inflammatory responses generated by macrophages and dendritic cells in response to LPS. However, the *in vivo* role of SAG on modulation of macrophages is not known. We generated novel LysM-Cre/$Sag^{fl/fl}$ mice and observed that in contrast to *in vitro* observations, they showed greater levels of proinflammatory cytokines and enhanced mortality in response to LPS. Although $Sag^{-/-}$ macrophages released less proinflammatory cytokines, $Sag^{-/-}$ neutrophils exhibited increased proinflammatory cytokines suggesting Sag plays a differential role in these cells.

INTRODUCTION

The innate immune system consists of several cell types and is the first line of defense in the host, functioning as a barrier to infection from invading organisms[207]. Macrophages and neutrophils –two cell types of the innate immune system– derive from the myeloid progenitor lineage that are critical for the initiation of inflammation in the context of antimicrobial immunity[208]. Innate immune cells recognize and bind to pathogen associated molecular patterns (PAMPs) of pathogens via pattern recognition receptors (PRRs). Toll-like receptors (TLRs), a type of PRR, regardless of the innate immune cells that express them, utilize similar signal pathways that lead to the activation of the nuclear factor-kappa B (NF-κB) pathway[178] and initiates the release of proinflammatory cytokines[209,210]. These mutual and complementary features of innate immune cells likely favor their interaction and cooperation in generating complimentary innate immune responses[208]. However, whether there are differences in the mechanisms through which specific innate immune cells are activated in response to infection remains unknown. In this context, specifically, whether the critical LysM-enzyme expressing innate immune cells – namely macrophages and neutrophils – utilize the same pathway to produce differential inflammatory responses is not known.

SAG –also known as RING box protein 2 (RBX2), Regulator of Cullins 2 (ROC2), or RING Finger Protein 7 (RNF7)– was originally cloned by differential display in our laboratory as a redox-inducible antioxidant protein which scavenges ROS by forming intra- and inter- molecular disulfide bonds[69,70]. As a member of the SCF E3 ubiquitin ligase complex, SAG binds to ubiquitin-loaded E2 and catalyzes the ubiquitin

transfer from the E2 molecule to a substrate for subsequent degradation by the proteasome. By promoting the degradation of a variety of substrates through its ligase activity, SAG regulates diverse signaling pathways and biological processes, including cell apoptosis, embryonic development, vasculogenesis, angiogenesis, and tumorigenesis[211]. This degradative process is known as neddylation and is responsible for the regulation of several cellular pathways. SAG was previously reported to maintain macrophage survival and to regulate the levels of inflammatory cytokines in response to infection by ubiquitinating the pro-apoptotic proteins Bax and SARM[201,212]. Further, inhibitor-κB (IκBα), a classical inhibitor of NF-κB activation, is a direct substrate of the SAG-SCF$^{\beta\text{-TrCP}}$ E3 ubiquitin ligase[213]

It is well known that the activation and translocation of NF-κB to the nucleus is responsible for the transcription of the proinflammatory cytokines tumor necrosis factor-alpha (TNFα) and interleukin-6 (IL-6)[214,215]. The accumulation of IκB upon SAG disruption leads to the inhibition of NF-κB activation and thus decreases inflammatory responses by dendritic cells (DCs) in vitro[50,213]. Thus, inhibition of SAG may regulate the innate immune response of macrophages in a similar manner as in DCs[50]. LysM$^+$ cells (i.e. macrophages and neutrophils) are keys to the in vivo inflammatory response. In light of the regulation of NF-κB by SAG, we tested the hypothesis that *Sag* deficient LysM$^+$ cells would release less proinflammatory cytokines in response to LPS and mitigate LPS induced mortality. Surprisingly, we found that loss of Sag protein in these cells resulted in a net increase in proinflammatory cytokines and furthermore increased LPS-induced mortality. Mechanistic studies showed that disruption of Sag in macrophages, consistent with previous reports[212], reduced the release of inflammatory cytokines by preventing the

degradation of IκBα and thus inhibiting subsequent NF-κB activation. By contrast, Sag deficiency in neutrophils up-regulated the release of inflammatory cytokines and ROS that likely contributed to the net increase in systemic levels of proinflammatory cytokines and increased LPS-induced mortality in response to LPS *in vivo*. Together, these findings suggest that the same molecular pathway – namely Sag – plays a differential role in the activation of macrophages and neutrophils.

RESULTS

Characterization of LysM-Cre/*Sag*$^{fl/fl}$ mice

To determine the role of SAG in the innate inflammatory response – specifically macrophages – we crossed *Sag*$^{fl/fl}$ mice with LysM-Cre transgenic mice, which express Cre recombinase in myeloid cells[216]. Inactivation of *Sag* was verified in macrophages of the peritoneal cavity by RT-PCR analysis (Fig. 3.1).

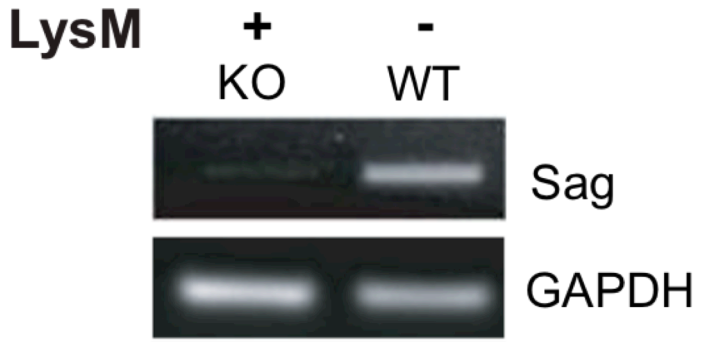

Fig. 3.1 – Characterization of LysM-Cre/*Sag*$^{fl/fl}$ mice. Sag expression is significantly decreased in peritoneal macrophages from LysM-Cre/*Sag*$^{fl/fl}$ mice. Residential peritoneal macrophages were flushed from LysM-Cre^{-}/*Sag*$^{fl/fl}$ wild type (WT) and LysM-Cre^{+}/*Sag*$^{fl/fl}$ knockout (KO) mice, and then subjected to mRNA extraction, followed by RT-PCR.

The mRNA levels of *Sag* were significantly decreased in resident peritoneal macrophages from LysM-Cre^{+}/*Sag*$^{fl/fl}$ (KO) mice compared to LysM-Cre^{-}/*Sag*$^{fl/fl}$ (WT) mice. To determine whether hematopoietic deficiency of Sag in LysM^{+} cells affects their development and/or other cells, we performed serial complete blood count (CBC) analysis of mice at 4 and 12 weeks of age. Sag-deficiency in the myeloid lineage had no significant effect on the total cell numbers of white blood cells, neutrophils, lymphocytes, monocytes, eosinophils, basophils, red blood cells, and platelets in the peripheral blood (Table 3.1).

Parameter	Unit	4 Weeks		12 Weeks	
		WT ($LysM^-$)	KO ($LysM^+$)	WT ($LysM^-$)	KO ($LysM^+$)
WBC#	K/uL	3.72 ± 0.07	4.08 ± 1.52	7.67 ± 1.24	7.64 ± 3.27
NE#	K/uL	0.54 ± 0.13	0.42 ± 0.07	1.98 ± 1.08	1.96 ± 1.00
LY#	K/uL	2.99 ± 0.17	3.38 ± 1.34	5.01 ± 0.89	5.08 ± 1.83
MO#	K/uL	0.16 ± 0.03	0.26 ± 0.14	0.38 ± 0.09	0.49 ± 0.33
EO#	K/uL	0.02 ± 0.03	0.02 ± 0.02	0.23 ± 0.37	0.08 ± 0.11
BA#	K/uL	0.00 ± 0.01	0.00 ± 0.00	0.07 ± 0.05	0.04 ± 0.06
RBC	M/uL	5.70 ± 0.26	6.66 ± 2.12	9.41 ± 2.10	10.55 ± 0.88
HB	g/dL	8.38 ± 0.58	9.46 ± 2.73	12.97 ± 2.64	14.7 ± 0.42
HCT	%	29.68 ± 1.63	33.86 ± 10.03	48.43 ± 11.03	52.75 ± 2.52
PLT	K/uL	469.8 ± 51.9	543.4 ± 150.4	689.7 ± 126.3	725.5 ± 165.4
MPV	fL	3.82 ± 0.26	4.18 ± 0.60	4.23 ± 1.22	4.12 ± 0.33

Table 3.1 – Mouse complete blood count (CBC).

Next, we determined whether deficiency of Sag affected the phenotype of macrophages by performing immunophenotypical analysis of macrophages isolated from the spleen, bone marrow, and peripheral lymph nodes. No differences were observed between WT and KO animals in either absolute numbers of macrophages ($CD11b^+$&$F4/80^+$) or expression of co-stimulatory molecules (MHCII, CD80, CD86, CD40, PD-L1, PD-L2) (Table 3.2). These data indicate that targeted deletion of *Sag* in the myeloid lineage does not result in altered development, total numbers, or phenotype of these cells.

Organ	Marker	WT ($LyzM^-$)	KO ($LyzM^+$)
Spleen	Total Count	4.18e7 ± 7.10e6	4.47e6 ± 1.25e6
	CD11b/F4.80	1.81e6 ± 1.96e5	1.95e6 ± 1.37e5
	MHCII	1.53e6 ± 1.53e5	1.65e6 ± 1.11e5
	CD80	1.29e6 ± 2.01e5	1.41e6 ± 1.29e5
	CD86	1.07e6 ± 1.70e5	1.21e6 ± 8.09e4
	CD40	1.89e5 ± 6.99e4	1.77e5 ± 2.67e4
	PDL1	1.22e6 ± 1.56e5	1.31e6 ± 1.09e5
	PDL2	3.08e5 ± 9.94e4	3.23e5 ± 1.10e4
Bone Marrow	Total Count	2.64e7 ± 2.01e6	2.32e7 ± 2.95e6
	CD11b/F4.80	7.60e6 ± 1.19e6	7.80e6 ± 4.70e5
	MHCII	2.28e6 ± 4.01e5	1.93e6 ± 2.19e5
	CD80	1.21e6 ± 2.43e5	1.25e6 ± 1.28e5
	CD86	1.14e6 ± 2.84e5	1.40e6 ± 3.53e4
	CD40	1.80e5 ± 1.99e4	2.56e5 ± 4.59e4
	PDL1	6.41e5 ± 1.34e5	7.31e5 ± 9.92e4
	PDL2	1.73e5 ± 3.61e3	3.21e5 ± 7.12e3
Peripheral Lymph Nodes	Total Count	6.29e6 ± 1.69e6	8.39e6 ± 5.87e5
	CD11b/F4.80	2.67e5 ± 5.14e4	2.81e5 ± 1.82e4
	MHCII	2.60e5 ± 5.04e4	2.75e5 ± 1.93e4
	CD80	1.25e5 ± 2.58e4	1.42e5 ± 1.21e4
	CD86	2.07e5 ± 2.86e4	2.20e5 ± 2.28e4
	CD40	3.43e4 ± 9.63e3	2.64e4 ± 5.26e3
	PDL1	2.01e5 ± 3.72e4	2.19e5 ± 1.29e4
	PDL2	7.06e4 ± 1.89e4	5.81e4 ± 1.10e4

Table 3.2 – Mouse naïve phenotype.

The *in vivo* responses of Sag-deficiency in myeloid lineage to LPS

Previous studies have shown that SAG knockdown in macrophages results in decreased release of inflammatory cytokines upon LPS challenge[50,212]. Therefore we next tested the hypothesis whether *in vivo* LPS stimulation would result in decreased proinflammatory cytokines and decreased mortality in KO animals. We injected intraperitoneally (i.p) WT and KO mice with a lethal dose of LPS (25 mg/kg). To our surprise, the survival study demonstrated significantly increased mortality in KO mice with Sag deficient myeloid cells (Fig. 3.2).

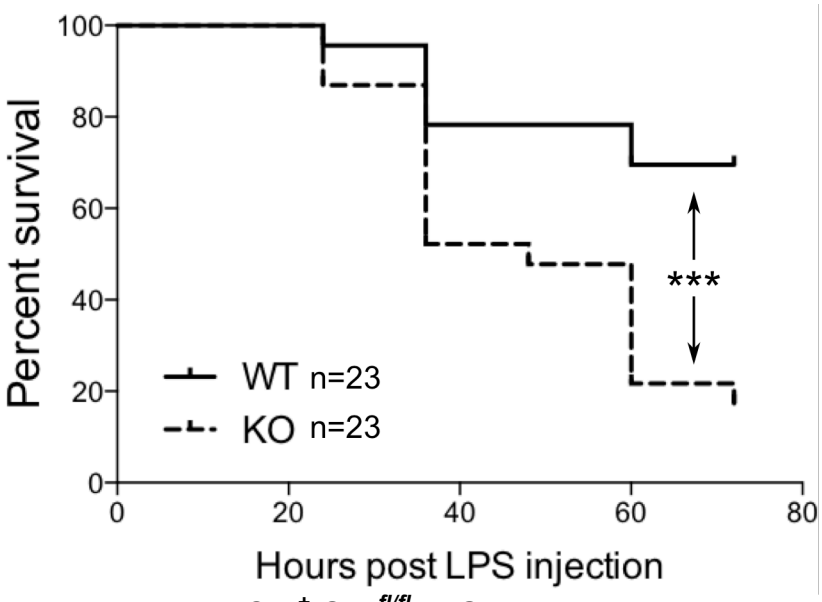

Fig. 3.2 – LysM-Cre^{+}/*Sag*$^{fl/fl}$ (KO) mice exhibit increased mortality to LPS injection. WT and KO mice were injected i.p. with LPS (25 mg/kg body weight), and their survival was monitored and plotted every 12 hours up to 72 hours. n=23 for WT or KO group. *p*=0.0006, log-rank test.

We next measured LPS-induced production of proinflammatory cytokines and observed that the levels of TNFα and IL-6 in the sera of KO mice were significantly higher than those of WT mice 18 hours post LPS injection (Fig. 3.3A-B). These surprising data suggested that mice with LysM Sag deficiency were hypersensitive to LPS.

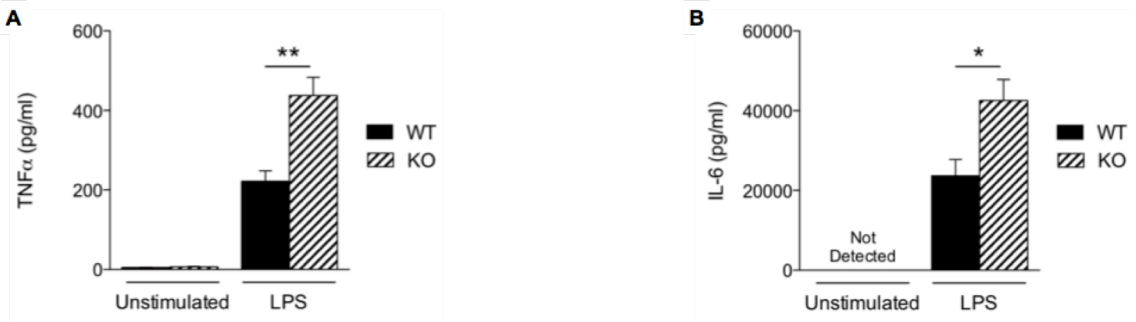

Fig. 3.3 – LysM-Cre^{+}/*Sag*$^{fl/fl}$ (KO) mice exhibit increased LPS-induced proinflammatory cytokines in the sera. TNFα and (**D**) IL-6 in the cardiac sera of mice 18 hours after LPS injection; measured by ELISA. * P < 0.05; ** P < 0.01

The *in vitro* responses of Sag-deficient macrophages to LPS

Previous studies have demonstrated that SAG regulates other innate immune cell responses, such as DCs[50] and macrophages during infection[212]. We next analyzed the response of Sag-deficient peritoneal macrophages stimulated with LPS. We observed that the release of the proinflammatory cytokines TNFα and IL-6 were significantly reduced by Sag-deficient macrophages (Fig. 3.4A-B) with a similar decrease in mRNA transcripts for TNFα and IL-6 (Fig. 3.4C-D) from these cells.

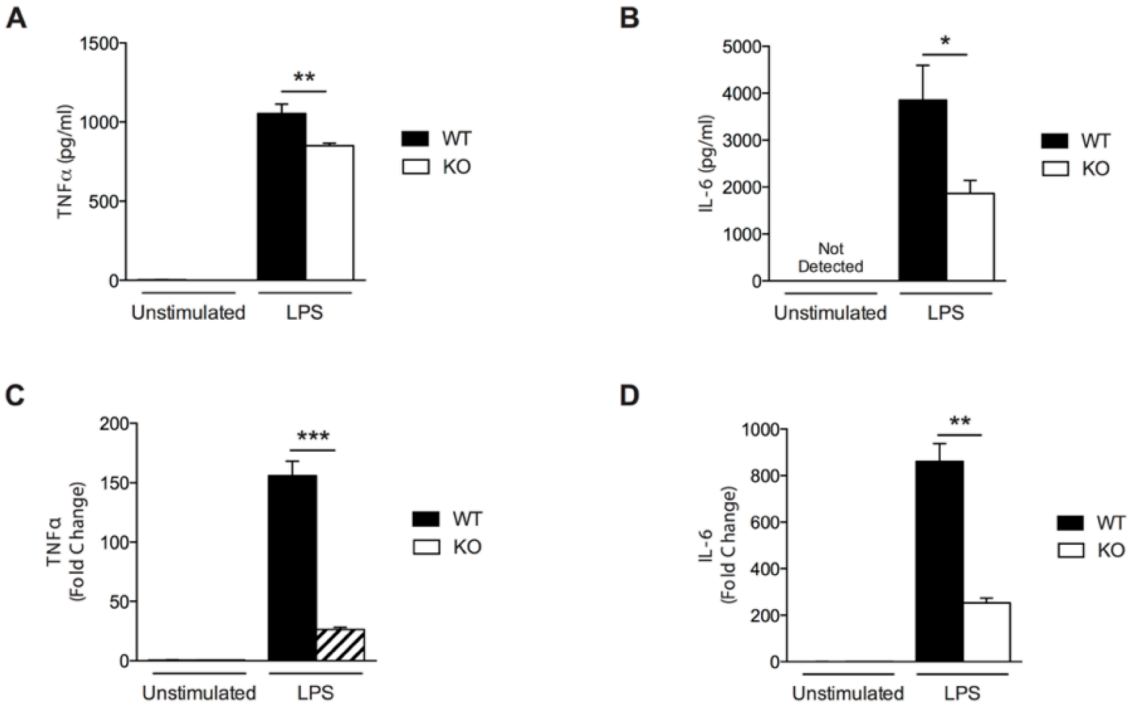

Fig. 3.4 – Sag-deficient macrophages release less TNFα and IL-6 *in vitro*. (**A-D**) Reduced production of proinflammatory cytokines in thioglycollate-elicited peritoneal macrophages from LysM-cre/*Sag*$^{fl/fl}$ mice. Cells were left unstimulated or stimulated with 100 ng/ml LPS for 24 hours. TNFα and IL-6 protein concentrations were measured in cell culture supernatants by **(A&B)** ELISA and (**C**&**D**) mRNA transcript in cells by qPCR.* $P < 0.05$; ** $P < 0.01$

Studies have shown that inactivation of SAG reduces the viability of tumor cells[71]. However, primary bone marrow derived DCs do not exhibit increased apoptosis

upon inhibition of SAG E3 ligase complex[50] suggesting that inactivation of SAG in healthy, non-cancerous cells may not affect cell survival. Thus, we next tested whether primary WT and Sag-deficient macrophages stimulated with LPS resulted in altered cell viability. Once again, we observed no difference between WT and Sag-deficient peritoneal macrophages (Fig. 3.5A).

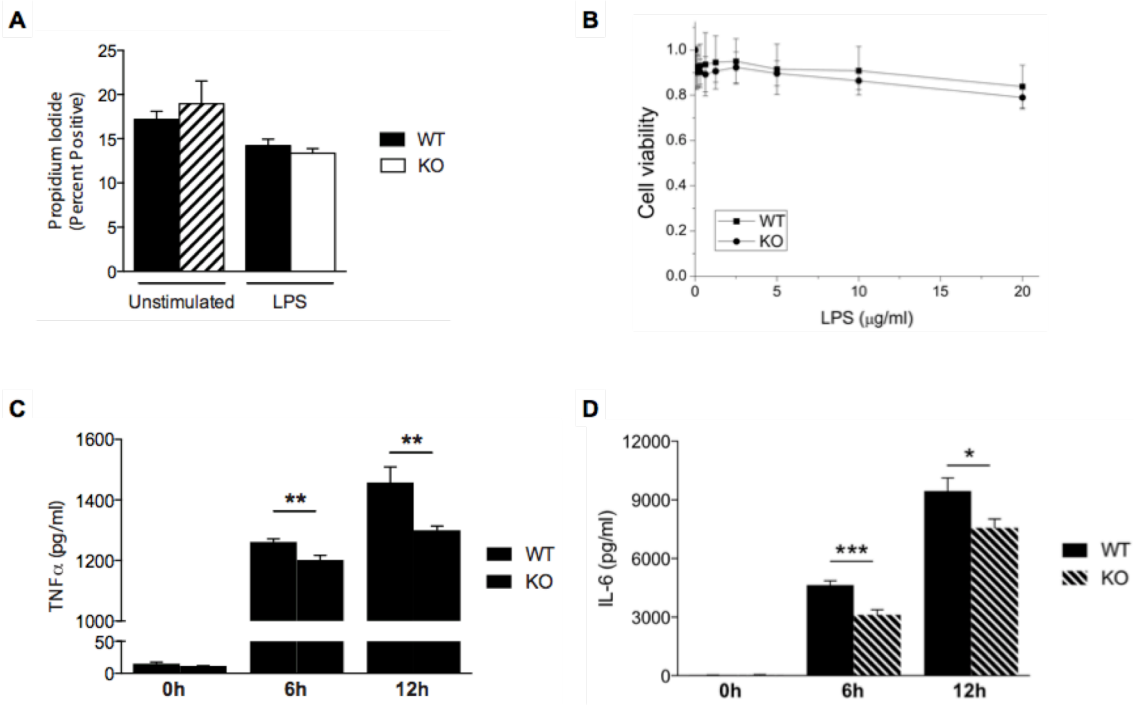

Fig. 3.5 – Sag-deficient macrophage viability and BMDM function. (**A**&**B**) Sag deficiency has no effect on the (**A**) apoptosis (Annexin V/PI) of peritoneal macrophages or (**B**) viability of BMDMs in response to LPS. BMDMs derived from LysM-cre/*Sag*$^{fl/fl}$ mice were treated with 100 ng/ml LPS for 72 hours. The viability of BMDMs treated with various concentrations of LPS for 72 hours in triplicates were normalized to untreated cells and shown as mean ± SEM (n=2) (**B**). (**C&D**) Reduced production of proinflammatory cytokines in BMDMs derived from LysM-cre/*Sag*$^{fl/fl}$ mice. BMDMs were stimulated with 100 ng/ml LPS for 6 and 12 hours. (**C**) TNFα and (**D**) IL-6 release were measured in cell culture supernatants by ELISA. * $p<0.05$; ** $p<0.01$; *** $p<0.001$.

To ensure that the results observed were not specific to macrophages isolated from a particular compartment, we next examined bone marrow derived macrophages (BMDMs). Consistent with our results from peritoneal macrophages, no significant

differences in viability of BMDMs from WT or KO mice were observed (Fig. 3.5B). Further, the release of TNFα and IL-6 cytokines by BMDMs in response to LPS stimulation over a total time period of 12 hours was significantly reduced in the absence of Sag (Fig. 3.5C-D). These data together suggest that Sag deficiency in macrophages significantly impairs LPS-induced release of proinflammatory cytokines, but had no significant effect on the viability of macrophages.

Sag deficient macrophages release less cytokines *in vivo*

To further explore why KO mice were hypersensitive to LPS, we next measured LPS-induced production of proinflammatory cytokines *in vivo*. We injected LPS i.p. (25mg/kg) as before and analyzed macrophages of the peritoneum and spleen by flow cytometry 18 hours later.

Organ	Marker	WT ($LyzM^-$)	KO ($LyzM^+$)
Peritoneal Macrophages	PBS Elicited	3.69e6 ± 4.88e5	4.71e6 ± 9.13e5
	LPS Elicited	2.19e6 ± 9.11e5	2.19e6 ± 2.55e5
Splenic Macrophages	PBS Elicited	8.04e7 ± 1.80e7	7.14e7 ± 2.60e6
	LPS Elicited	9.30e7 ± 1.24e7	8.73e7 ± 1.31e7

Table 3.3 – Elicited macrophages.

However, although the total numbers of macrophages were comparable between WT and KO mice (Table 3.3), the total number of macrophages isolated from the peritoneum and spleen that were producing TNFα and IL-6 were significantly lower (Fig. 3.6A-D) in KO animals, compared to WT. Taken together, these data suggest that in the absence of Sag in myeloid cells mice show increased LPS-induced mortality and increased proinflammatory cytokines in the sera, but the increases were not due to increased cytokine release from macrophages. Thus, these data indicated that the increase in

proinflammatory cytokines contributing to mortality might be from another type of myeloid cell capable of responding to LPS and secreting increased proinflammatory cytokines.

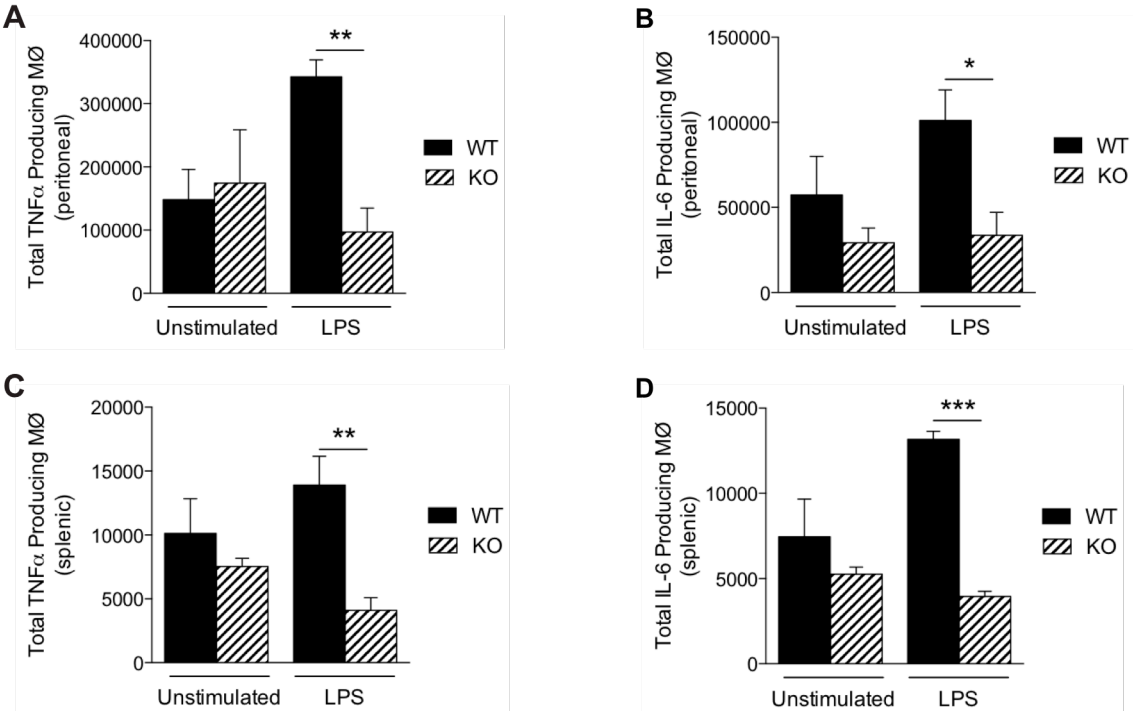

Fig. 3.6 – Sag-deficient macrophages release less cytokines *in vivo*. LysM-cre/*Sag*$^{fl/fl}$ (KO) and *Sag*$^{fl/fl}$ (WT) mice were i.p. injected with PBS or LPS (25 mg/kg body weight). The cells and the blood samples were harvested 18 hours post injection. The total numbers of macrophages producing **(A&C)** TNFα and (**B&D**) IL-6 in the (**A**-**B**) peritoneal cavity and (**C**-**D**) spleen were determined by flow cytometry. N=4 for PBS elicited; N=6 for LPS elicited. * $p<0.05$; ** $p<0.01$; *** $p<0.001$.

Impact of Sag deficiency in macrophages: IκB accumulation

We next pursued the mechanism by which *Sag* deletion causes reduction of proinflammatory cytokines with focus on IκBα/NF-κB, since our previous studies have shown that IκBα is a direct substrate of SAG E3 ligase[213],and SAG disruption prevents the activation and translocation of NF-κB, which contributes to decreased inflammatory cytokines from DCs and to the increased radiosensitivity observed in Sag-null murine

embryonic stem cells[50,213]. Upon stimulation of a cell by TLR4, IκBα is phosphorylated and degraded as a direct substrate of SAG- $SCF^{\beta\text{-}TrCP}$ E3 ubiquitin ligase. To determine if IκBα and NF-κB play a similar role in macrophages as was previously shown in dendritic cells[50], we examined the protein levels of phosphorylated and total IκB in macrophages and found that LPS stimulation resulted in accumulation of phosphorylated IκBα as well as total IκBα in Sag-deficient macrophages (Fig. 3.7), indicating that the degradation of IκB was impaired in the absence of Sag.

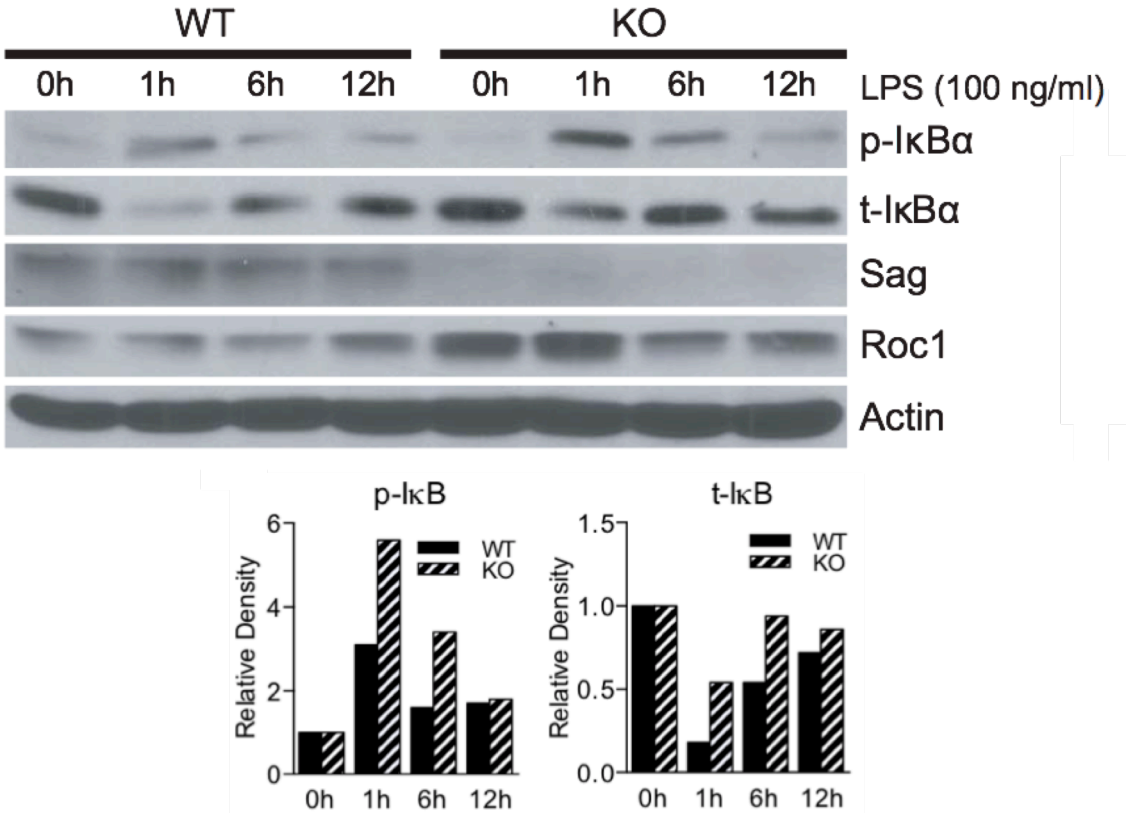

Fig. 3.7 – IκB accumulation in Sag-deficient macrophages. BMDMs derived from bone marrow cells from WT (n=4) and KO (n=4) mice were pooled by group and stimulated with 100 ng/ml LPS for indicated time periods, followed by immunoblot with indicated Abs. Densitometric analysis is shown on the right of blots after normalization with α-tubulin.

Consistent with this notion, we found that nuclear translocation of p65 NF-κB to the nucleus was significantly reduced in Sag-deficient macrophages compared to Sag-competent WT controls (Fig. 3.8).

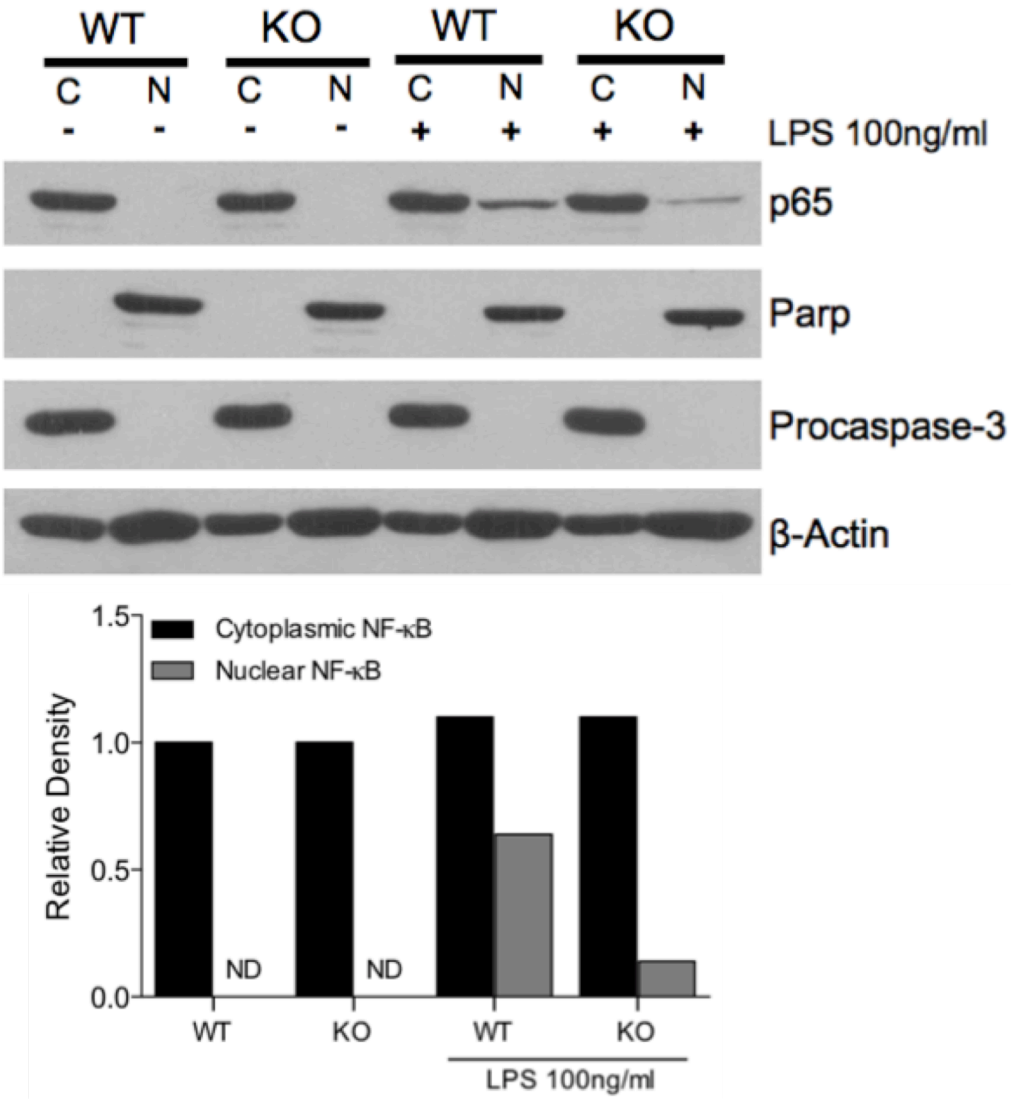

Fig. 3.8 – NF-κB translocation is inhibited in Sag-deficient macrophages. Western blot analysis of p65 isoform of NF-κB protein using nuclear [N] and cytosolic [C] fractions of peritoneal WT and KO macrophages, stimulated concurrently with LPS (100 ng/ml) for 1 hour. Plot on the right of blots shows densitometric analysis of p65 level in the nuclear fraction vs. cytosolic fraction. Parp and Procaspase-3 serve as biomarkers of nuclear and cytoplasmic fractions, respectively.

These data suggest that similar to the effects seen in DCs, Sag disruption affects LPS-induced IκBα degradation, which inhibits NF-κB activation in macrophages, leading to reduced levels of proinflammatory cytokines, such as TNFα and IL-6.

Sag deficiency increases proinflammatory responses by neutrophils

Similar to macrophages, neutrophils are myeloid lineage cells, which also express LysM. Thus, to determine the origin of increased LPS-induced cytokine production in the sera of mice with Sag deficient myeloid lineage cells, we next analyzed the response of neutrophils ($CD11b^+$ & $Gr\text{-}1^+$) to LPS stimulation. We stimulated whole splenocyte cultures with LPS for 6 hours and 18 hours and observed a significant increase in Sag-deficient $CD11b^+$ $Gr\text{-}1^+$-neutrophils producing TNFα (Fig. 3.9A-B).

Fig. 3.9 – Sag-deficient neutrophils release less TNFα and IL-6 in response to LPS. Increased TNFα and ROS production in Sag-deficient neutrophils in response to LPS. Splenocytes from LysM-Cre^-/$Sag^{fl/fl}$ (WT) and LysM-Cre^+/$Sag^{fl/fl}$ (KO) mice (n=5 for each genotype) were stimulated with LPS (100 ng/ml) and TNFα production was analyzed by flow cytometry (**A**) 6 hours and (**B**) 18 hours following stimulation. ** $P < 0.01$; *** $P < 0.001$

As NF-κB is the transcription factor for TNFα, we next examined the translocation of NF-κB from the cytoplasm to the nucleus in neutrophils. In contrast to the results seen in macrophages (Fig. 4B), we did not see a difference in the translocation

of NF-κB in neutrophils (Fig. 3.10). These data suggested that Sag deficiency had a differential role in neutrophils as compared with macrophages.

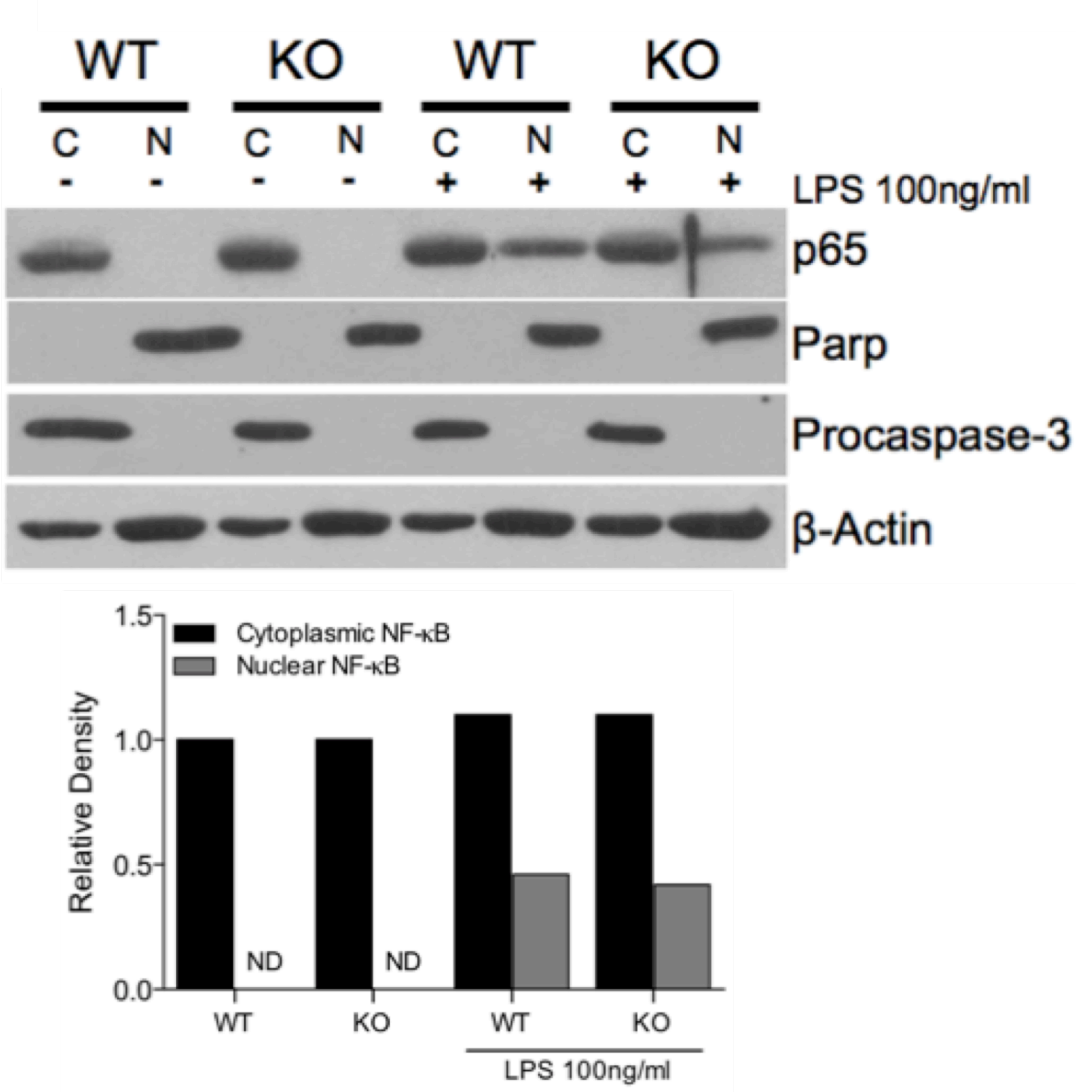

Fig. 3.10 – NF-κB translocation is not inhibited in Sag-deficient neutrophils. Protein analysis by western blot of p65 isoform of NF-κB protein using nuclear [N] and cytosolic [C] fractions of peritoneal WT and KO neutrophils, stimulated concurrently with LPS (100 ng/ml) for 1 hour. Plot at right of blots shows densitometric analysis of p65 NF-κB presence in the nuclear fraction and cytosolic fraction. Parp and Procaspase-3 serve as biomarkers of nuclear and cytoplasmic fractions, respectively.

We next explored why Sag deficiency in neutrophils causes an increase in TNFα release in contrast to what was observed in macrophages. Given that neutrophils are

mediators of ROS[217] and SAG is known to be an ROS scavenger[69,70], we tested the hypothesis that increased cytokine release from neutrophils might be due to increased ROS in these cells upon *Sag* deletion. We harvested and stimulated splenocytes with LPS (100ng/ml) from WT and KO mice and gated for ROS in neutrophils. We observed a significant increase in the production of ROS in neutrophils of KO mice, although the basal level of ROS was relatively lower (Fig. 3.11A-B). To determine the mechanism by which the ROS level could be induced to a higher degree in Sag-deficient neutrophils, we focused on NRF2, an antioxidant transcription factor, which is induced by ROS[218,219]. We stimulated whole splenocyte cultures with hydrogen peroxide (H_2O_2) and examined the percentage of neutrophils expressing NRF2. Following H_2O_2 stimulation for 3 hrs, we observed significantly less NRF2-positive neutrophils in Sag-deficient mice (Fig. 3.11C).

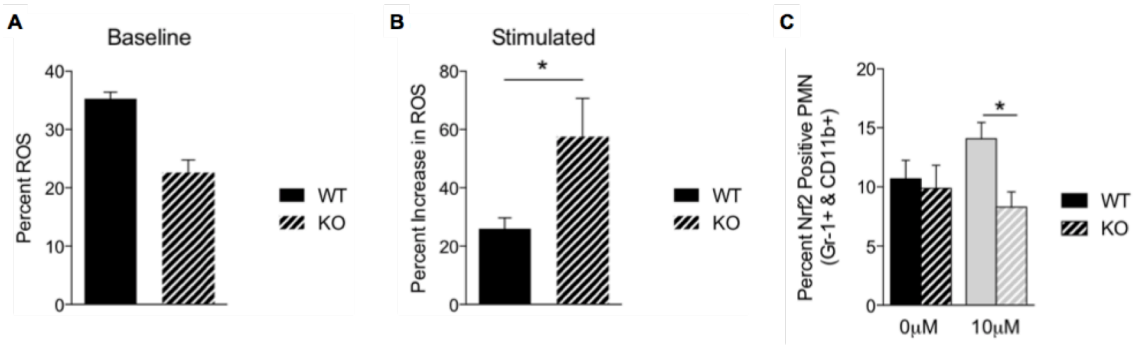

Fig. 3.11 – Sag-deficient neutrophils exhibit increased ROS and decrease NRF2 transcription factor. (**A-B**) ROS production upon stimulation with LPS: (**A**) Baseline ROS levels and (**B**) LPS stimulated levels (100 ng/ml for 1 hour) of ROS in WT and KO mice (n=5). (**C**) Percentage of Nrf2 positive cells in WT and KO mice (n=5) analyzed by flow cytometry after 3 hours of stimulation with hydrogen peroxide (H_2O_2).

These data together suggest that increased ROS levels in Sag-deficient neutrophils in response to stimuli is likely due to lack of Sag-mediated ROS scavenging and reduced NRF2 expression with subsequent reduced production of other antioxidants.

We next ensured that cells that did not express LysM enzyme were unaffected. We, therefore, stimulated WT and KO bone marrow derived DCs (BMDCs) with LPS and examined the production of TNFα and IL-6, and found no difference in either the release of TNFa (Fig. 3.12A) and IL-6 (Fig. 3.12B) or in the mRNA expression of these proinflammatory cytokines (Fig. 3.12C-D). These data indeed suggested that Sag deficiency in $LysM^{+}$ cells did not affect non-LysM expressing cells.

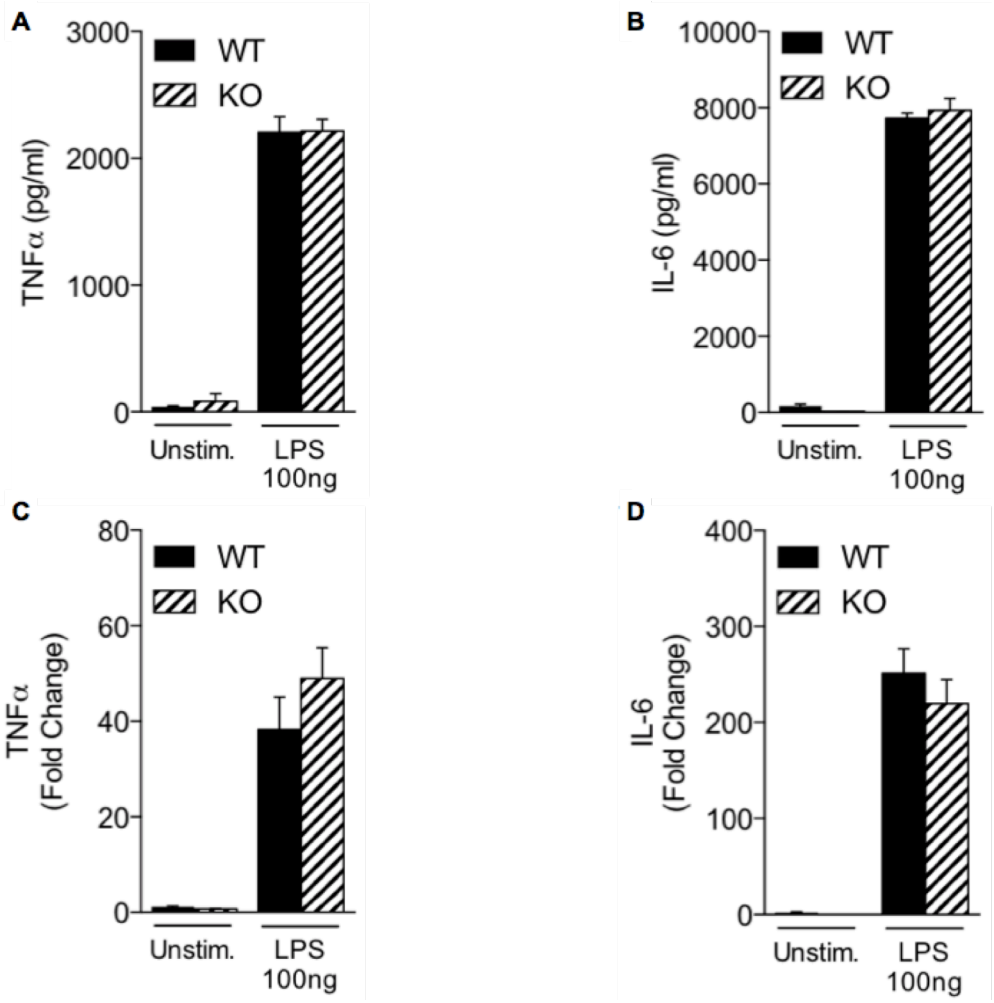

Fig. 3.12 – The function of BMDC from SAG-deficient mice are not different from SAG-competent mice. (**A**) TNFα (**B**) and IL-6 cytokines and (**C-D**) corresponding mRNA expression released by bone marrow derived dendritic cells (BMDCs) stimulated with LPS (100ng/ml) for 6 hours. * $p<0.05$; ** $p<0.01$; *** $p<0.001$.

DISCUSSION

Our data has shown that Sag deficiency in $LysM^{+}$ mice has no effect on the total CBC including myeloid cells of the innate immune system, specifically macrophages and PMNs (Table 3.1). However, although the cell number in myeloid lineage was unaltered upon *Sag* deletion, a significant LPS-induced increase in proinflammatory cytokines in the sera as well as an increase in mortality were observed in KO mice. Macrophages and neutrophils are the first cells of the innate immune system to respond to pathogenic insult to the host. Both cell types are known to release proinflammatory cytokines in response to PRR ligation, but whether disparate mechanisms exist of inducing inflammatory cytokines, remains unknown. Thus, we explored cell-specific responses to LPS and found that Sag deficient macrophages release less proinflammatory cytokines with a concomitant decrease in IκB degradation and subsequent decrease NF-κB translocation to the nucleus, when compared to WT controls. Further, there was no alteration in the KO cells viability, similar to our previous examination of DCs[50]. Despite the decreased release of LPS induced proinflammatory cytokines by macrophages both *in vitro* and *in vivo*, mice with Sag deficient myeloid cells intriguingly exhibited an increased mortality rate in response to LPS injection i.p. Hence, we next examined the response of neutrophils to LPS stimulation and found a surprising increase in release of TNFα and a concurrent increase in ROS with a corresponding decrease in NRF2 transcription factor, responsible for the transcription of antioxidant molecules.

The reasons for the differential response to Sag deficiency in macrophages and neutrophils are unclear at the present time. We posit that these responses are likely due to differences in cell context in which different Sag substrates are targeted for degradation

in cell-type dependent manner. Indeed, the degradation of IκB is inhibited in macrophages and dendritic cells[50], but this inhibition is not seen in neutrophils upon *Sag* deletion.

Innate immune signaling is poorly understood. Our finding that Sag protein plays a differential role in macrophages and neutrophils is significant and novel as it is the first demonstration that Sag function can be determined by targeting – or not targeting – IκBα in two types of critical cells of the innate immune system. This observation is consistent with our recent finding that Sag plays a tissue specific role during Kras-triggered tumorigenesis, in which Sag functions as a Kras-cooperator in the lung[220], or Kras-antagonist in the skin[221]. Furthermore, *Sag* deletion in keratinocytes results in NRF2 accumulation [221], whereas deletion of *Sag* in neutrophils causes NRF2 reduction (Fig. 3.11C). Future studies will be directed to further dissect the underlying mechanism.

In summary, our findings demonstrate that Sag protein differentially regulates inflammatory responses of myeloid cell subsets. In macrophages, disruption of Sag reduces the release of inflammatory cytokines by preventing the degradation of IκBα, which blocks translocation of NF-κB to the nucleus (Fig. 3.13).

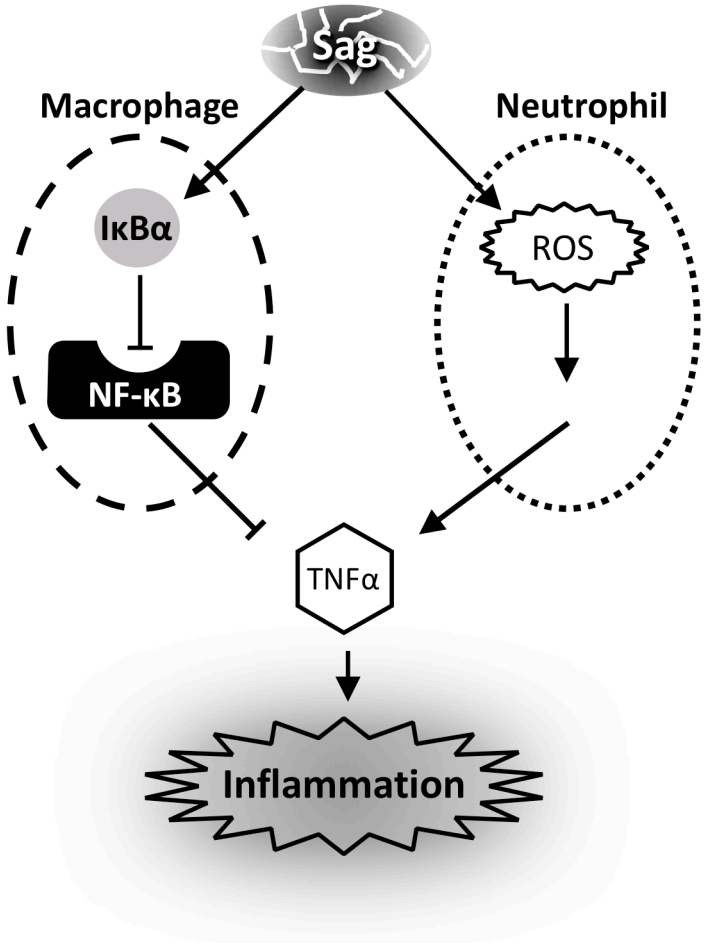

Fig. 3.13 – Model of mechanism. Disruption of Sag in macrophages (left arrow) prevents the degradation of IκBα, which blocks NF-κB from translocating to the nucleus, thus blocking the transcription of proinflammatory cytokines. In neutrophils (right arrow), the depletion of SAG, here acting as a ROS scavenger, results in increased ROS production, decreased NRF2, and increased ROS-induced TNFα to trigger inflammation

In neutrophils, disruption of Sag increases the release of inflammatory cytokines by increased ROS production, thus contributing to increased mortality *in vivo* in response to LPS (Fig. 3.13).

MATERIALS AND METHODS

Mouse studies

The *Sag*$^{fl/fl}$ mice were generated as previously described[222,223]. The LysM-cre mice were purchased from the Jackson Laboratory (Stock number: 004781). All procedures were approved by the University of Michigan Committee on Use and Care of Animals. Animal care was provided in accordance with the principles and procedures outlined in the National Research Council Guide for the Care and Use of Laboratory Animals.

Macrophage preparation

For BMDMs preparation, bone marrow cells were flushed from the femurs and tibiae of mice and cultured in complete RPMI in the presence of 20% medium conditioned by L929 mouse fibroblasts, as described[224]. On day 7, BMDMs were split and used as indicated. To isolate thioglycollate-elicited macrophages, mice were i.p. injected with 1.5 ml of 5% thioglycollate and peritoneal macrophages were flushed out 3 days post injection.

Dendritic cell preparation

Bone marrow cells were flushed from the femurs of 8- to 12-week- old female C57BL/6 mice and cultured in 150 x 15-mm CytoOne petri dishes (USA Scientific, Ocala, FL) at $1x10^7$ in 20ml of RPMI supplemented with 10% FCS, 4mM L-glutamine, 10 U/ml penicillin, 100 μg/ml streptomycin, 0.5 mM 2-ME, 20ng/ml GM-CSF. On day 4, 20ml of fresh complete RPMI containing 20ng/ml GM-CSF was added to each culture. After 7

days of culture, the loosely adherent cells were harvested and purified using anti-CD11c magnetic microbeads (Miltenyi Biotec Ltd., Auburn, CA) and the autoMACS (Miltenyi Biotec).

LPS administration

Mice at 2 months old were subjected to i.p. injection of *Escherichia coli* LPS (0111:B4, Sigma, L4391) at 25 mg/kg body weight and were monitored for survival. For short-term studies, mice were sacrificed 18 hours post LPS i.p. injection, followed by blood collection with cardiac puncture. Peritoneal cavity was then washed with PBS and spleens were collected.

Gene expression

Total RNA was isolated from cells with Trizol reagent (Invitrogen). Complementary DNA was made from RNA with Superscript III (Inivitrogen) and subjected to reverse transcription PCR or quantitative real-time PCR (qRT-PCR) with a 7500 Real Time PCR system (Applied Biosystems). The cycling program for qRT-PCR was set as follows: 50 °C 2 min, 95 °C 10 min for the PCR initial activation and 45 cycles of denaturation at 95 °C for 15 sec, annealing and extension at 60 °C for 1 min. The sequences of Sag, TNFα, IL-1β, IL-6, IL-10, and GAPDH are as follows: SAG-Fwd: 5'- CGC TGA GCC ACC GTA CCT -3', SAG-Rev: 5'- TTA CAC TCT CCC CAG ACC ACA A -3'; TNF-Fwd: 5'- CCC CAA AGG GAT GAG AAG TT -3', TNF-Rev: 5'- CTT GGT GGT TTG CTA CGA CG -3'; IL6-Fwd: 5'- TCA TAT CTT CAA CCA AGA GGT AAA A -3', IL6-Rev:

5’- CGC ACT AGG TTT GCC GAG TA -3’; GAPDH-Fwd: 5’- GCC GCC TGG AGA AAC CTG CC -3’, GAPDH-Rev: 5’- GGT GGA AGA GTG GGA GTT GC -3’.

Western blot analysis

BMDM cells stimulated with LPS for different time periods were harvested, lysed and subjected to Western blotting, using various antibodies as follows: Sag monoclonal mouse antibody was raised against the RING domain (AA44-113) [225], Roc1 polyclonal rabbit antibody [226], pho-IκBα (Cell Signaling), IκBα (Santa Cruz), p65 (Santa Cruz), Parp (Cell Signaling), Procaspase-3 (Santa Cruz), and actin (Sigma), as a loading control.

ATPlite assay

BMDM cells were seeded into 96-well plates with 5,000 cells per well in triplicate and treated with various concentrations of LPS for 3 days followed by ATPlite assay using an ATPlite kit (Perkin Elmer) according to the manufacturer's instructions.

Cytokine detection

Isolated peritoneal and BMDC were seeded on 6-well plates at $3x10^6$ cells/well. Unstimulated and LPS-stimulated cells were cultured for indicated period. Supernatants were subsequently collected and stored at -20°C until analysis. TNFα and IL-6 ELISA kits were purchased from R&D Systems and performed as per the manufacturers’ instructions and read at 450nm by a SpectraMax microplate reader (Molecular Devices, Sunnyvale, CA).

Flow cytometry

To analyze macrophage surface phenotype, peritoneal macrophages were incubated in the presence or absence LPS (Sigma). Cells were then harvested and stained with CD11b-conjugated FITC (Clone: M1/70) and F4.80-conjugated APC with the following per triplicate group: Annexin V (BD Biosciences), CD80 (Clone: 16-10A1), CD86 (Clone: GL-1), CD40 (Clone: 3/23), MHCII-I-Ab (Clone: AF6-120.1), PD-L1 (Clone: MIH5), PD-L2 (Clone: TY25). All flow cytometry Abs were purchased from eBiosciences except for NRF2 (Clone: D1Z9C) obtained from Cell Signaling (Beverly, MA). Stained cells were then analyzed with an Accuri C6 Flow Cytometer (BD Biosciences).

Statistical analysis

The two-tailed Student *t*- test was used for the comparison of parameters between groups. Survival analysis was performed by Kaplan-Meier analysis. Statistical significance was determined as $p<0.05$.

CHAPTER IV

SAG/RBX2 DEPENDENT NEDDYLATION REGULATES T CELL RESPONSES

ABSTRACT

Neddylation is crucial for the degradation of certain proteins. However its role in regulating T cells is poorly understood. Neddylation activates the cullin RING ligase (CRL) complex, an E3 ligase, responsible for the ubiquitination of a specific subset of proteins. An adapter element of the CRL – sensitive to apoptosis gene (SAG) – is critical for the function of CRL-mediated ubiquitination and thus deletion of SAG regulates the neddylation pathway. We explored the role of SAG and thus neddylation in T cells by utilizing two different, but complementary approaches, namely, chemical inhibition with small molecule MLN4924 and a novel genetic knockout (KO). We generated T cell-specific SAG deficient animals by crossing B6 LCK-Cre mice with B6 $SAG^{fl/fl}$ mice. The KO animals were viable and splenic and thymic analyses showed no significant differences in the numbers of conventional T cells (Tcons) and Tregs between KO and WT littermate controls. In vitro functional analysis of Tcons, however, revealed that stimulation of $SAG^{-/-}$ T cells with allogeneic irradiated splenocytes, exhibited significantly decreased proliferation of allo-T cells. Phenotypic analysis following stimulation demonstrated that $SAG^{-/-}$ T cells showed fewer activated cells ($CD69^{+}$, $CD62L^{-}CD44^{+}$) and greater expression of naïve ($CD62L^{+}CD44^{-}$) cells when compared to

WT-SAG competent T cells. The SAG deficient T cells also demonstrated reduced expression of T effector signature cytokines, IL-17, IFN-γ and IL-4. Similar reduction in proliferation, activation marker expression, and release of cytokines was observed when the WT-T cells were treated with small molecule inhibitor of neddylation, MLN4924. We next determined the in vivo relevance of SAG and neddylation in Tcons by utilizing the clinically relevant, major histocompatibility complex (MHC) disparate (C57BL/6→BALB/c) model of allogeneic BMT and received T cells from either the WT B6 or $SAG^{-/-}$ B6 animals. The allogeneic animals that received $SAG^{-/-}$ T cells demonstrated markedly reduced clinical GVHD and significantly increased survival when compared to those that received WT-B6 T cells. Similar results were observed in B6→B6D2F1 model. To further confirm our results and to determine potential translational application, we utilized the small molecule MLN4924, once again in the B6→BALB/c system. Mice receiving MLN4924 demonstrated significantly decreased clinical GVHD and improved survival. Our studies thus demonstrate that SAG is a novel molecular target for regulating T cell responses and mitigating GVHD. Furthermore, the clinical availability of the small molecule, MLN4924, suggests that this strategy could be tested in carefully designed human clinical trials for attenuating GVHD.

INTRODUCTION

T cell function is critical for a competent immune response[19]. T cell activation is the result of the stimulation of T cell receptor (TCR) and necessary co-stimulatory receptors which trigger signaling cascades ultimately resulting in cytokine production, clonal proliferation, lineage differentiation, and adaptive immune memory[227,228]. There are two main subsets of T cells that express either $CD4^+$ glycoprotein or $CD8^+$ glycoprotein[19]. $CD4^+$ T cells recognize cognate peptide presented by antigen presenting cells (APCs) expressing major histocompatibility complex (MHC) class II molecules and subsequently differentiate into several T effector subtypes including T_H1, T_H2 and T_H17 cells that express IFNγ, IL-4, and IL-17, respectively[20]. These lineage 'signature' cytokines direct the function and response of accessory-immune cell functions, such as macrophages or B cells. By contrast, $CD8^+$ T cells recognize viral peptides presented by cells expressing MHC class I molecules leading to the release of cytotoxic granules causing the target cell to undergo apoptosis[229]. Thus, $CD8^+$ T cells are known as cytotoxic T lymphocytes (CTLs).

T cells are central to the efficacy of allogeneic bone marrow transplantation (allo-BMT) – a critical and curative interventional therapy for patients with aggressive hematological malignancies[230,231]. However, 40-50% of allo-BMT recipients experience severe transplant related complications known as graft versus host disease (GVHD), leading to high transplant related mortality[83]. Recent advances have indicated that post translational protein modifications (PTMs) play an important role in GVHD pathophysiology[57,232,233].

PTMs modulate cellular processes[234]. However, the role of T cell PTMs in the initiation of GVHD is unknown. Moreover, intracellular protein signaling pathways that are critical for T cell functions – and the regulation thereof – are poorly understood. The PTM ubiquitination, typically demarcates a protein for degradation thereby regulating the proteins location, function, and lifespan – although ubiquitin attachment can activate a protein under certain circumstances[204]. Neddylation, a type of PTM, modulates the ubiquitination of a specific subset of proteins[68] through the activation of the cullin ring ligase (CRL) degradation scaffolding (an E3 ligase) through the attachment of the ubiquitin-like molecule, neural precursor cell expressed developmentally downregulated protein 8 (NEDD8) to the cullin protein backbone of the CRL complex[67]. NEDD8 molecule must be activated by an ATP-dependent specific E1 enzyme known as NEDD8 activating enzyme (NAE) prior to its transfer to the E2 molecule called NEDD-conjugating enzyme (Ubc12), which in turn transfers NEDD8 to the cullin E3 ligase backbone. NEDD8 attachment to cullin serves as a critical activating step that results in the recruitment of the multi-subunit components composing the CRL complex[67]. There are seven known cullin proteins (CUL1, CUL2, CUL3, CUL4A, CUL4B, CUL5, and CUL7) that each facilitates the ubiquitination of proteins based upon their own CRL-complex substrate specificity[67]. One component of the CRL-5 complex – an adaptor molecule known as sensitive to apoptosis gene (SAG) / RING box protein 2 (RBX2) / RING finger protein 7 (RNF7) – interfaces with E2-ubiquitin conjugates bringing them into close proximity with the target substrate protein and thus leading to mono- or poly-ubiquitination[69-71]. Previous studies have shown that silencing SAG by siRNA inhibits

the CRL complex, thereby regulating the neddylation pathway[50,71-73,211,226]. However, such molecular knockdown methods are prone to off target effects[235-237].

Another method of regulating the neddylation pathway is through the use of a pharmacological small-molecule inhibitor that was recently developed, MLN4924. MLN4924 showed remarkable specificity and potency for inhibiting NAE, thus preventing the initial activation of NEDD8 molecule and thereby blocking the neddylation pathway[75]. Subsequent studies utilizing MLN4924 have exhibited its ability to potently suppress inflammatory responses[50,201] and others have shown MLN4924 to be a promising agent in the inhibition of cancer cells lines – including human pancreatic cells[79], breast cancer cells[80], and liver cancer cells[81]. These promising preclinical results have led to the advancement of MLN4924 to phase 1 clinical trials for the treatment of both hematological and non-hematological cancers[205,206].

Neddylation has been shown to be critical for the function of select immune cell subsets[50,238,239]. Furthermore, previous studies have partially examined the role of neddylation in T cells, albeit only in the $CD4^+$ T cell subset[239]. To that end, Jin et. al. utilized the primary methodology of shRNA knockdown of Ubc12 (E2) molecule (encompassing the possibility of a number of off-target effects) [235-237], which globally inhibited all seven CRL complexes.

In this study, we report the generation of a targeted knockout mouse possessing a deficiency of T cell-specific SAG protein – thereby selectively inhibiting CRL-2 and -5, which is in stark contrast to previous studies utilizing global inhibition of all seven CRL

complexes. We found that T cell-specific SAG deficiency resulted in diminished allo-T cell proliferation and cytokine release *in vitro* and decreased GVHD clinical scores, improved survival, and decreased inflammatory cytokines in the sera following allo-BMT, *in vivo*. These *in vivo* results corresponded with fewer activated donor T cells ($CD44^{hi}$ and $CD69^{+}$) and increased naïve donor T cells ($CD62L^{+}CD44^{-}$) in allo-BMT recipients of KO T cells, 7 days and 14 day following allo-BMT. Furthermore, mechanistic studies suggested that the decreased T cell functions observed were not due to inhibition of NF-κB as in other immune cell subsets[50,201], but rather through a disparate accumulation of the suppressor of cytokine signaling (SOCS) protein. Utilizing a different yet complementary approach, we treated recipients of allo-BMT with MLN4924 that recapitulated the results seen in mice with a targeted deletion of SAG in T cells.

Our data thus represent a novel *in vivo* method of targeting specific CRL complexes allowing for the discovery of CRL-subtype specific substrates. Furthermore, we report a novel molecular mechanism of neddylation in T cells, which was heretofore unknown. Additionally, the results of our studies utilizing the small molecule inhibitor of neddylation, MLN4924, and its clinical availability suggest that this strategy could be tested in carefully designed human clinical trials for attenuating GVHD.

RESULTS

MLN4924 inhibits neddylation but is not cytotoxic to T cells: We have previously shown that inhibition of neddylation decreases the function of DCs[50]. Therefore, we hypothesized that deficiency of neddylation will regulate T cell proliferative responses. MLN4924 has previously been shown to inhibit neddylation in a variety of cell types, including immune cells[50,75]. Thus, we incubated CD90.2^{+} T cells in the presence of MLN4924 at 100nm and 500nm. We observed only a 25% decrease in neddylation – indicated by the presence of the higher molecular weight band of Cul-1 – at the 100nm concentration (Fig. 4.1A) over a time period of 6 hours. By contrast, when T cells were treated with MLN4924 at 500nm we observed the higher molecular weight band was absent within two hours of treatment (Fig. 4.1B) suggesting that MLN4924 indeed inhibited neddylation in T cells.

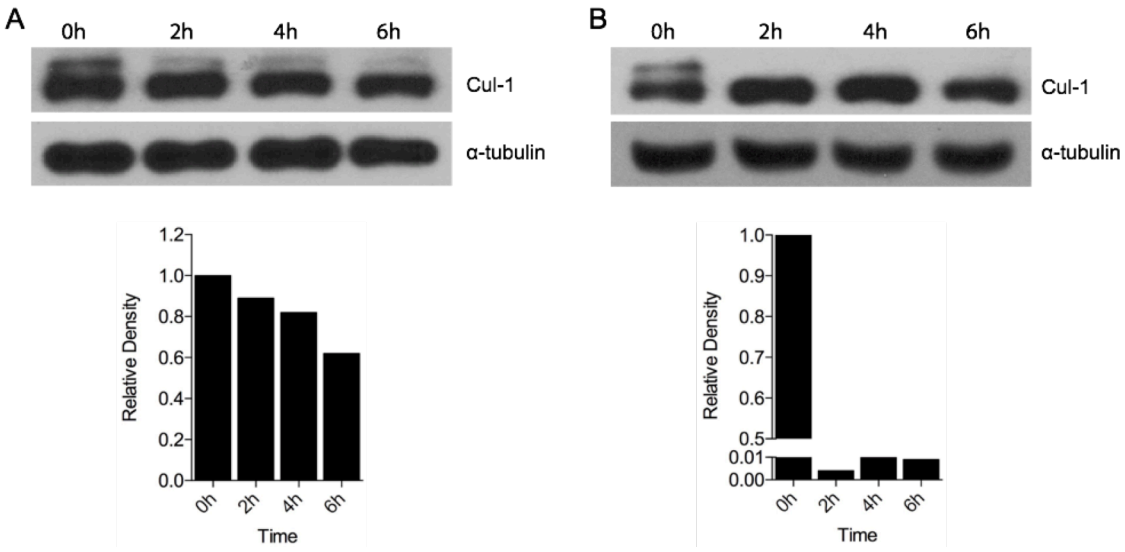

Fig. 4.1 – MLN4924 inhibits neddylation in T cells. Incubation of MLN4924 with CD90.2+ T cells at (**A**) 100nm and (**B**) 500nm. 100nm resulted in only partial inhibition of neddylation over a course of 6 hours. By contrast 500nm inhibited neddylation within 2 hours.

Although MLN4924 does not affect viability of DCs[50], it has been shown to by cytotoxic to cancer cells[79-81]. Thus we next wanted to ensure that MLN4924 was not cytotoxic to T cells at doses that deneddylated cullin protein. Therefore, we cultured T cells in the presence or absence of the indicated concentrations of MLN4924 and examined the cells resulting Annexin V positivity. We saw no difference in the viability of T cells at either 100nm or 500nm (Fig. 4.2).

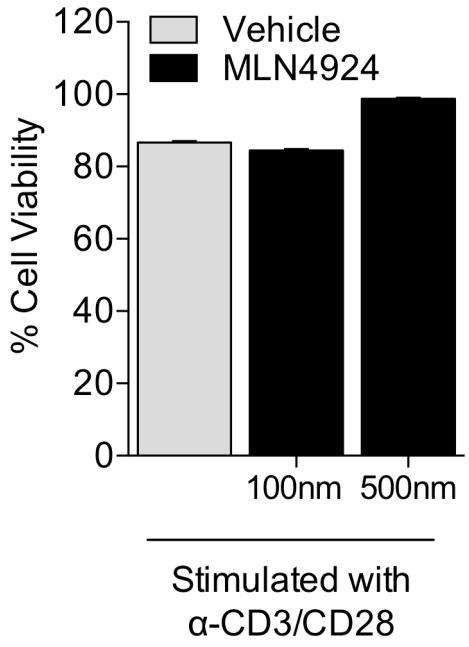

Fig. 4.2 – MLN4924 does not alter viability of T cells. Incubation of MLN4924 with CD90.2+ T cells at 100nm and 500nm does not alter the viability of T cells over the course of 16 hours.

Inhibiting neddylation decreases T cell functions: We have previously shown that culture of DCs with MLN4924 decreases allo-T cell responses and further, that MLN4924 has a DC intrinsic effect by decreasing their stimulatory capacity[50]. However, whether inhibition of neddylation in T cells diminishes their proliferative capacity is unknown. To test this, we next utilized a mixed lymphocyte reaction (MLR) in which $^{[3]}$H

is taken up and incorporated into proliferating cells. We cultured irradiated C57BL/6 (H-2^b) BMDC with BALB/c (H-2^d) CD90.2^+ T cells in the following experimental culture groups: 1) vehicle treated, 2) MLN4924 was applied to the culture at the time of plating, 3) T cells that had been pretreated with MLN4924 for 6 hours were co-cultured with DCs in the absence of drug, and 4) MLN4924 pretreated T cells were cultured with MLN4924 present throughout the co-culture. We observed a significant decrease in all groups cultured with MLN4924, compared to vehicle treated controls after 72 hours (Fig. 4.3A) and 96 hours (Fig. 4.3B) of culture. Interestingly, cultures that contained pretreated T cells, but that did not have MLN4924 present during co-culture, still exhibited a significant decrease in T cell proliferation suggesting that inhibition of neddylation has a T cell-intrinsic effect (Fig. 4.3A). Further, culture of MLN 4924-pretreated T cells with drug present throughout co-culture, resulted in an even greater decrease in T cell proliferation suggesting that MLN4924 also has an impact on DCs, confirming our previous data[50] (Fig. 4.3A).

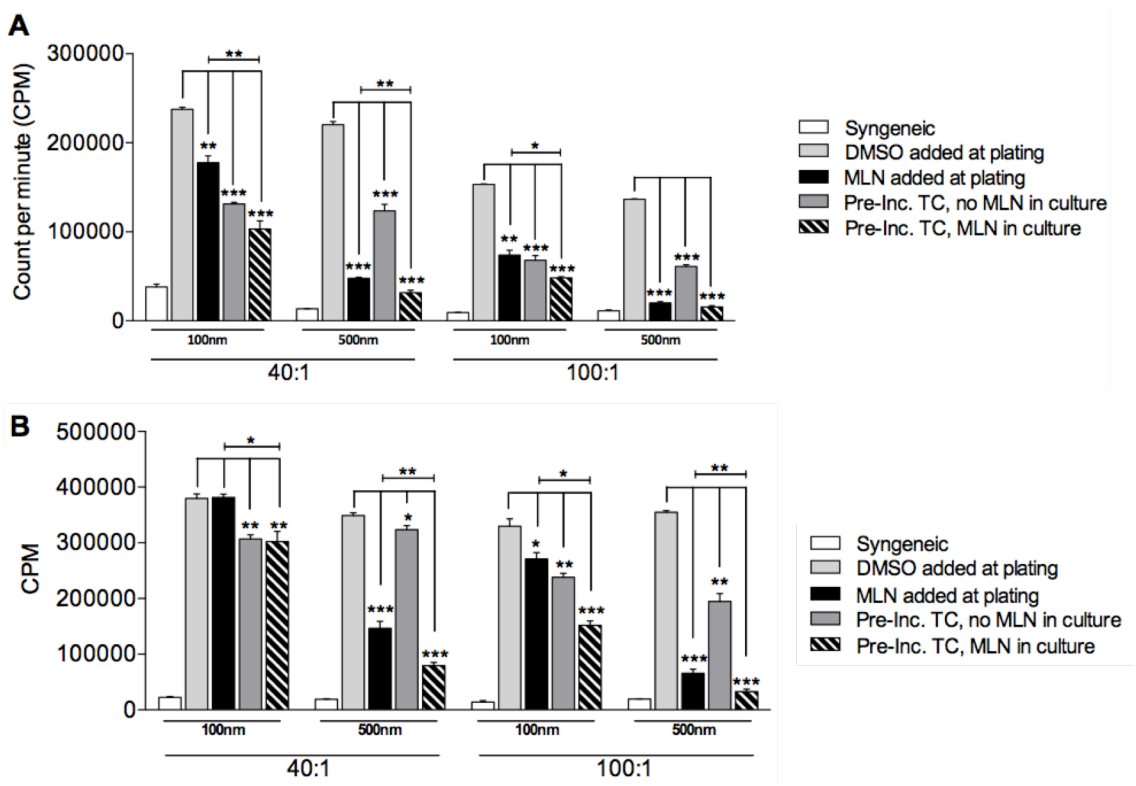

Fig. 4.3 – Neddylation has intrinsic role in T cell function. Mixed lymphocyte reaction of irradiated DC and CD90.2+ T cells for (**A**) 72 hours and (**B**) 96 hours at 40:1 and 100:1 ratios. * $P < 0.05$; ** $P < 0.01$; *** $P < 0.001$

In addition to proliferating in response to stimulation, T cells release lineage specific cytokines that have many paracrine effects on other immune cell subsets[20]. Thus, we next examined IL-2 (an activation cytokine) and IFNγ, IL-4, and IL-17, which are Th1, Th2 and Th17 lineage cytokines, respectively. We saw that all groups treated with MLN4924 exhibited decreased cytokine production (Fig. 4.4A-D). When we next utilized another method of TCR/co-receptor stimulation, α-CD3 and α-CD28, we observed a similar decrease T cell proliferation (Fig. 4.4E).

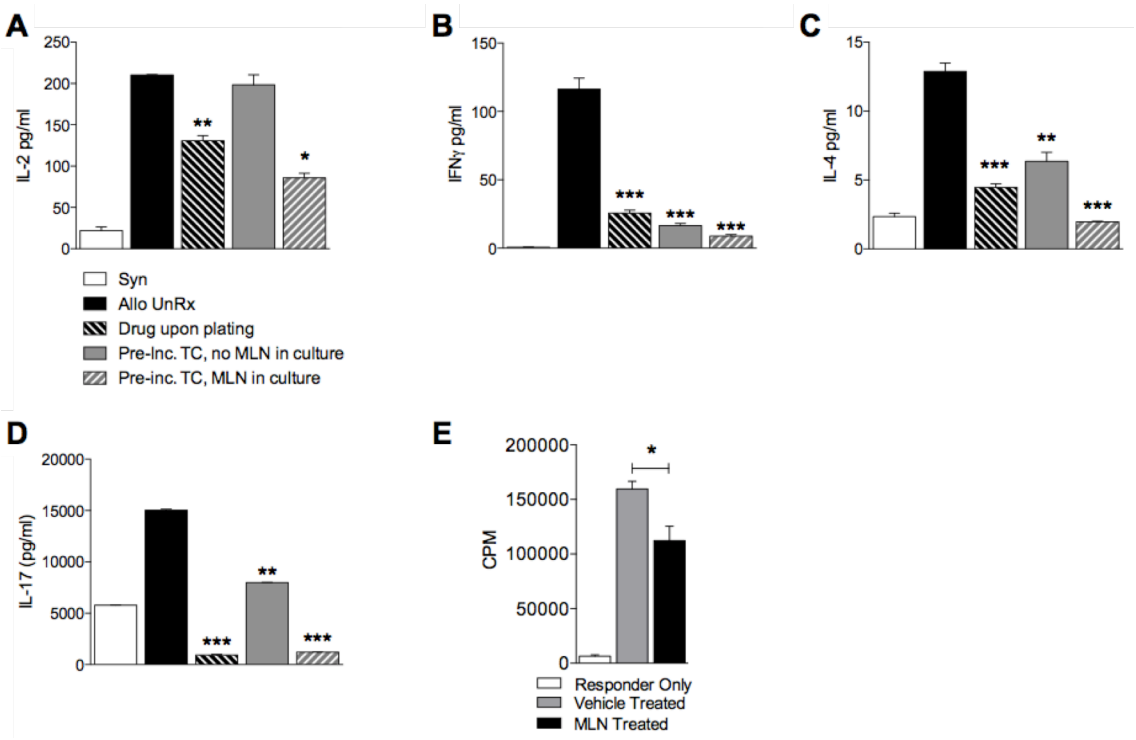

Fig. 4.4 – Inhibiting neddylation decreases T cell cytokines. Neddylation inhibition of T cells with MLN4924 decreases the realease of (**A**) IL-2, (**B**) IFNγ, (**C**) IL-4, and (**D**) IL-17 after allogeneic stimulation.
* P < 0.05; ** P < 0.01; *** P < 0.001

Next, we utilized CFSE and Annexin V staining to measure the proliferation and viability dynamics of T cells treated in the presence or absence of vehicle or MLN4924 and stimulated with α-CD3 and α-CD28 for 48 hours. We saw that proliferation of T cells treated with MLN4924 at the time of plating was significantly reduced compared to vehicle control without an increase in cell apoptosis (Fig. 4.5A, plot 4). Further, when T cells were stimulated and allowed to proliferate for 24 hours prior to the addition of MLN4924, we still observed a significant decrease in T cell proliferation (Fig. 4.5A, plot 3). Indeed, comparison of the T cells that proliferated unimpeded for 24 hours with the T cells treated with vehicle alone show a dramatic decrease in proliferation upon inhibition of neddylation with MLN4924 (Fig. 4.5B).

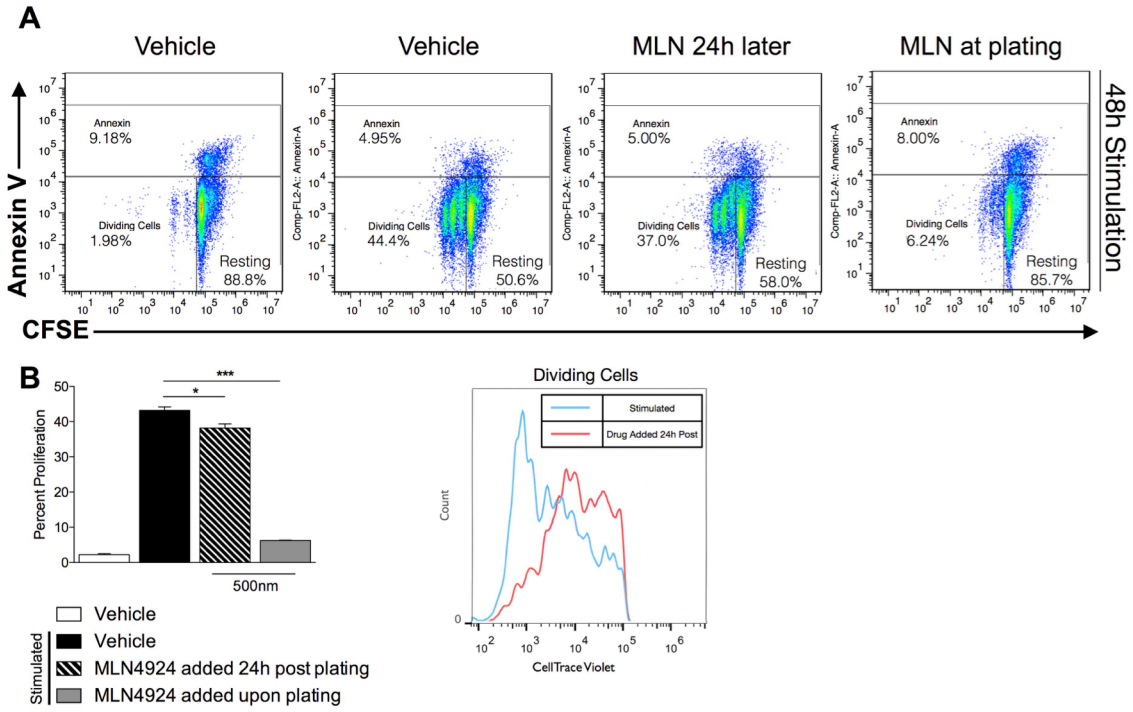

Fig. 4.5 – Inhibiting neddylation decreases T cell proliferation without increasing apoptosis. (**A**) Incubating T cells with MLN4924 decreases proliferation but does not result in increased Annexin V. (**B**) Quantification of proliferation dynamics in (A). * P < 0.05; *** P < 0.001

Phenotype of stimulated T cells following inhibition of neddylation: We next wanted to determine if T cells with inhibited neddylation displayed an activated phenotype upon stimulation. Following treatment of T cells with MLN4924 and stimulation with α-CD3 and α-CD28 for 48 hours and 72 hours, we observed decreased activation markers ($CD44^{hi}$, $CD69^{+}$) and increased naïve T cells ($CD44^{-}CD62L^{+}$) (Fig. 4.6). Likewise, cultures in which T cells were allowed to proliferate for 24 hours prior to the addition of MLN4924 contained fewer $CD69^{+}$ and $CD44^{hi}$ T cells (Fig 4.6). These data suggested that inhibition of neddylation in T cells mitigates their proliferation and response following stimulation.

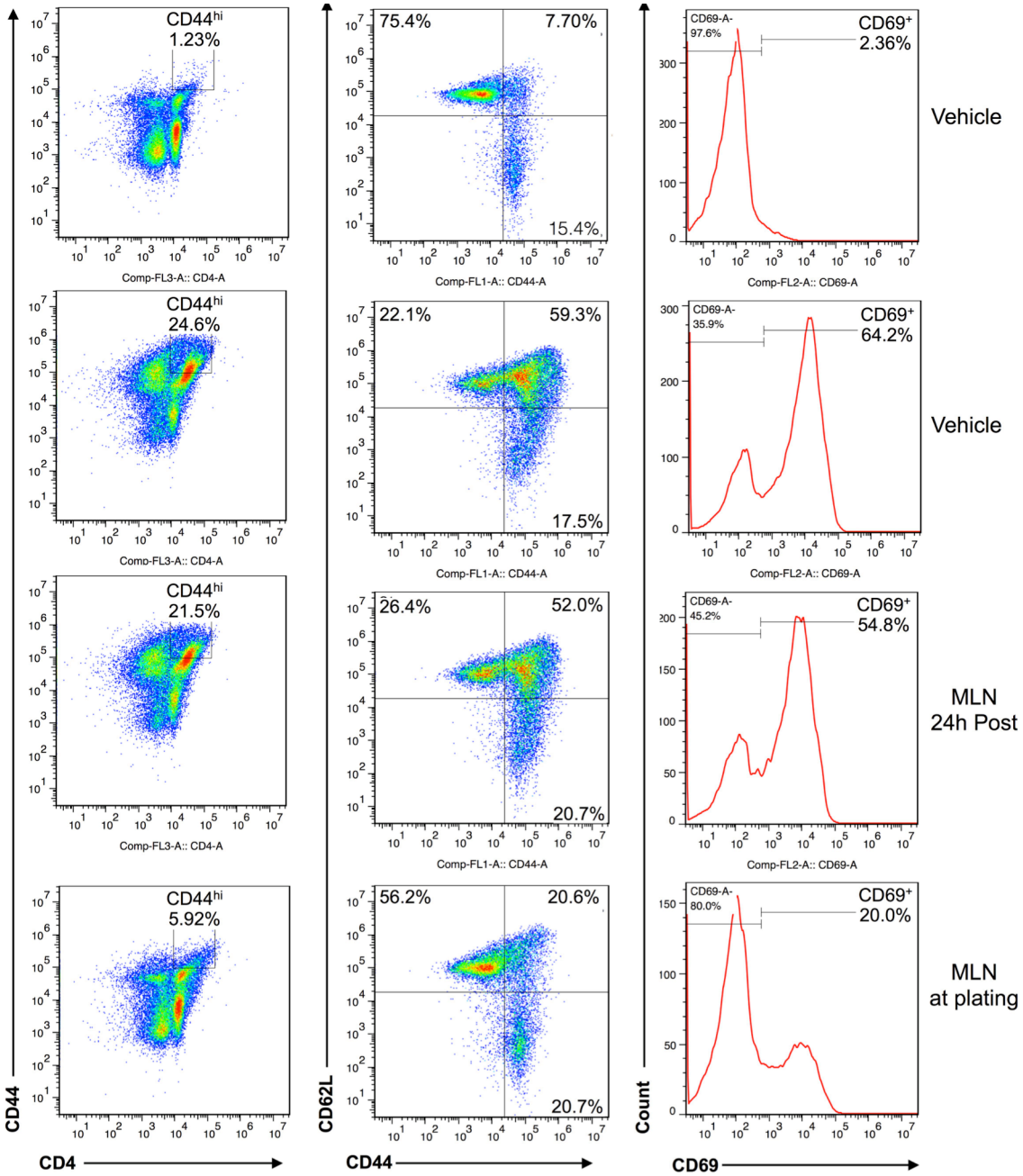

Fig. 4.6 – Phenotype of neddylation inhibited T cells. CD90.2+ T cells treated with vehicle or MLN4924 and stimulated with α-CD3 & α-CD28 where analyzed using flow cytometry for phenotypical markers CD69, CD44, and CD62L.

Generation of novel T cell conditional SAG knockout mouse: The loss of SAG protein has previously been shown to regulate the neddylation pathway[69-71] and we have shown

knockdown of SAG decreases DC functions[50]. The results of the previous experiments with pharmacological inhibitor of neddylation could be due to off-target effects of MLN4924. Thus we next generated knockout mice with a T cell specific deficiency of SAG protein by crossing LCK-Cre mice with *Sag*$^{fl/fl}$ (Fig. 4.7). We then crossed the F1 heterozygous generations to obtain LCK-Cre^{-}/*Sag*$^{fl/fl}$ (WT) and LCK-Cre^{+}/*Sag*$^{fl/fl}$ (KO) mice that had deletion of *Sag* only in T cells.

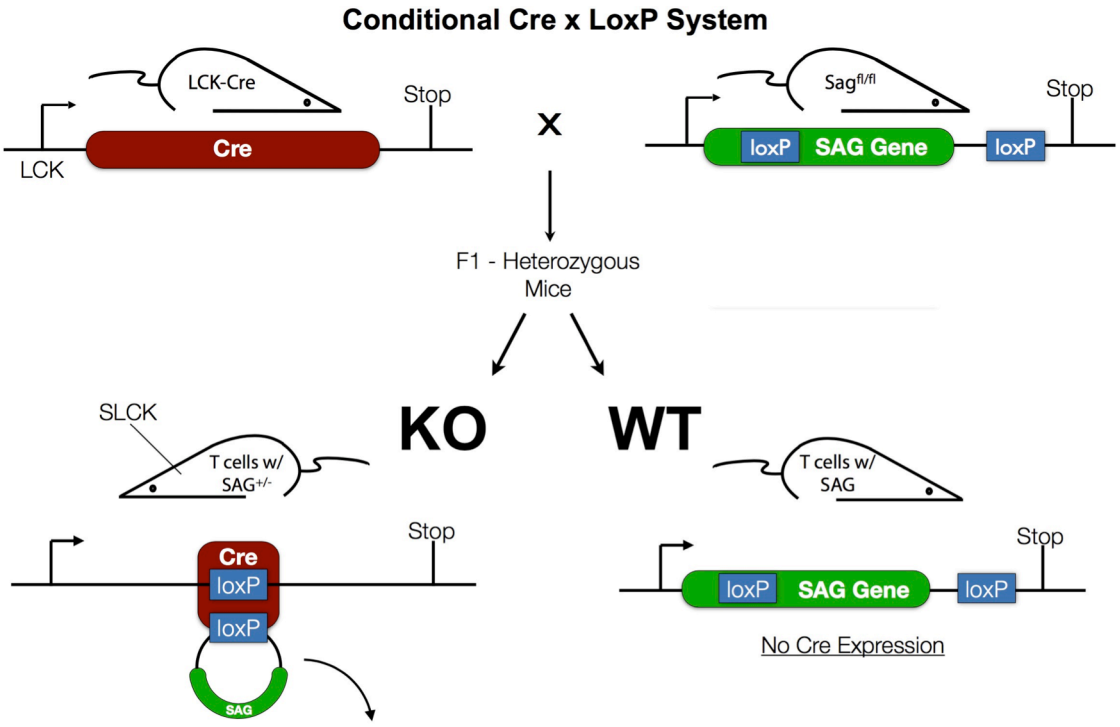

Fig. 4.7 – Breeding scheme of T cell conditional SAG knockout mouse. Breeding of LCK-Cre mice with SAG$^{fl/fl}$ mice led to novel mice with a deletion of *Sag* only in T cells.

Upon confirming that SAG was indeed deleted in T cells (Fig. 4.8), we examined whether the loss of SAG protein affected the development of T cells in the thymus.

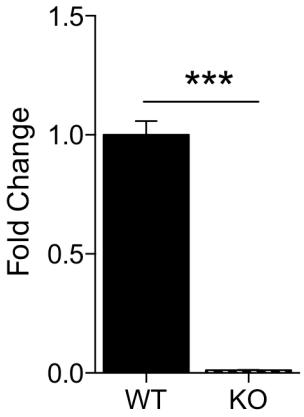

Fig. 4.8 – SAG protein is knocked out in T cells of mice. Analysis of FACS-purified T cells (~98% pure) show significantly decreased SAG protein. *** P < 0.001

We did not observe any difference in the total number of thymocytes nor in the total number of double positive T cells ($CD4^+CD8^+$) (Fig. 4.9A-B) suggesting thymopoiesis functions normally.

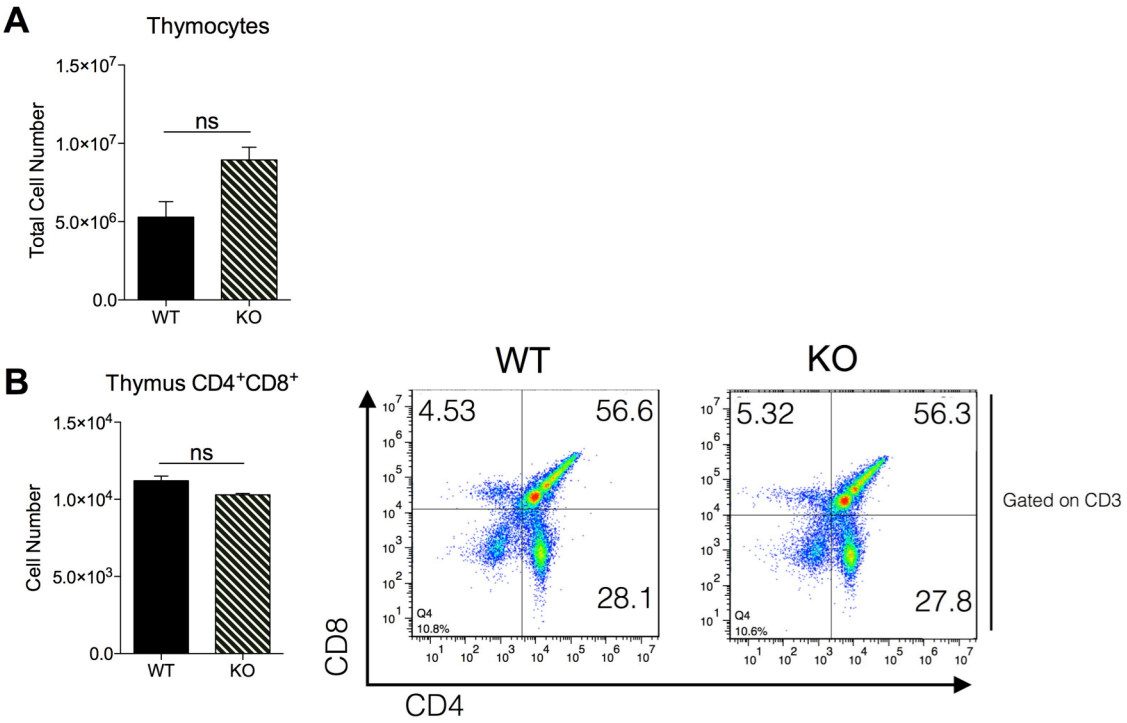

Fig. 4.9 – Thymopoiesis is normal in KO mice. Phenotypical analysis of naïve mice exhibit no difference in the thymus.

Further, phenotypical analysis of the cellular contents of the secondary lymphoid organs – spleen and peripheral lymph nodes – revealed no difference in the total number of $CD3^+$ T cells (Fig. 4.10A) nor was there a difference in the total number of naïve T cells ($CD62L^+CD44^-$) suggesting normal T cell development occurs in the conditional knockout mouse (Fig. 4.10B-C).

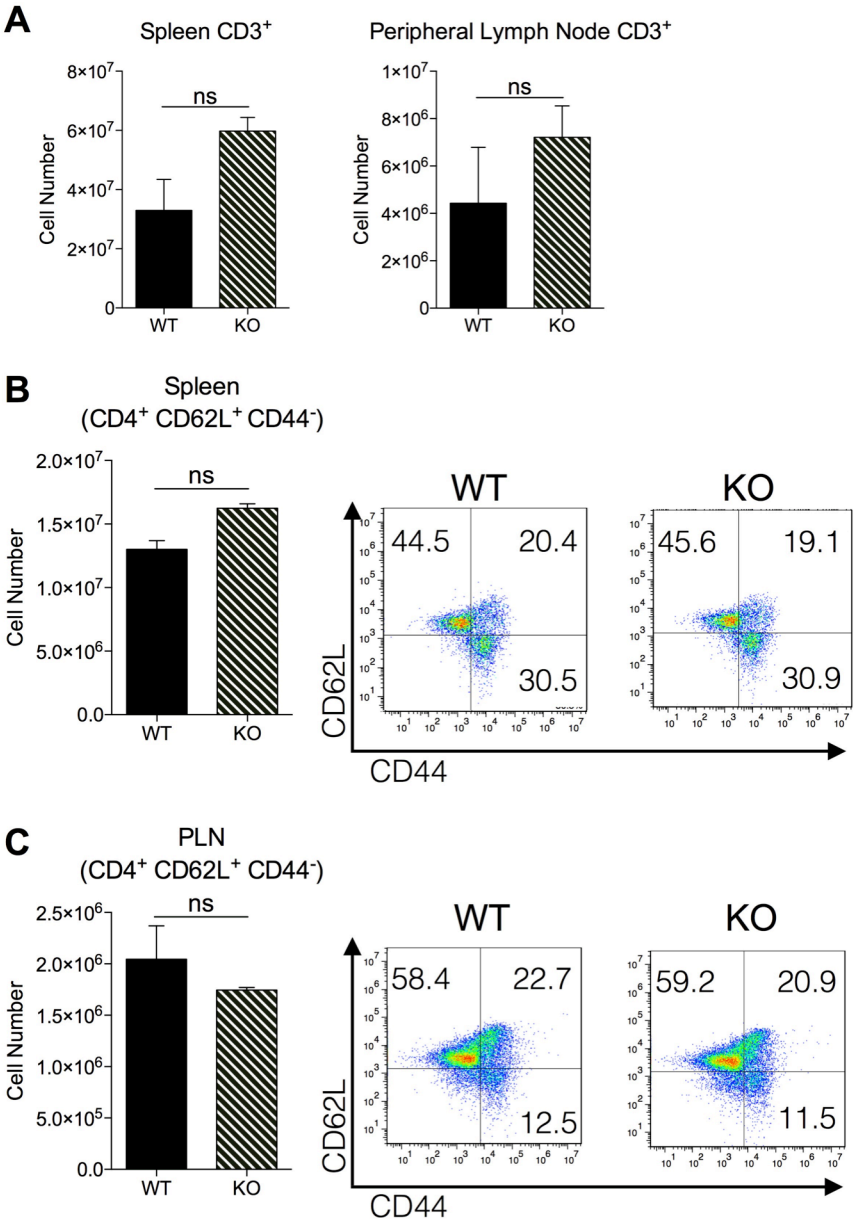

Fig. 4.10 – Phenotype is not different in KO mouse. Phenotypical analysis of naïve mice exhibit no differences in the peripheral organs.

Next, we wanted to examine the allo-proliferative capacity of SAG-deficient T cells. We therefore cultured WT or KO T cells with irradiated BALB/c splenocytes for 96 hours. Consistent with pharmacological neddylation inhibition, we observed significantly fewer SAG-deficient T cells proliferating, when compared with WT-SAG competent controls (Fig. 4.11A). To again examine the viability dynamics of proliferating cells, we stained KO T cells with CFSE and subjected them to allogeneic stimulation by irradiated splenocytes. We observed a similar decrease in prolifeDation without an increase in annexin V (Fig. 4.11B) suggesting that although the cells were living, there was a defect in their ability to proliferate.

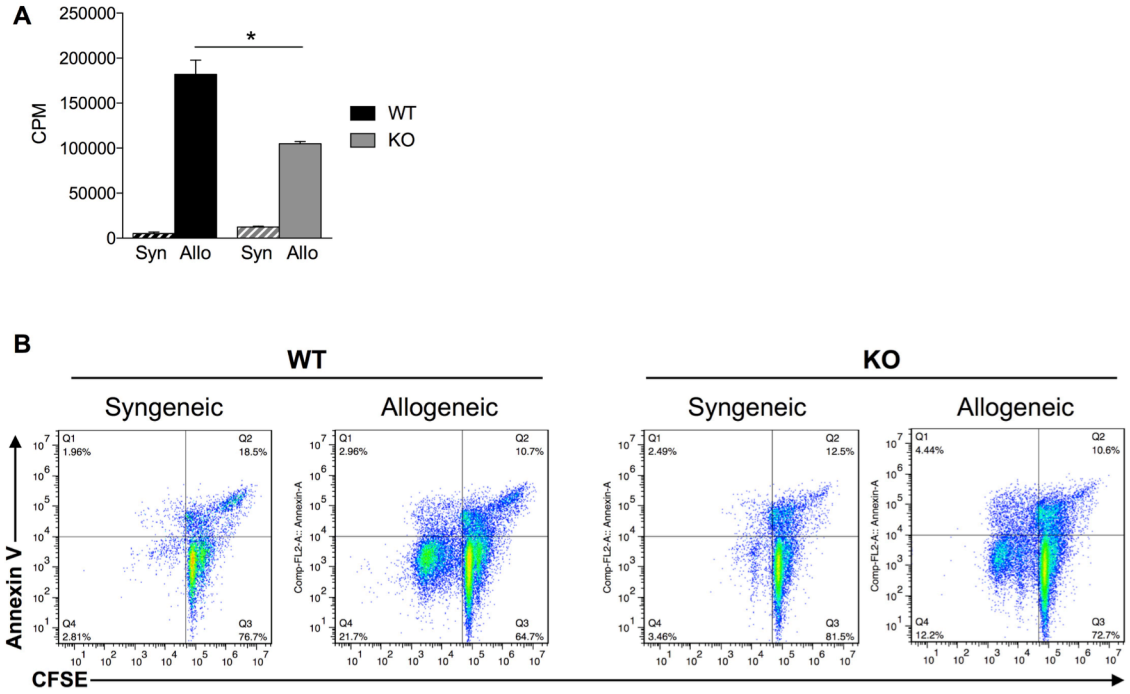

Fig. 4.11 – Allogeneic stimulation of KO T cells results in less proliferation. CD90.2+ purified T cells from KO mice proliferate to a lesser degree than WT controls without increased apoptosis. Measured by (**A**) ^{3}[H] uptake and (**B**) divisions of CFSE stained cells.

Mechanism of neddylation in T cells: Inhibition of neddylation – either by MLN4924 treatment or molecular knockdown of SAG – is known to regulate the degradation of IκB thereby preventing the function of the transcription factor NF-κB[50,213]. T cell receptor (TCR) signaling is known to trigger the NF-κB pathway[240] thus, we wanted to determine if inhibition of NF-κB translocation was responsible for the decrease in SAG-deficient T cell functions. To test this, we assessed p65 NF-κB translocation to the nucleus in WT and KO T cells following TCR stimulation. Contrary to the aforementioned results in DCs[50] following inhibition of neddylation, we saw that NF-κB translocation to the nucleus was only mildly impacted by deletion of SAG (Fig. 4.12A) after α-CD3 and α-CD28 stimulation. Likewise, T cells treated with MLN4924 exhibited only a partial inhibition of NF-κB translocation following similar stimulation (Fig. 4.12B).

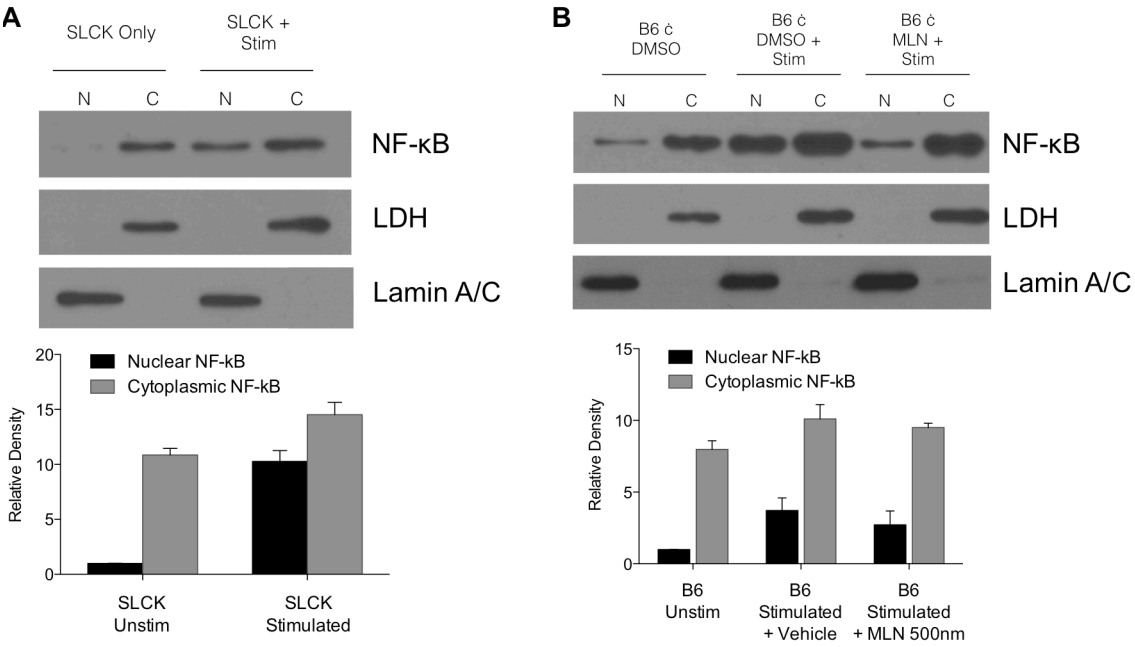

Fig. 4.12 – Inhibition of neddylation does not impact NF-κB translocation. CD90.2+ purified T cells from (**A**) KO mice (**B**) MLN treated WT mice were stimulated with α-CD3/α-CD28 and examined for NF-κB translocation from the [C] cytoplasm to the [N] nucleus.

Next, we visualized the dynamics of p65 translocation utilizing a complementary method – immunocytochemistry and confocal microscopy analysis. We treated T cells with vehicle or MLN4924 and stimulated these cells with α-CD3 and α-CD28. Both vehicle and MLN4924 treated cells exhibited similar NF-κB localization (Fig. 4.13). These data together suggest that inhibition of neddylation in T cells utilizes a disparate mechanism for regulating T cell function, compared to macrophages and DCs.

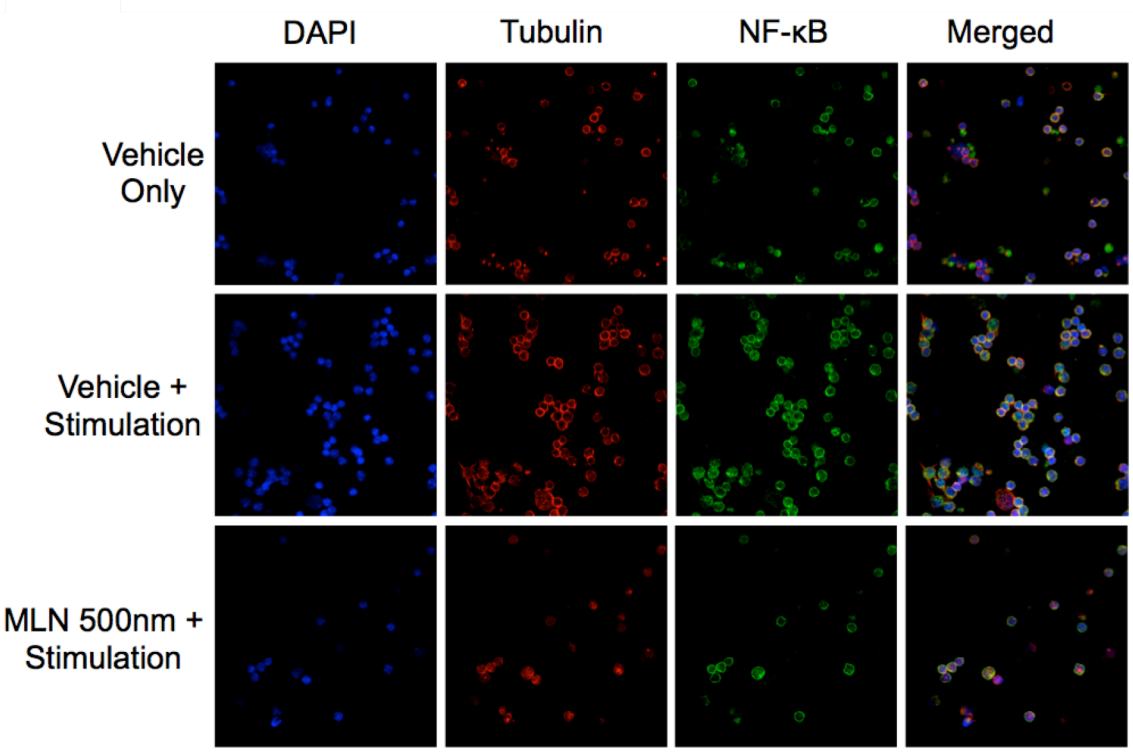

Fig. 4.13 – Confocal imaging of MLN4924 impact on NF-κB. CD90.2+ purified T cells from (**A**) KO mice (**B**) MLN treated WT mice were stimulated with α-CD3/α-CD28 and examined for NF-κB translocation using immunocytochemistry and confocal microscopy.

Because neddylation is a pathway that regulates the degradation of proteins, and proteins are known to have positive and negative feedback upon their own, or other protein, transcription and translation[241,242], we next examined the mRNA transcripts present in WT and KO T cells using microarray. Following analysis, we found lower levels of

RNF7 / SAG in the KO T cells confirming that SAG was indeed deficient in these cells (Fig. 4.14). More importantly, we saw an increased expression of suppressor of cytokine signaling (SOCS) proteins in KO T cells (Fig. 4.14).

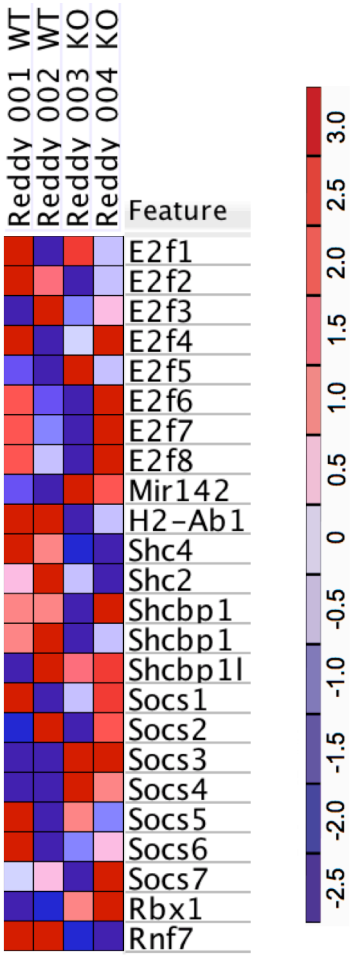

Fig. 4.14 – Microarray of mRNA transcripts in WT and KO T cells. mRNA was extracted from FACS-purified T cells from WT and KO mice.

SOCS proteins are involved in the regulation of intracellular signaling following TCR and cytokine-receptor ligation[243]. Furthermore, SOCS proteins are known to recruit the Cul5/SAG complex thereby regulating the ubiquitination of substrate proteins[243]. Thus, based upon the increased expression of SOCS mRNA transcripts in KO T cells, we next examined the protein expression of SOCS1 in T cells treated with MLN4924. We saw that inhibition of neddylation indeed increased the presence of SOCS1 protein following

stimulation (Fig. 4.15A). To determine if the degradation of SOCS proteins were regulated by CRL5-specific neddylation, we next stimulated WT and KO T cells with irradiated allogeneic whole splenocytes for 96 hours and measured SOCS1 and SOCS 3 dynamics. We observed that although SOCS proteins were induced in a similar fashion in WT and KO T cells, degradation was significantly lower in KO T cells (Fig. 4.16B)

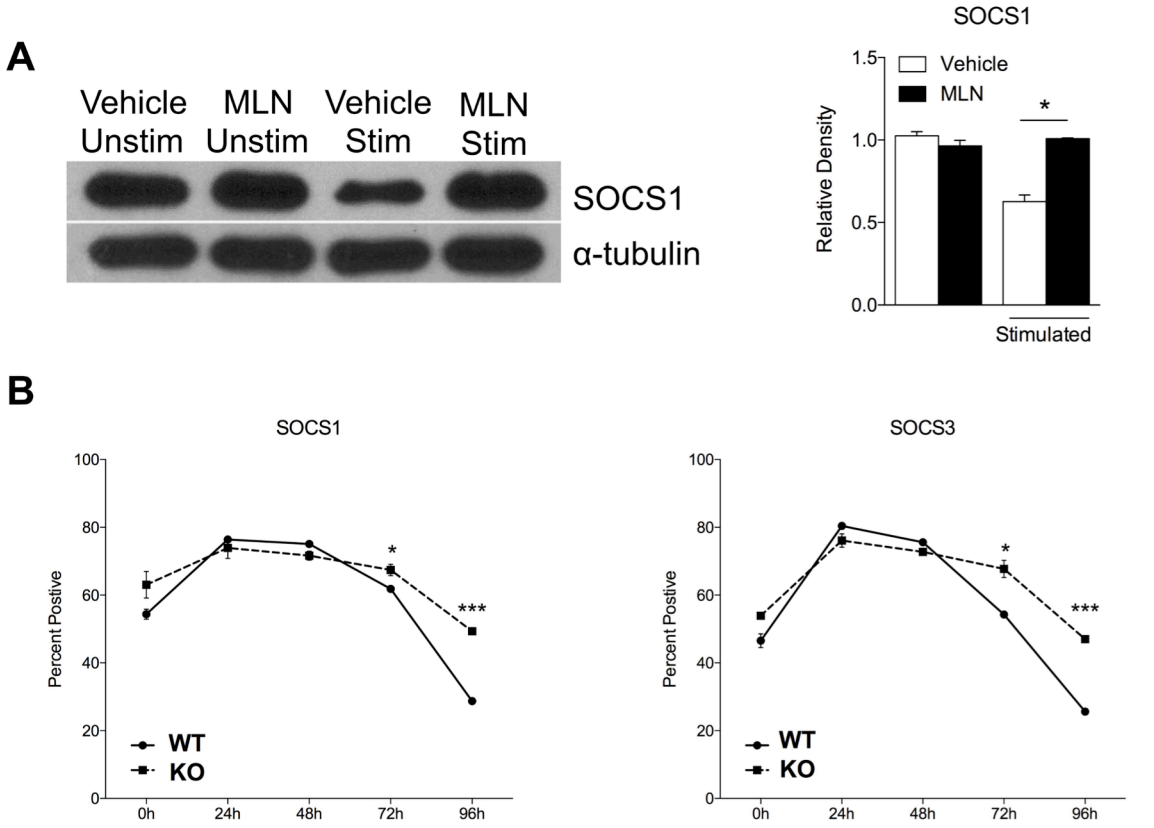

Fig. 4.15 – SOCS1 is increased when neddylation is blocked in T cells. (**A**) Whole cell lysates were quantified and examined by western blot. Relative density was determined based on the α-tubulin loading control. (**B**) T cells ($2x10^6$/ml) were stimulated with irradiated allogeneic splenocytes ($5x10^6$/ml) for indicated times. Presence of SOCS1 and SOCS3 were analyzed by flow cytometry.

Neddylation inhibition decreases GVHD and improves survival: To determine if SAG-deficient T cells proliferated to a lesser degree *in vivo*, we performed a clinically

relevant major MHC mismatch allo-BMT in which C57BL/6 (H-2^b) cells are transferred to BALB/c (H-2^d) mice following lethal irradiation of the recipient with 800 cGy, or a syngeneic BALB/c to BALB/c transplant as a control. The recipients received 5 x 10^6 T cell depleted (TCD) bone marrow and 0.5 x 10^6 $CD90.2^+$ T cells from either conditional KO SAG-deficient mice or WT SAG-competent mice on day +0. We then analyzed the donor-cell immunophenotype in the recipients 7- and 14 days after transplant. On day +7 after transplant we saw that while there was no significant difference in donor $CD4^+$ or $CD8^+$ T cell numbers, there were significantly fewer donor activated T cells ($CD4^+CD44^{hi}$ and $CD8^+CD44^{hi}$) and significantly greater donor naïve T cells ($CD4^+CD62L^+CD44^-$ and $CD8^+CD62L^+CD44^-$) (Fig. 4.16A). A similar immunophenotype was seen on day +14 following transplant (Fig. 4.16B).

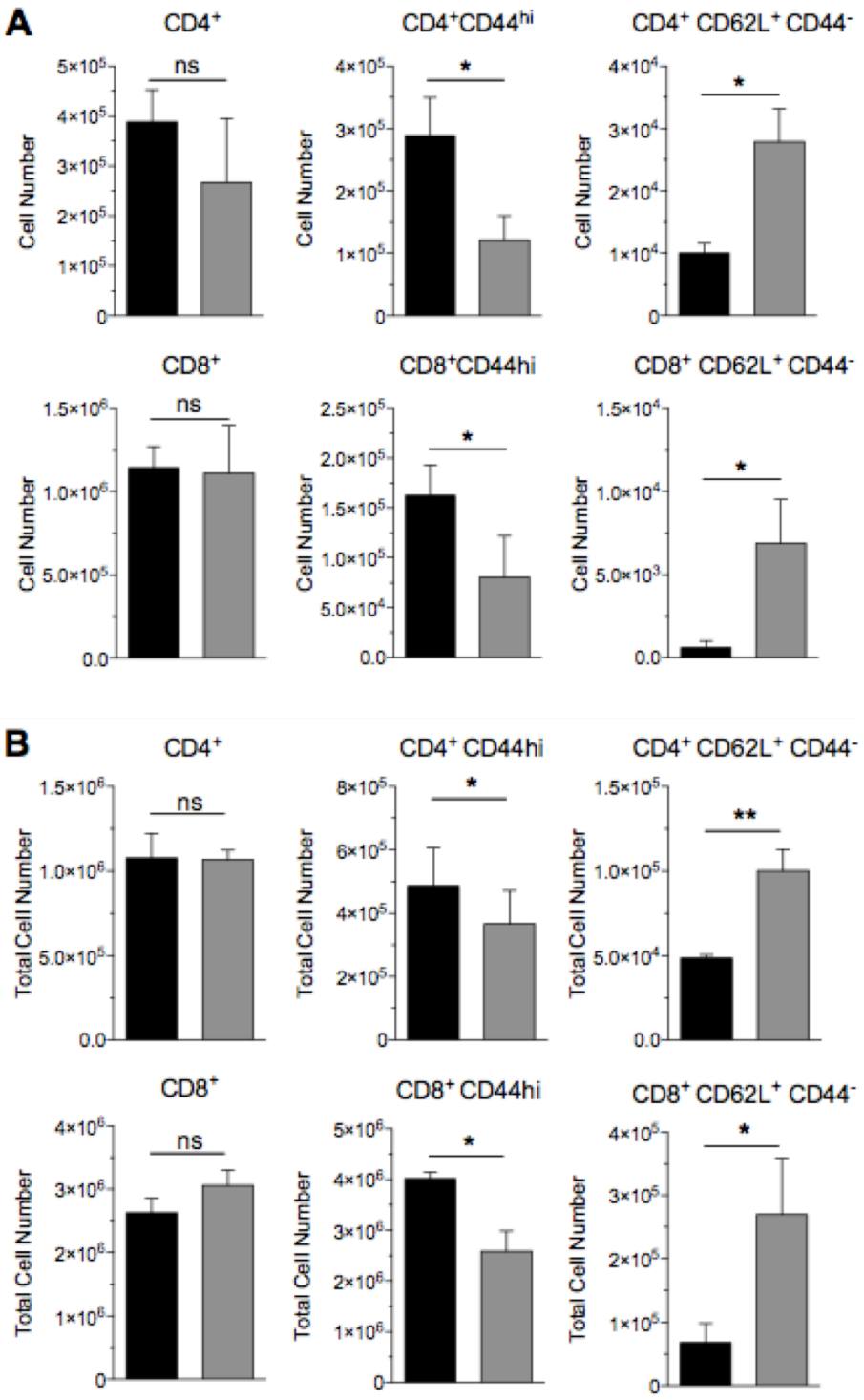

Fig. 4.16 – Immunophenotype following allogeneic BMT. Cellular analysis of the spleen (**A**) 7 days and (**B**) 14 days after allogeneic transplant (C57BL/6 [H-2^b] to BALB/c [H-2^d]). Recipients received either WT (SAG-competent) or KO (SAG-deficient) donor T cells and TCD bone marrow.

T cells release cytokines in response to TCR stimulation, which in turn mediate GVHD[244]. Thus, we examined the production of cytokines by donor T cells on day +14. We saw that IFNγ, IL-4, and IL-17 were significantly decreased in recipients of donor KO T cells (Fig. 4.17).

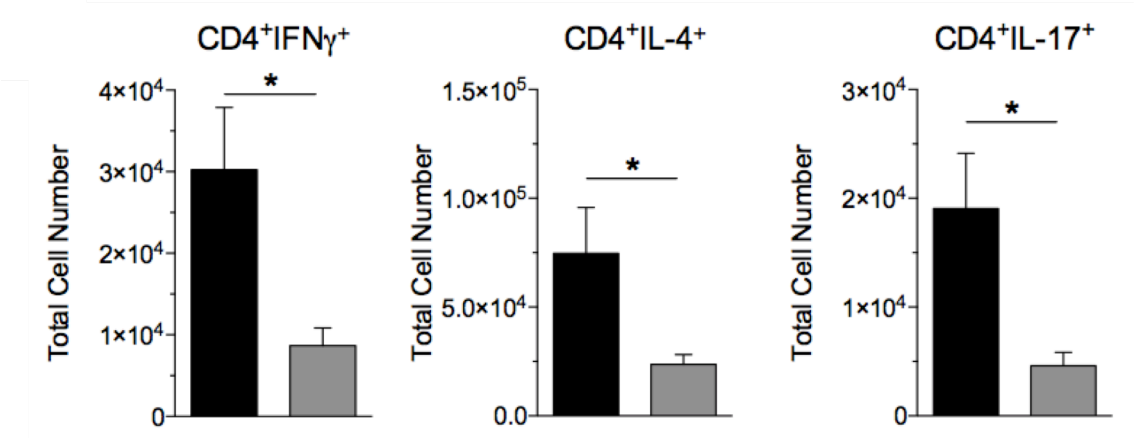

Fig. 4.17 – Diminished release of cytokines by KO T cells after allogeneic BMT. Whole splenocytes were stimulated with PMA/ionomycin for 6 hours then analyzed by flow cytometry.

Next, we scored recipients of syngeneic and allogeneic BMT recipient mice for clinical signs of GVHD and observed their survival. The allogeneic recipients that received WT donor T cells exhibited signs of severe GVHD (Fig. 4.18A) and greater mortality (Fig. 4.18B), compared with recipients of syngeneic transplant. By contrast, allo-BMT recipients that received donor KO T cells exhibited decreased signs of GVHD and significantly improved survival (Fig. 4.18A-B) when compared with recipients of WT donor T cells.

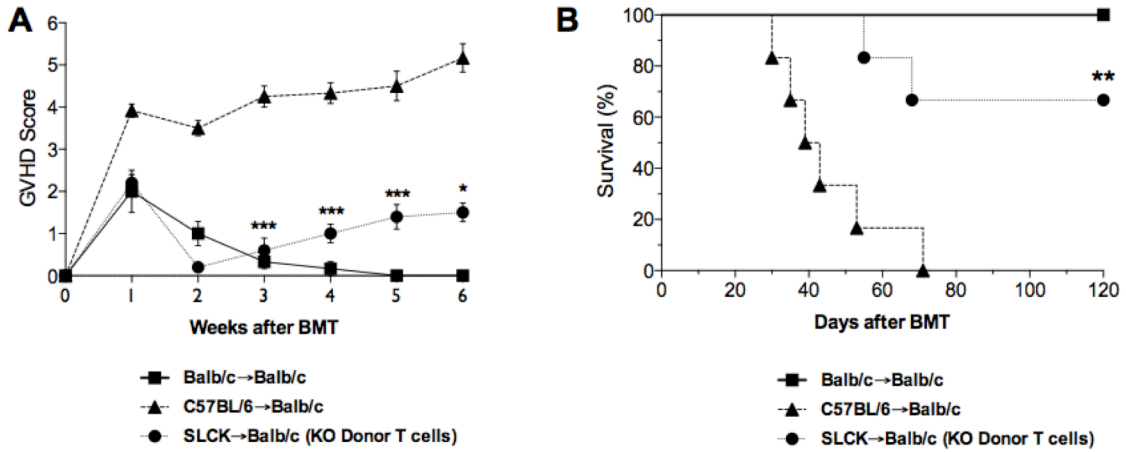

Fig. 4.18 – Decreased GVHD and increased survival of recipients of KO donor T cells. Recipients of KO T cells exhibited less severe clinical signs of GVHD and decreased mortality, compared to allogeneic recipients of WT donor T cells.

To test if there were any clinical and therapeutic implications of this data, we next wanted to determine if MLN4924 could decrease T cell proliferative responses following allo-BMT. Therefore, we performed a similar major MHC mismatch allo-BMT as above but instead transferred WT C57BL/6 T cells (0.5 x 10^6 $CD90.2^+$) and whole bone barrow (5 x 10^6) to BALB/c mice following lethal irradiation of the recipients. We began injecting recipient mice with either vehicle or MLN4924 (20mg/kg, sub-q) starting day -1 and continued daily administration through day +3, relative to BMT on day 0. All recipients of syngeneic BMT survived, indicating MLN4924 did not have non-specific toxicity. More importantly, allo-BMT recipients treated with MLN4924 resulted in decreased GVHD clinical scores (Fig. 4.19A) and increased survival (Fig. 4.19B) compared with allo-BMT recipients of vehicle control.

Together, these data suggest that inhibition of neddylation in T cells may have possible therapeutic relevance and could be used as a novel agent to mitigate GVHD in the clinic.

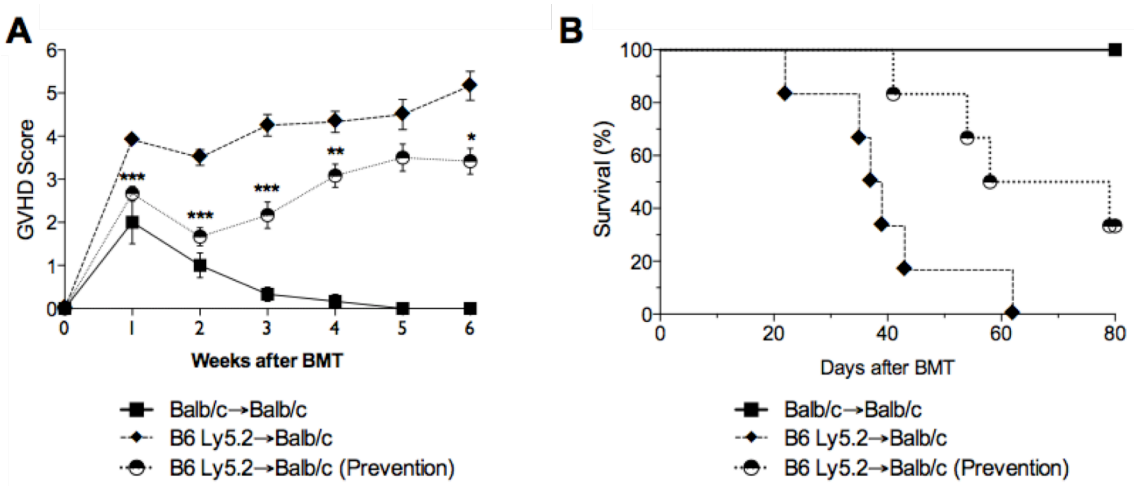

Fig. 4.19 – Inhibition of neddylation with MLN4924 decreases GVHD and improves survival. Allo-BMT recipients were injected with MLN4924 (20 mg/kg) for 5 days, starting day -1 relative to BMT on day 0.

DISCUSSION

Previous studies have shown that global inhibition of all CRL complexes inhibit neddylation and regulate T cell functions[239]. Our data utilizing the pharmacological small molecule inhibitor of neddylation, MLN4924, confirm and extend these observations of neddylation in T cells. More specifically, our use of MLN4924 revealed an intrinsic effect of neddylation in T cells, decreased release of T cell-specific cytokines, and a defect in T cell proliferation. Furthermore, when T cells were stimulated unimpeded for 24 hours prior to the addition of MLN4924, proliferation was dramatically halted following addition of neddylation inhibitor. These data suggest that T cell responses can be mediated through regulation of the neddylation pathway, even after TCR stimulation (Fig. 4.3 to 4.5). Additionally, following stimulation we observed fewer activated T cells ($CD69^{+}$, $CD44^{hi}$) and an increased number of naïve T cells ($CD62L^{+}CD44^{-}$) in cells treated with MLN4924.

However, the impacts that specific CRL complexes have on T cell functions have, thus far, been unknown. In contrast to global CRL inhibition, our results provide a novel perspective on the role of a particular CRL complex – CRL5 – in T cell proliferative responses. Here, we generated a novel knockout mouse with a conditional SAG protein deletion in T cells, thus allowing the selective inhibition of specific E3 ligases involved in the neddylation pathway. Allogeneic stimulation of SAG-deficient T cells too resulted in a decrease in proliferation as well as a diminished release of T cell lineage and activation cytokines.

Previous studies have shown that the regulation that neddylation confers is through the prevention of IκB degradation, thus inhibiting NF-κB translocation to the nucleus[50,213]. However, examination of NF-κB dynamics in T cells, utilizing either MLN4924 or SAG-deficient T cells, revealed that the NF-κB pathway was only minimally impacted. This suggested that a disparate pathway may be responsible for the diminished T cell functions observed. We thus profiled the total mRNA expression and found that transcripts for SOCS proteins were increased in KO T cells compared with WT SAG-competent controls. Therefore, we stimulated T cells and found an increase in SOCS1 protein in neddylation-inhibited WT cells treated with MLN4924 and increased SOCS1 and SOC3 protein in KO T cells after 96 hours of stimulation (Fig. 4.15). These results suggest that the increased presence of SOCS protein may be responsible for decreased T cell functions following inhibition of neddylation, as SOCS is a known component of the CRL5 complex[67,243]. This disparate mechanism in regulating neddylation is intriguing and future studies will serve to further explore the role of SOCS in neddylation-mediated regulation of T cell responses.

T cells play a central role in many immune mediated diseases including GVHD[83,230]. Upon transfer of SAG-deficient T cells into MHC mismatched recipients, we observed significantly less severe GVHD clinical scores and increased survival. These results confirmed our *in vitro* observations that SAG-deficient T cells have diminutive responses following allo-stimulation. Using the same MHC mismatched model, but instead transferring WT T cells, we treated recipient mice with MLN4924 and recapitulated the results of decreased GVHD and improved survival seen following transfer of KO T cells.

In conclusion, our novel finding that the *in vivo* regulation of a specific neddylation E3 ligase – CRL5 – plays a specific role in regulating T cells brings new insights to the understanding of the neddylation pathway. The data demonstrate an additional heretofore unknown mechanism through which neddylation may confer its regulatory effects. Our findings may have important clinical implications and suggest that regulation of neddylation may mitigate T cell mediated diseases. More specifically, these results together suggest that MLN4924 (currently in phase I/II clinical trials) [205,206] may be a novel strategy for attenuating GVHD in carefully designed clinical trials.

MATERIALS AND METHODS

Mice: Female C57BL/6 (H-2^b; CD45.2^+), BALB/c (H-2^d) mice were purchased from National Cancer Institute and C3H.sw (H-2^b) mice were purchased from The Jackson Laboratory (Bar Harbor, ME). The age of mice used for experiments ranged between 7 and 12 weeks. All animals were cared for under regulations reviewed and approved by the University Committee on Use and Care of Animals of the University of Michigan, based on University Laboratory Animal Medicine guidelines.

Cell isolation and cultures: Briefly, bone marrow cells were flushed from the femurs of 8- to 12-week-old female C57BL/6 mice and cultured in 150 x 15-mm CytoOne petri dishes (USA Scientific, Ocala, FL) at $1x10^7$ in 20ml of RPMI supplemented with 10% FCS, 4mM L-glutamine, 10 U/ml penicillin, 100 μg/ml streptomycin, 0.5 mM 2-ME, 20ng/ml GM-CSF. On day 4, 20ml of fresh complete RPMI containing 20ng/ml GM-CSF was added to each culture. After 7 days of culture, the loosely adherent cells were harvested and purified using anti-CD11c magnetic microbeads (Miltenyi Biotec Ltd., Auburn, CA) and the autoMACS (Miltenyi Biotec).

T cells were isolated from whole splenoctye homogenates, incubated with CD90.2+ microbeads and separated using the autoMACS, following the manufacturers instructions.

Bone Marrow Transplantation (BMT): BMTs were performed as previously described [39,245]. Briefly, syngeneic (BALB/c → BALC/c or C57BL/6 → C57BL/6) and allogeneic (C57BL/6 → BALB/c or C3H.sw → C57BL/6) recipients received lethal irradiation. On

day -1, BALB/c recipients received a total of 800 cGy of irradiation (split dose separated by 3 hours) and B6 animals received a single dose of 1000 cGy. Donor splenic CD90.2^{+} T cells were magnetically separated using an autoMACs (Miltenyi Biotec; Bergisch Gladbach, Germany) and 0.5 x 10^6 – 1 x 10^6 T cells were transferred to BALB/c recipients and 2 x 10^6 T cells were transferred to C57BL/6 recipients. 5 x 10^6 donor whole bone marrow was transferred to all recipients. Survival was monitored daily and the recipient body weight and GVHD clinical scores were determined weekly, as described previously [39]. Histopathologic analysis of the gastrointestinal (GI) tract was performed as described [39]. Animals received vehicle (sterile water) or butyrate (10mg/kg) by flexible 20G-1.5" intragastric gavage needle daily for 1 week, then every other day thereafter.

Cytokine Detection: Isolated CD90.2+ T cells were seeded on 60mm culture dishes at 3x10^6 cells/well and a 24-well plate at 2x10^5 cells/well, respectively. Pretreated cells were cultured with DMSO (Sigma), MLN4924 (Active Biochem), dexamethasone (APP Pharmaceuticals), or bortezomib (Fisher Scientific) at the indicated dosages for 2 hours. Cells were then stimulated α-CD3 and α-CD28 at the indicated concentrations for indicated time period. Supernatants were subsequently collected and stored at -20ºC until analysis. TNFα and IL-6 ELISA kits were purchased from R&D Systems and performed as per the manufacturers' instructions and read at 450nm by a SpectraMax microplate reader (Molecular Devices, Sunnyvale, CA).

Quantitative PCR: Using 1μg of each RNA template, cDNA was synthesized using SuperScript VILO (Invitrogen; Carlsbad, CA). qPCR primers for murine GAPDH (Forward: CCACAGTCCATGCCATCACTGC; Reverse: GCCCAAGATGCCCTTCAGTGGG), TNF α (Forward: CGACGTGGAGGCAGAAGAGGC; Reverse: CGTGGGCTACAGGCTTGTCACTC).

Flow Cytometry: To analyze immunophenotype surface markers, lymphocytes contained in the IEC fraction or spleen were harvested, stained and gated on CD4-conjugated PerCP/Cy5.5 (Clone: GK1.5) or CD8-conjugated APC (Clone: 53-6.7) and configurations of the following per mouse in duplicate: CD69-PE (Clone: H1.2F3), CD62L-PE (Clone: MEL-14), CD25-PE (Clone: 3C7), CD44-PerCP/Cy5.5 (Clone: IM7), CD44-APC (Clone: IM7), FoxP3-APC (Clone: FJK-16s). All flow cytometry Abs were purchased from eBiosciences. Stained cells were then analyzed with an Accuri C6 Flow Cytometer (BD Biosciences).

Western Blot and Subcellular Fractionation: T cells were seeded in 60mm dishes with $3x10^6$ cells per dish. Pretreated cells were cultured with DMSO (Sigma), MLN4924 (Active Biochem), or dexamethasone (APP Pharmaceuticals) at the indicated dosages for 2 hours followed by concurrent stimulation with α-CD3 and α-CD-28. Following treatment and stimulation, whole cell lysates where obtained and protein concentrations determined with Pierce BCA Protein Assay (Thermo Scientific). Equal amounts of protein were separated by SDS-PAGE gel (120V, 1.5h) and subsequently transferred to nitrocellulose membrane (20V, 1h). The following antibodies were used to analyze the

membranes: Nedd8 (19E3), α-tubulin (11H10), NF-κB p65 (D14E12), Lamin A/C (4C11), pIκBα (5A5), IκBα (L35A5), pERK (D13.14.4E), ERK (137F5) were purchased from Cell Signaling (Danvers, MA). Cullin1 (EPR3103Y) and LDH (EP1566Y) were purchased from abcam (Cambridge, MA). Secondary antibodies conjugated to HRP (Jackson ImmunoResearch) were used to detect primary antibodies. Densitometric analysis performed by ImageJ software. Subcellular fractionation was performed on $3x10^6$ BMDC seeded in 60mm dishes. Cells were pretreated in the presence or absence of vehicle, MLN4924, or dexamethasone for 2 hours followed by concurrent LPS stimulation for 30 minutes. The cytoplasmic and nuclear fractions were isolated using the Nuclear Extract Kit (Active Motif) per the manufacturers instructions. The extracts where then analyzed via western blot.

Mixed Lymphoctye Reaction (MLR): Splenic T cells ($2x10^5$/well) were magnetically separated from WT-B6 or WT-BALB/c mice by autoMACS using CD90.2 microbeads and subsequently cultured with irradiated (30 Gy) WT-B6 DC at 40:1 ($5x10^3$/well) and 100:1 ($2x10^3$/well) for 72 hours and 96 hours. Human MLRs were performed by co-culture of PBMCs ($1x10^5$/well) and moDCs at 1:1($1x10^5$) and 10:1 ($1x10^4$) ratios for 96 hours and 120 hours. Incorporation of ^{3}H-thymidine (1μCi/well) by proliferating T cells or PBMCs during the final 6 hours of culture was measured by a TopCount (PerkinElmer).

Confocal Microscopy: T cells were seeded onto Corning glass cover slips ($1x10^5$ cells/slip) (Fisher Scientific) using cytospin technique. Pretreated cells were cultured with

DMSO (Sigma) or MLN4924 (Active Biochem) at the indicated dosages for 2 hours followed by concurrent stimulation with α-CD3 and α-CD28 for an additional 24 hours. Cover slips were then washed, fixed with 4% paraformaldehyde for 20 minutes, and subsequently permeabilized with 0.3% Triton X. Cells were stained with NF-κB p65 (D14E12) primary (1:500) and Alexa Fluor 488 (Molecular Probes) secondary (1:1000), DAPI (Invitrogen), and Alexa Fluor 555 Phalloidin (1:500). Coverslips were then mounted using ProLong Gold Antifade Reagent (Molecular Probes) and Z-stack images were acquired at room temperature using a Nikon A-1 confocal microscope (Mellville, NY) using an oil immersion 60X objective with a numerical aperture = 1.4 and imported into NIS-Elements Software (Nikon). Excitation lasers 405nm, 488nm, and 561nm were used. Microscope laser exposure and settings were obtained using appropriate isotype controls and were retained for each experimental group.

CHAPTER V

UNBIASED PROFILING UNCOVERS A CRUCIAL ROLE FOR TARGETED GUT MICROBIOME DERIVED METABOLITES IN MODULATING GI EPITHELIAL CELL DAMAGE AND MITIGATING GVHD

ABSTRACT

Changes in the community structure of the intestinal microbiota are being progressively associated with many diseases, including graft-versus host disease (GVHD). However, the impact of these alterations on microbial metabolites and by-products and their impact on disease processes, such as GVHD, are not known. Here we utilized unbiased and blinded analysis to identify novel alterations in targeted microbial metabolite levels including the short chain fatty acids (SCFA) after allogeneic bone marrow transplant (allo-BMT). Surprisingly, alterations were observed only in the intestinal tissue but not in the luminal contents. The reduced butyrate in $CD326^{+}$ intestinal epithelial cells (IECs) after allo-BMT resulted in decreased histone acetylation, which was restored upon local administration of exogenous butyrate. This resulted in improved IEC junctional integrity, increased anti-apoptotic proteins, decreased GVHD, and improved survival. Furthermore, alteration of the indigenous microbiota with 17 rationally selected strains of high butyrate producing Clostridia also decreased GVHD and increased survival following allo-BMT in experiments performed at two different institutions. These data demonstrate a heretofore unrecognized role of microbial metabolites and suggest that local and specific

alteration of microbial metabolites has direct salutary effects on GVHD target tissues and can mitigate its severity.

INTRODUCTION

Alterations in the intestinal microbiome are associated with several disease processes[110,133,134,246,247]. However, the effect that changes in the community structure of the microbiome have on the production of microbial-derived metabolites is poorly explored. Microbial metabolites influence disease severity, but whether these alterations in microbial metabolites can impact outcomes after allogeneic bone marrow transplant (allo-BMT) are not known. Allo-BMT is a critical interventional therapy for patients with aggressive hematological malignancies[230,248]. Although allo-BMT is a curative and widely used treatment, approximately 40-50% of patients experience severe gastrointestinal damage from graft-versus-host disease (GVHD), which leads to high transplant-related mortality[88,230].

Studies have revealed that the intestinal microbiota is significantly altered in patients with GVHD and the alterations correlate with GVHD severity and pathogenesis[139]. Nevertheless, the direct causality of the changes in the host microbiota on GVHD severity is unclear. More relevantly, whether changes in the microbiota result in alterations in levels of microbial metabolites and by-products that have biological impact on allogeneic-BMT remain unknown.

We therefore profiled the levels of microbial metabolites with a specific focus on short chain fatty acids (SCFA), which are exclusively derived from the microbiota and are not made by the host. Some of these fatty acids (FAs), specifically the histone deacetylase inhibitor (HDACi) butyrate, is a preferred energy source for intestinal epithelial cells (IECs)[60,61,249] and administration of exogenous HDACi regulates GVHD[57,245,250]. But the

impact that host indigenous microbial metabolites that function as HDACi have on GVHD remains unknown[60,61,249].

We performed unbiased profiling of the microbial metabolome not just in the bowel lumen, but also in the intestinal tissue, serum, spleen, and liver with a specific focus on targeted FAs after experimental allo-BMT. We found that only one SCFA, namely butyrate was significantly reduced only in the intestinal tissue of allo-BMT recipients resulting in decreased histone-H4 acetylation within IECs. Intragastric administration of butyrate restored histone-H4 acetylation, improved the junctional integrity of IECs, enhanced IEC resistance to apoptosis, decreased the severity of GVHD, and increased survival following allo-BMT. Furthermore, rationally altering host GI microbiota to high butyrate producers[103] mitigated GVHD.

RESULTS

Targeted microbial metabolite profiling: We hypothesized that alterations in the composition of the microbiota in the GI lumen would result in an altered microbial metabolome after GVHD[133,251]. We determined the concentration of microbial FA metabolites, both short-chain FAs (which are exclusively derived from the microbiome and not made by the host) and long-chain FAs up to 18 carbons in length (which are host endogenous metabolites), from several sites seven days (day +7) after BMT. Specifically, we analyzed the serum, spleen, liver, intestines, and luminal contents (stool) of the intestines with gas chromatography mass spectrometry (GC/MS) (Fig. 5.1).

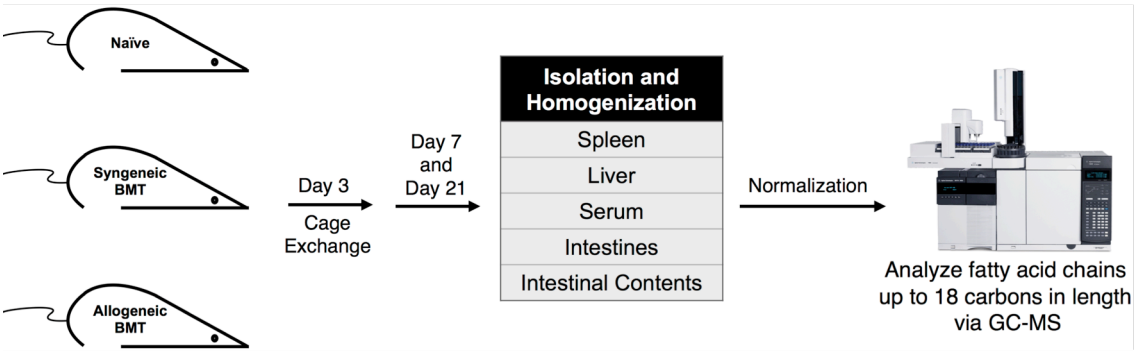

Fig. 5.1 – GC/MS experimental analysis. Schematic of fatty acid analysis. Animal cages of naïve animals and those receiving syngeneic or allogeneic BMT were exchanged on day 3 relative to transplant. All groups were sacrificed on day 7 and day 21 (Fig. 5.5). Homogenized samples were normalized and analyzed via gas chromatography mass spectrometry.

We utilized a well established and clinically relevant model of MHC-mismatched BMT with C57BL/6 (H-2^b) cells transferred to lethally irradiated Balb/c (H-2^d) mice and compared it to syngeneic transplant and naïve animals. The animal cages were exchanged on day 3 to take any alterations in the microbial environment into account, and analysis following GC/MS was performed in a blinded manner. Surprisingly, the concentrations

of the FAs were not significantly different in the luminal contents of the intestines between any of the groups (Fig. 5.2A and Fig. Fig. 5.3A).

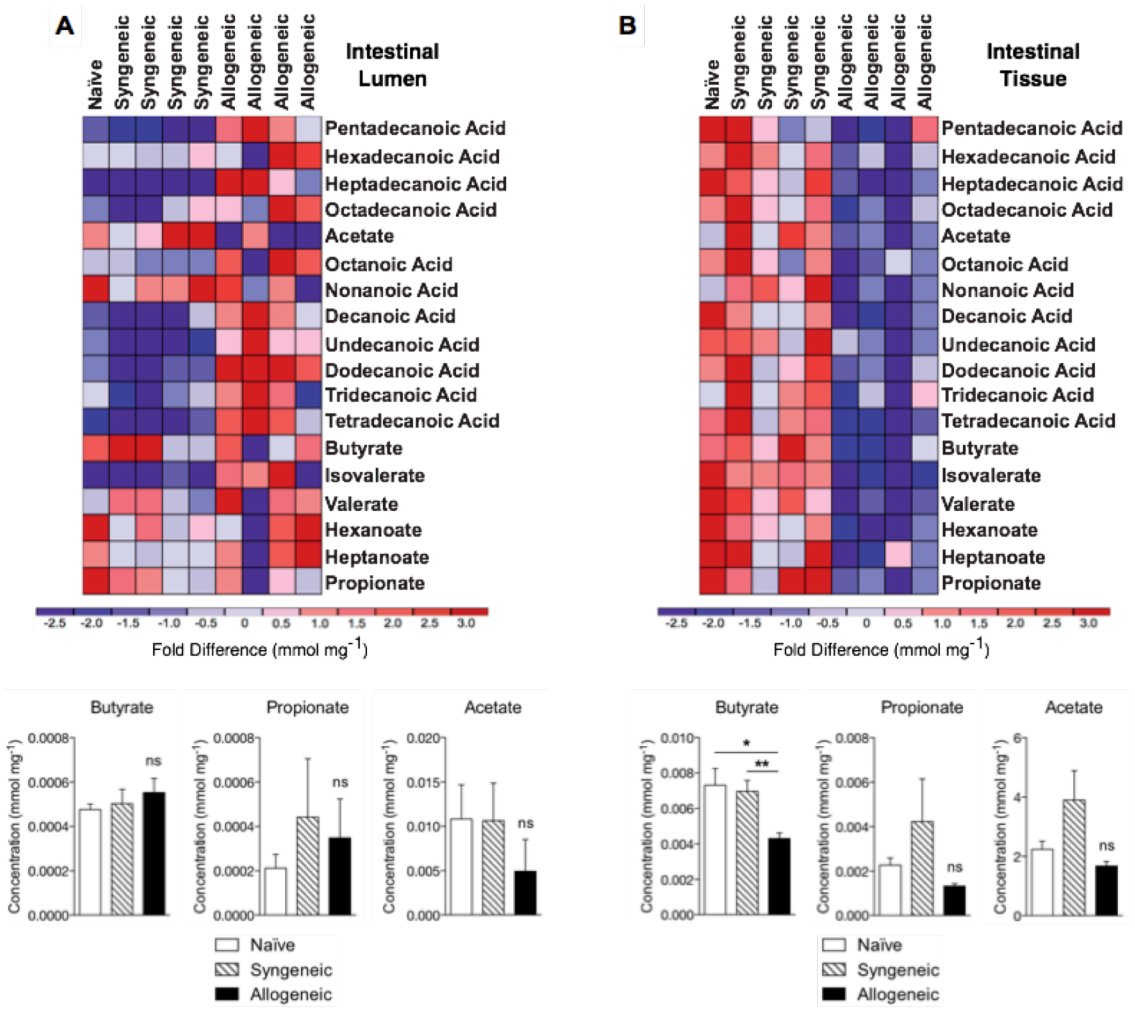

Fig. 5.2 – Fatty acid levels on day +7. (**A**) Fatty acid levels (short and long chain) on day 7 in the intestinal luminal contents (stool) and (**B**) in the intestinal tissue of animals in experimental groups. Only butyrate was different in the intestinal tissue of recipients of allogeneic transplant. Representative heatmaps are shown of n = 9-10 animals per group. * P < 0.05; ** P < 0.01

They were also not significantly different in the serum or the tissues such as the spleen and liver of allogeneic animals (Fig. 5.4) compared with syngeneic animals and naïve controls. However, the greatest and the only statistically significant difference –was unexpectedly– observed in just one SCFA, butyrate, which was significantly decreased only in the intestinal tissue at day 7 (Fig. 5.2B and Fig. 5.3B).

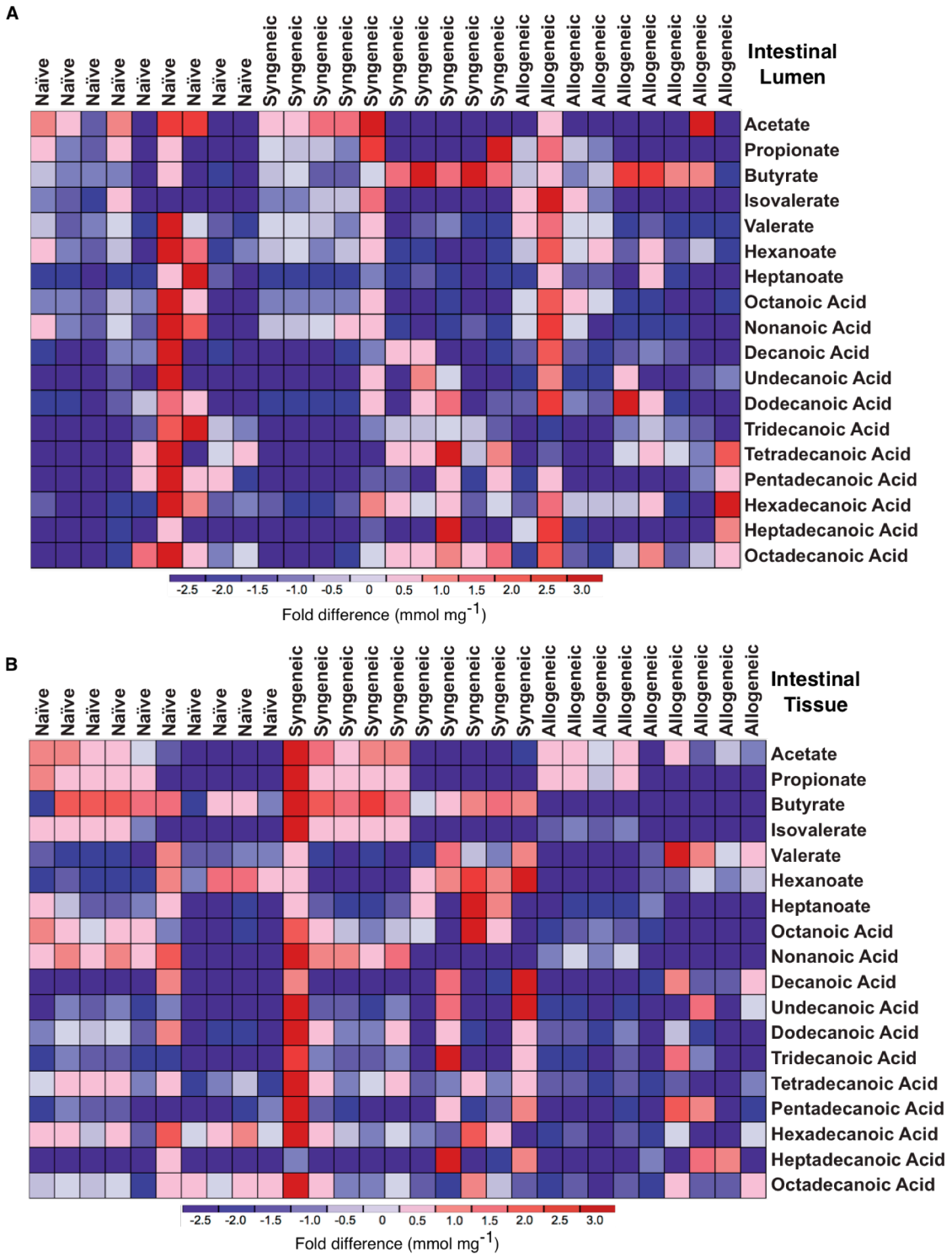

Fig. 5.3 – Heatmap of fatty acid profiles (short and long chain) of all animals combined. All animals were sacrificed 7 days following syngeneic (BALB/c → BALB/c) or allogeneic (C57BL/6 → BALB/c) transplant in the (**A**) intestinal luminal contents (stool) and (**B**) in the intestinal tissue. n = 9 – 10 animals per group.

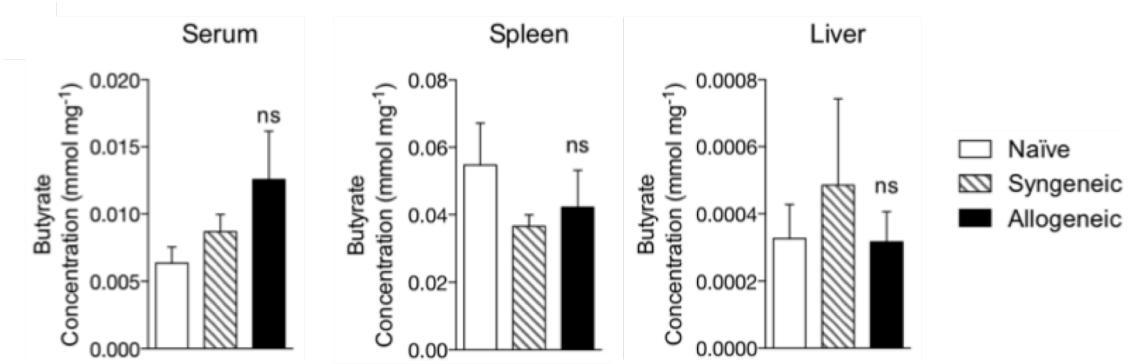

Fig. 5.4 – Butyrate levels in the periphery. Butyrate concentration was not different in the serum, spleen, and liver of naïve animals or recipients of syngeneic or allogeneic BMT.

We next determined if the lack of significant change in the FAs from all other sites, and the only significant change noted in the intestinal tissue (butyrate) was altered at later time points by performing similar analysis on day 21. We once again observed similar results on day 21 as on day 7 (Fig. 5.5).

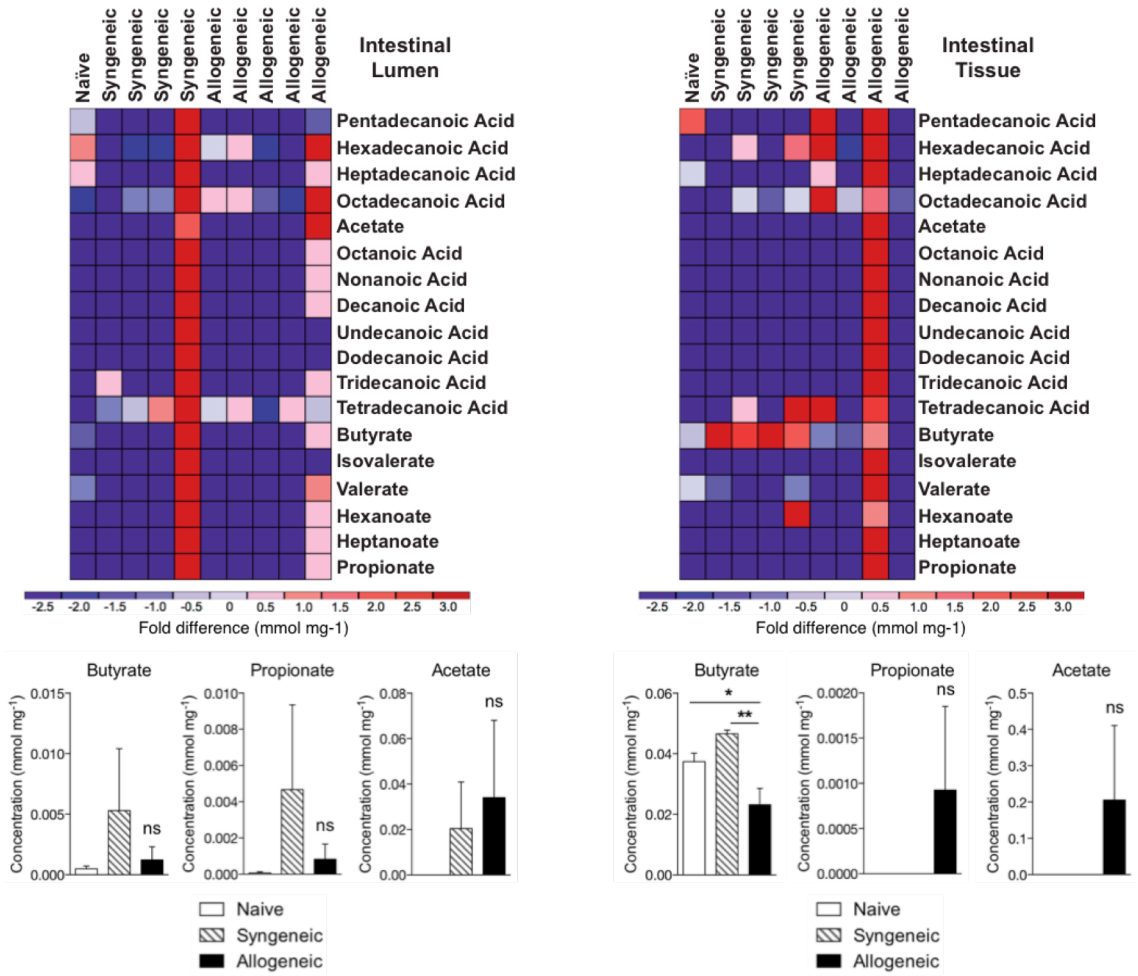

Fig. 5.5 – Fatty acids analysis on day +21. Fatty acid levels (short and long chain) 21 days following transplant in the (left) intestinal luminal contents (stool) and in the (right) intestinal tissue. Quantifications of the short chain fatty acids acetate, propionate, and butyrate are shown below representative heatmaps; n= 5 animals per group.

Functional impact of altered levels of SCFA in the IECs: In light of the reduction of butyrate in allogeneic animals only in the intestinal tissue, we next analyzed the potential functional impact of reduced butyrate in IECs. Because butyrate is an HDACi[60,252,253], we examined the level of histone acetylation in purified IECs ($CD326^{+}$) after transplant. The level of acetylated histone-H4 was significantly decreased day 21 (Fig. 5.6A) and day 7

(Fig. 5.6B) following allo-BMT demonstrating that reduced butyrate resulted in decreased histone acetylation.

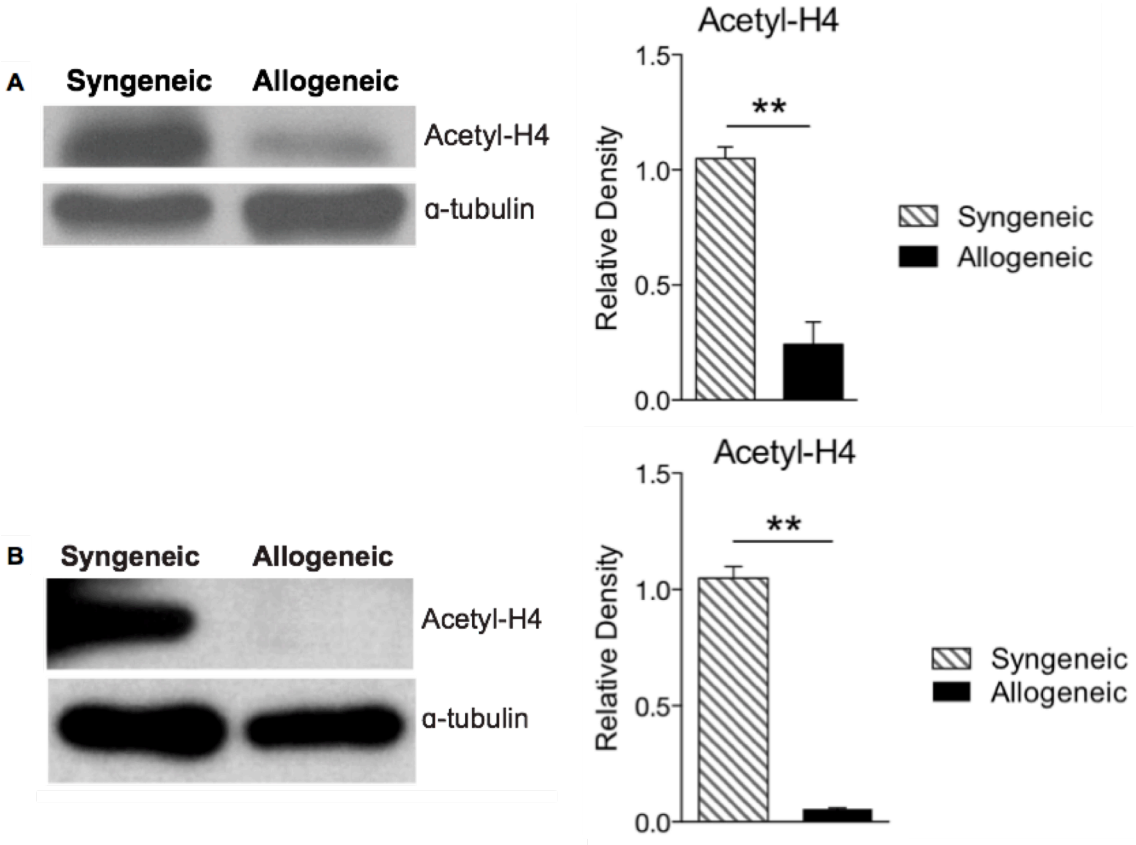

Fig. 5.6 – Loss of butyrate decreases levels of acetylated histone H4 in IECs. Protein expression of acetyl-histone H4 (top blot) and densitometric analysis normalized to presence of α-tubulin (lower blot) (**A**) 21 days and (**B**) 7 days following syngeneic (BALB/c → BALB/c) or allogeneic (C57BL/6 → BALB/c) BMT. Representative immunoblots; densitometric analysis of three similar experiments combined is shown right of blot.
** $P < 0.01$

Histone acetylation is the result of a balance between the activity of histone acetyl transferases (HATs) and histone deacetylases (HDACs). Therefore to confirm if the decreased acetylation is secondary to decreased HDAC inhibition from reduction in butyrate and not due to potential alterations in HDAC and HAT enzyme levels[254] following transplant, we analyzed the expression of HDACs and HATs in IECs after BMT. We observed similar levels of several HDACs (HDAC 1,4,7,9, and 10) (Fig. 5.7A)

and HATs (p300 and TIP60) (Fig. 5.7C) in the IECs ($CD326^{+}$) of both syngeneic and allogeneic BMT recipients. Furthermore both HDAC (Fig. 5.7B) and HAT (Fig. 5.7D) enzyme activity were not different in these animals suggesting that reduction in histone acetylation in the IECs after allo-BMT is from reduced levels of butyrate.

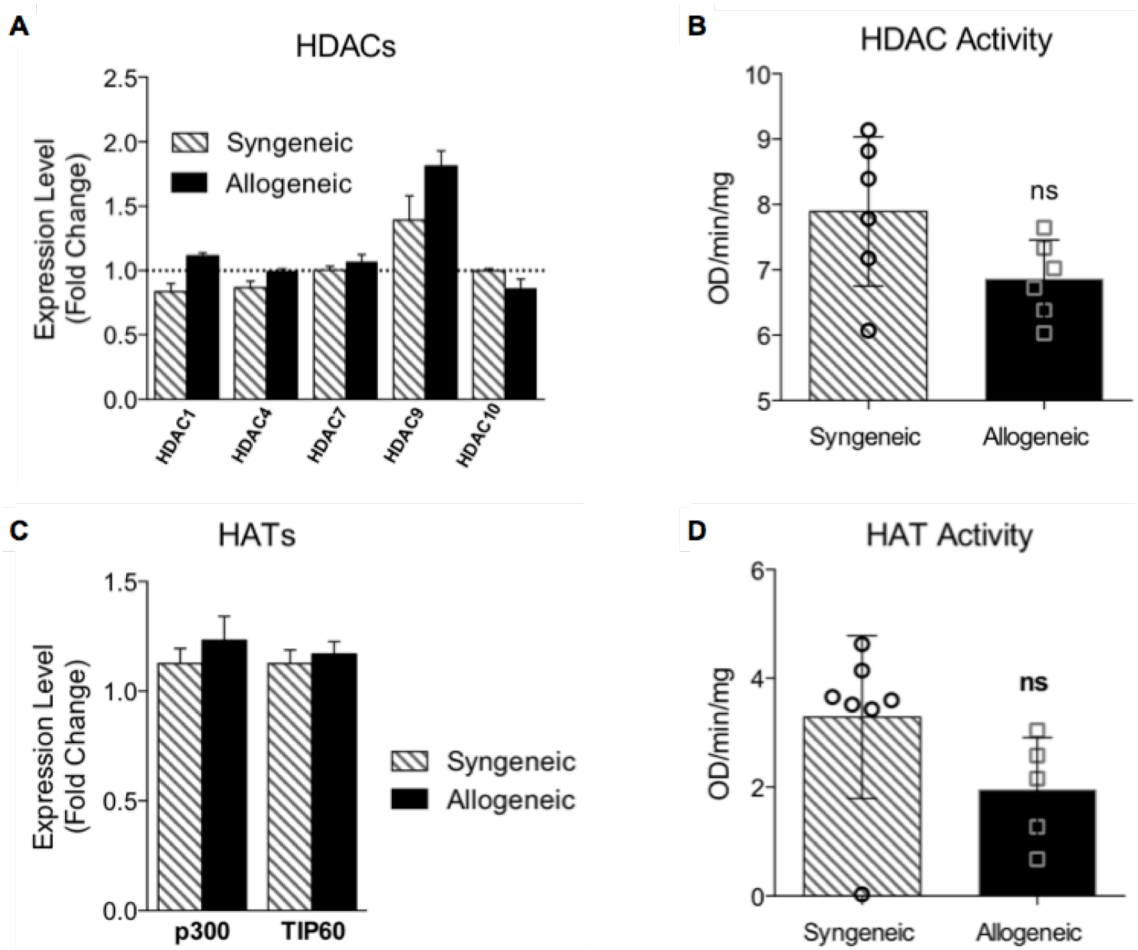

Fig. 5.7 – Loss of butyrate decreases levels of acetylated histone H4 in IECs. (**A**)-(**B**) Analysis of histone deactylase (HDAC) enzymes and (**C**)-(**D**) histone acetyltransferase (HAT) enzymes in IECs ($CD326^{+}$) 21 days following syngeneic and allogeneic BMT. (**A**) Gene expression of representatives of class I, II, and IV HDAC enzymes, (**B**) HDAC activity, (**C**) histone acetyltransferase (HAT) enzyme levels, and (**D**) HAT activity in syngeneic and allogeneic CD326+ IECs.

Reduced uptake of butyrate by the IECs: Because butyrate can only be generated by luminal microbiota and not by the host tissues, we next explored whether the diminished concentration of butyrate observed in the intestinal tissue was from impaired uptake of butyrate following allo-BMT. To this end, we examined the expression of the known butyrate monocarboxylate transporter (SLC5A8) and the receptor of butyrate (GPR43) in IECs following allo-BMT[104,252].

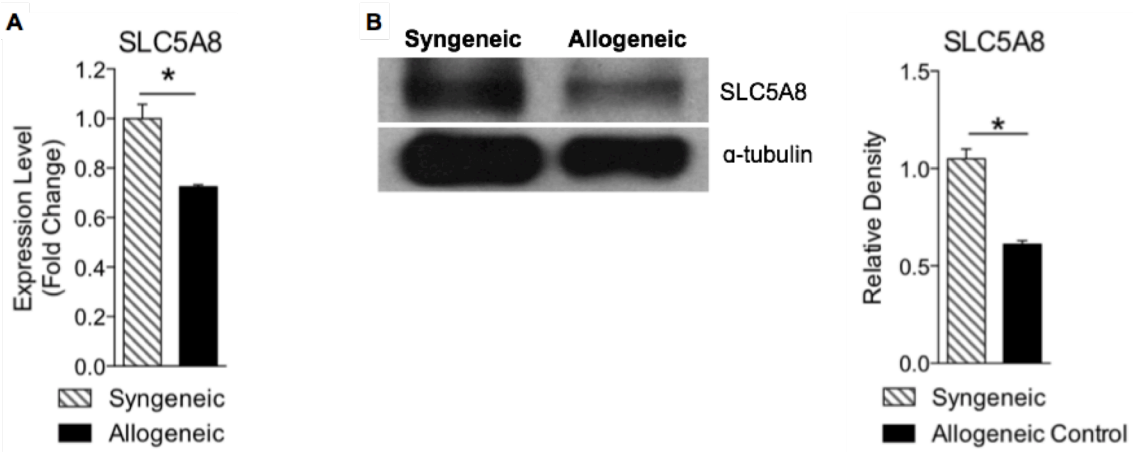

Fig. 5.8 – Loss of butyrate decreases levels of butyrate transporter, SLC5A8. (**A**) Gene expression and (**B**) protein levels of SLC5A8 (monocarboxylate transporter of butyrate) in IECs ($CD326^{+}$) of syngeneic and allogeneic transplant recipients 21 days following BMT. Representative immunoblots; densitometric analysis of three similar experiments combined is shown right of blot.

Decreased gene expression (Fig. 5.8A) and protein levels (Fig. 5.8B) of both SLC5A8 and GPR43 (Fig. 5.9A to B) were observed in IECs from allogeneic animals following transplant on day +21 and also on day +7 (Fig. Fig. 5.9C) suggesting that reduction in butyrate levels in the IECs is due to reduced uptake of the microbiota-derived luminal butyrate.

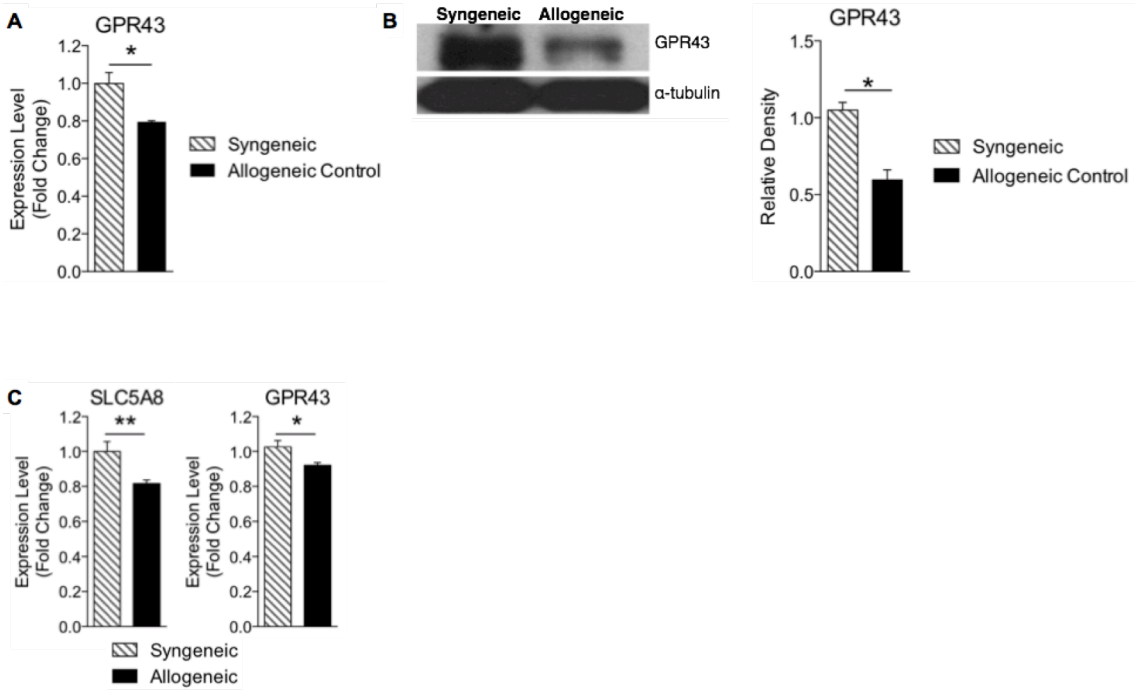

Fig. 5.9 – Loss of butyrate decreases level of butyrate receptor and transporter. (**A**) Gene expression and (**B**) protein level of GPR43 in IECs ($CD326^+$) of syngeneic or allogeneic BMT recipients 21 days following transplant. (**C**) Gene expression of SLC5A8 (left) and GPR43 (right) in IECs ($CD326^+$) 7 days following syngeneic or allogeneic BMT. Representative immunoblots; densitometric analysis of three similar experiments combined, are shown below blots. * $P < 0.05$; ** $P < 0.01$

We next analyzed the potential reasons for the reduction in the expression of butyrate transporter on IECs after allo-BMT. To this end we cultured primary IECs ($CD326^+$) with proinflammatory mediators (IFNγ and/or TNFα) and analyzed the expression of the butyrate transporter SLC5A8. Exposure of IECs to inflammatory cytokines significantly decreased the expression of SLC5A8 (Fig. 5.10). These data indicate that the intense inflammatory milieu following allo-BMT causes reduced expression of butyrate transporters and receptors leading to reduction in butyrate levels and histone acetylation in IECs.

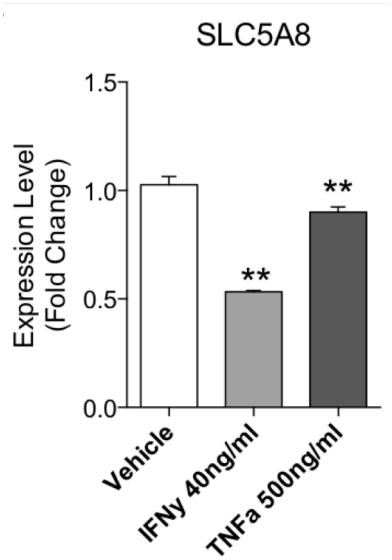

Fig. 5.10 – Inflammatory cytokines decrease expression of butyrate transporter. Primary IECs ($CD326^+$) cultured in the presence or absence of inflammatory cytokines IFNγ (40ng/ml) or TNFα (500ng/ml) for 6 hours. Expression of SLC5A8 is significantly decreased in cells cultured in the presence of IFNγ or TNFα, compared to vehicle control. ** $P < 0.01$

Rescuing the cellular effects of reduced butyrate: We next determined if the reduced levels of butyrate in IECs could be restored *in vivo* and further, whether this would have a functional impact on histone acetylation. In addition to utilizing transporters, butyrate can also diffuse across the mucosal barrier into IECs when present in high concentrations[252,255]. Therefore, we hypothesized that administration of high levels of butyrate locally would restore histone acetylation of IECs, *in vivo*. To test this, we again utilized the clinical model of MHC-mismatched BMT model in which C57BL/6 ($H\text{-}2^b$) cells are transferred to Balb/c ($H\text{-}2^d$) mice and administered vehicle or butyrate via daily intragastric gavage. We found that daily intragastric butyrate administration for 21 days significantly restored histone-H4 acetylation when compared with untreated allo-BMT recipients (Fig. 5.11A).

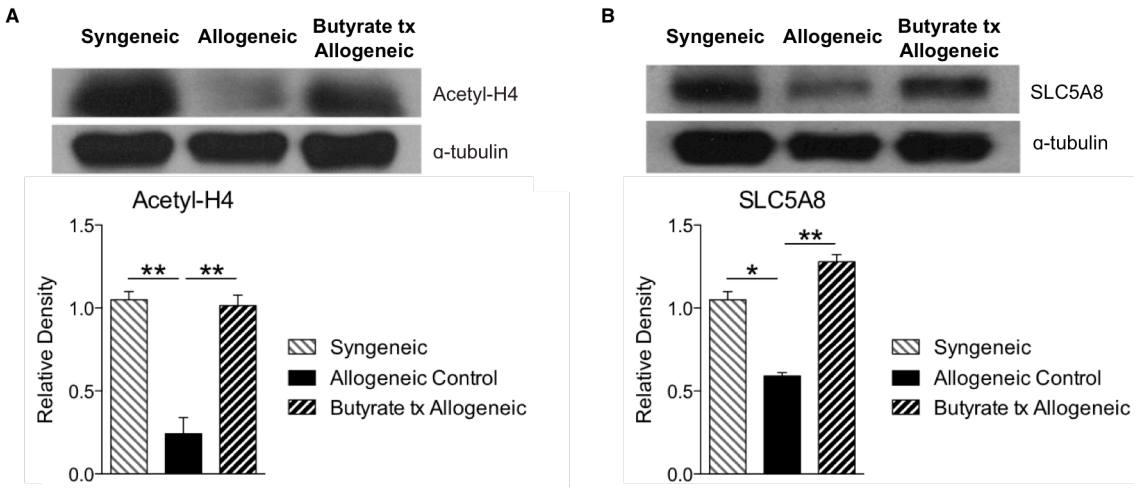

Fig. 5.11 – Local intragastric administration of butyrate increases acetylated-H4 and SLC5A8 in IECs. Immunoblot of CD326^{+} purified intestinal epithelial cells from syngeneic (BALB/c → BALB/c) or allogeneic (C57BL/6 → BALB/c) BMT recipients treated daily with intragastric vehicle or butyrate (10mg/kg) exhibit restored (**A**) acetylated histone-H4 and (**B**) SLC5A8 within 21 days of BMT with densitometric analysis of three experiments combined, shown below blots. Representative immunoblots shown. * $P < 0.05$; ** $P < 0.01$

Furthermore, daily intragastric gavage of butyrate resulted in an increase in butyrate transporter SLC5A8 (Fig. 5.11B), suggesting that butyrate may have a positive feedback mechanism resulting in an increase of its own transporter. To determine whether butyrate directly was responsible for induction of its own transporter, we analyzed the level of histone acetylation at the promoter of SLC5A8 with chromatin immunoprecipitation assay (ChIP). We found an increased association of acetylated histone H4 in the promoter region of SLC5A8 in IECs (CD326^{+}) treated with butyrate (Fig. 5.12).

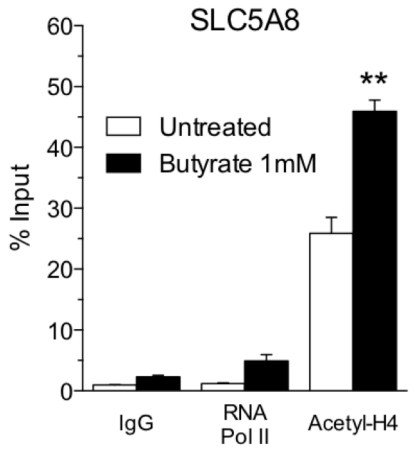

Fig. 5.12 – Butyrate increases association of acetyl-H4 with SLC5A8. Chromatin immunoprecipitation (ChIP) of butyrate treated IECs ($CD326^{+}$) exhibit increased acetylated histone H4 in the promoter region of SLC5A8.
** $P < 0.01$

Increase in intestinal butyrate mitigated GVHD severity: Systemic administration of HDACi decreases inflammation, enhances Tregs, and reduces *in vivo* biological responses such as acute GVHD[48,245,250]. We therefore determined if increasing local levels of endogenous HDACi, butyrate, would impact *in vivo* biological responses such as GVHD. Again using the C57BL/6 into Balb/c model, we administered vehicle control or butyrate via daily intragastric gavage for one week, followed by administration every other day for the remainder of the experiment.

Local intragastric administration of butyrate resulted in decreased weight loss (Fig. 5.13A) and GVHD clinical scores (Fig. 5.13B) culminating in increased survival (Fig. 5.13C) of allo-BMT recipients compared with vehicle control recipients.

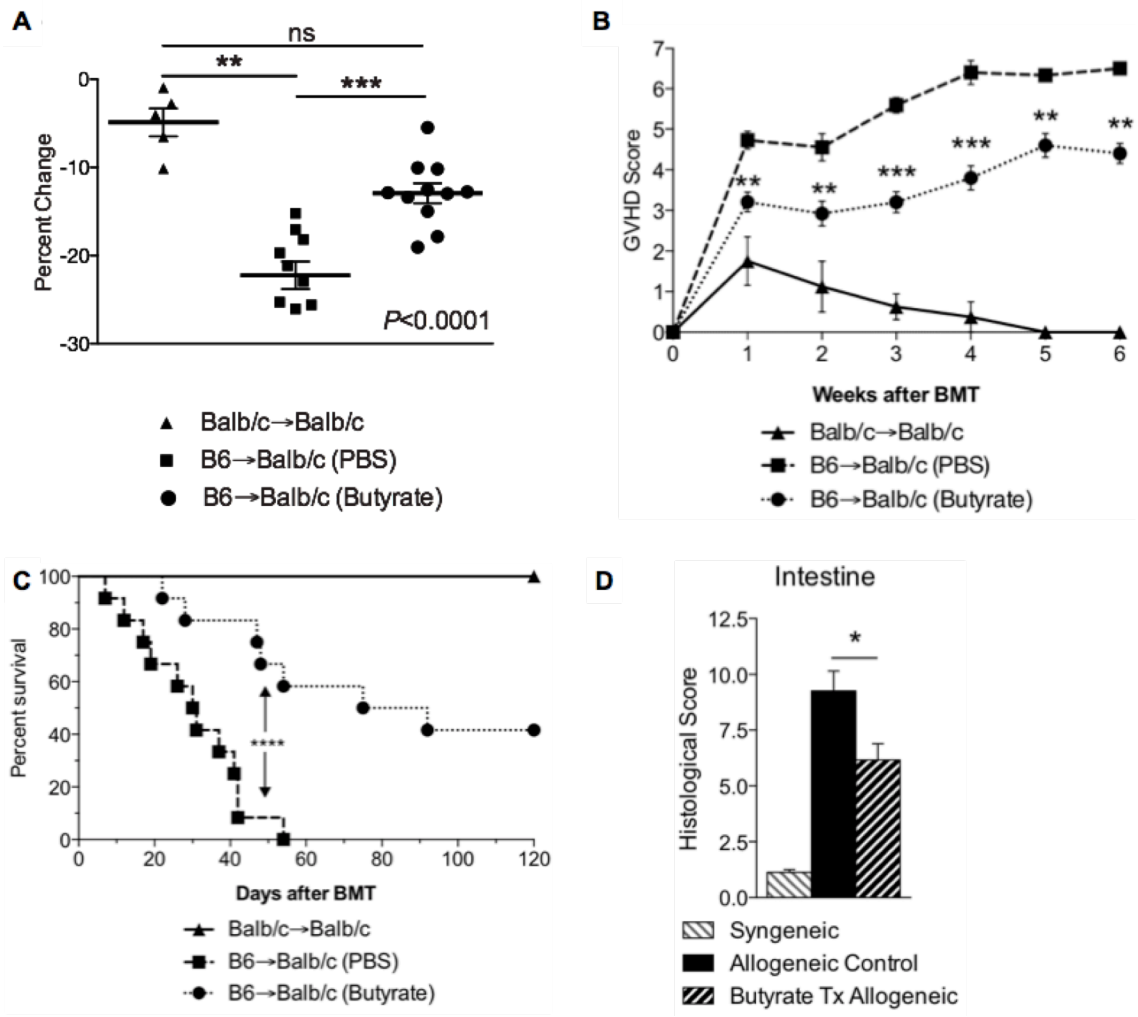

Fig. 5.13 – Intragastric gavage of butyrate decreases GVHD and improves survival. (**A**) Decreased weight loss on day 21 with (**B**) decreased**,** GVHD clinical score, (**C**) improved survival, and (**D**) decreased 21 day post- BMT intestinal histopathology of recipients of syngeneic or allogeneic BMT treated with intragastric butyrate or vehicle. * P < 0.05; ** P < 0.01; *** P < 0.001

We found similar improved survival using a second clinical model of BMT utilizing a MHC-matched, minor antigen mismatched model in which C3H.SW (H-2^b) cells are transferred to C57BL/6 (H-2^b) mice, thus demonstrating strain-independent results (Fig. 5.14). Furthermore, histopathological analysis 21 days following BMT revealed that recipients of butyrate intragastric gavage exhibited decreased histological scores in the intestines (Fig. 5.13D).

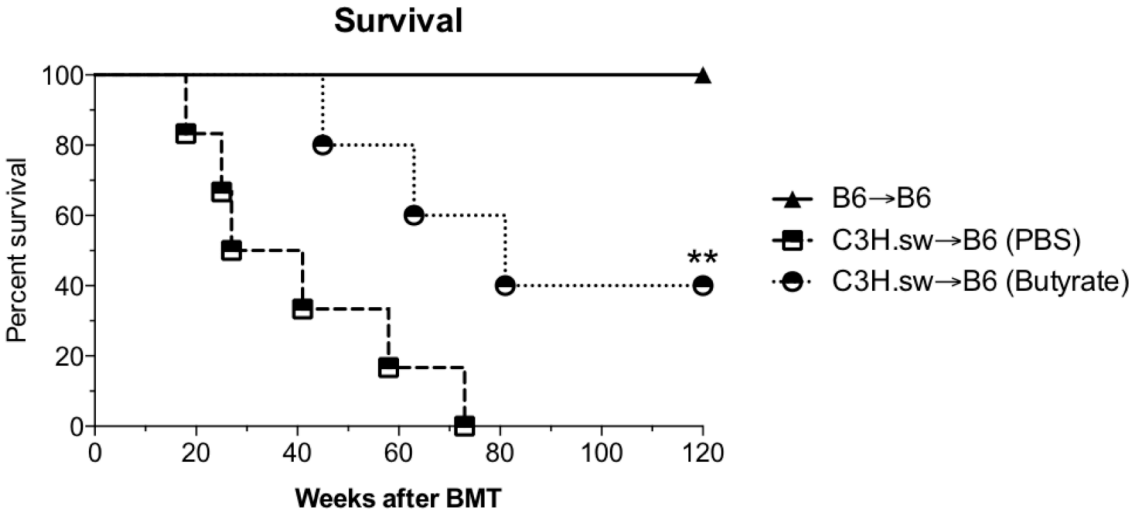

Fig. 5.14 – Intragastric gavage of butyrate improves survival of mMHC-mismatch BMT. Improved survival was observed using a second model of syngeneic (C57BL/6 → C57BL/6) and allogeneic (C3H.sw → C57BL/6) BMT indicating strain independent effects. Each recipient received 2 x 106 T cells and 5 x 106 bone marrow cells following lethal irradiation (1000 cGy) on day -1. ** $P < 0.01$

Increase in intracellular butyrate protects GI epithelium: We next determined if the decreased GI GVHD resulted in reduced translocation of luminal contents and improved epithelial integrity. Because allogeneic targeting of IECs disrupts cellular tight junctions[256-258], we utilized transmission electron microscopy (TEM) to examine the ability of butyrate to preserve cellular junctions following allo-BMT. Significantly, intense leakage of the electron dense stain ruthenium red[257] was found in the cell-cell interstitial space of allo-BMT recipients treated with vehicle alone (Fig. 5.15A, middle panel). However, the integrity of the IEC junction was preserved at both day 7 (Fig. 5.15A, right panel) and day 21 (Fig. 5.15B) in allo-BMT recipients that received local intragastric administration of butyrate.

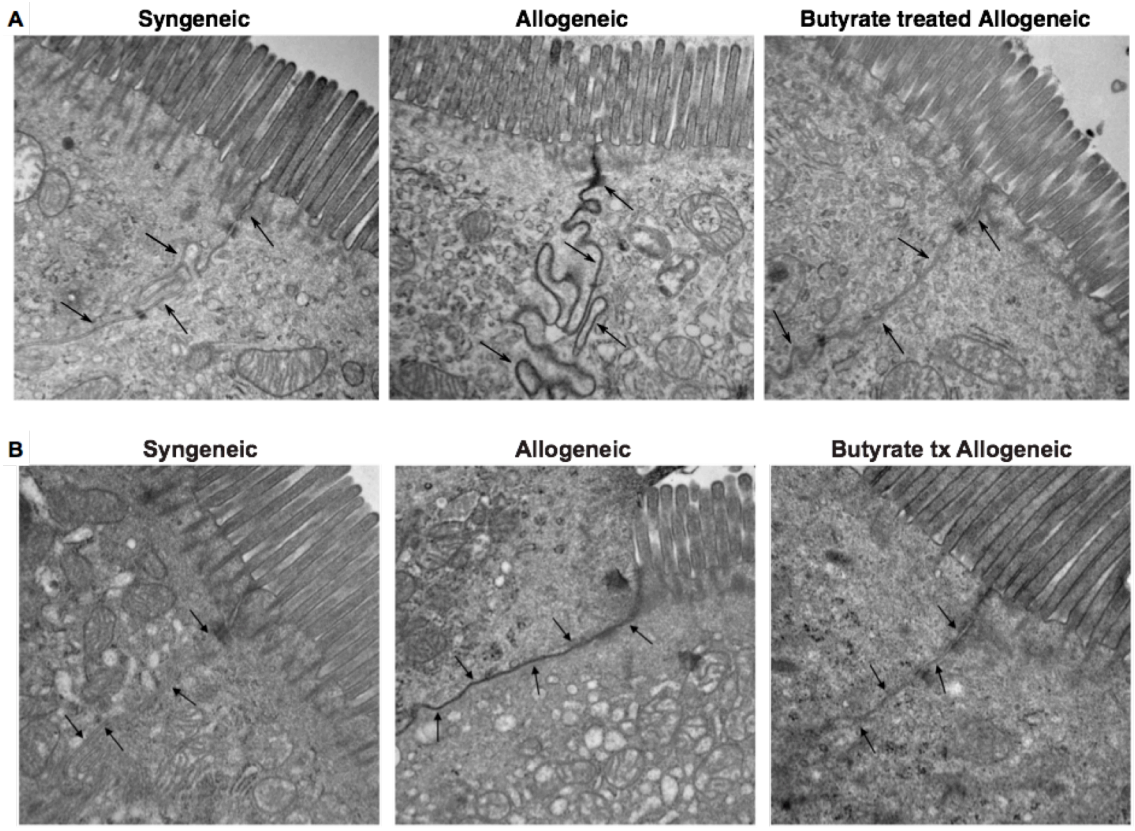

Fig. 5.15 – Butyrate improves IEC junctions. Transmission electron microscopy (TEM) of intestines, isolated from recipients of syngeneic (BALB/c → BALB/c) or allogeneic (C57BL/6 → BALB/c) transplant with or without intragastric gavage of butyrate for duration of experiment; all samples were isolated (**A**) 7 and (**B**) 21 days following BMT and stained with ruthenium red (0.1%). Intense ruthenium red leakage observed in recipients of allogeneic transplant treated with vehicle compared to butyrate treatment or syngeneic BMT; arrows indicate cell interface.

Utilizing a complementary methodology, we further assessed the intestinal permeability after allo-BMT by intragastric administration of FITC-dextran, a non-metabolized carbohydrate[259]. Butyrate-treated allo-BMT recipients exhibited significantly less detectable FITC-dextran in the serum at 21 days (Fig. 5.16) following transplant.

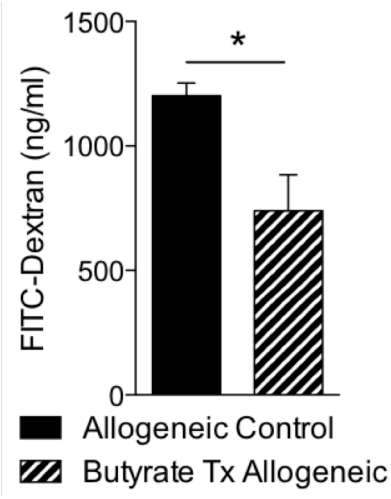

Fig. 5.16 – Less FITC-dextran traverses IEC barrier in butyrate treated allo-BMT recipients. Decreased level of FITC-dextran translocation across the GI-barrier into blood serum in butyrate treated allogeneic BMT recipients, compared to vehicle control 21 days post BMT. * $P < 0.05$

Reduction in GVHD is independent of donor Tregs: We next explored the potential mechanisms of butyrate-induced protection in GI GVHD and examined several possibilities. First, T regulatory cells (Tregs) mitigate GVHD and butyrate has been shown to increase intestinal Tregs[103,260] in certain model systems. We therefore analyzed the cellular contents of the intestine 21 days after allo-BMT to determine whether butyrate had an impact on local Tregs. The total numbers of recovered cells from the intestine were not different between vehicle- and butyrate-treated allo-BMT recipients (Fig. 5.17A). By contrast, immunophenotypical analysis following allo-BMT revealed that intestinal infiltration of donor $CD4^+$ and $CD8^+$ T cells and activated T cells ($CD69^+$ and $CD44^{hi}$) was decreased in animals that received local intragastric butyrate administration (Fig. 5.17B).

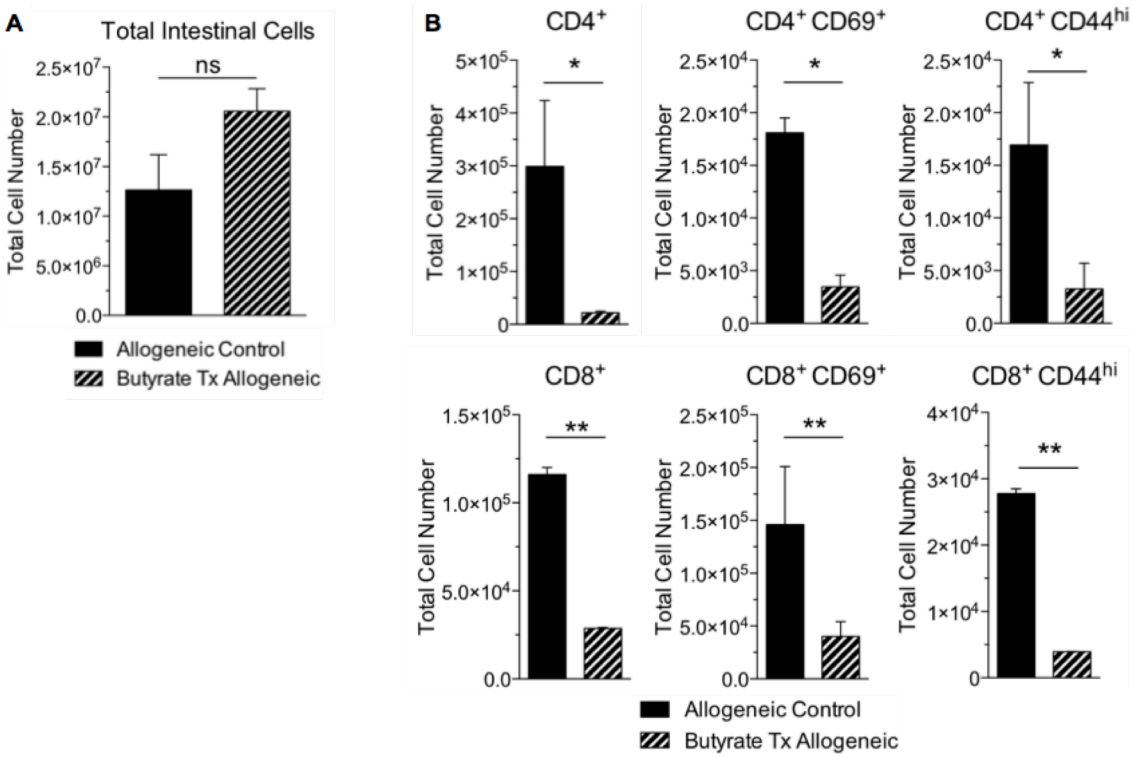

Fig. 5.17 – Fewer activated T cells in butyrate treated allo-BMT recipients. Intestinal immunophenotypical analysis of recipients 21 days following allogeneic (C57BL/6 → BALB/c) BMT treated with either butyrate or vehicle via intragastric gavage. (**A**) Total intestinal cell numbers harvested were not different between recipients of allogeneic BMT treated with butyrate or vehicle. (**B**) Total cell numbers of intestinal $CD4^+$ & $CD8^+$ T cells (left column) and activated T cells: $CD69^+$ T cells (middle column) & $CD44^{hi}$ T cells (right column). * $P < 0.05$; ** $P < 0.01$

However, the ratio of donor Tregs to effector T cells was not different in the intestine of these animals (Fig. 5.18A). Microbiota derived butyrate has been shown to increase immune-regulatory macrophages in the GI tract which increased Tregs[261]. Therefore we next determined whether administration of butyrate altered donor macrophage recovery from the intestinal tract. However we observed no difference in the total number of donor macrophages in the intestine of allogenenic recipients that were treated with either vehicle or butyrate (Fig. 5.18B).

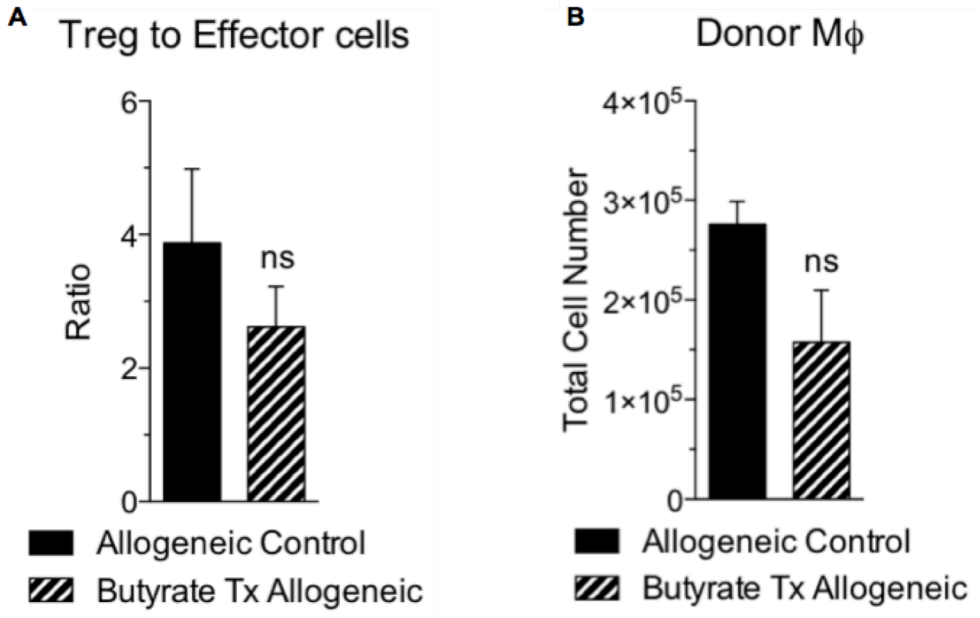

Fig. 5.18 – Intragastric gavage of butyrate does not alter Treg ratio or number of donor macrophages in the intestine. (**A**) Ratio of intestinal Tregs ($CD4^+CD25^+FoxP3^+$) to effector cells ($CD4^+FoxP3^-$) and (**B**) total cell number of intestinal donor macrophages ($CD11b^+F4.80^+$) in recipients of allo-BMT treated with vehicle or butyrate.

To further determine whether the salutary effects of local treatment with butyrate on GI GVHD were dependent on donor Tregs, we next performed a BMT, utilizing the same MHC-mismatched BMT model in which C57BL/6 ($H\text{-}2^b$) cells are transferred to Balb/c ($H\text{-}2^d$) mice. We transferred T cell-depleted (TCD) bone marrow and purified $CD4^+$ $CD25^-$ T cells from donors and administered vehicle or butyrate to the recipients daily for 1 week, then every other day thereafter as above. We still observed decreased GVHD clinical scores (Fig. 5.19A) and improved survival (Fig. 5.19B) in the animals that received butyrate despite the absence of donor Tregs.

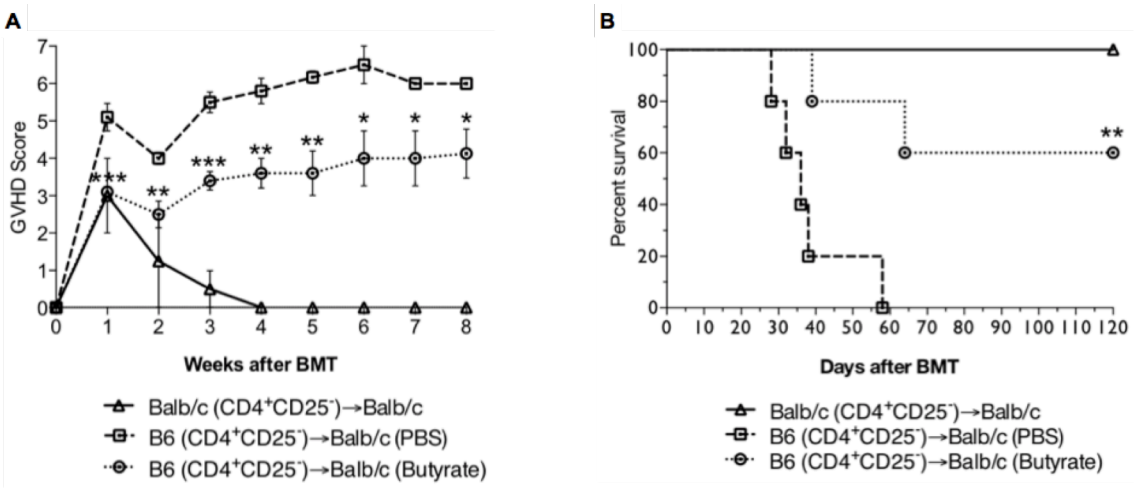

Fig. 5.19 – Improved GVHD score and increased survival were still observed in the absence of Tregs. Syngeneic (BALB/c → BALB/c) and allogeneic (C57BL/6 → BALB/c) BMT and butyrate treatment in recipients that received $CD4^{+}CD25^{-}$ (Treg depleted) donor T cells and T cell depleted (TCD) bone marrow resulting in (**A**) decreased GVHD score and (**B**) improved survival in animals treated with butyrate (10mg/kg).

To further examine whether the local administration of butyrate impacted donor T cells directly, we determined the HDAC and HAT enzymatic activity in donor T cells harvested from the recipient animals. Both the HDAC activity (Fig. 5.20A) or HAT activity (Fig. 5.20B) in the donor T cells harvested from the recipient spleen were similar between butyrate and vehicle treated allogeneic animals. These results suggest that the reduction in GI GVHD upon intragastric administration of butyrate is independent of its potential effects from donor Tregs.

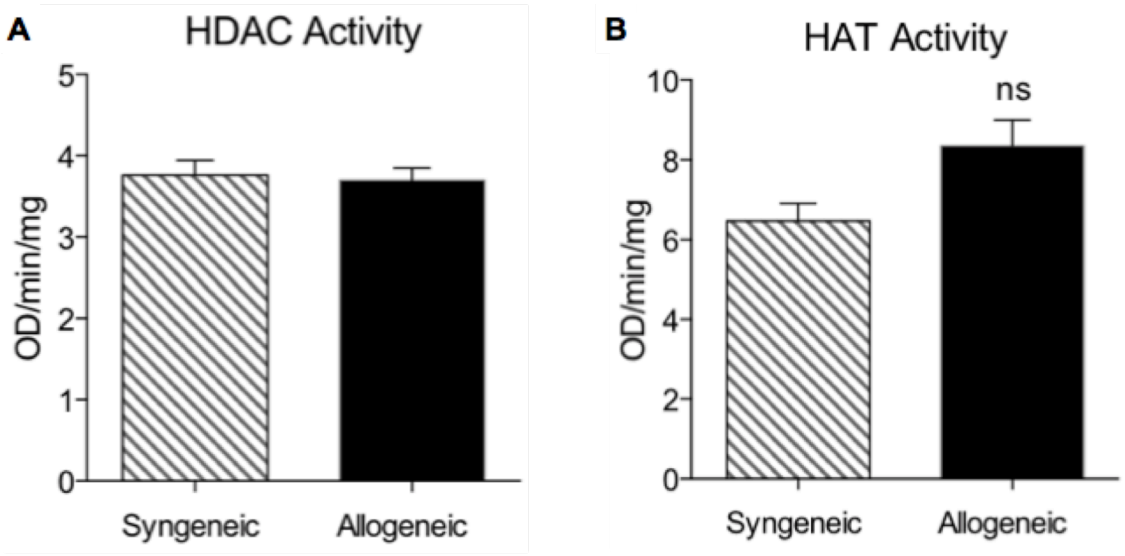

Fig. 5.20 – No difference in splenic T cell HDAC or HAT activity. (**A**) HDAC activity and (**B**) HAT activity was not altered in T cells of the spleen 21 days following syngeneic or allogeneic BMT.

Microbial metabolite, butyrate protects IECs from conditioning and allo-T cell mediated damage: We next sought to explore the potential mechanisms that contribute to butyrate-induced protection from severe GVHD. Because (a) butyrate is decreased in IECs, (b) administration of butyrate mitigated GI GVHD independent of Tregs, but (c) improved junction integrity, we therefore explored whether butyrate had direct effects on protecting IECs from allo-T cell mediated damage and conditioning. We hypothesized that the absence of butyrate would result in increased irradiation-induced apoptosis and allogeneic-mediated damage of IECs. To test this we treated IECs *ex vivo* with vehicle or butyrate for 24 hours and withheld or subjected the cells to irradiation (6 Gy), followed by 24 hours of additional incubation with butyrate. We observed that butyrate was not toxic to IECs (Fig. 5.21A, left) and more importantly conferred protection from irradiation-induced apoptosis (Fig. 5.21A, right).

Furthermore, to determine if butyrate protected IECs from allogeneic T cell-mediated damage, we next determined the ability of butyrate-treated IECs to withstand damage mediated by alloreactive T cells. We isolated and cultured primary IECs with butyrate or vehicle control, overnight. The pre-treated IECs were next co-cultured with primed allogeneic $CD8^+$ T cells, in the absence of butyrate. Fewer butyrate pre-treated IECs succumbed to $CD8^+$ T cell killing within 6 hours (Fig. 5.21B, left) and 16 hours (Fig. 5.21B, right) following co-culture, compared with control.

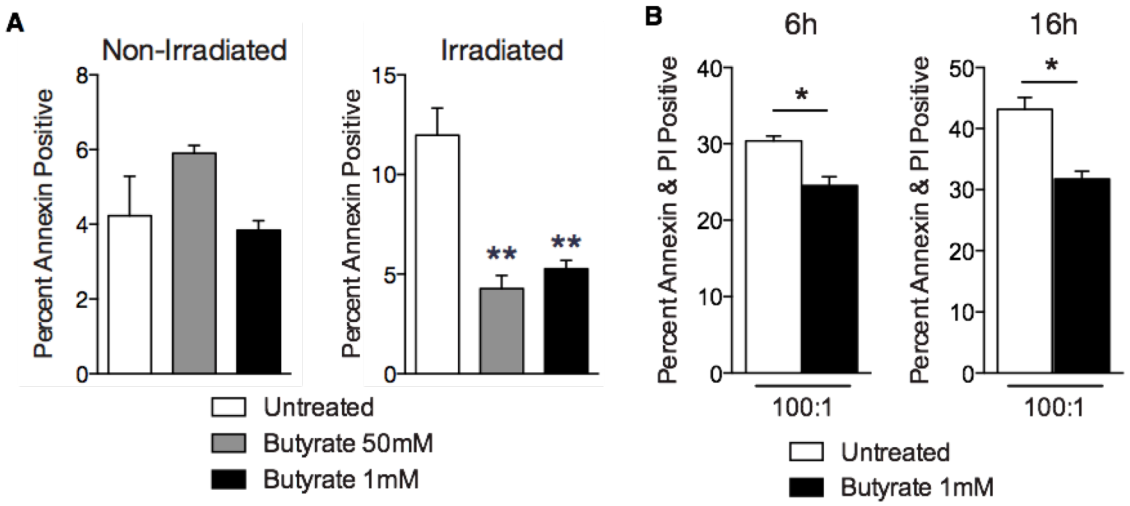

Fig. 5.21 – Butyrate protects from irradiation- and allo-induced apoptosis. (**A**) $CD326^+$ purified intestinal epithelial cells (IECs) cultured in the presence or absence of butyrate and withheld (left panel) or subjected to (right panel) irradiation (6 Gy). Butyrate did not effect the viability of IECs but protected these cells from irradiation induced apoptosis. (**B**) Allogeneic $CD8^+$ T cell killing assay. $CD326^+$ IECs incubated with or without butyrate overnight followed by co-culture with allo-primed $CD8^+$ T cells resulted in less allo-induced apoptosis in butyrate pretreated IECs. * $P < 0.05$; ** $P < 0.01$

Because butyrate is a primary energy source for IECs[60,61,249], we next determined whether butyrate enhances survival and growth of IECs *in vitro*. To this end, we cultured intestinal organoids in the presence or absence of butyrate. We observed that culture in the presence of butyrate significantly increased organoid size (Fig. 5.22A). Next we

confirmed the impact of butyrate on IEC junctional function in the organoid cultures by determining the expression levels of claudins (Fig. 5.22B). We further observed that culture of organoids with butyrate significantly increased the expression of several junctional proteins such as claudins (1, 5, 6, 10, 11, 13, 14, 17, and 18).

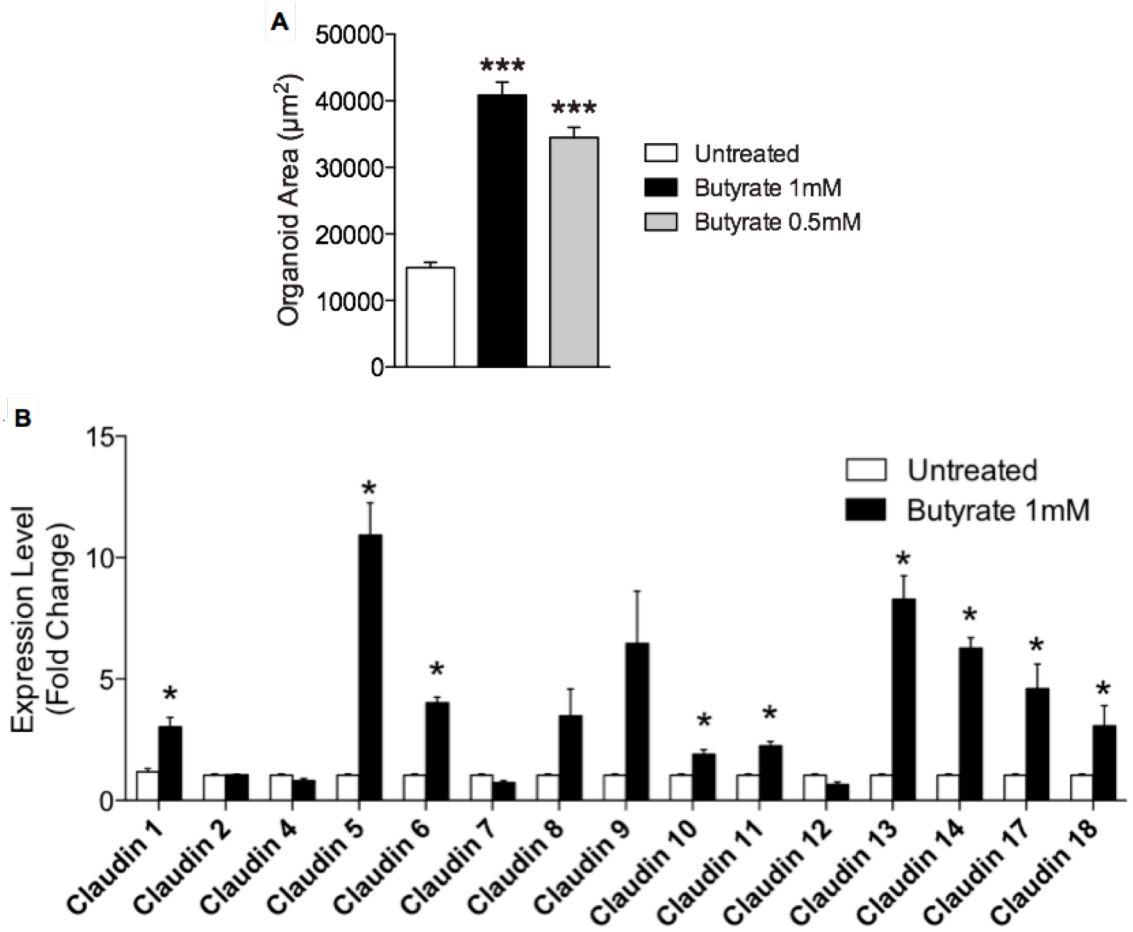

Fig. 5.22 – Butyrate increases organoid size and improves organoid junctions. (**A**) Butyrate treatment (0.5mM and 1mM) resulted in increased size (area, μm^2) of cultured primary intestinal organoids, compared to control. (**B**) Butyrate treatment (1mM) resulted in increased expression of junctional claudins (1, 5, 6, 10, 11, 13, 14, 17, and 18) in cultured primary intestinal organoids, compared to control. * $P < 0.05$; *** $P < 0.001$

Molecular mechanisms of IEC protection: To determine the potential molecular mechanism for enhanced protection from irradiation- and allogeneic T cell-mediated

apoptosis, we hypothesized that butyrate would increase anti-apoptotic genes by modulation of histone acetylation. We analyzed pro- and anti-apoptotic gene expression levels[262] and found that BAK and BAX were significantly decreased (Fig. 5.23A), whereas transcripts of the anti-apoptotic protein BCL-B were significantly increased (Fig. 5.23B) in butyrate treated IECs ($CD326^{+}$).

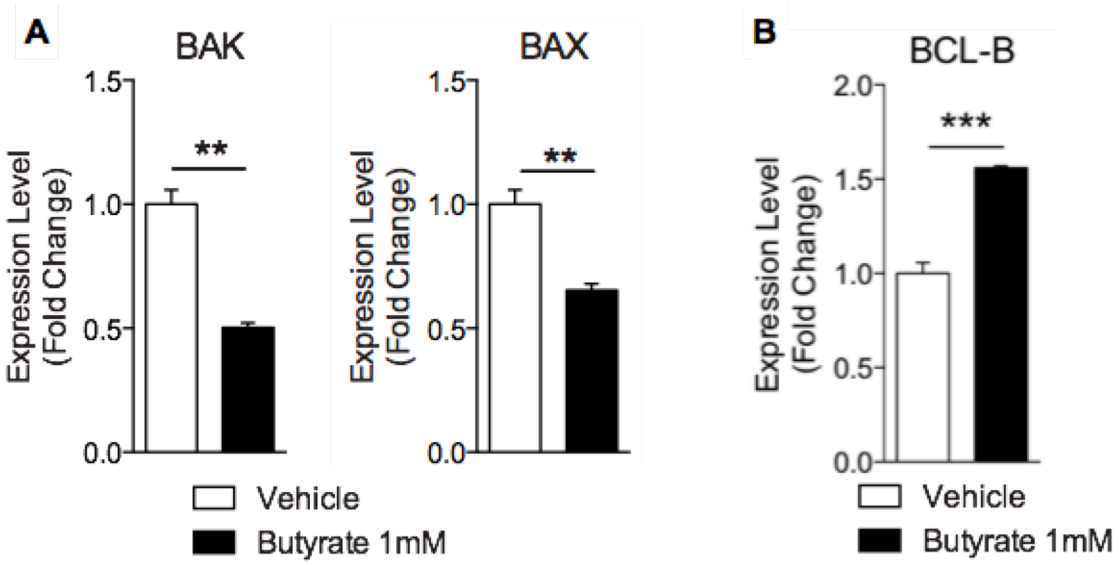

Fig. 5.23 – Butyrate treatment of IECs decreases pro-apoptotic proteins and increases anti-apoptotic proteins. (**A**) Decreased gene expression of the pro-apoptotic proteins BAK (left) and BAX (right) and (**B**) increased expression of the anti-apoptotic protein BCL-B ** $P < 0.01$; *** $P < 0.001$

Next we determined whether butyrate had direct impact on the improved junctional integrity of IECs. We therefore examined expression levels of junctional proteins such as occludin and JAM (Fig. 5.24) in IECs ($CD326^{+}$) following butyrate treatment, which significantly increased their expression.

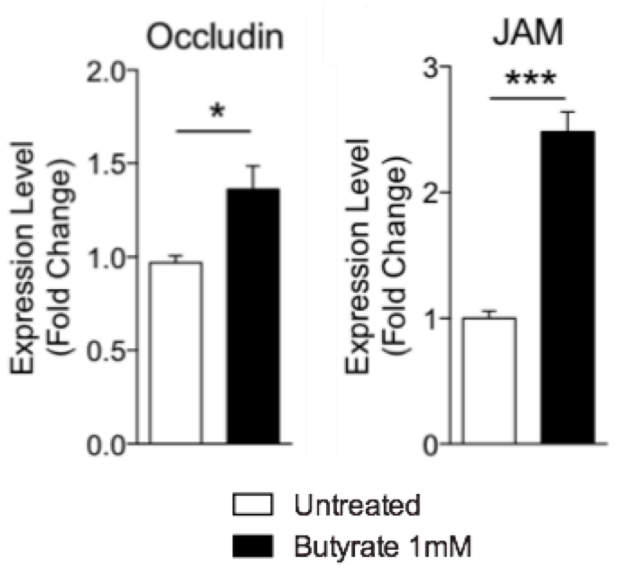

Fig. 5.24 – Butyrate treatment of IECs increases mRNA expression of junctional proteins. Gene expression level junctional proteins occludin and JAM in primary CD326^{+} IECs is increased when cultured in the presence of butyrate 1mM. * P < 0.05; *** P < 0.001

We also determined if the restored levels of histone-H4 acetylation observed in butyrate-treated allo-BMT recipients was responsible for increased BCL-B and JAM expression via ChIP. We found that acetylated histone-H4 was indeed associated with the promoter region of BCL-B (Fig. 5.25A) and JAM (Fig. 5.25B) in butyrate treated IECs (CD326^{+}).

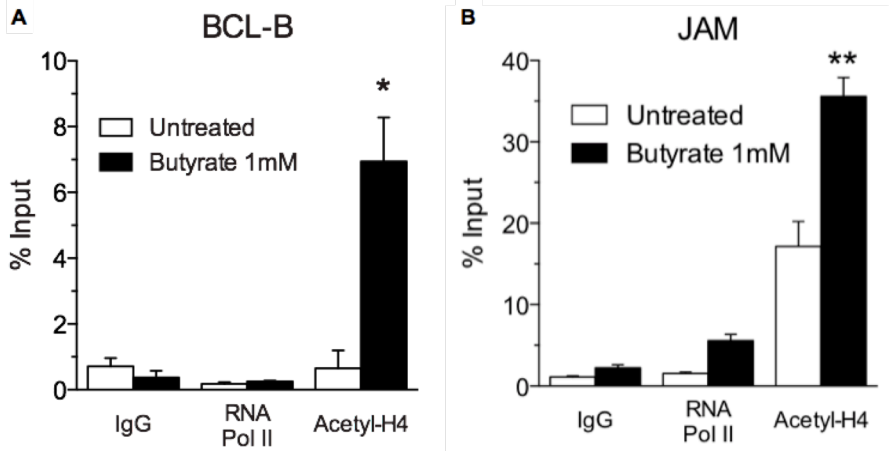

Fig. 5.25 – Butyrate treatment of IECs increases acetyl-H4 association with BCL-B and JAM. Butyrate has direct effects on BCL-B and JAM as chromatin immunoprecipitation assay (ChIP) of butyrate treated IECs (CD326^{+}) exhibit increased acetylated histone H4 in the promoter region of (**A**) BCL-B and (**B**) JAM. * P < 0.05; ** P < 0.01

These data thus collectively suggest butyrate has several salutary effects on IECs that may or may not be mutually exclusive, such as regulating the expression of genes involved in decreased IEC apoptosis and increased junctional proteins in IECs. To determine if these are involved in *in vivo* protection from GVHD, we determined the expression of pro- and anti-apoptotic proteins as well as junctional proteins in IECs ($CD326^+$) isolated 21 days following allo-BMT.

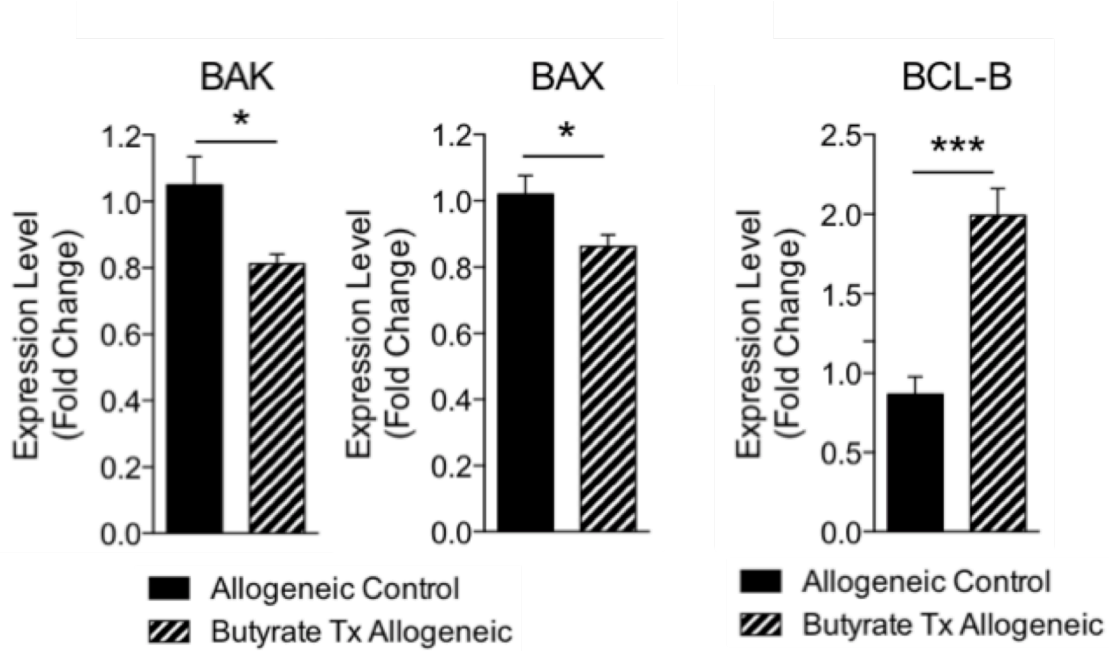

Fig. 5.26 – Intragastric gavage of butyrate increases anti-apoptotic gene expression, *in vivo*. Analysis of IECs ($CD326^+$) isolated from recipients of syngeneic (BALB/c → BALB/c) and allogeneic (C57BL/6 → BALB/c) BMT treated with butyrate or vehicle daily via intragastric gavage for 21 days. Butyrate treatment of allogeneic recipients decreased gene expression level of pro-apoptotic proteins BAK (left) and BAX (middle), increased the anti-apoptotic protein BCL-B (right) * $P < 0.05$; *** $P < 0.001$

We once again observed similar results as seen *in vitro* with pro-apoptotic proteins BAK and BAX significantly decreased in allo-BMT recipients that received intragastric butyrate treatment (Fig. 5.26) and significantly increased transcripts of the anti-apoptotic protein BCL-B (Fig. 5.26). Further, gene expression of junctional proteins were, again,

similarly increased in butyrate treated animals (Fig. 5J). Overall, our results identify several ways in which butyrate can directly enhance epithelial cell function ranging from protection from irradiation and allo-T cell mediated apoptosis to proliferation and junctional protein expression, both *in vitro* and *in vivo*.

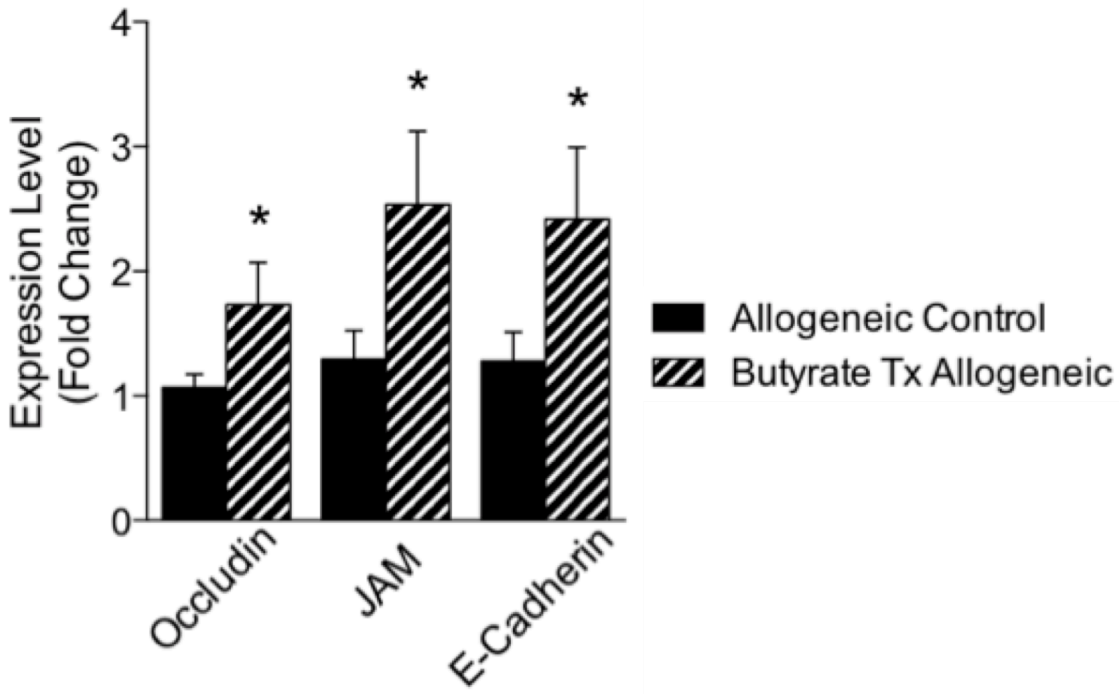

Fig. 5.27 – Intragastric gavage of butyrate increases junctional protein gene expression, *in vivo*. Increased junctional protein gene expression in $CD326^{+}$ purified IECs isolated 21 days following allo-BMT. * $P < 0.05$

Increasing butyrate levels by administration of rationally designed microbiota mitigates GVHD: The endogenous HDACi butyrate is a by-product of microbial fermentation[163] and our data suggested that increased local butyrate decreases GVHD. Therefore, we next tested the hypothesis that altering the composition of indigenous GI microbiota in hosts to those that can produce high levels of butyrate will mitigate GVHD. To test this hypothesis, we utilized 17 rationally selected strains of Clostridia that have been shown to increase butyrate both *in vitro* and *in vivo*[103,263]. We administered these 17

strains via intragastric gavage every other day to naïve mice starting 14 days prior to allo-BMT and continued administration of the 17-strain cocktail for 21 days post-BMT. Prior to BMT, we wanted to determine whether these strains could establish colonization despite the presence of an indigenous host microbiota. Therefore, we characterized the microbiota in feces collected from animals that received vehicle and 17-strain administration by 16S rRNA-encoding gene sequencing. In animals that received the 17 Clostridial strains, 16S analysis[264-266] revealed an important biologically significant shift in the microbiota indicating that these organisms could be detected as part of the gut microbiota with increased colonization of the 17 strains in naïve mice within 14 days (day -1 relative to BMT) of commencing administration (Fig. 5.28A and Fig. 5.28B).

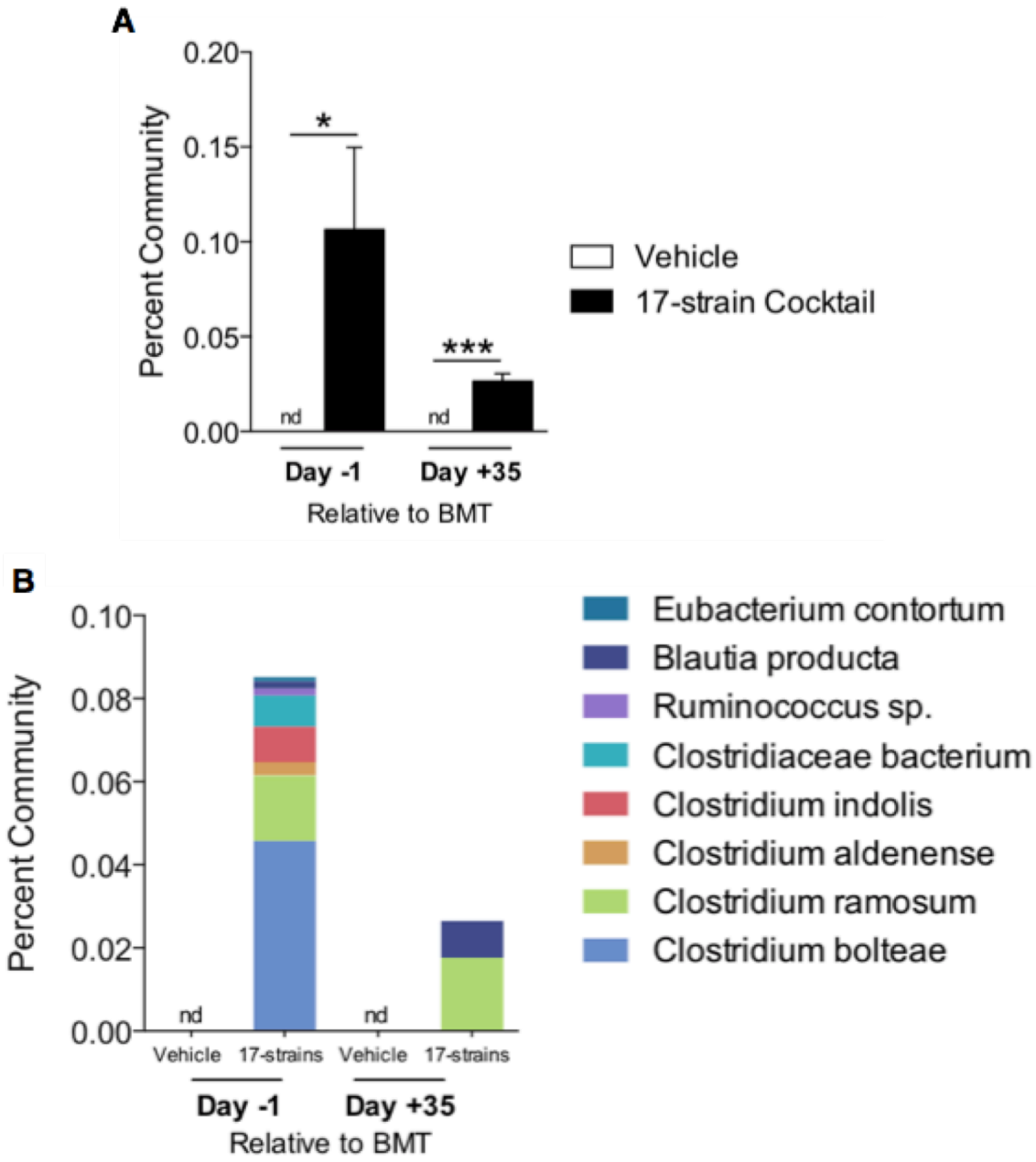

Fig. 5.28 – Intragastric gavage of 17 strains of Clostridia take hold amongst indigenous microbiota. (**A**) 16S rRNA-encoding gene sequencing of stool for percent of 17 Clostridal strains in total GI community on day -1 and day +35, relative to allogeneic (C57BL/6 → BALB/c) BMT on day 0. Vehicle or 17-strain cocktail were administered to recipients every other day via intragastric gavage beginning day -14 and continued through day +21, relative to BMT. (**B**) Detailed presence of bacterial strains found in animals colonized with 17-strain cocktail. nd – not detected. * $P < 0.05$; *** $P < 0.001$

Furthermore, GC/MS analysis 21 days following allo-BMT revealed an increased trend of butyrate in the luminal contents (Fig. 5.29A) and a significantly increased level of butyrate in the intestinal tissues (Fig. 5.29B) of animals that received intragastric gavage of the 17 Clostridial strains.

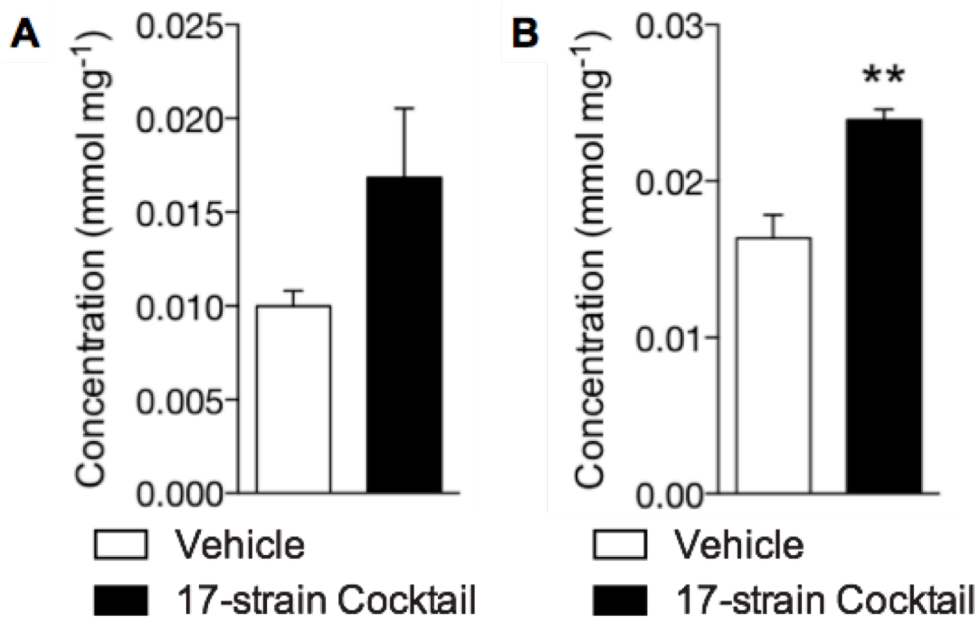

Fig. 5.29 – Intragastric gavage of 17 strains of Clostridia increase butyrate in the intestinal tissue. Recipients of allogeneic BMT gavaged with vehicle or colonized with 17-strain cocktail were sacrificed 21 days following BMT. Intestinal luminal contents (stool) and intestinal tissue were harvested and analyzed via GC/MS. (**A**) Allo-BMT recipients colonized with 17 Clostridial strains exhibited butyrate levels that trended higher in the intestinal lumen and (**B**) butyrate levels that were significantly higher in the intestinal tissue.
** $P < 0.01$

Importantly, the recipients of intragastric gavage of the 17 strains and allo-BMT exhibited significantly decreased GVHD (Fig. 5.30A) and increased survival (Fig. 5.30B). Detectable levels of the 17 Clostridial strains were diminished within 2 weeks (day +35) of ceasing intragastric administration (Fig. 5.28).

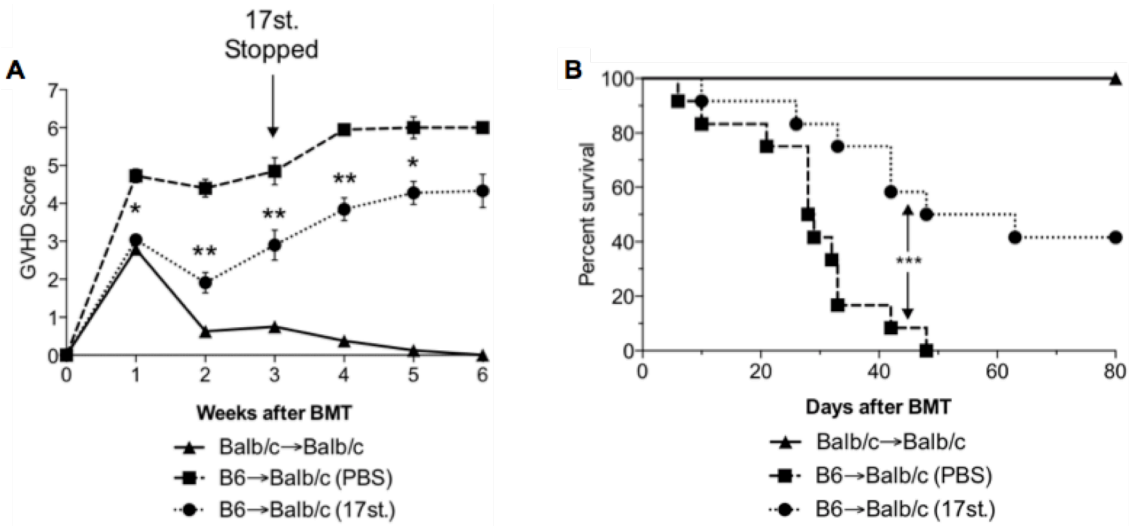

Fig. 5.30 – Intragastric gavage of 17 strains of Clostridia decreases GVHD and improves survival. (**A**) Decreased GVHD clinical score and (**B**) increased survival following syngeneic (BALB/c → BALB/c) and allogeneic BMT (C57BL/6 → BALB/c) with vehicle or 17-strain administration.
* P < 0.05; ** P < 0.01; ** P < 0.01

Because microbiota variations are known to occur in different colonies of mice, we also determined whether mice housed at another institution (Memorial Sloan Kettering Cancer Center) and treated with the same 17 Clostridial strains would also mitigate GVHD. Additionally, because clinical BMT patients are often treated with antibiotics, as an alternative approach to colonizing the indigenous microbiota, we treated C57BL/6 (H-2^b) mice with an antibiotic cocktail (ampicillin 5mg, metronidazole 4mg, clindamycin 5mg, vancomycin 5mg) daily by intragastric gavage for 6 days to target obligate anaerobes. The mice were then colonized 4 and 6 days later with either human E. faecalis or the same cocktail of 17 strains of human Clostridia[103] by intragastric gavage. Once again, we characterized the fecal microbiota by 16S gene sequence analysis on day -1, relative to BMT. Upon analysis, we observed increased presence of the Clostridial strains in recipients that received the cocktail of Clostridia (Fig. 5.31A), compared to recipients of

E. faecalis. The animals were next used as recipients of a MHC-mismatched B10.BR (H-2^k) BMT and followed for survival. Once again, we observed significantly increased survival in the animals treated with the cocktail of 17 Clostridial strains (Fig. 5.31B).

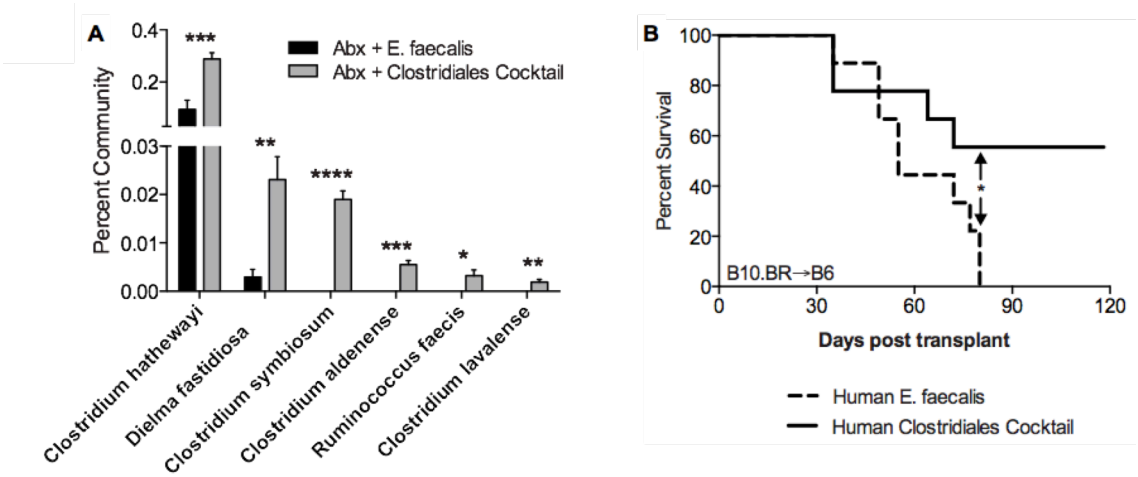

Fig. 5.31 – Intragastric gavage of 17 strains of Clostridia decreases GVHD and improves survival - MSKCC. (**A**) Decreased GVHD clinical score and (**B**) increased survival following syngeneic (BALB/c → BALB/c) and allogeneic BMT (C57BL/6 → BALB/c) with vehicle or 17-strain administration.
* P < 0.05; ** P < 0.01; ** P < 0.01

These results suggest that altering the indigenous microbiota with rationally selected strains of Clostridia, known to produce high levels of butyrate[103,263], can decrease the severity of GVHD and improve survival across multiple institutions with strain independent results.

DISCUSSION

Previous studies have shown that the community structure of the microbiota is altered following allo-BMT[133,134]. The impacts that these alterations in microbial diversity have on the GI metabolome have thus far been unknown. Our results provide a novel perspective on microbial metabolites and their impact on GVHD. Here, we use an unbiased, blinded method to analyze targeted by-products of microbial fermentation. Our FA profiling revealed that the greatest and only significantly decreased SCFA, butyrate, is diminished in the intestinal tissue after allogeneic transplant (Fig. 5.2B). Reduction of butyrate in allo-BMT IECs decreased histone-H4 acetylation while increasing butyrate via intragastric gavage restored acetylated histone-H4 levels, protected epithelial integrity, decreased the severity of GVHD, and increased survival following allogeneic BMT. An important and surprising observation was the lack of changes in luminal (stool) butyrate, despite a documented shift in the microbiome species that produce less butyrate after allo-BMT[133]. While it remains to be formally tested, we posit that this may be because of reduced uptake into IECs due to decreased butyrate transporter, thus leaving overall butyrate levels not significantly reduced in the lumen because less is being taken into the IECs despite a decreased production by the shift in the microbiota after allo-BMT.

While at high concentrations, some amount of butyrate can passively diffuse across epithelial cell membranes[252]. At low concentrations, the effects of butyrate on IECs are dependent upon the sodium-coupled monocarboxylate transporter SLC5A8 and the G-protein coupled signaling receptor (GPCR) GPR43[252]. By contrast the reasons for

decreased transporter proteins after allo-BMT are intriguing. Previous reports observed a decrease in SLC5A8 following alterations in the microbiota[267]. Thus, our findings that SLC5A8 and GPR43 are decreased in IECs ($CD326^{+}$) following allo-BMT are consistent with this report and other studies revealing taxonomic changes in the microbiota occur after allo-BMT[133,134]. Furthermore we demonstrate for the first time to our knowledge that exposure of IECs to inflammatory cytokines leads to reduction in the expression of butyrate transporters. Moreover our data suggest that butyrate appears to have a positive feedback effect on its own transporter expression. These data suggest that the inflammatory milieu early after allo-BMT reduces the levels of butyrate transporter SLC5A8 leading to its reduction in the IECs and further reducing transporter expression and butyrate intake in a feedback mechanism. These insights will need to be formally tested further in future studies. Nonetheless, our data suggest increased local butyrate, either by exogenous source or by increased microbiota-derived butyrate, could increase IEC butyrate by passive diffusion and enhance expression of SLC5A8, break the feedback loop, and mitigate GI damage and decrease GVHD[252].

Previous studies have shown that 17 rationally selected strains of Clostridia, which produce high levels of butyrate, increase Tregs in the intestines[103]. Although we did not observe an increase in Treg cells in the intestine following butyrate treatment of allo-BMT recipients, we cannot formally rule out the contribution of butyrate-mediated effects on Tregs (directly or indirectly via macrophages) for decreased GVHD when they are present in the donor inoculum. Nonetheless our data do suggest that butyrate administration could mitigate GVHD despite stringent depletion of mature donor Tregs.

Our data do however suggest that butyrate has direct salutary effects on the intestinal epithelial target tissue in GVHD. Thus, the effect of butyrate on GVHD target cells, namely GI epithelium, likely contributes to protection from GVHD. Our data does not directly address the impact of butyrate on various other cells that make up GI epithelium besides IECs. Clearly, butyrate and HDACi also have a multitude of effects on immune cells and our data cannot directly measure their impact on GVHD protection. However, a growing body of evidence indicates that GVHD pathophysiology can be regulated by manipulation of the host response to injury, and not just by suppressing the donor immune system[259,268,269]. Our results extend these observations and suggest that direct modulation of target tissues could be an additional important strategy to decrease GVHD without resorting to further global immunosuppression.

In conclusion, our novel finding that alterations in microbial diversity after allo-BMT change the microbial metabolic profile, specifically that of butyrate, is a paradigm shift in our understanding of the mechanisms through which the microbiota confer their effects on host homeostasis. The data demonstrate a complex nexus between microbiota, metabolism and epigenetic regulation of target tissues in determining the severity of GVHD. Our findings may have important clinical implications and suggest that increasing local levels of butyrate in the GI tract may mitigate GVHD severity without causing global immunosuppression. Thus, increasing the endogenous local levels of the HDACi butyrate by enhancing the microbiota with 17 high butyrate-producing rationally selected Clostridia strains[103,263], reduces the severity of GVHD in clinical models and thus may be a novel therapeutic strategy for management of clinical GVHD.

MATERIALS AND METHODS

Reagents: RPMI, penicillin and streptomycin, and sodium pyruvate were purchased from Gibco (Grand Island, NY); FCS from GemCell (Sacramento, CA); 2-ME from Sigma (St. Louis, MO); murine GM-CSF from Peprotech (Rocky Hill, NJ). All antibodies (Abs) used for FACS were purchased from eBioscience (San Diego, CA). DMSO and butyrate were obtained from Sigma (St. Louis, MO), and lipopolysaccharide (LPS) from InvivoGen (San Diego, CA).

Mice: Female C57BL/6 (H-2^b; CD45.2^+), BALB/c (H-2^d) mice were purchased from National Cancer Institute and C3H.sw (H-2^b) mice were purchased from The Jackson Laboratory (Bar Harbor, ME). The age of mice used for experiments ranged between 7 and 12 weeks. All animals were cared for under regulations reviewed and approved by the University Committee on Use and Care of Animals of the University of Michigan, based on University Laboratory Animal Medicine guidelines.

Cell isolation and cultures: Primary intestinal epithelial cells (IECs) were obtained from C57BL/6 mice as described previously [270]. Briefly, luminal contents of intestine were flushed with CMF solution. Intestine was then minced into 0.5cm pieces, washed with CMF four times, transferred to CMF/FBS/EDTA, and incubated at 37 °C for 60 minutes (shaking tubes every 10 minutes). Supernatant containing IECs was then transferred through 100 μM cell filter followed by incubation on ice for 10 minutes to allow sedimentation. Supernatant was again transferred through a 75 μM cell filter. CD326$^+$

IECs were next purified utilizing either FACS or anti-APC magnetic microbeads (Miltenyi Biotec Ltd., Auburn, CA) and an autoMACs (Miltenyi Biotec).

For viability assay, $CD326^+$ IECs were seeded on gelatin coated 100mm culture dishes and treated in the presence of absence of indicated butyrate concentrations overnight. Cells were then subjected to or withheld from irradiation (6 Gy) and cultured for another 24 hours.

Bone Marrow Transplantation (BMT): BMTs were performed as previously described [39,245]. Briefly, syngeneic (BALB/c → BALC/c or C57BL/6 → C57BL/6) and allogeneic (C57BL/6 → BALB/c or C3H.sw → C57BL/6) recipients received lethal irradiation. On day -1, BALB/c recipients received a total of 800 cGy of irradiation (split dose separated by 3 hours) and B6 animals received a single dose of 1000 cGy. Donor splenic $CD90.2^+$ T cells were magnetically separated using an autoMACs (Miltenyi Biotec; Bergisch Gladbach, Germany) and $0.5 \times 10^6 - 1 \times 10^6$ T cells were transferred to BALB/c recipients and 2×10^6 T cells were transferred to C57BL/6 recipients. 5×10^6 donor whole bone marrow was transferred to all recipients. Survival was monitored daily and the recipient body weight and GVHD clinical scores were determined weekly, as described previously [39]. Histopathologic analysis of the gastrointestinal (GI) tract was performed as described [39]. Animals received vehicle (sterile water) or butyrate (10mg/kg) by flexible 20G-1.5" intragastric gavage needle daily for 1 week, then every other day thereafter.

For BMTs performed at MSKCC, C57BL/6 mice were treated with an antibiotic cocktail to target obligate anaerobes (ampicillin 5 mg, metronidazole 4 mg, clindamycin 5 mg,

and vancomycin 5 mg) gavaged daily for 6 days (BMT days -18 to -13) followed 4 and 6 days later by oral gavage with indicated bacteria (BMT days -9 and -7) or PBS. Clostridial bacteria were cultured individually on plates and resuspended in anaerobic PBS at a final OD (600nm) of 0.02 to 0.06. One week later, mice were irradiated (12 Gy single dose) and transplanted with B10.BR BM (5×10^6) and T cells (0.5×10^6 CD5 MACS), and followed for development of clinical GVHD.

Gas chromatography mass spectrometry (GC/MS): To determine targeted fatty acid quantitation, samples (plasma, spleen, liver, intestine, and intestinal fecal content) from mice 7d and 21d post-transplant were harvested, homogenized, and snap-frozen in liquid N_2. Equal volumes of plasma and homogenized tissue were utilized, while fecal content was weighed at necropsy. Samples were dispersed in acidified water spiked with stable isotope-labeled SCFA standards and extracted with diethyl ether. The ether layer was immediately analyzed by gas chromatography/mass spectroscopy using a Phenomenex ZB-WAX column on an Agilent 6890 GC with a 5973MS detector. Quantitation was performed by calibration to internal standards. The tissue levels were normalized by protein concentration of the homogenized tissue. Heatmap data was generated using GenePattern software from the Broad Institute (Cambridge, MA). Metabolomic data, mass spectral analytical parameters and spectral raw data from the study and meta data will be deposited in the National Institutes of Health Metabolomics Data Repository Coordinating Center (DRCC) at the University of California San Diego (http://www.metabolomicsworkbench.org/data/index.php).

16S deep sequencing: On indicated days, fecal pellets were collected from mice and stored at -80°C. DNA was extracted and purified with phenol-chloroform following bead-based lysis. Sequencing and analysis was performed as described [271]. Briefly, the V4 region of the 16S rRNA gene was sequenced using Ilumina MiSeq technology. Sequencers were trimmed and analyzed using Mothur [264]. The 16S rRNA gene sequence from each strain in the 17 strain cocktail was added to the version 9 trainset sequences from the Ribosomal Database Project [272]. The resulting sequences were classified by comparing to described trainset with the requirement that the confidence score is 100%. MSKK 16S experiment were analyzed using the Illumina MiSeq platform to sequence the V4-V5 region of the 16S rRNA gene. Sequence data were compiled and processed using mothur version 1.34 [264], screened and filtered for quality [265], then classified to the species level [273] using the Greengenes reference database [266].

17 strain mixture: The 17 strain mix was prepared as described [103]. Briefly all strains were grown in 5 ml of EG media for 24 hours at 37°C under anaerobic conditions. Each strain was grown to confluence, with the exception of St 3,8,13,26, and 29. Cells were scraped from EG agar plates and added to the 5 ml culture to obtain the same approximate optical density as the other strains. All cultures were then mixed and glycerol was added to a final concentration of 20%. Aliqouts (1 ml) were individually frozen and stored at -80°C.

Transmission Electron Microscopy (TEM): Samples were stained as previously described [257]. Briefly, the intestines from mice that received butyrate or vehicle treatment

were harvested 7 days and 21 days following syngeneic and allogeneic BMT and flushed with 0.1 M Sorensen's phosphate buffer (pH 7.4) to remove luminal contents using a 20G needle. The intestines were next gently flushed with 0.1% ruthenium red (RR) containing 2.5% glutaraldehyde fixative in Sorensen's buffer and immediately placed in a dish containing the stain/fixative. Cross sections were immediately sliced (2mm wide) from the duodenum, jejunum, and illium. The tissue was then rinsed three times with Sorensen's buffer, containing 0.1 percent RR and post-fixed for one hour in one percent osmium tetroxide in the same buffer containing RR. The samples were again rinsed with Sorensen's buffer containing RR. Next, the tissue was dehydrated in ascending concentrations of ethanol, treated with propylene oxide, and embedded in Epon epoxy resin. Semi-thin sections were stained with toluidine blue for tissue identification. Selected regions of interest were ultra-thin sectioned (70 nm thick) mounted on copper grids, and post stained with uranyl acetate and lead citrate. The samples were examined using a Philips CM100 electron microscope at 60 kV. Images were recorded digitally using a Hamamatsu ORCA-HR digital camera system operated using AMT software (Advanced Microscopy Techniques Corp., Danvers, MA).

FITC-dextran assay: Food and water was withheld from all mice for four hours on day 21 post bone marrow transplant. FITC-dextran (Sigma-Aldrich; St. Louis, MO) was administered by 20G-1.5" flexible intragastric gavage needle (Braintree Scientific; Braintree, MA) at a concentration of 50mg/ml in PBS. BMT recipients received 800mg/kg (~16mg/mouse). Four hours later, serum was collected from peripheral blood, diluted 1:1 with PBS, and analyzed on a plate reader at excitation/emission wavelength of

485nm/535nm. Concentrations of FITC-dextran experimental samples were determined based on a standard curve.

Western Blot: $CD326^+$ purified IECs were harvested from animals that received syngeneic (BALB/c → BALB/c) or allogeneic (C57BL/6 → BALB/c) BMT. Whole cell lysates were next obtained and protein concentrations determined with Pierce BCA Protein Assay (Thermo Scientific). Equal amounts of protein (20 μg) were separated by SDS-PAGE gel electrophoresis (120V, 1.5h) and subsequently transferred to polyvinylidene difluoride (PVDF) membrane using a Bio-Rad semi-dry transfer cell (Hercules, CA) (20V, 1h). The following antibodies were used to analyze the membranes: α-tubulin (Cell Signaling, clone 11H10) and Acetyl histone H4 (Lys5/8/12/16) (EMD Millipore, clone 3HH-4C10). Secondary antibodies conjugated to HRP (Jackson ImmunoResearch) were used to detect primary antibodies, where needed. Densitometric analysis was performed using ImageJ software (National Institutes of Health; Bethesda, MA).

Quantitative PCR: mRNA was isolated from samples using RNeasy kit following manufacturers instructions (Qiagen; Venlo, Netherlands). Using 1μg of each mRNA template, cDNA was synthesized using SuperScript VILO (Invitrogen; Carlsbad, CA). qPCR primers were designed for murine targets:

qPCR Probe	Forward	Reverse
GAPDH	CCACAGTCCATGCCATCACTGC	GCCCAAGATGCCCTTCAGTGGG
SLC5A8	GCTGGATTTGCATCCGTAAT	TGGGACTGGTTGACACCATA
GPR43	CACGGCCTACATCCTCATCT	TTGGTAGGTACCAGCGGAAG
p300	TGCCTCCCATTGTTGATCCT	ACTCGTTGCAGGTGTAGACA

TIP60	TGGACGGAAGCGGAAATCTA	CGGCCAAGCTCAATACACTC
BAK	CAGATGGATCGCACAGAGAG	TCTGTGTACCACGAATTGGC
BAX	ACTAAAGTGCCCGAGCTGAT	ATGGTCACTGTCTGCCATGT
BCL-B (Bcl2l10)	TCATAGTGACCCGAGACTGC	TGTTGCAAAGAAGCCTGACA
JAM	ACTGCTCAATCTGACGTCCA	ATAGGGAGCTGTGATCTGGC
Occludin	CTCTCAGCCAGCGTACTCTT	CTCCATAGCCACCTCCGTAG
E-Cadherin	CCTGTCTTCAACCCAAGCAC	CAACAACGAACTGCTGGTCA
HDAC1	TGGGGCTGGCAAAGGCAAGT	GACCACTGCACTAGGCTGGAACA
HDAC4	AGCTCTGGCAACGTCAGCACT	AAGTGGGGCGACTGAGCCTTCT
HDAC7	GCTCAGCATGTGCATGTGGAACAC	TGAGAGCCTGGTGTGTCTGGCT
HDAC9	TGCACCTTTGCCTCAGAGCACG	TGGCTGCCTGGTTGCTTCAGT
HDAC10	TAGCAGCCAAACATGCCAAGCAGA	ATGCTCATAGCGGTGCCAAGAGAAA

All primers were verified for the production of a single specific PCR product using a melting curve program.

Chromatin Immunoprecipitation: Primary CD326^{+} IECs were seeded on gelatin (Cell Biologics; Chicago, IL) coated cell culture dishes (100mm) overnight followed by treatment with butyrate 1mM for 24 hours. Cells were harvested and used for ChIP analysis using EZ-Magna ChIP kit from EMD Millipore (Billerica, MA) following the manufacturers instructions. Briefly, cells were cross-linked with 1% formaldehyde and extracted chromatin was sonicated using a Bioruptor Pico by Diagenode (Denville, NJ) to yield DNA fragments predominately in the range of 200 – 1000bp. Sonicated lysates were immunoprecipitated (IP) utilizing either ChIP grade specific antibodies purchased from EMD Millipore for acetylated histone-H4 and RNA Pol II or IgG control antibody. De-crosslinked DNA was next examined by qPCR using primers designed in the promoter region of the target gene BCL-B (Forward: CCTACTCTGCCTGGCTCTTT; Reverse: ACCCTTCTGAGTCCCTGAGA), SLC5A8 (Forward: CACAGCACAGCCTTCTTTGT; Reverse: TCCAGTTCACAGTCCAGGTC), and JAM (Forward: TGCCGGGATTAAAAGCATGG; Reverse:

ACAGGGACAGCAGGATTAGG). IP efficiency of all samples was verified by qPCR analysis of the promoter region of GAPDH (Forward: CTGCAGTACTGTGGGGAGGT; Reverse: CAAAGGCGGAGTTACCAGAG). Data analysis was determined as percent of input utilizing the equations: $\Delta Ct_{[\text{normalized ChIP}]} = (Ct_{[\text{ChIP}]} - (Ct_{[\text{Input}]} - \text{Log2 } (6.644)))$ and % Input = $2^{(-\Delta Ct\ [\text{normalized ChIP}])}$.

Flow Cytometry: To analyze immunophenotype surface markers, lymphocytes contained in the IEC fraction or spleen were harvested, stained and gated on CD4-conjugated PerCP/Cy5.5 (Clone: GK1.5) or CD8-conjugated APC (Clone: 53-6.7) and configurations of the following per mouse in duplicate: CD69-PE (Clone: H1.2F3), CD62L-PE (Clone: MEL-14), CD25-PE (Clone: 3C7), CD44-PerCP/Cy5.5 (Clone: IM7), CD44-APC (Clone: IM7), FoxP3-APC (Clone: FJK-16s). All flow cytometry Abs were purchased from eBiosciences. Stained cells were then analyzed with an Accuri C6 Flow Cytometer (BD Biosciences).

IECs were stained with CD326-conjugated APC (Clone: G8.8) and DAPI and sorted to 98% purity using a FACSAria III (BD Biosciences) gating on live cells.

CTL Assay: $CD8^+$ T cells were isolated from Balb/c ($H\text{-}2^d$) mice using anti-CD8 microbeads and LS columns (Miltenyi Biotec) following the manufacturers instructions. $CD8^+$ T cells were primed in the presence of irradiated (30 Gy) C57BL/6 ($H\text{-}2^b$) splenocytes for 6 days prior to culture with primary IECs for 6h and 16h. Primary C57BL/6 IECs were harvested and incubated overnight in the presence or absence of

butyrate 1 mM in gelatin coated (Cell Biologics Inc.; Chicago, IL) 100 mm-culture dishes (Fisher Scientific).

Statistics: Bars and error bars represent the means and standard errors of the mean, respectively. Non-survival analysis was performed using students unpaired t test between two groups. ANOVA was used for comparisons with more than two groups. Survival data analysis was performed using a Mantel-Cox log-rank test.

CHAPTER VI

CONCLUSION

Collectively, the data presented in this thesis demonstrate a novel role for the PTM neddylation in the function of the immune system. Specifically, inhibition of neddylation in both murine and human DCs decreases the release of the inflammatory cytokines TNFα and IL-6. Mechanistic studies in DCs of mice showed that blockade of the neddylation pathway prevented the loss of IκB, a protein that binds to and sequesters the transcription factor for TNFa and IL-6 in the cytoplasm, NF-κB, thus preventing its translocation to and function in the nucleus[50,51]. Not only did neddylation inhibition confer an anti-inflammatory effect on DCs, but it also decreased the DCs ability to stimulate allogeneic T cells both *in vitro* and in *in vivo* clinical models of allo-BMT. The diminished DC functions resulted in decreased GVHD pathogenesis and improved mortality. Future studies will address the mechanism of how inhibiting neddylation decreases the allo-stimulatory capacity of DCs. Although GVHD is a complex syndrome in which there are many mediators of disease, it is possible that the diminutive NF-κB pathway seen in neddylation-inhibited DCs, plays a role[274,275]. Our data suggest that MHCII expression was not impacted on DCs treated with MLN4924, but these results remain to be formally tested. Furthermore, the decreased inflammatory cytokine environment may also serve to decrease autocrine signaling in DCs and paracrine signaling in accessory cells that are known to modulate GVHD[91,244].

The generation of a novel conditional knockout mouse that is SAG-deficient only in LysM expressing cells uncovered a disparate role of neddylation in myeloid cells, specifically macrophages and neutrophils. Injection of these KO mice with LPS resulted in increased mortality and inflammatory cytokines in the sera. However, cellular analysis revealed that KO macrophages released less inflammatory cytokines (TNFα and IL-6) in response to LPS stimulation *in vitro* and *in vivo*. By contrast, examination of SAG deficient neutrophils interestingly revealed a significant increase in the expression of TNFα. Concomitantly, ROS expression was increased in KO neutrophils corresponding with decreased NRF2, a transcription factor with anti-oxidative functions. Future in-depth studies will examine why NRF2 is diminished in KO neutrophils. SAG protein has multiple roles in quotidian cell activity 1) it serves as an adaptor protein for CRL2/5 complexes and 2) it is a redox-inducible antioxidant protein which scavenges ROS by forming intra- and inter-molecular disulfide bonds[67,69,70]. Thus we hypothesize that disruption of SAG protein results in increased ROS activity due to diminutive ROS-scavenger functions.

Through the generation of a novel conditional T cell knockout mouse that too, lacked SAG protein, led to the discovery that inhibition of neddylation in T cells decreases their proliferative capacity *in vitro* and *in vivo*. Indeed, KO T cells stimulated by allogeneic APCs exhibit less proliferation without an increase in apoptosis. Surprisingly, when neddylation is inhibited in T cells, NF-κB translocation is only mildly impacted – suggesting that a disparate mechanism from that of DCs and macrophages is responsible for the effects of neddylation blockade. To that end, mechanistic studies found that

inhibition of neddylation resulted in the increase of SOCS1 protein, a known suppressor of T cell functions. Furthermore, utilization of the small molecule inhibitor, MLN4924, too resulted in decreased allo-responses (fewer activated T cells following allo-BMT and decreased GVHD translating to improved survival) suggesting that carefully designed clinical trials may find MLN4924 to be a possible therapeutic agent for the treatment of GVHD pathogenesis in patients. Future studies will serve to address the mechanism of why more SOCS1 protein is present following stimulation of neddylation-inhibited T cells. SOCS proteins are known to recruit CRL2 and CRL5 – that use SAG as an adaptor molecule – to degrade signaling proteins within cells[243]. Furthermore, SOCS proteins are known to be putative targets of neddylation[68]. It is thus our hypothesis that due to the inhibition of neddylation, SOCS proteins are not degraded and thus accumulate, enabling increased suppression of T cell signaling.

Furthermore, the data in this thesis present a heretofore unknown role for the SCFA microbial metabolite, butyrate. Butyrate is an endogenous HDAC inhibitor that is made exclusively by the microbiota[60,61]. Unbiased and blinded profiling of several target sites of GVHD revealed that butyrate was diminished only in the intestinal tissue following allogeneic BMT, but not after syngeneic BMT. Surprisingly, butyrate was not decreased in the lumen (stool) of the intestine suggesting that there was a defect in butyrate uptake. Indeed, examination of CD326-purified IECs revealed that the transporter of butyrate, SLC5A8, was decreased both at the transcriptional and protein level. Loss of butyrate within IECs resulted in a decrease in acetylated histone-H4 and increased junctional permeability of IECs. Intragastric gavage of butyrate resulted in restoration of these

functions, protected mice from GVHD, and improved their survival after allo-BMT. Butyrate has been shown to increase intestinal Tregs[103], but our data show that the improved results were still observed even in the absence of donor Tregs – suggesting that butyrate treatment had a salutary effect on the IECs. Indeed, treatment of purified IECs with butyrate conferred protection from irradiation- and allo-induced apoptosis. Future studies will further dissect why the expression of SLC5A8 (the transporter of butyrate) is decreased following allo-BMT. Our data show that when IECs are cultured with TNFα or IFNγ, SLC5A8 expression is decreased. However, further studies are needed to formally test this. Furthermore, whether the signaling receptor of butyrate, GPR43 – that too is decreased after allo-BMT – plays a role in conferring protection from GVHD will be formally tested utilizing GPR43$^{-/-}$ mice. Ongoing experiments in the lab are examining the severity of GVHD in GPR43 chimeric recipients. We hypothesize that GPR43$^{-/-}$ into WT mice (thus having no GPR43 on hematopoietic cells, but GPR43 on IECs) will exhibit protection from GVHD. By contrast, WT into GPR43$^{-/-}$ animals (thus no GPR43 on IECs) will exhibit decreased protection from GVHD.

Together, the data presented in this thesis highlight the – heretofore unknown – important roles of neddylation and acetylation in the immune system.

CHAPTER VII

FUTURE DIRECTIONS

The data presented in this thesis further our understanding of the roles of PTMs in the immune system and answer important questions regarding the regulation of immune cell function, activation, and proliferation. However, these novel studies reveal new gaps in our knowledge of the roles of PTMs in immunity. Thus, this chapter will discuss future studies to highlight specific approaches that build upon the novel data.

Chapter II revealed an important role for neddylation in murine and human DC function through the utilization of a specific small molecule inhibitor of neddylation, MLN4924. Future studies will further validate the findings revealed by pharmacological inhibitor with a genetic model of neddylation inhibition by crossing SAG-floxed mice with CD11c-Cre mice. In addition to validating the small molecule results, these novel mice with a DC-specific deletion of SAG protein will allow us to further understand the role of SAG in DC ontogeny. Furthermore, we will characterize the biochemical and molecular mechanisms through which neddylation regulates IκB degradation in further detail.

Chapter III described a novel disparate mechanism of macrophage and neutrophil regulation. Indeed, deletion of SAG in Lys-M specific myeloid cells revealed a positive regulation of NF-κB in macrophages but a negative regulation of NF-κB in neutrophils. Further analysis of SAG-deficient neutrophils revealed that the loss of SAG resulted in

increased ROS release upon stimulation with these cells exhibiting a concomitant decrease in a transcription factor for antioxidant mediators, NRF2. Future studies will explore the role of the compensatory mechanism observed in the genetic knockout system by utilizing other complimentary approaches such as small molecule inhibition of neddylation (MLN4924) and molecular knockdown of SAG protein. The reasons that macrophage and neutrophils are regulated differently by neddylation are intriguing, yet unknown. Thus future studies will determine the practical mechanisms for the differential effects in macrophages and neutrophils.

Chapter IV highlighted an important role for neddylation in the function and proliferation of T cells. We utilized two complementary methods of regulating neddylation – utilization of MLN4924 and the generation of a novel mouse that is genetically deficient in SAG, only in T cells. In depth examination, revealed that inhibition of neddylation either pharmacologically or by genetic knockout of SAG confers a deficiency in the function, activation, and proliferation of T cells by preventing the degradation of SOCS1 and SOCS3 proteins. Thus, in future studies we will further characterize the molecular mechanisms with gain and loss of function experiments of SOCS in WT and KO cells, by either knocking down or overexpressing SOCS proteins. Furthermore, the results presented in this chapter suggest that MLN4924 – which is currently in phase I/II clinical trials) may represent a novel strategy to mitigate clinical GVHD.

Chapter V presented novel data examining the role of acetylation in GVHD target tissue pathology (non-immune cells). To that end, we found that the endogenous HDACi butyrate is decreased in the intestinal tissue following allo-BMT, but not syngeneic BMT, compared with naïve controls. The diminutive levels of butyrate in the allo-intestinal

tissues lead to a decrease in acetylation of histone-H4, increased junctional permeability, and increased allo-mediated damage – the effects of which were restored upon local intragastric gavage of exogenous butyrate resulting in mitigated GVHD severity and improved mortality. Although we show that levels of the transporter of butyrate (SLC5A8) are decreased following allo-BMT, butyrate also enters IECs through passive diffusion. Thus, future studies will evaluate the key molecular pathway for butyrate uptake. In addition, we will probe the molecular pathways of IEC resistance to allo-damage, such as tissue bioenergetics.

REFERENCES

1. Murphy, K. *Janeway's Immunobiology (Immunobiology: The Immune System (Janeway))*. (Garland Science, 2011).
2. Boehm, T. Design principles of adaptive immune systems. *Nat. Rev. Immunol.* 11, 307–317 (2011).
3. Nemazee, D. Receptor editing in lymphocyte development and central tolerance. *Nat. Rev. Immunol.* 6, 728–740 (2006).
4. Arstila, T. P. A Direct Estimate of the Human T Cell Receptor Diversity. *Science* 286, 958–961 (1999).
5. Bouillet, P. & O'Reilly, L. A. CD95, BIM and T cell homeostasis. *Nat. Rev. Immunol.* (2009).
6. Sprent, J. & Surh, C. D. Normal T cell homeostasis: the conversion of naive cells into memory-phenotype cells. *Nat. Immunol.* 12, 478–484 (2011).
7. Steinert, E. M. *et al.* Quantifying Memory CD8 T Cells Reveals Regionalization of Immunosurveillance. *Cell* 161, 737–749 (2015).
8. Sprent, J. & Surh, C. D. T cell memory. *Annu. Rev. Immunol.* 20, 551–579 (2002).
9. Cook, D. N., Pisetsky, D. S. & Schwartz, D. A. Toll-like receptors in the pathogenesis of human disease. *Nat. Immunol.* 5, 975–979 (2004).
10. Gay, N. J., Symmons, M. F., Gangloff, M. & Bryant, C. E. Assembly and localization of Toll-like receptor signalling complexes. *Nat. Rev. Immunol.* 14, 546–558 (2014).
11. Abdullah, Z. & Knolle, P. A. Scaling of immune responses against intracellular bacterial infection. *EMBO J* 33, 2283–2294 (2014).
12. Ogura, Y. *et al.* Nod2, a Nod1/Apaf-1 family member that is restricted to monocytes and activates NF-kappaB. *J Biol Chem* 276, 4812–4818 (2001).
13. Shaw, M. H., Reimer, T., Kim, Y.-G. & Nuñez, G. NOD-like receptors (NLRs): bona fide intracellular microbial sensors. *Curr. Opin. Immunol.* 20, 377–382 (2008).
14. Lechtenberg, B. C., Mace, P. D. & Riedl, S. J. Structural mechanisms in NLR inflammasome signaling. *Curr. Opin. Struct. Biol.* 29C, 17–25 (2014).
15. Villadangos, J. A. & Schnorrer, P. Intrinsic and cooperative antigen-presenting functions of dendritic-cell subsets in vivo. *Nat. Rev. Immunol.* 7, 543–555 (2007).
16. Toubai, T., Mathewson, N. & Reddy, P. The Role of Dendritic Cells in Graft-Versus-Tumor Effect. *Front Immunol* 5, 66 (2014).
17. Cocco, R. E. & Ucker, D. S. Distinct modes of macrophage recognition for

apoptotic and necrotic cells are not specified exclusively by phosphatidylserine exposure. *Mol. Biol. Cell* 12, 919–930 (2001).
18. Stavnezer, J., Guikema, J. E. J. & Schrader, C. E. Mechanism and regulation of class switch recombination. *Annu. Rev. Immunol.* 26, 261–292 (2008).
19. Germain, R. N. T-cell development and the CD4–CD8 lineage decision. *Nat. Rev. Immunol.* 2, 309–322 (2002).
20. Bevan, M. J. Helping the CD8+ T-cell response. *Nat. Rev. Immunol.* 4, 595–602 (2004).
21. Romagnani, S. T-cell subsets (Th1 versus Th2). *Annals of Allergy, Asthma & Immunology* 85, 9–21 (2000).
22. Korn, T., Bettelli, E., Oukka, M. & Kuchroo, V. K. IL-17 and Th17 Cells. *Annu. Rev. Immunol.* 27, 485–517 (2009).
23. Miossec, P. & Kolls, J. K. Targeting IL-17 and TH17 cells in chronic inflammation. *Nature Reviews Drug Discovery* 11, 763–776 (2012).
24. Yadav, M., Stephan, S. & Bluestone, J. A. Peripherally induced tregs - role in immune homeostasis and autoimmunity. *Front Immunol* 4, 232 (2013).
25. Couper, K. N., Blount, D. G. & Riley, E. M. IL-10: the master regulator of immunity to infection. *The Journal of Immunology* 180, 5771–5777 (2008).
26. Marshall, N. B. & Swain, S. L. Cytotoxic CD4 T Cells in Antiviral Immunity. *Journal of Biomedicine and Biotechnology* 2011, 1–8 (2011).
27. Fang, M. *et al.* Perforin-dependent CD4+ T-cell cytotoxicity contributes to control a murine poxvirus infection. *Proc Natl Acad Sci USA* 109, 9983–9988 (2012).
28. Appay, V. The physiological role of cytotoxic CD4(+) T-cells: the holy grail? *Clin. Exp. Immunol.* 138, 10–13 (2004).
29. Chowdhury, D. & Lieberman, J. Death by a thousand cuts: granzyme pathways of programmed cell death. *Annu. Rev. Immunol.* 26, 389–420 (2008).
30. Pipkin, M. E. & Lieberman, J. Delivering the kiss of death: progress on understanding how perforin works. *Curr. Opin. Immunol.* 19, 301–308 (2007).
31. Peter, M. E. & Krammer, P. H. The CD95(APO-1/Fas) DISC and beyond. *Cell Death Differ.* 10, 26–35 (2003).
32. Stalder, T., Hahn, S. & Erb, P. Fas antigen is the major target molecule for CD4+ T cell-mediated cytotoxicity. *The Journal of Immunology* 152, 1127–1133 (1994).
33. Buller, R. M., Holmes, K. L., Hügin, A., Frederickson, T. N. & Morse, H. C. Induction of cytotoxic T-cell responses in vivo in the absence of CD4 helper cells. *Nature …* 328, 77–79 (1987).
34. Rahemtulla, A. *et al.* Normal development and function of CD8+ cells but markedly decreased helper cell activity in mice lacking CD4. *Nature …* 353, 180–184 (1991).
35. Wu, Y. & Liu, Y. Viral induction of co-stimulatory activity on antigen-presenting cells bypasses the need for CD4+ T-cell help in CD8+ T-cell responses. *Curr. Biol.* 4, 499–505 (1994).
36. Shedlock, D. J. & Shen, H. Requirement for CD4 T cell help in generating

functional CD8 T cell memory. *Science* 300, 337–339 (2003).
37. Sun, J. C. & Bevan, M. J. Defective CD8 T cell memory following acute infection without CD4 T cell help. *Science* 300, 339–342 (2003).
38. Cresswell, P., Ackerman, A. L., Giodini, A., Peaper, D. R. & Wearsch, P. A. Mechanisms of MHC class I-restricted antigen processing and cross-presentation. *Immunol. Rev.* 207, 145–157 (2005).
39. Reddy, P. *et al.* A crucial role for antigen-presenting cells and alloantigen expression in graft-versus-leukemia responses. *Nat. Med.* 11, 1244–1249 (2005).
40. Yaneva, R., Springer, S. & Zacharias, M. Flexibility of the MHC class II peptide binding cleft in the bound, partially filled, and empty states: a molecular dynamics simulation study. *Biopolymers* 91, 14–27 (2009).
41. Schwartz, R. H. T cell anergy. *Annu. Rev. Immunol.* 21, 305–334 (2003).
42. Gardner, D., Jeffery, L. E. & Sansom, D. M. Understanding the CD28/CTLA-4 (CD152) pathway and its implications for costimulatory blockade. *Am. J. Transplant.* 14, 1985–1991 (2014).
43. Parry, R. V. *et al.* CTLA-4 and PD-1 receptors inhibit T-cell activation by distinct mechanisms. *Mol. Cell. Biol.* 25, 9543–9553 (2005).
44. Vieira, P. L. *et al.* ICOS-mediated signaling regulates cytokine production by human T cells and provides a unique signal to selectively control the clonal expansion of Th2 helper cells. *Eur J Immunol* 34, 1282–1290 (2004).
45. Potempa, J. Posttranslational modifications in innate immunity. *J Innate Immun* 4, 119–120 (2012).
46. Cloos, P. A. C. & Christgau, S. Post-translational modifications of proteins: implications for aging, antigen recognition, and autoimmunity. *Biogerontology* 5, 139–158 (2004).
47. Grotenbreg, G. & Ploegh, H. Chemical biology: dressed-up proteins. *Nature …* 446, 993–995 (2007).
48. Sun, Y. *et al.* Cutting edge: Negative regulation of dendritic cells through acetylation of the nonhistone protein STAT-3. *J Immunol* 182, 5899–5903 (2009).
49. Magnani, M., Crinelli, R., Bianchi, M. & Antonelli, A. The ubiquitin-dependent proteolytic system and other potential targets for the modulation of nuclear factor-kB (NF-kB). *Curr Drug Targets* 1, 387–399 (2000).
50. Mathewson, N. *et al.* Neddylation plays an important role in the regulation of murine and human dendritic cell function. *Blood* (2013). doi:10.1182/blood-2013-02-486373
51. Mowen, K. A. & David, M. Unconventional post-translational modifications in immunological signaling. *Nat. Immunol.* 15, 512–520 (2014).
52. Sterner, D. E. & Berger, S. L. Acetylation of histones and transcription-related factors. *Microbiol. Mol. Biol. Rev.* 64, 435–459 (2000).
53. Arrowsmith, C. H., Bountra, C., Fish, P. V., Lee, K. & Schapira, M. Epigenetic protein families: a new frontier for drug discovery. *Nature Reviews Drug Discovery* 11, 384–400 (2012).
54. Eberharter, A. & Becker, P. B. Histone acetylation: a switch between repressive and permissive chromatin. Second in review series on chromatin

dynamics. *EMBO Rep* 3, 224–229 (2002).
55. Bose, P., Dai, Y. & Grant, S. Histone deacetylase inhibitor (HDACI) mechanisms of action: emerging insights. *Pharmacol. Ther.* 143, 323–336 (2014).
56. Marks, P. A. & Jiang, X. Histone Deacetylase Inhibitors in Programmed Cell Death and Cancer Therapy. *Cell Cycle* 4, 549–551 (2005).
57. Choi, S. W. *et al.* Vorinostat plus tacrolimus and mycophenolate to prevent graft-versus-host disease after related-donor reduced-intensity conditioning allogeneic haemopoietic stem-cell transplantation: a phase 1/2 trial. *Lancet Oncol.* 15, 87–95 (2014).
58. Watanabe, T. Investigational histone deacetylase inhibitors for non-Hodgkin lymphomas. *Expert Opin Investig Drugs* 19, 1113–1127 (2010).
59. Mathewson, N. *et al.* Unbiased Metabolic Profiling Uncovers a Crucial Role for the Microbial Metabolite Butyrate in Modulating GI Epithelial Cell Damage from Gvhd. *American Society of Hematology* (2014). at <https://ash.confex.com/ash/2014/webprogram/Paper75934.html>
60. Sealy, L. & Chalkley, R. The effect of sodium butyrate on histone modification. *Cell* 14, 115–121 (1978).
61. Cook, S. I. & Sellin, J. H. Review article: short chain fatty acids in health and disease. *Aliment. Pharmacol. Ther.* 12, 499–507 (1998).
62. Arnim, von, A. G. A Hitchhiker's Guide to the Proteasome. *Science Signaling* 2001, pe2 (2001).
63. Fulda, S., Rajalingam, K. & Dikic, I. Ubiquitylation in immune disorders and cancer: from molecular mechanisms to therapeutic implications. *EMBO Mol Med* 4, 545–556 (2012).
64. Ikeda, F. & Dikic, I. Atypical ubiquitin chains: new molecular signals. 'Protein Modifications: Beyond the Usual Suspects' review series. *EMBO Rep* 9, 536–542 (2008).
65. Metzger, M. B., Hristova, V. A. & Weissman, A. M. HECT and RING finger families of E3 ubiquitin ligases at a glance. *J. Cell. Sci.* 125, 531–537 (2012).
66. Hua, Z. & Vierstra, R. D. The Cullin-RING Ubiquitin-Protein Ligases. *Annual Review of Plant Biology* (2011).
67. Enchev, R. I., Schulman, B. A. & Peter, M. Protein neddylation: beyond cullin–RING ligases. *Nat. Rev. Mol. Cell Biol.* 16, 30–44 (2014).
68. Emanuele, M. J. *et al.* Global Identification of Modular Cullin-RING Ligase Substrates. *Cell* 147, 459–474 (2011).
69. Duan, H. *et al.* SAG, a novel zinc RING finger protein that protects cells from apoptosis induced by redox agents. *Mol. Cell. Biol.* 19, 3145–3155 (1999).
70. Swaroop, M. *et al.* Expression, purification, and biochemical characterization of SAG, a ring finger redox-sensitive protein. *Free Radic. Biol. Med.* 27, 193–202 (1999).
71. Jia, L. *et al.* Validation of SAG/RBX2/ROC2 E3 ubiquitin ligase as an anticancer and radiosensitizing target. *Clin. Cancer Res.* 16, 814–824 (2010).
72. Zhou, W., Wei, W. & Sun, Y. Genetically engineered mouse models for functional studies of SKP1-CUL1-F-box-protein (SCF) E3 ubiquitin ligases. *Cell Res.* 23, 599–619 (2013).

73. Zhao, Y. & Sun, Y. Cullin-RING ligases (CRLs) as attractive anti-cancer targets. *Curr. Pharm. Des.* (2012).
74. Sun, Y. & Li, H. Functional characterization of SAG/RBX2/ROC2/RNF7, an antioxidant protein and an E3 ubiquitin ligase. *Protein Cell* 4, 103–116 (2013).
75. Soucy, T. A. *et al.* An inhibitor of NEDD8-activating enzyme as a new approach to treat cancer. *Nature …* 458, 732–736 (2009).
76. Walden, H. *et al.* The structure of the APPBP1-UBA3-NEDD8-ATP complex reveals the basis for selective ubiquitin-like protein activation by an E1. *Mol Cell* 12, 1427–1437 (2003).
77. Walden, H., Podgorski, M. S. & Schulman, B. A. Insights into the ubiquitin transfer cascade from the structure of the activating enzyme for NEDD8. *Nature …* 422, 330–334 (2003).
78. Rock, K. L. *et al.* Inhibitors of the proteasome block the degradation of most cell proteins and the generation of peptides presented on MHC class I molecules. *Cell* 78, 761–771 (1994).
79. Wei, D. *et al.* Radiosensitization of human pancreatic cancer cells by MLN4924, an investigational NEDD8-activating enzyme inhibitor. *Cancer Res* 72, 282–293 (2012).
80. Yang, D., Tan, M., Wang, G. & Sun, Y. The p21-Dependent Radiosensitization of Human Breast Cancer Cells by MLN4924, an Investigational Inhibitor of NEDD8 Activating Enzyme. *PLoS ONE* 7, e34079 (2012).
81. Luo, Z. *et al.* The Nedd8-activating enzyme inhibitor MLN4924 induces autophagy and apoptosis to suppress liver cancer cell growth. *Cancer Res* (2012). doi:10.1158/0008-5472.CAN-12-0388
82. Blazar, B. R., Murphy, W. J. & Abedi, M. Advances in graft-versus-host disease biology and therapy. *Nat. Rev. Immunol.* 12, 443–458 (2012).
83. Choi, S. W. & Reddy, P. Current and emerging strategies for the prevention of graft-versus-host disease. *Nat Rev Clin Oncol* 11, 536–547 (2014).
84. Negrin, R. S. Sources of hematopoietic stem cells. *uptodate.com* at <http://www.uptodate.com/contents/sources-of-hematopoietic-stem-cells>
85. Storek, J. *et al.* Reconstitution of the immune system after hematopoietic stem cell transplantation in humans. *Semin Immunopathol* 30, 425–437 (2008).
86. Chunduri, S. *et al.* Comparable kinetics of myeloablation between fludarabine/full-dose busulfan and fludarabine/melphalan conditioning regimens in allogeneic peripheral blood stem cell transplantation. *Bone Marrow Transplant.* 38, 477–482 (2006).
87. Jacobsohn, D. A. & Vogelsang, G. B. Acute graft versus host disease. *Orphanet J Rare Dis* 2, 35 (2007).
88. Ferrara, J. L. M., Levine, J. E., Reddy, P. & Holler, E. Graft-versus-host disease. *Lancet* 373, 1550–1561 (2009).
89. Paczesny, S., Hanauer, D., Sun, Y. & Reddy, P. New perspectives on the biology of acute GVHD. *Bone Marrow Transplant.* 45, 1–11 (2010).
90. Nestel, F. P., Price, K. S., Seemayer, T. A. & Lapp, W. S. Macrophage priming

and lipopolysaccharide-triggered release of tumor necrosis factor alpha during graft-versus-host disease. *J. Exp. Med.* 175, 405–413 (1992).
91. Ferrara, J. L., Abhyankar, S. & Gilliland, D. G. Cytokine storm of graft-versus-host disease: a critical effector role for interleukin-1. *Transplant. Proc.* 25, 1216–1217 (1993).
92. Tawara, I. *et al.* Interleukin-6 modulates graft-versus-host responses after experimental allogeneic bone marrow transplantation. *Clin. Cancer Res.* 17, 77–88 (2011).
93. Hill, G. R. *et al.* Total body irradiation and acute graft-versus-host disease: the role of gastrointestinal damage and inflammatory cytokines. *Blood* 90, 3204–3213 (1997).
94. Bäckhed, F., Ley, R. E., Sonnenburg, J. L., Peterson, D. A. & Gordon, J. I. Host-bacterial mutualism in the human intestine. *Science* 307, 1915–1920 (2005).
95. Savage, D. C. Microbial ecology of the gastrointestinal tract. *Annu. Rev. Microbiol.* 31, 107–133 (1977).
96. Nuding, S., Antoni, L. & Stange, E. F. The host and the flora. *Dig Dis* 31, 286–292 (2013).
97. Khosravi, A. *et al.* Gut microbiota promote hematopoiesis to control bacterial infection. *Cell Host Microbe* 15, 374–381 (2014).
98. Blaser, M. J. The microbiome revolution. *J. Clin. Invest.* 124, 4162–4165 (2014).
99. Reikine, S., Nguyen, J. B. & Modis, Y. Pattern Recognition and Signaling Mechanisms of RIG-I and MDA5. *Front Immunol* 5, 342 (2014).
100. Natarajan, N. & Pluznick, J. L. From Microbe to Man: the role of microbial short chain fatty acid metabolites in host cell biology. *Am. J. Physiol., Cell Physiol.* ajpcell.00228.2014 (2014). doi:10.1152/ajpcell.00228.2014
101. Young, V. B. The intestinal microbiota in health and disease. *Current Opinion in Gastroenterology* 28, 63–69 (2012).
102. Donohoe, D. R. *et al.* The microbiome and butyrate regulate energy metabolism and autophagy in the mammalian colon. *Cell Metab.* 13, 517–526 (2011).
103. Atarashi, K. *et al.* Treg induction by a rationally selected mixture of Clostridia strains from the human microbiota. *Nature …* (2013). doi:10.1038/nature12331
104. Furusawa, Y. *et al.* Commensal microbe-derived butyrate induces the differentiation of colonic regulatory T cells. *Nature …* (2013). doi:10.1038/nature12721
105. Bouma, G. & Strober, W. The immunological and genetic basis of inflammatory bowel disease. *Nat. Rev. Immunol.* 3, 521–533 (2003).
106. Palm, N. W. & Medzhitov, R. Not so fast: adaptive suppression of innate immunity. *Nat. Med.* 13, 1142–1144 (2007).
107. Geuking, M. B. *et al.* Intestinal bacterial colonization induces mutualistic regulatory T cell responses. *Immunity* 34, 794–806 (2011).
108. Turnbaugh, P. J. *et al.* The effect of diet on the human gut microbiome: a metagenomic analysis in humanized gnotobiotic mice. *Sci Transl Med* 1,

6ra14 (2009).
109. Zivkovic, A. M., German, J. B., Lebrilla, C. B. & Mills, D. A. Human milk glycobiome and its impact on the infant gastrointestinal microbiota. *Proc Natl Acad Sci USA* 108 Suppl 1, 4653–4658 (2011).
110. David, L. A. *et al.* Diet rapidly and reproducibly alters the human gut microbiome. *Nature …* 505, 559–563 (2014).
111. De Vadder, F. *et al.* Microbiota-generated metabolites promote metabolic benefits via gut-brain neural circuits. *Cell* 156, 84–96 (2014).
112. Stecher, B. & Hardt, W.-D. Mechanisms controlling pathogen colonization of the gut. *Curr. Opin. Microbiol.* 14, 82–91 (2011).
113. Sonnenburg, J. L., Angenent, L. T. & Gordon, J. I. Getting a grip on things: how do communities of bacterial symbionts become established in our intestine? *Nat. Immunol.* 5, 569–573 (2004).
114. Chairatana, P. & Nolan, E. M. Molecular basis for self-assembly of a human host-defense Peptide that entraps bacterial pathogens. *J. Am. Chem. Soc.* 136, 13267–13276 (2014).
115. Yount, N. Y. & Yeaman, M. R. Peptide antimicrobials: cell wall as a bacterial target. *Ann. N. Y. Acad. Sci.* 1277, 127–138 (2013).
116. Zhao, L. & Lu, W. Defensins in innate immunity. *Current Opinion in Hematology* 21, 37–42 (2014).
117. Oppenheim, J. J., Biragyn, A., Kwak, L. W. & Yang, D. Roles of antimicrobial peptides such as defensins in innate and adaptive immunity. *Ann. Rheum. Dis.* 62 Suppl 2, ii17–21 (2003).
118. Ricciardi-Castagnoli, P. & Granucci, F. Opinion: Interpretation of the complexity of innate immune responses by functional genomics. *Nat. Rev. Immunol.* 2, 881–889 (2002).
119. Cash, H. L., Whitham, C. V., Behrendt, C. L. & Hooper, L. V. Symbiotic bacteria direct expression of an intestinal bactericidal lectin. *Science* 313, 1126–1130 (2006).
120. Mukherjee, S., Zheng, H., Derebe, M. G. & Callenberg, K. M. Antibacterial membrane attack by a pore-forming intestinal C-type lectin. *Nature …* (2013).
121. Wang, G. Pharmaceuticals | Free Full-Text | Human Antimicrobial Peptides and Proteins | HTML. *Pharmaceuticals* (2014).
122. Kolios, G., Valatas, V. & Ward, S. G. Nitric oxide in inflammatory bowel disease: a universal messenger in an unsolved puzzle. *Immunology* 113, 427–437 (2004).
123. van BEKKUM, D. & VOS, O. Treatment of secondary disease in radiation chimaeras. *Int. J. Radiat. Biol.* 3, 173–181 (1961).
124. van Bekkum, D. W., De Vries, M. J. & van der Waay, D. Lesions characteristic of secondary disease in germfree heterologous radiation chimeras. (1967).
125. Jones, J. M., Wilson, R. & Bealmear, P. M. Mortality and gross pathology of secondary disease in germfree mouse radiation chimeras. *Radiat. Res.* 45, 577–588 (1971).
126. van Bekkum, D. W., Roodenburg, J., Heidt, P. J. & van der Waaij, D. Mitigation of secondary disease of allogeneic mouse radiation chimeras by modification

of the intestinal microflora. *J. Natl. Cancer Inst.* 52, 401–404 (1974).
127. van der Waaij, D., Berghuis-de Vries, J. M. & Lekkerkerk Lekkerkerk-v. Colonization resistance of the digestive tract in conventional and antibiotic-treated mice. *J Hyg (Lond)* 69, 405–411 (1971).
128. Navari, R. M. *et al.* Prophylaxis of infection in patients with aplastic anemia receiving allogeneic marrow transplants. *Am. J. Med.* 76, 564–572 (1984).
129. Pérez-Simón, J. A. *et al.* Antibiotic prophylaxis with meropenem after allogeneic stem cell transplantation. *Bone Marrow Transplant.* 33, 183–187 (2004).
130. Passweg, J. R. *et al.* Influence of protective isolation on outcome of allogeneic bone marrow transplantation for leukemia. *Bone Marrow Transplant.* 21, 1231–1238 (1998).
131. Russell, J. A. *et al.* Early outcomes after allogeneic stem cell transplantation for leukemia and myelodysplasia without protective isolation: a 10-year experience. *Biol. Blood Marrow Transplant.* 6, 109–114 (2000).
132. Petersen, F. B. *et al.* Infectious Complications in Patients Undergoing Marrow Transplantation: A Prospective Randomized Study of the Additional Effect of Decontamination and Laminar Air Flow Isolation among Patients Receiving Prophylactic Systemic Antibiotics. *… journal of infectious …* (1987).
133. Jenq, R. R. *et al.* Regulation of intestinal inflammation by microbiota following allogeneic bone marrow transplantation. *Journal of Experimental Medicine* 209, 903–911 (2012).
134. Eriguchi, Y. *et al.* Graft-versus-host disease disrupts intestinal microbial ecology by inhibiting Paneth cell production of α-defensins. *Blood* 120, 223–231 (2012).
135. Vermeulen, L. & Snippert, H. J. Stem cell dynamics in homeostasis and cancer of the intestine. *Nature Reviews Cancer* 14, 468–480 (2014).
136. Sato, T. *et al.* Paneth cells constitute the niche for Lgr5 stem cells in intestinal crypts. *Nature …* 469, 415–418 (2011).
137. Selsted, M. E. & Harwig, S. S. Determination of the disulfide array in the human defensin HNP-2. A covalently cyclized peptide. *J Biol Chem* 264, 4003–4007 (1989).
138. Bevins, C. L. Innate immune functions of α-defensins in the small intestine. *Dig Dis* 31, 299–304 (2013).
139. Taur, Y. *et al.* The effects of intestinal tract bacterial diversity on mortality following allogeneic hematopoietic stem cell transplantation. *Blood* 124, 1174–1182 (2014).
140. Bleich, A. *et al.* CpG motifs of bacterial DNA exert protective effects in mouse models of IBD by antigen-independent tolerance induction. *Gastroenterology* 136, 278–287 (2009).
141. Furusawa, Y., Obata, Y. & Hase, K. Commensal microbiota regulates T cell fate decision in the gut. *Semin Immunopathol* (2014). doi:10.1007/s00281-014-0455-3
142. Tawara, I. *et al.* Influence of donor microbiota on the severity of experimental graft-versus-host-disease. *Biol. Blood Marrow Transplant.* 19, 164–168 (2013).

143. Heidegger, S., van den Brink, M. R. M., Haas, T. & Poeck, H. The role of pattern-recognition receptors in graft-versus-host disease and graft-versus-leukemia after allogeneic stem cell transplantation. *Front Immunol* 5, 337 (2014).
144. Bayston, K., Baumgartner, J. D., Clark, P. & Cohen, J. Anti-endotoxin antibody for prevention of acute GVHD. *Bone Marrow Transplant.* 8, 426–427 (1991).
145. Cooke, K. R. *et al.* LPS antagonism reduces graft-versus-host disease and preserves graft-versus-leukemia activity after experimental bone marrow transplantation. *J. Clin. Invest.* 107, 1581–1589 (2001).
146. Cohen, J. *et al.* Antibody titres to a rough-mutant strain of Escherichia coli in patients undergoing allogeneic bone-marrow transplantation. Evidence of a protective effect against graft-versus-host disease. *Lancet* 1, 8–11 (1987).
147. Li, H. *et al.* Graft-versus-host disease is independent of innate signaling pathways triggered by pathogens in host hematopoietic cells. *J Immunol* 186, 230–241 (2011).
148. Elmaagacli, A. H. *et al.* Mutations in Innate Immune System NOD2/CARD 15 and TLR-4 (Thr399Ile) Genes Influence the Risk for Severe Acute Graft-versus-Host Disease in Patients Who Underwent an Allogeneic Transplantation. *Transplantation* 81, 247–254 (2006).
149. Calcaterra, C. *et al.* Critical role of TLR9 in acute graft-versus-host disease. *J Immunol* 181, 6132–6139 (2008).
150. Taylor, P. A. *et al.* TLR agonists regulate alloresponses and uncover a critical role for donor APCs in allogeneic bone marrow rejection. *Blood* 112, 3508–3516 (2008).
151. Penack, O., Holler, E. & van den Brink, M. R. M. Graft-versus-host disease: regulation by microbe-associated molecules and innate immune receptors. *Blood* 115, 1865–1872 (2010).
152. Schwab, L. *et al.* Neutrophil granulocytes recruited upon translocation of intestinal bacteria enhance graft-versus-host disease via tissue damage. *Nat. Med.* 20, 648–654 (2014).
153. Penack, O. *et al.* NOD2 regulates hematopoietic cell function during graft-versus-host disease. *J. Exp. Med.* 206, 2101–2110 (2009).
154. Shin, O. S. & Harris, J. B. Innate immunity and transplantation tolerance: the potential role of TLRs/NLRs in GVHD. *Korean J Hematol* 46, 69–79 (2011).
155. Granell, M. *et al.* Common variants in NLRP2 and NLRP3 genes are strong prognostic factors for the outcome of HLA-identical sibling allogeneic stem cell transplantation. *Blood* 112, 4337–4342 (2008).
156. Zeiser, R., Penack, O., Holler, E. & Idzko, M. Danger signals activating innate immunity in graft-versus-host disease. *J. Mol. Med.* 89, 833–845 (2011).
157. Wilhelm, K. *et al.* Graft-versus-host disease is enhanced by extracellular ATP activating P2X7R. *Nat. Med.* 16, 1434–1438 (2010).
158. Crocker, P. R., Paulson, J. C. & Varki, A. Siglecs and their roles in the immune system. *Nat. Rev. Immunol.* 7, 255–266 (2007).
159. Toubai, T. *et al.* Siglec-G-CD24 axis controls the severity of graft-versus-host disease in mice. *Blood* 123, 3512–3523 (2014).
160. Vaziri, N. D., Yuan, J. & Norris, K. Role of urea in intestinal barrier

dysfunction and disruption of epithelial tight junction in chronic kidney disease. *Am. J. Nephrol.* 37, 1–6 (2013).
161. Pluznick, J. L. *et al.* Olfactory receptor responding to gut microbiota-derived signals plays a role in renin secretion and blood pressure regulation. *Proc Natl Acad Sci USA* 110, 4410–4415 (2013).
162. DuPont, A. W. & DuPont, H. L. The intestinal microbiota and chronic disorders of the gut. *Nat Rev Gastroenterol Hepatol* 8, 523–531 (2011).
163. Wong, J. M. W., de Souza, R., Kendall, C. W. C., Emam, A. & Jenkins, D. J. A. Colonic health: fermentation and short chain fatty acids. *J. Clin. Gastroenterol.* 40, 235–243 (2006).
164. Nizet, V. *et al.* Innate antimicrobial peptide protects the skin from invasive bacterial infection. *Nature …* 414, 454–457 (2001).
165. Bals, R., Weiner, D. J., Meegalla, R. L. & Wilson, J. M. Transfer of a cathelicidin peptide antibiotic gene restores bacterial killing in a cystic fibrosis xenograft model. *J. Clin. Invest.* 103, 1113–1117 (1999).
166. Wehkamp, J., Salzman, N. H. & Porter, E. Reduced Paneth cell α-defensins in ileal Crohn's disease. in (2005).
167. Salzman, N. H. Paneth cell defensins and the regulation of the microbiome: détente at mucosal surfaces. *Gut Microbes* 1, 401–406 (2010).
168. Ferrara, J. L. M. *et al.* Regenerating islet-derived 3-alpha is a biomarker of gastrointestinal graft-versus-host disease. *Blood* 118, 6702–6708 (2011).
169. Satpathy, A. T., Wu, X., Albring, J. C. & Murphy, K. M. Re(de)fining the dendritic cell lineage. *Nat. Immunol.* 13, 1145–1154 (2012).
170. Hespel, C. & Moser, M. Role of inflammatory dendritic cells in innate and adaptive immunity. *Eur J Immunol* 42, 2535–2543 (2012).
171. Turley, S. J. *et al.* Transport of peptide-MHC class II complexes in developing dendritic cells. *Science* 288, 522–527 (2000).
172. Mellman, I. & Steinman, R. M. Dendritic cells: specialized and regulated antigen processing machines. *Cell* 106, 255–258 (2001).
173. Tabas, I. & Glass, C. K. Anti-inflammatory therapy in chronic disease: challenges and opportunities. *Science* 339, 166–172 (2013).
174. Martin, G. S. Sepsis, severe sepsis and septic shock: changes in incidence, pathogens and outcomes. *Expert Rev Anti Infect Ther* 10, 701–706 (2012).
175. Lee, J. Adipose tissue macrophages in the development of obesity-induced inflammation, insulin resistance and type 2 Diabetes. *Arch. Pharm. Res.* (2013). doi:10.1007/s12272-013-0023-8
176. Honda, K. & Taniguchi, T. IRFs: master regulators of signalling by Toll-like receptors and cytosolic pattern-recognition receptors. *Nat. Rev. Immunol.* 6, 644–658 (2006).
177. Moynagh, P. N. The Pellino family: IRAK E3 ligases with emerging roles in innate immune signalling. *Trends Immunol.* 30, 33–42 (2009).
178. Razani, B., Reichardt, A. D. & Cheng, G. Non-canonical NF-κB signaling activation and regulation: principles and perspectives. *Immunol. Rev.* 244, 44–54 (2011).
179. Sun, S.-C. Non-canonical NF-κB signaling pathway. *Cell Res.* 21, 71–85 (2011).

180. Dai, L., Aye Thu, C., Liu, X.-Y., Xi, J. & Cheung, P. C. F. TAK1, more than just innate immunity. *IUBMB Life* 64, 825–834 (2012).
181. Xirodimas, D. P. Novel substrates and functions for the ubiquitin-like molecule NEDD8. *Biochem. Soc. Trans.* 36, 802–806 (2008).
182. Saha, A. & Deshaies, R. J. Multimodal activation of the ubiquitin ligase SCF by Nedd8 conjugation. *Mol Cell* 32, 21–31 (2008).
183. Petroski, M. D. & Deshaies, R. J. Function and regulation of cullin-RING ubiquitin ligases. *Nat. Rev. Mol. Cell Biol.* 6, 9–20 (2005).
184. Sun, Y., Tan, M. & Duan, H. SAG/ROC/Rbx/Hrt, a Zinc RING Finger Gene Family: Molecular Cloning, Biochemical Properties, and Biological Functions. *Antioxidants and Redox …* (2001).
185. Brownell, J. E. *et al.* Substrate-assisted inhibition of ubiquitin-like protein-activating enzymes: the NEDD8 E1 inhibitor MLN4924 forms a NEDD8-AMP mimetic in situ. *Mol Cell* 37, 102–111 (2010).
186. Swords, R. T. *et al.* Inhibition of NEDD8-activating enzyme: a novel approach for the treatment of acute myeloid leukemia. *Blood* 115, 3796–3800 (2010).
187. Grauer, O. *et al.* Analysis of maturation states of rat bone marrow-derived dendritic cells using an improved culture technique. *Histochem. Cell Biol.* 117, 351–362 (2002).
188. Torri, A. *et al.* Gene expression profiles identify inflammatory signatures in dendritic cells. *PLoS ONE* 5, e9404 (2010).
189. Barr, T. A., Brown, S., Ryan, G., Zhao, J. & Gray, D. TLR-mediated stimulation of APC: Distinct cytokine responses of B cells and dendritic cells. *Eur J Immunol* 37, 3040–3053 (2007).
190. Tynan, G. A., McNaughton, A., Jarnicki, A., Tsuji, T. & Lavelle, E. C. Polymyxin B inadequately quenches the effects of contaminating lipopolysaccharide on murine dendritic cells. *PLoS ONE* 7, e37261 (2012).
191. Stamatos, N. M. *et al.* LPS-induced cytokine production in human dendritic cells is regulated by sialidase activity. *J. Leukoc. Biol.* 88, 1227–1239 (2010).
192. Herter, J. R. & Fuchs, S. Y. Recognition of substrate and Skp1 by the Homologue of Slimb (HOS) ubiquitin ligase receptor D role of the F-box. *Med. Sci. Monit.* 8, BR283–8 (2002).
193. Guindi, C. *et al.* Differential role of NF-κB, ERK1/2 and AP-1 in modulating the immunoregulatory functions of bone marrow-derived dendritic cells from NOD mice. *Cell. Immunol.* 272, 259–268 (2012).
194. Sharif, O., Bolshakov, V. N., Raines, S., Newham, P. & Perkins, N. D. Transcriptional profiling of the LPS induced NF-kappaB response in macrophages. *BMC Immunol.* 8, 1 (2007).
195. Ghosh, S. Handbook of transcription factor NF-kappaB. (2006).
196. Viatour, P., Merville, M.-P., Bours, V. & Chariot, A. Phosphorylation of NF-kappaB and IkappaB proteins: implications in cancer and inflammation. *Trends Biochem. Sci.* 30, 43–52 (2005).
197. Milhollen, M. A. *et al.* MLN4924, a NEDD8-activating enzyme inhibitor, is active in diffuse large B-cell lymphoma models: rationale for treatment of NF-{kappa}B-dependent lymphoma. *Blood* 116, 1515–1523 (2010).
198. Brunton, L., Lazo, J. & Parker, K. *Goodman & Gilman's The Pharmacological*

Basis of Therapeutics, Eleventh Edition (Goodman and Gilman"S the Pharmacological Basis of Therapeutics). (McGraw-Hill Professional, 2005).
199. Coutinho, A. E. & Chapman, K. E. The anti-inflammatory and immunosuppressive effects of glucocorticoids, recent developments and mechanistic insights. *Molecular and cellular endocrinology* (2011).
200. De Bosscher, K. The Interplay between the Glucocorticoid Receptor and Nuclear Factor- B or Activator Protein-1: Molecular Mechanisms for Gene Repression. *Endocrine Reviews* 24, 488–522 (2003).
201. Chang, F.-M. *et al.* Inhibition of neddylation represses lipopolysaccharide-induced proinflammatory cytokine production in macrophage cells. *J Biol Chem* 287, 35756–35767 (2012).
202. Zinser, E. *et al.* Inhibition of the proteasome influences murine and human dendritic cell development in vitro and in vivo. *Immunobiology* 214, 843–851 (2009).
203. Gottipati, S., Rao, N. L. & Fung-Leung, W.-P. IRAK1: a critical signaling mediator of innate immunity. *Cell. Signal.* 20, 269–276 (2008).
204. Wang, C. *et al.* TAK1 is a ubiquitin-dependent kinase of MKK and IKK. *Nature …* 412, 346–351 (2001).
205. Pharmaceuticals, M. Study of MLN4924 in Adult Patients With Nonhematologic Malignancies. *Study of MLN4924 in Adult Patients With Nonhematologic Malignancies* at <http://clinicaltrials.gov/ct2/show/record/NCT00677170>
206. *MLN4924 for the Treatment of Acute Myelogenous Leukemia, Myelodysplastic Syndrome, and Acute Lymphoblastic Leukemia*. (2009). at <http://clinicaltrials.gov/ct2/show/record/NCT00911066>
207. Akira, S., Uematsu, S. & Takeuchi, O. Pathogen recognition and innate immunity. *Cell* 124, 783–801 (2006).
208. Silva, M. T. When two is better than one: macrophages and neutrophils work in concert in innate immunity as complementary and cooperative partners of a myeloid phagocyte system. *J. Leukoc. Biol.* 87, 93–106 (2010).
209. Takeuchi, O. & Akira, S. Pattern recognition receptors and inflammation. *Cell* 140, 805–820 (2010).
210. Spooner, R. & Yilmaz, O. The role of reactive-oxygen-species in microbial persistence and inflammation. *Int J Mol Sci* 12, 334–352 (2011).
211. Sun, Y. & Li, H. Functional characterization of SAG/RBX2/ROC2/RNF7, an antioxidant protein and an E3 ubiquitin ligase. *Protein Cell* (2013).
212. Chang, S. C. & Ding, J. L. Ubiquitination by SAG regulates macrophage survival/death and immune response during infection. *Cell Death Differ.* 21, 1388–1398 (2014).
213. Tan, M., Zhu, Y., Kovacev, J., Zhao, Y. & Pan, Z. Q. Disruption of Sag/Rbx2/Roc2 induces radiosensitization by increasing ROS levels and blocking NF-κB activation in mouse embryonic stem cells. *Free Radical Biology …* (2010).
214. Lawrence, T. The nuclear factor NF-κB pathway in inflammation. *Cold Spring Harbor Perspectives in Biology* (2009).
215. Tak, P. P. & Firestein, G. S. NF-κB: a key role in inflammatory diseases.

Journal of Clinical Investigation (2001).
216. Clausen, B. E., Burkhardt, C., Reith, W., Renkawitz, R. & Förster, I. Conditional gene targeting in macrophages and granulocytes using LysMcre mice. *Transgenic Res.* 8, 265–277 (1999).
217. Wright, H. L., Moots, R. J., Bucknall, R. C. & Edwards, S. W. Neutrophil function in inflammation and inflammatory diseases. *Rheumatology (Oxford)* 49, 1618–1631 (2010).
218. Kumagai, Y., Kanda, H., Shinkai, Y. & Toyama, T. The role of the Keap1/Nrf2 pathway in the cellular response to methylmercury. *Oxid Med Cell Longev* 2013, 848279 (2013).
219. Kobayashi, M. & Yamamoto, M. Nrf2-Keap1 regulation of cellular defense mechanisms against electrophiles and reactive oxygen species. *Adv. Enzyme Regul.* 46, 113–140 (2006).
220. Li, H. *et al.* Inactivation of SAG/RBX2 E3 ubiquitin ligase suppresses KrasG12D-driven lung tumorigenesis. *J. Clin. Invest.* 124, 835–846 (2014).
221. Xie, C.-M. *et al.* Erbin is a novel substrate of the Sag-βTrCP E3 ligase that regulates KrasG12D-induced skin tumorigenesis. *J. Cell Biol.* 209, 721–738 (2015).
222. Li, H. *et al.* Inactivation of SAG/RBX2 E3 ubiquitin ligase suppresses KrasG12D-driven lung tumorigenesis. *The Journal of clinical …* (2014).
223. Tan, M., Li, H. & Sun, Y. Endothelial deletion of Sag/Rbx2/Roc2 E3 ubiquitin ligase causes embryonic lethality and blocks tumor angiogenesis. *Oncogene* (2013).
224. Weischenfeldt, J. & Porse, B. Bone Marrow-Derived Macrophages (BMM): Isolation and Applications. *CSH Protoc* 2008, pdb.prot5080 (2008).
225. Tan, M. *et al.* SAG/RBX2/ROC2 E3 ubiquitin ligase is essential for vascular and neural development by targeting NF1 for degradation. *Dev. Cell* 21, 1062–1076 (2011).
226. Tan, M., Davis, S. W., Saunders, T. L., Zhu, Y. & Sun, Y. RBX1/ROC1 disruption results in early embryonic lethality due to proliferation failure, partially rescued by simultaneous loss of p27. *Proc Natl Acad Sci USA* 106, 6203–6208 (2009).
227. Malissen, B., Grégoire, C., Malissen, M. & Roncagalli, R. Integrative biology of T cell activation. *Nat. Immunol.* 15, 790–797 (2014).
228. Sallusto, F., Geginat, J. & Lanzavecchia, A. Central memory and effector memory T cell subsets: function, generation, and maintenance. *Annu. Rev. Immunol.* 22, 745–763 (2004).
229. Zhang, N. & Bevan, M. J. CD8+ T Cells: Foot Soldiers of the Immune System. *Immunity* 35, 161–168 (2011).
230. Choi, S. & Reddy, P. Graft-versus-host disease. *Panminerva Med* 52, 111–124 (2010).
231. Ferrara, J. & Antin, J. H. The Pathophysiology of Graft-Versus-Host Disease. *Thomas' Hematopoietic Cell …* (2009).
232. Choi, S. & Reddy, P. HDAC inhibition and graft versus host disease. *Mol Med* 17, 404–416 (2011).
233. Reddy, P. Targeting deacetylases to improve outcomes after allogeneic bone

marrow transplantation. *Trans. Am. Clin. Climatol. Assoc.* 124, 152–162 (2013).
234. Wang, Y.-C., Peterson, S. E. & Loring, J. F. Protein post-translational modifications and regulation of pluripotency in human stem cells. *Cell Res.* 24, 143–160 (2014).
235. Baek, S. T. *et al.* Off-target effect of doublecortin family shRNA on neuronal migration associated with endogenous microRNA dysregulation. *Neuron* 82, 1255–1262 (2014).
236. Gu, S. *et al.* The loop position of shRNAs and pre-miRNAs is critical for the accuracy of dicer processing in vivo. *Cell* 151, 900–911 (2012).
237. Singh, S., Narang, A. S. & Mahato, R. I. Subcellular Fate and Off-Target Effects of siRNA, shRNA, and miRNA. *Pharm Res* 28, 2996–3015 (2011).
238. Li, L. *et al.* Neddylation pathway regulates the proliferation and survival of macrophages. *Biochem Biophys Res Commun* 432, 494–498 (2013).
239. Jin, H.-S., Liao, L., Park, Y. & Liu, Y.-C. Neddylation pathway regulates T-cell function by targeting an adaptor protein Shc and a protein kinase Erk signaling. *Proc Natl Acad Sci USA* 110, 624–629 (2013).
240. Paul, S. & Schaefer, B. C. A new look at T cell receptor signaling to nuclear factor-κB. *Trends Immunol.* 34, 269–281 (2013).
241. Cho, J.-H., Dimri, M. & Dimri, G. P. A positive feedback loop regulates the expression of polycomb group protein BMI1 via WNT signaling pathway. *J Biol Chem* 288, 3406–3418 (2013).
242. Rodrigues, G. A., Falasca, M., Zhang, Z., Ong, S. H. & Schlessinger, J. A novel positive feedback loop mediated by the docking protein Gab1 and phosphatidylinositol 3-kinase in epidermal growth factor receptor signaling. *Mol. Cell. Biol.* 20, 1448–1459 (2000).
243. Yoshimura, A., Naka, T. & Kubo, M. SOCS proteins, cytokine signalling and immune regulation. *Nat. Rev. Immunol.* 7, 454–465 (2007).
244. Ferrara, J. L. Cytokine dysregulation as a mechanism of graft versus host disease. *Curr. Opin. Immunol.* 5, 794–799 (1993).
245. Reddy, P. *et al.* Histone deacetylase inhibition modulates indoleamine 2,3-dioxygenase-dependent DC functions and regulates experimental graft-versus-host disease in mice. *J. Clin. Invest.* 118, 2562–2573 (2008).
246. Turnbaugh, P. J. *et al.* A core gut microbiome in obese and lean twins. *Nature …* 457, 480–484 (2009).
247. Mathewson, N. & Reddy, P. The Microbiome and Graft Versus Host Disease. *Curr Stem Cell Rep* (2015).
248. Jenq, R. R. & van den Brink, M. R. M. Allogeneic haematopoietic stem cell transplantation: individualized stem cell and immune therapy of cancer. *Nature Reviews Cancer* 10, 213–221 (2010).
249. Fleming, L. L. & Floch, M. H. Digestion and absorption of fiber carbohydrate in the colon. *Am. J. Gastroenterol.* 81, 507–511 (1986).
250. Reddy, P. *et al.* Histone deacetylase inhibitor suberoylanilide hydroxamic acid reduces acute graft-versus-host disease and preserves graft-versus-leukemia effect. *Proc Natl Acad Sci USA* 101, 3921–3926 (2004).
251. Hill, G. R. & Ferrara, J. L. The primacy of the gastrointestinal tract as a target

organ of acute graft-versus-host disease: rationale for the use of cytokine shields in allogeneic bone marrow transplantation. *Blood* 95, 2754–2759 (2000).
252. Ganapathy, V., Thangaraju, M., Prasad, P. D., Martin, P. M. & Singh, N. Transporters and receptors for short-chain fatty acids as the molecular link between colonic bacteria and the host. *Curr Opin Pharmacol* 13, 869–874 (2013).
253. Gao, S.-M. *et al.* Histone deacetylases inhibitor sodium butyrate inhibits JAK2/STAT signaling through upregulation of SOCS1 and SOCS3 mediated by HDAC8 inhibition in myeloproliferative neoplasms. *Exp. Hematol.* 41, 261–70.e4 (2013).
254. Ell, B. & Kang, Y. Transcriptional control of cancer metastasis. *Trends Cell Biol.* 23, 603–611 (2013).
255. Charney, A. N., Micic, L. & Egnor, R. W. Nonionic diffusion of short-chain fatty acids across rat colon. *Am. J. Physiol.* 274, G518–24 (1998).
256. Noth, R. *et al.* Increased intestinal permeability and tight junction disruption by altered expression and localization of occludin in a murine graft versus host disease model. *BMC Gastroenterol* 11, 109 (2011).
257. Soler, A. P. *et al.* Increased tight junctional permeability is associated with the development of colon cancer. *Carcinogenesis* 20, 1425–1431 (1999).
258. Suzuki, T. Regulation of intestinal epithelial permeability by tight junctions. *Cell. Mol. Life Sci.* 70, 631–659 (2013).
259. Hanash, A. M. *et al.* Interleukin-22 protects intestinal stem cells from immune-mediated tissue damage and regulates sensitivity to graft versus host disease. *Immunity* 37, 339–350 (2012).
260. Arpaia, N. *et al.* Metabolites produced by commensal bacteria promote peripheral regulatory T-cell generation. *Nature …* 504, 451–455 (2013).
261. Chang, P. V., Hao, L., Offermanns, S. & Medzhitov, R. The microbial metabolite butyrate regulates intestinal macrophage function via histone deacetylase inhibition. *Proc Natl Acad Sci USA* 111, 2247–2252 (2014).
262. Topham, C. H. & Taylor, S. S. Mitosis and apoptosis: how is the balance set? *Curr. Opin. Cell Biol.* 25, 780–785 (2013).
263. Narushima, S. *et al.* Characterization of the 17 strains of regulatory T cell-inducing human-derived Clostridia. *Gut Microbes* 5, 333–339 (2014).
264. Schloss, P. D. *et al.* Introducing mothur: open-source, platform-independent, community-supported software for describing and comparing microbial communities. *Appl. Environ. Microbiol.* 75, 7537–7541 (2009).
265. Schloss, P. D., Gevers, D. & Westcott, S. L. Reducing the effects of PCR amplification and sequencing artifacts on 16S rRNA-based studies. *PLoS ONE* 6, e27310 (2011).
266. DeSantis, T. Z. *et al.* Greengenes, a chimera-checked 16S rRNA gene database and workbench compatible with ARB. *Appl. Environ. Microbiol.* 72, 5069–5072 (2006).
267. Cresci, G. A., Thangaraju, M., Mellinger, J. D., Liu, K. & Ganapathy, V. Colonic gene expression in conventional and germ-free mice with a focus on the butyrate receptor GPR109A and the butyrate transporter SLC5A8. *J.*

Gastrointest. Surg. 14, 449–461 (2010).
268. Takashima, S. *et al.* The Wnt agonist R-spondin1 regulates systemic graft-versus-host disease by protecting intestinal stem cells. *J. Exp. Med.* 208, 285–294 (2011).
269. Iyengar, S., Zhan, C., Lu, J., Korngold, R. & Schwartz, D. H. Treatment with a rho kinase inhibitor improves survival from graft-versus-host disease in mice after MHC-haploidentical hematopoietic cell transplantation. *Biol. Blood Marrow Transplant.* 20, 1104–1111 (2014).
270. Lefrançois, L. & Lycke, N. *Isolation of Mouse Small Intestinal Intraepithelial Lymphocytes, Peyer's Patch, and Lamina Propria Cells*. (John Wiley & Sons, Inc., 2001). doi:10.1002/0471142735.im0319s17
271. Koenigsknecht, M. J. *et al.* Dynamics and Establishment of Clostridium difficile Infection in the Murine Gastrointestinal Tract. *Infect. Immun.* 83, 934–941 (2015).
272. Cole, J. R. *et al.* The Ribosomal Database Project: improved alignments and new tools for rRNA analysis. *Nucleic Acids Res.* 37, D141–5 (2009).
273. Wang, Q., Garrity, G. M., Tiedje, J. M. & Cole, J. R. Naive Bayesian classifier for rapid assignment of rRNA sequences into the new bacterial taxonomy. *Appl. Environ. Microbiol.* 73, 5261–5267 (2007).
274. Liu, X. *et al.* NF-kappaB signaling regulates functional expression of the MHC class I-related neonatal Fc receptor for IgG via intronic binding sequences. *The Journal of Immunology* 179, 2999–3011 (2007).
275. Molinero, L. L. *et al.* NF-kappa B regulates expression of the MHC class I-related chain A gene in activated T lymphocytes. *The Journal of Immunology* 173, 5583–5590 (2004).